Studying the functional relevance of lung cancer genetic drivers in their physiological niche

Jenni Lahtela

Institute for Molecular Medicine Finland (FIMM)
Faculty of Medicine
University of Helsinki
Helsinki, Finland

ACADEMIC DISSERTATION

To be presented for public examination with the permission of the Faculty of Medicine, University of Helsinki, in Lecture hall 3 at Biomedicum 1 (Haartmaninkatu 8, Helsinki), on the 19th of February 2016 at 12 noon.

Helsinki 2016

Supervised by

Emmy Verschuren, Ph.D
FIMM-EMBL Group Leader
Institute for Molecular Medicine Finland (FIMM)
University of Helsinki
Helsinki, Finland

Juha Klefström, Ph.D, Docent
Research Programs Unit/Translational Cancer Biology
Medical Faculty
University of Helsinki
Helsinki, Finland

Reviewers appointed by the Faculty

Satu Kuure, Ph.D, Docent
Institute of Biotechnology
University of Helsinki
Helsinki, Finland

Cecilia Sahlgren, Ph.D, Docent
Turku Centre for Biotechnology
Åbo Akademi University
Turku, Finland

Opponent appointed by the Faculty:

Anton Berns, Ph.D, Professor
Netherlands Cancer Institute
Amsterdam, The Netherlands

Custos appointed by the Faculty:

Tomi Mäkelä, Ph.D, Professor
Faculty of Medicine
University of Helsinki
Helsinki, Finland

Cover layout and image: Susanna Tuononen

ISBN 978-951-51-1918-6 (pbk.)
ISBN 978-951-51-1919-3 (PDF)

Press: Hansaprint Oy, Helsinki, 2016

To my family

"Strive not to be a success, but rather to be of value."
Albert Einstein

Contents

List of original publications

This thesis is based on the following publications:

I Lahtela, J., Corson, L.B., Hemmes, A., Brauer, M.J., Koopal, S., Lee, J., Hunsaker, T.L., Jackson, P.K., and Verschuren, E.W. A high- content cellular senescence screen identifies candidate tumor suppressors, including EPHA3. *Cell Cycle*. 2013:12:625-34.

II Lahtela, J., Pradhan, B., Närhi, K., Hemmes, A., Särkioja, M., Kovanen, P.E., Brown, A., and Verschuren, E,W. The putative tumor suppressor gene *EphA3* fails to demonstrate a crucial role in murine lung tumorigenesis or morphogenesis. *Dis. Model Mech*. 2015:8:393-401.

III Nagaraj, A.*, Lahtela, J.*, Hemmes, A., Salmenkivi, K., Närhi, K., and Verschuren EW. Cell-of-origin links histotype spectrum to immune microenvironment diversity in non-small cell lung cancer driven by mutant *Kras* and loss of *Lkb1*. Submitted.

*Co-first author

The publications are referred to in the text by their roman numerals

Abbreviations

AC	adenocarcinoma
Ad5-CC10-Cre	adenovirus expressing Cre-recombinase under CC10 promoter
Ad5-CMV-Cre	adenovirus expressing Cre-recombinase
Ad5-SPC-Cre	adenovirus expressing Cre-recombinase under SPC promoter
AIS	adenocarcinoma in situ
AKT	RAC-alpha serine/threonine-protein kinase
ALK	anaplastic lymphoma kinase
AMPK	AMP-activated protein kinase
Arg1	arginase 1
ASC	adenosquamous carcinoma
AT1 cell	alveolar type I cell
AT2 cell	alveolar type II cell
BADJ	bronchioalveolar duct junction
BASCs	bronchioalveolar stem cells
Bmp4	bone morphogenetic protein 4
BRAF	B-Raf proto-oncogene, serine/threonine kinase
CALCA/ CGRP	calcitonin gene-related peptide 1
CC10	Clara cell 10 kDa secretory protein
CD11b	integrin alpha-M
CD14	CD14 molecule
CD15	myeloid-specific alpha fucosyltransferase, FUT4
CD33	CD33 molecule
CDKI	cyclin-dependent kinase inhibitor
CDKN1A/p21	cyclin-dependent kinase inhibitor 1A
CDKN2A/p16INK4a /Arf	cyclin-dependent kinase inhibitor 2A
CK14	cytokeratin 14
CK5	cytokeratin 5
COPD	chronic obstructive pulmonary disease
CPPs	cardiopulmonary mesoderm progenitors
DDR	DNA damage response
DNA	deoxyribonucleic acid
ECM	extra cellular matrix
EGFR	epidermal growth factor receptor
EMT	epithelial-to-mesenchymal transition
EndMT	endothelial-to-mesenchymal transition

EPH	erythropoietin-producing hepatocellular (carcinoma)
EPHA3	EPH receptor A3
ERK	extracellular signal-regulated kinase
Fgf10	fibroblast growth factor 10
Fgf9	fibroblast growth factor 9
Fgfr2	fibroblast growth factor receptor 2
FOXJ1	forkhead box J1
GEMM	Genetically engineered mouse model
Gr-1	myeloid differentiation antigen Gr-1
GTPase	small guanosine triphosphatase
HRAS	harvey rat sarcoma viral oncogene homolog
IHC	immunohistochemical
i.e	id est
Il1b	interleukin-1b
ITH	intratumour heterogeneity
KDR	kinase insert domain receptor (vascular endothelial growth factor receptor 2, VEGFR2)
KL	$Kras^{LSL\text{-}G12D/+}$; $Lkb1^{fl/fl}$ / $Kras^{LSL\text{-}G12D/+}$; $Lkb1^{fl/-}$
KP	$Kras^{LSL\text{-}G12D/+;}$ $Trp53^{fl/fl}$
KRAS	kirsten rat sarcoma viral oncogene homolog
LCC	large cell carcinoma
LKB1/*STK11*	liver kinase B1 / serine/threonine kinase 11
LY6C	lymphocyte antigen 6 complex, locus C
LY6G	lymphocyte antigen 6 complex, locus G
MAPK	mitogen-activated protein kinase
MDM2	MDM2 proto-oncogene
MDSC	myeloid derived suppressor cell
MHC	major histocompatibility complex
MUC5AC	mucin 5AC, oligomeric mucus/gel-forming
NE	neuroendocrine
NEB	neuroepithelial body
NGFR	nerve growth factor receptor
Nkx2-1	NK2 homeobox 1
NSCLC	non-small-cell lung cancer
OIS	oncogene-induced senescence
p63	tumour protein 63
PAC	papillary adenocarcinoma
PAS	periodic acid Schiff's staining
PD-1	programmed death 1
PECAM1/CD31	platelet endothelial cell adhesion molecule
PI3K	phosphoinositide 3-kinase
PJS	Peutz-Jeghers syndrome
PNECs	pulmonary neuroendocrine cells

PTEN	phosphatase and tensin homolog
Q-PCR	quantitative polymerase chain reaction
RA	the retinoic acid
RB1	retinoblastoma 1
RTK	receptor tyrosine kinase
SA-β-gal	senescence-associated β-galactosidase
SASP	senescence-associated secretory phenotype
SCC	squamous cell carcinoma
Scgb1a1	secretoglobin, family 1A, member 1
SCLC	small-cell lung cancer
Shh	sonic hedgehog
siRNA	small interfering RNA
SO_2	sulfur dioxide
Sox2	SRY (sex determining region Y)-box 2
Sox9	SRY (sex determining region Y)-box 9
SPC / *Sftpc*	surfactant associated protein C
Spry1/2	sprouty homolog 1/2
TERT	telomerase reverse transcriptase
TetO	tetracycline 19-bp operator sequence
TNM	Tumour-Node-Metastasis system
Trp53/*TP53*	transformation related protein 53/tumour protein p53
tTA	tetracycline controlled transactivator
Vegfa	vascular endothelial growth factor-A

Abstract

Lung cancer is the leading cause of cancer related deaths worldwide. Major contributing factors include asymptomatic disease progression and a high level of intra- and intertumour genomic, molecular, and microenvironmental heterogeneity. Large lung cancer sequencing efforts have identified clear histopathology-specific genetic alteration patterns, which in the cases of lung adenocarcinomas (ACs) are applied in clinics to direct treatment. Unfortunately, in most patients acquired resistance to targeted treatment often develops within months. Recently, lung cancer immunotherapy approaches have shown promising results in clinical trials. However, a need for further development and accurate patient stratification to better counter the variability seen in the lung cancer immune microenvironment exists. Hence, a deeper understanding of the functional importance of novel lung cancer genes as well as the lung cancer-related niche and cell type specific propensities leading to molecular and microenvironmental tumour heterogeneity would be beneficial.

The first part of this thesis work concentrated on the functional *in vitro* and *in vivo* investigation of putative tumour suppressive characteristics of the EPH receptor A3 (*EPHA3*), a gene commonly mutated in human lung cancers. Our finding that silencing of *EPHA3* induces cellular senescence, a cell intrinsic mechanism for tumour suppression, prompted us to further validate its tumour suppressive characteristics. An *in vitro* kinase assay-based investigation of EPHA3 cancer point mutations indicated that EPHA3-mediated tumour suppression was specifically dependent on its kinase activity. However, we found that constitutive loss of *EphA3* did not co-operate with two known genetic alterations of human lung cancer, namely conditional oncogenic *Kras* or *Trp53*-loss, in murine lung tumourigenesis. Moreover, we did not find any defects in lung morphogenesis due to *EphA3*-loss, despite its expression being detected in developing murine lung mesenchyme. Hence, we conclude that our study demonstrates how functional validation of putative cancer genes can be challenged by biological complexity, which may result in acquired compensation or different functional roles in human and mice.

The second part of this thesis work investigated the propensities of the *in vivo* lung proximal and peripheral niche and lung epithelial cell types to respond to known lung cancer genetic alterations, namely conditional oncogenic *Kras* combined with loss of a tumour suppressor *Lkb1* (KL). Our results showed that cells in the airways of mouse lungs had a higher propensity to develop faster growing and progressing lung tumours than the cells in the alveolar space. These lung tumours, which were predominantly classified as adenosquamous carcinomas (ASCs), showed elevated levels of immune related genes, suggesting an ASC-specific immunosuppressive microenvironment. This conclusion was further supported by a notable ASC-specific immune cell infiltration

with an increase in the amount of myeloid cells, possibly representing a subpopulation of myeloid-derived suppressor cells (MDSCs) and decrease in the amount of tumour-infiltrating T-cells. The KL ASC model may thus represent a relevant preclinical model for the study of anti-MDSC immune therapy as a treatment for ASCs, which in humans represent a rare but aggressive type of lung cancer.

Thus, the findings presented in this thesis highlight the importance of the functional niche in the progression of lung cancer and, therefore, possibly affecting a response to treatment. Niche-specific investigation of lung cancer genetic alterations thus leads to a more accurate stratification of the preclinical *in vivo* models, simultaneously revealing relevant molecular mechanisms underlying lung cancer heterogeneity.

Tiivistelmä

Keuhkosyöpä on maailmanlaajuisesti eniten kuolemaan johtava syöpäsairaus, jonka hoito on aina yksilöllistä riippuen muun muassa syövän tyypistä ja levinneisyydestä. Huolimatta uusimmista keuhkosyövän hoitomuodoista, joilla pyritään vaikuttamaan kohdennetusti tiettyjen geenimutaatioiden aiheuttamaan pahalaatuisen syöpäkudoksen kasvuun, ei riittävän hyviä potilaan parantumiseen johtavia hoitoja ole vielä keksitty. Tämän ajatellaan johtuvan muun muassa yksittäisen syöpäkudoksen sisäisestä tai syöpäkasvainten välillä olevasta heterogeenisyydestä eli siitä, että syöpäsolut poikkeavat toisistaan ja reagoivat siksi eritavalla syöpähoitoihin. Laajat keuhkosyövän DNA-sekvensointitutkimukset ovat tunnistaneet valtavan määrän uusia mutaatiota, jotka ovat oletettavasti vaikuttaneet tutkittujen syöpien kehittymiseen. Näiden geneettisten muutosten syvempi toiminnallinen ymmärtäminen on tärkeää, jotta voimme paremmin käyttää hyväksi tätä suurta määrää uutta tietoa kehittäessämme uusia hoitomuotoja syöpiin.

Keuhkosyövät luokitellaan histopatologisesti kahteen pääluokkaan, ei-pienisoluisiin ja pienisoluisiin keuhkosyöpiin. Ei-pienisoluisten keuhkosyöpien, joiden esiintyvyys on noin 85% kaikista keuhkosyövistä, kaksi yleisintä alaluokkaa ovat adenokarsinooma (~60%) ja levyepiteelikarsinooma (~30%), joiden diagnostiset tutkimukset ja hoitolinjat poikkeavat toisistaan. Potilaan oman immuunipuolustuksen valjastaminen syöpäkasvainta vastaan on syövän hoitomuotona keksitty jo 1900-luvun alussa, mutta vasta viimeaikaiset tutkimukset ovat selvittäneet immuunipuolustukseen liittyvää kasvaimen mikroympäristön ja molekyylisäätelyn taustaa.

Tämän väitöskirjatyön tavoitteena oli selvittää useissa keuhkosyövissä mutatoituneen EPH-reseptori A3- (*EPHA3*) geenin osuutta keuhkosyövän synnyssä ja etenemisessä, sekä tutkia kyseisen geenin toimintaa keuhkon kehityksessä. Tutkimustuloksemme osoittavat, että *EPHA3*-geenin ilmentymisen väheneminen soluissa johtaa senesenssiin eli solun palautumattomaan lepotilaan. Tämän mekanismin on osoitettu toimivan solujen luontaisena keinoina puolustautua normaalista poikkeavaa kasvua vastaan. Jatkotutkimuksemme osoittivat, että keuhkosyöpäsoluista löytyneet *EPHA3*-geenin mutaatiot vähentävät EPHA3-proteiinin kinaasiaktiivisuutta, tukien *EPHA3*-geenin syövän kasvua estävää eli tuumorisuppressivista tehtävää soluissa. Keuhkosyöpähiirimalleilla saadut tuloksemme eivät kuitenkaan tukeneet *EPHA3*-geenin tuumorisuppressivista toimintaa. Lisäksi, vaikka EPHA3-proteiinin osoitettiin ilmentyvän hiiren alkion keuhkojen mesenkymaalisissa soluissa, *EphA3*-poistogeenisten hiirten alkioiden keuhkojen havaittiin kehittyvän normaalisti. Näiden *in vivo* hiirimallista saatujen tulosten perusteella teimme johtopäätöksen, että hiiren *EphA3*- geenin poisto voi esimerkiksi johtaa saman geeniperheen geenien ilmentymisen aikaansaamaan

kompensaatioon ja/tai *EPHA3*-geenin poistolla voi olla eri merkitys hiirelle kuin ihmiselle.

Toinen tämän väitöskirjatyön tavoite oli tutkia eri keuhkosolutyyppien alttiutta kehittyä ei-pienisoluisen keuhkosyövän eri histopatologiatyypeiksi. Tutkimustuloksemme keuhkosyöpähiirimallilla, jossa tunnettujen keuhkosyöpägeenien, *KRAS* ja *LKB1*, muutokset aikaansaavat ei-pienisoluisen keuhkosyövän synnyn, osoittivat, että keuhkojen kahdella eri solutyypillä on erilainen alttius kehittyä adenoskvamoosi karsinoomaksi. Ihmisellä adenoskvamoosi karsinooma on harvinainen, mutta aggressiivinen keuhkosyöpätyyppi. Tutkimustuloksemme osoittivat, että keuhkosyöpähiirimallin adenoskvamooseissa karsinoomissa, joiden havaittiin kasvavan nopeammin kuin adenokarsinoomien, on immuunipuolustuksen vaimentamiseen viittaava immuunisoluympäristö. Tämän on osoitettu liittyvän syövän huonoon ennusteeseen. Tulevaisuudessa kyseistä hiirimallia voidaan mahdollisesti käyttää uusien potilaan omaa immuunipuolustusta hyväksi käyttävien hoitomuotojen kehityksessä.

Tämä väitöskirjatyö on tuottanut merkittävää uutta tietoa *EPHA3*-geenin toiminnallisesta tehtävästä syövässä, jonka valossa kyseiseen geeniin liittyvää syöpätutkimusta pystytään ohjaamaan tulevaisuudessa oikeaan suuntaan. Lisäksi tämä väitöskirjatyö avasi uusia näkökulmia keuhkosyövän heterogeenisyyteen johtavista tekijöistä sekä osoitti aggressiivisen keuhkosyöpätyypin mahdollisesti omaavan erityisen kasvaimen immuunisoluympäristön, jota voidaan tulevaisuudessa käyttää hyväksi uusien hoitomuotojen kehityksessä.

1 Introduction

Cancer is a disease caused by rapid and abnormal expansion of cells growing beyond their normal tissue boundaries. Cancer can affect any part of the body, invade neighbouring tissues, and/or spread to distant organs via a process called metastasis. Cancer is among the leading cause of morbidity and mortality worldwide (Stewart *et al.*, 2014).

Cancerous growth of cells is caused by genetic errors in genes normally regulating tissue homeostasis. These errors can be inherited or occur sporadically due to exposure to environmental agents, such as ultraviolet radiation, components of tobacco smoke, and infections by specific viruses. Cancer-causing genetic alterations functionally either promote cellular growth or inhibit it and are referred to as oncogenes and tumour suppressor genes, respectively. The multistep process that leads to development of malignant cancer is composed of acquired biological capabilities of the cancer cells, generally referred to as 'hallmarks of cancer'. These capabilities include sustaining proliferative signalling, evading growth suppression and cell death, enabling replicative immortality, inducing angiogenesis, activating invasion and metastasis, reprogramming of energy metabolism, and evading immune destruction (Hanahan and Weinberg, 2000, 2011).

Cellular senescence is a cell-intrinsic mechanism to arrest cell growth, and its bypass is considered one of the cancer hallmarks (Hanahan and Weinberg, 2000, 2011). In embryonic development and normal physiology, senescence takes part in tissue remodelling and removal of damaged cells (Munoz-Espin *et al.*, 2013; Munoz-Espin and Serrano, 2014; Storer *et al.*, 2013). Replicative senescence, which acts as a mechanism to protect cells from unlimited proliferation, is triggered by DNA damage to allow DNA repair during the DNA damage response (DDR) (Campisi and d'Adda di Fagagna, 2007; Evan and d'Adda di Fagagna, 2009). The mechanisms that lead to cellular senescence are context-dependent. In general, induction of cellular senescence is mediated by up-regulation of cell cycle inhibitors including cyclin-dependent kinase inhibitors (CDKIs) p21 (encoded by *CDKN1A*) and $p16^{INK4a}$ (encoded by *CDKN2A*), and often up-regulation and activation of transcription factor p53 (encoded by *TP53* in humans and *Trp53* in mice) (Munoz-Espin and Serrano, 2014). Recently, it has been also reported that senescent cells acquire a pro-inflammatory senescence-associated secretory phenotype (SASP), which can affect neighbouring cells in a paracrine manner and trigger responses including inflammation. This response leads to elimination of senescent cells as well as promotion of cell growth (Munoz-Espin and Serrano, 2014; Rodier and Campisi, 2011). Thus, cellular senescence has pleiotropic effects on tissue homeostasis.

The tumour suppressive role of cellular senescence is demonstrated both *in vitro* and *in vivo*. Expression of the constitutively active, oncogenic small guanosine

triphosphatase *HRAS* (harvey rat sarcoma viral oncogene homolog) in murine and human cells induces cellular senescence (Serrano *et al.*, 1997). This process is named oncogene-induced senescence (OIS). *In vivo*, OIS is detected in lung lesions induced by oncogenic *Kras* (Kirsten rat sarcoma viral oncogene homolog) and oncogenic *BRAF*, a downstream effector of Ras (Collado *et al.*, 2005; Dankort *et al.*, 2007). In both cases, OIS, characterised by expression of $p16^{INK4a}$ and senescence-associated β-galactosidase (SA-β-gal) positivity, is bypassed in the more progressed AC lesions or by introduction of p53- or $p16^{INK4a}$-loss. Additionally, loss of the tumour suppressor phosphatase and tensin homologue (*Pten*) in mouse prostate induces p53-dependent cellular senescence, which is bypassed with inactivation of p53 (Chen *et al.*, 2005). Taken together, OIS acts as a mechanism to suppress tumourigenesis, initiated by an oncogene or by loss of a tumour suppressor gene. Furthermore, acquired bypass of OIS with alterations in genes such as *TP53* and *CDKN2A* may be needed for cancers to progress.

The development of malignant cancer is characterised by aberrant activation or deactivation of molecules generally regulating embryonic development. An example is observed with the members of the EPH receptor family (Nievergall *et al.*, 2012). Specifically, concepts gained with studies exploring mechanisms of developmental biology can be crucial in understanding the functional importance of cancer-promoting genetic alterations. Furthermore, the tissue-specific niches in adult organs, which are composed of cells specialised to control physiologically distinct processes, are crucial determinants of cancer heterogeneity (Leeman *et al.*, 2014). In lungs, different parts of the proximo-distal axis are highly specialised for maintenance of organ homeostasis, enabling uninterrupted respiration providing oxygen to and removing carbon dioxide from the body. The lung injury model-based identification of lung epithelial stem and progenitors cells and following progenitor cell specific modulation of genes have revealed new insights to several lung pathologies including lung cancer (Leeman *et al.*, 2014; Sutherland and Berns, 2010; Sutherland *et al.*, 2014).

Lung cancer is the leading cause of cancer-related deaths worldwide (Ferlay *et al.*, 2015). It is characterised by high levels of genetic, epigenetic, and histopathological tumour heterogeneity within and between the lung tumours. In addition to heterogeneity detected in the epithelial tumour cell compartment, cancer heterogeneity is also detected within the tumour microenvironment, which includes tumour-infiltrating innate immune cells, such as natural killer cells, macrophages, and neutrophils, as well as adaptive immune cells including B- and T-lymphocytes (de Visser *et al.*, 2006; Hanahan and Coussens, 2012). Recently, much progress has been made applying cancer immunotherapy approaches in which the patient's own immune system is harnessed against the cancer cells (Wolchok and Chan, 2014). Inhibition of molecules which cancer cells use to escape from an immune attack, in combination with standard chemotherapy treatment, is being pursued in clinical trials and showing promising results (Creelan, 2014). Thus, there is a need for a deeper understanding of the functional importance of novel lung cancer genes as well as the molecular and microenvironmental

tumour heterogeneity caused by factors including lung cancer related niche and cell type specific propensities.

This thesis work concentrated on the *in vitro* and *in vivo* investigation of the functional tumour suppressor role of the EPH receptor A3 (*EPHA3*) gene, a result from a cellular senescence screen executed to identify novel putative tumour suppressors. Since *EPHA3* is commonly mutated in human lung cancers, the work presented in this thesis focused on the *in vivo* role of EPHA3 in lung cancer development. Considering the well-established roles of EPH receptors in embryonic development, the possible role of *EphA3* in mouse lung morphogenesis was addressed with the aim to gain biological insight into its putative function during lung cancer progression. Finally, this thesis work established the differential contributions of *in vivo* lung proximal and peripheral niches, and specific epithelial cell progenitor types, to growth of murine NSCLC. Using a murine NSCLC model driven by known lung cancer drivers, namely oncogenic *Kras* and loss of the tumour suppressor *Lkb1,* the investigation of lung progenitor cell niche-specific tumour heterogeneity analysed lung lesion-specific immunosuppressive mechanisms and established a link between the tumour histopathology spectrum and the immune microenvironment.

2 Review of the literature

2.1 The lung

The lung is a complex organ with a primary function to provide oxygen and remove carbon dioxide from the body. Different parts of the lung are highly specialized for maintaining organ homeostasis and enabling uninterrupted flow of gasses. The lung belongs to the group of organs that have a low steady-state cell turnover but can robustly respond to injury and repair damaged tissue. During recent years excellent progress has been made through murine studies to gain information about the composition and organization of the distinct epithelial cell populations of mouse lung, (Leeman et al., 2014) which in many aspects resemble the composition of the cells in human lung (Rock et al., 2010). Much work has focused on the identification of lung epithelial stem and progenitors cells, key players of normal lung tissue homeostasis. Dysfunction of these cells is likely the cause of several lung pathologies such as chronic obstructive pulmonary disease (COPD), asthma, and lung cancer (Leeman et al., 2014) (for literature review of lung cancer see section 2.3.1.4). Therefore, current mechanistic studies are focusing on the functional differences between the distinct epithelial stem and progenitor cells of the lung to better understand the aetiology of these lung diseases.

2.1.1 Structure and cell types of the lung

The lung consists of conducting proximal airways and gas-exchanging distal alveolar space that is surrounded by a dense capillary network. The proximal airways are composed of cartilaginous trachea, which in mice is lined by pseudostratified columnar epithelial cells and noncartilaginous bronchioles, made of simple columnar epithelium. The epithelial cells in the distal alveolar space form the gas-exchanging alveolar structures. The epithelial cell types in the proximo-distal axis of the lungs vary and are highly specialised to carry out functions needed for the maintenance of the tissue homeostasis and/or defence against inhaled harmful gases, particulates, and microorganisms, as well as the gas-exchanging process (Figure 1). Lung cell types with mesenchymal origin and resident to the epithelial and endothelial cells, take part in respiration and contribute to the maintenance of the airway, alveolar structures, and stem cell niches, as well as support the formation of a capillary network (Barkauskas *et al.*,

2013; Hogan *et al.*, 2014). The importance of these non-epithelial cell types to lung tissue homeostasis is axiomatic. However, this thesis work concentrated on lung cancers of epithelial origin (carcinomas), and thus the following sections describe the known epithelial cell types of mammalian lung and their properties as progenitor cells and thus possible contributors to lung carcinomas.

The epithelial cell types within the proximal part of the lung vary in its different regions (Figure 1). The basal cells, which are found in the trachea in mice, but interestingly, all along the airway to distal bronchioles in humans, are a population of multipotent stem cells that take care of both homeostasis of the normal epithelium as well as its regeneration after injury. These cells divide symmetrically and asymmetrically in the steady state murine lung, thus are capable of self-renewal as well as production of luminal ciliated and Clara cells (Watson et al., 2015). Furthermore, basal cells, marked with cytokeratin 14 (CK14) expression, serve as progenitor cells for Clara and ciliated cells (see sections below) after naphthalene treatment-induced Clara cell selective injury (Ghosh et al., 2011; Hong et al., 2004). Basal cells can be identified by expression of markers including nerve growth factor receptor (NGFR), tumour protein 63 (p63), cytokeratin 5 (CK5), and CK14 (Rock et al., 2010).

Nonciliated columnar secretory cells, which are the source of secretoglobins, such as Clara cell 10 kDa secretory protein (CC10, also known as CCSP) encoded by the *Scgb1a1* gene, are a heterogeneous population of cells generally referred to as Clara (or club) cells. They are capable of self-renewal and are found toward the distal parts of airways in increasing numbers (Rawlins *et al.*, 2009b). Specific $CC10^+$ Clara cells in the neuroepithelial body (NEB) microenvironment represent a naphthalene-resistant subpopulation of Clara cells indicating variety among the $CC10^+$ cells and pointing out a possible Clara cell progenitor population (Hong et al., 2001). Functionally, Clara cells have been linked to the lung inflammatory response. Specifically, Clara cell depletion, as well as CC10 deficiency, increases the lung inflammatory response induced by both pseudomonas aeruginosa lipopolysaccharide (Snyder et al., 2010) and adenovirus (Harrod et al., 1998).

Clara cells are progenitors for at least two other cell types of the lung airways, namely ciliated cells and goblet cells, both of which take part in mucociliary clearance, the process by which inhaled microorganisms and particulates are cleared from the lung. Multiciliated cells expressing the forkhead transcription factor (FOXJ1) are not capable of self-renewal (Rawlins et al., 2007). During normal regeneration of the epithelium, as well as in response to tracheal sulfur dioxide (SO_2) ciliated cell injury, ciliated cells originate from Clara cells (Rawlins *et al.*, 2009b). Mucin, which is composed of large glycoproteins, is produced by MUC5AC-expressing goblet cells. In comparison to humans, the amount of goblet cells in in adult mice, which are maintained under laboratory conditions, is low. However, the number increases in response to inflammation. For example, the differentiation of Clara cells into mucin-producing goblet cells, which are not capable of self-renewal, increases in ovalbumin-induced allergen inflammation in the mouse lungs (Chen et al., 2009; Rock et al., 2009).

Columnar pulmonary neuroendocrine cells (PNECs), which secrete calcitonin gene-related peptide 1 (CALCA also known as CGRP), sense stimuli within the airway lumen, including hypoxia and nicotine (Fu et al., 2002; Schuller et al., 2003). PNECs are found either as single cells in proximal airways or in clusters called neuroepithelial bodies (NEBs) closer to the distal alveolar space.

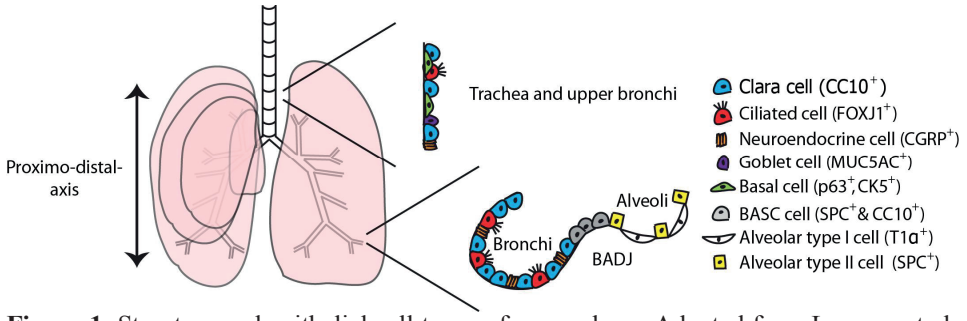

Figure 1. Structure and epithelial cell types of mouse lung. Adapted from Leeman et al. 2014.

The most distal parts of the bronchioles, which are called the terminal bronchioles, lead to the distal alveolar space. This peripheral part of the lungs consists of alveolar surface tension-reducing surfactant-associated protein C (SPC)-secreting alveolar type II (AT2) cells and gas-exchanging, alveolar type I (AT1) cells characterised with podoplanin (PDPN, also known as T1α) (Leeman et al., 2014) (Figure 1). The self-renewing and proliferating AT2 cells are progenitors of AT1 cells (Desai et al., 2014; Evans et al., 1972). Interestingly, low levels of CC10 expression, which expression is high in airway Clara cells, have been detected in mouse AT2 cells (Rawlins *et al.*, 2009b). The region between the terminal bronchioles and the alveolar space is called the bronchioalveolar duct junction (BADJ) where rare cells, positive for both CC10 and SPC and identified as bronchioalveolar stem cells (BASCs), are capable of differentiation to both Clara and alveolar cells (Kim et al., 2005).

Taken together multiple epithelial cell types have been identified of which five, namely basal, Clara, ciliated, goblet, and neuroendocrine cells, are described here. Two of these, basal and Clara cells, are capable of self-renewing and functioning as progenitors. Of the two types of alveolar epithelial cells, namely AT1 and AT2 cells, the latter have been shown to act as progenitors. Additionally, BASCS at the BADJ are shown to function as progenitors for both Clara and alveolar cells. As shown for the Clara cells, variety among within these defined cell type clusters may exist and more research is needed to characterise this possible, yet undefined heterogeneity.

2.1.2 Lung development

Lung development starts around embryonic (E) day 9.5 in mice and around 4–5 weeks gestation in humans when two primary lung buds appear in a region of the ventral wall of the anterior foregut. These primary lung buds express the transcription factor *Nkx2-1* (also known as *Titf1*) (Lazzaro et al., 1991; Morrisey and Hogan, 2010). NKX2-1 is one of the key molecules in lung morphogenesis. Lungs of *Nkx2-1*-null mice do not branch and show decreased expression levels of respiratory-system-specific genes *Sftpc* and the *Scgb1a1*-encoding SPC and CC10, respectively (Kimura et al., 1996; Minoo et al., 1999). The ventral side of the foregut tube develops into trachea, making a connection with the lung buds. Simultaneously, the dorsal side of the single foregut tube starts to separate and form the oesophagus, leading to the stomach. The two primary lung buds are composed of a simple endodermal epithelium, which is surrounded by mesoderm and a vascular plexus. These tissues are further surrounded by a thin layer of mesothelium, which also gives rise to a proportion of the mesenchymal cells (Dixit et al., 2013).

The branching morphogenesis, which follows the bud initiation phase (embryonic stage E9.5-E12.5), continues until E16.5 in mice, generating a tree-like structure with thousands of branches (Morrisey and Hogan, 2010) (Figure 2). This period is called the pseudoglandular stage of lung development due to the glandular looking structures that eventually form the airways. The branching follows an organised program of three branching modes, called domain branching, planar bifurcation, and orthogonal bifurcation (Metzger et al., 2008). Tracing of the different modes during branching has indicated specific functions for the different modes. The central architecture of each lobe is formed by domain branching, whereas the planar bifurcation and orthogonal bifurcations form the thin edges of lobes, create lobe surfaces, and fill the interior (Metzger et al., 2008). The tip of the epithelial bud is composed of inhibitor of DNA binding 2 (*Id2*)-expressing multipotent progenitor cells which give rise to cell types in the bronchi and bronchioles (Hogan *et al.*, 2014; Rawlins *et al.*, 2009a). The airway epithelial cell differentiation creates multiple specialized cell types in the proximal airways starts at this stage (Morrisey and Hogan, 2010). One of the crucial determinants of airway epithelial cell differentiation is Notch signalling, which has been shown to control the balance between ciliated and secretory cell fate by silencing the ciliated cell program (Tsao *et al.*, 2009).

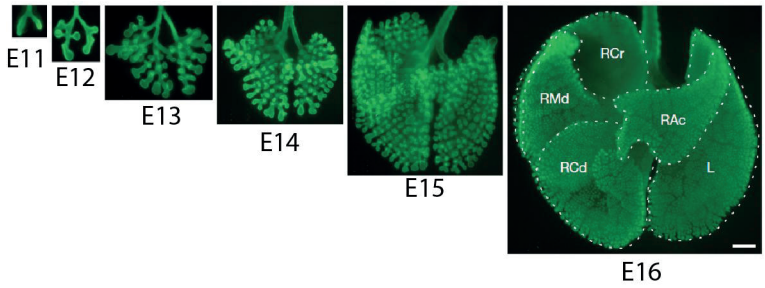

Figure 2. The branching morphogenesis of murine lungs. Dotted lines at embryonic day (E) 16 show the right cranial (RCr), right middle (RMd), accessory (RAc), right caudal (RCd) and left (L) lobes. Scale bar, 500 mm. Adapted from Metzger et al. 2008.

The pseudoglandular stage of lung development is followed by the canalicular (E16.5-E17.5) and saccular (E18.5-postnatal day (P) 5) stages which are part of the alveologenesis, a critical stage in preparing the structures for gas exchange. During the canalicular stage, when the canalisation of the lung parenchyma occurs, a population of columnar progenitor cells of the epithelial tips starts to become either flat AT1 cells specialized for gas exchange or cuboidal AT2 cells expressing surfactant proteins which are needed for reduction of surface tension. The saccular phase involves the generation of tiny peripheral sacs separated by primary septa. The development of alveoli continues postnatally as the number and surface area increase. Development continues for weeks after birth in mice and months in humans (Hogan et al., 2014). In support of the bipotential alveolar progenitor cell type, a single cell transcriptomic analysis of the developing mouse lung at E18.5 identified cells expressing markers for both AT1 and AT2 cells (Treutlein *et al.*, 2014). This observation was further supported by another study that identified cells expressing a subset of AT1 and AT2 markers giving rise to either AT1 or AT2 cells by shutting off the expression of specific cell type markers (Desai *et al.*, 2014). Throughout the whole process of lung development, dynamic and reciprocal signalling between the branching epithelium and the surrounding mesenchyme is needed for correct assembly of the formed organ. This assembly results in four right lobes (cranial, medial, caudal, and accessory) in humans and one left lobe in mice (Morrisey and Hogan, 2010).

2.1.2.1 Regulation and signalling networks of branching morphogenesis

Distinct genes along the axis of the developing lung have been identified to regulate the controlled process of lung branching. Examples of the dynamic control of branching morphogenesis are regulation mediated by the transcription factors SRY (sex determining region Y)-box 2 (*Sox2*) and -9 (*Sox9*). *Sox2* is a key regulator of cell

differentiation in the ventral early foregut. Its expression is detected in proximal and non-branching regions and is switched off in branch initiation sites (Gontan et al., 2008; Ishii et al., 1998). Conditional loss of *Sox2* expression in the ventral side of the early anterior foregut results in abnormal differentiation of the epithelium in the conducting airways with an increase in the amount of mucus-producing cells and decrease in the amount of basal, ciliated and Clara cells, indicating a role for *Sox2* in regulation of cell differentiation (Que et al., 2009). In contrast to *Sox2*, *Sox9* is expressed in the tips of the branching epithelia, and deletion of Sox9 in developing lung epithelium impairs branching morphogenesis resulting in smaller lungs with dilated airway branches (Chang et al., 2013). Furthermore, *Sox9* expression is suggested to suppress alveolar differentiation during the pseudoglandular stage of lung development (Chang et al., 2013).

The key signalling molecules regulating the lung branching process include members of the fibroblast growth factor (Fgf), bone morphogenic protein (Bmp), transforming growth factor beta (Tgfb), and sonic hedgehog (Shh) families in addition to retinoic acid (RA). The dynamic and reciprocal signalling between these molecules in branching epithelia and surrounding mesenchyme and mesothelium is needed for proper development (Morrisey & Hogan, 2010) (Figure 3).

Distal mesenchymal fibroblast growth factor 10 (encoded by *Fgf10*) and fibroblast growth factor receptor 2 (encoded by *Fgfr2*) in the branching epithelial tip (De Moerlooze et al., 2000; Min et al., 1998; Sekine et al., 1999) are two key signalling molecules in lung branching morphogenesis. The *Fgf10*$^{-/-}$ mouse embryos display complete absence of lungs leading to perinatal lethality (Min et al., 1998; Sekine et al., 1999). Furthermore, the lung phenotype of embryos expressing the IIIb-isoform specific mutation of *Fgfr2* and fusion chimera embryos of homozygous *Fgfr2* mutants resemble closely that of *Fgf10*-null mouse lungs (Arman et al., 1999; De Moerlooze et al., 2000), strongly indicating an important role for FGF10-FGFR2 signalling in the initiation of branching morphogenesis. Interestingly, recent data suggest that the level, rather than the localized expression, of *Fgf10* surrounding the distal epithelial bud controls the correct formation of a new branch point in developing lung (Volckaert et al., 2013).

The *Fgf10*-positive distal mesenchyme acts as an organizing and signalling centre working together with the epithelium- and mesothelium via reciprocal interactions between specifically expressed signalling molecules to coordinate epithelial branching (Figure 3). This section describes selected genes encoding signalling molecules which have been shown to control lung branching morphogenesis often by regulating *Fgf10* expression. Fibroblast growth factor 9 (*Fgf9*), is expressed first in the epithelium and mesothelium during embryonic stage (Colvin et al., 1999), and later, during the pseudoglandular stage, its expression is mostly restricted to the epithelium (del Moral et al., 2006a). *Fgf9*-null embryonic lungs are hypoplastic, showing thinning of the mesenchyme and lack *Fgf10* expression at E13.5-E14.5, indicating FGF10-FGF9-dependent regulation of mesenchymal proliferation (Colvin et al., 2001). Also, the

reciprocal interplay between mesenchymal *Fgf10* and epithelial *Shh* is linked to the control of mesenchymal cell proliferation as well as to alveolar differentiation in embryonic lungs. Overexpression of *Shh* in the developing lung epithelium leads to hyperproliferation of mesenchyme and absence of normal alveoli, and, interestingly, to decreased expression of mesenchymal *Fgf10* (Bellusci et al., 1997a; Bellusci et al., 1997b; Pepicelli et al., 1998). Similarly, epithelial overexpression of *Bmp4*, which is normally expressed in the branching epithelial tip of the developing lung, causes reduced epithelial cell proliferation, a small increase in mesenchymal cell proliferation but simultaneous increased cell death leading to dilated terminal buds incompatible with normal lung function (Bellusci et al., 1996). Addition of BMP4 to an embryonic lung epithelial culture system inhibits FGF10-induced epithelial budding and cell proliferation (Weaver et al., 2000), suggesting that BMP4, and possibly also SHH, function as a negative feedback loop for an FGF10-induced epithelial branching process. *Fgf10* is also linked to retinoic acid (RA)-dependent lung branching initiation. In a foregut explant culture system, pan-retinoic acid receptor (RAR) antagonist (BMS493) treatment, results in failure of the induction of *Fgf10* expression and epithelial bud formation (Desai et al., 2004). This result was later confirmed *in vivo* using a retinaldehyde dehydrogenase 2 (*Raldh2*)-null mouse model that furthermore linked the RA-FGF10 axis to regulation of TGFB signalling (Chen et al., 2007). Thus, multiple signalling molecules in the developing lung mesenchyme, epithelium, and mesothelium contribute to the lung branching morphogenesis often via regulation of mesenchymal *Fgf10*.

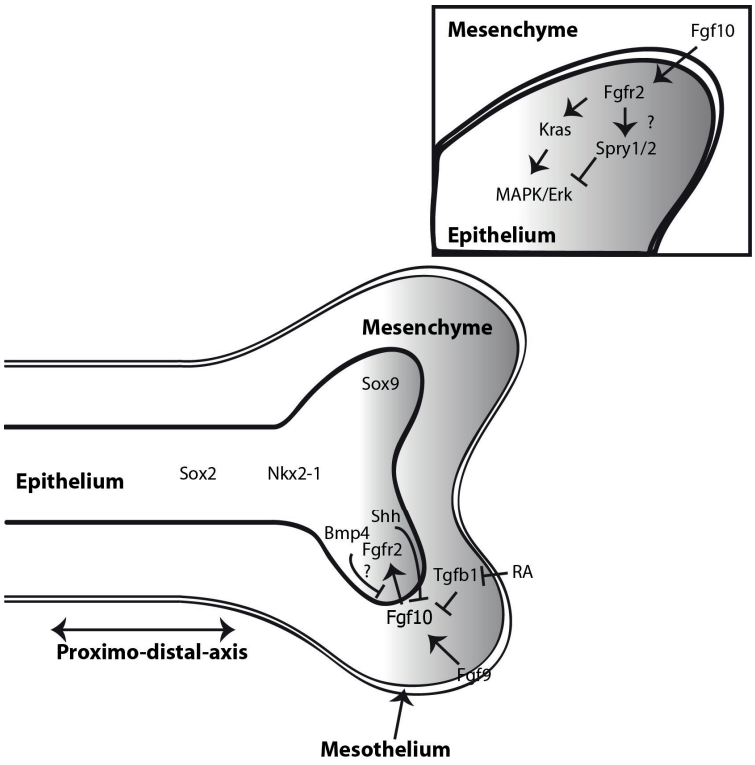

Figure 3. Multiple signalling pathways control lung branching morphogenesis. The diagram represents expression and known interplay between selected signalling molecules in the branching epithelium and surrounding mesenchyme during lung development. These include members of Fgf, Tgfb, Shh, Bmp, and Wnt families as well as RA and transcription factors *Sox2*, *Sox9*, and *Nkx2-1*. Also the signalling interplay between Fgf and Ras is shown.

Epidermal growth factor receptor (*Egfr*) and *Kras*, genes which both harbour key human lung cancer driver mutations (see section 2.2.3), have been functionally implicated in murine lung morphogenesis (Figure 3). *Egfr*-null embryos show impaired lung branching morphogenesis and deficient alveolisation and septation, resulting in significant reduction of alveolar volume and leading to reduced epithelial surface for gas exchange (Miettinen et al., 1997). Expression of constitutively active oncogenic *Kras* results in reduced cell differentiation in developing lung epithelia. Furthermore, developing lung expressed oncogenic *Kras* leads to abnormal localization of mitogen-activated protein kinase (MAPK) cascade activity and reduced expression levels of ciliated and Clara cell markers resulting in defects in lung branching morphogenesis (Shaw *et al.*, 2007). In contrast, silencing of *Spry2*, an antagonist of MAPK, rescues oncogenic *Kras*-induced lung morphogenesis defects (Shaw et al., 2007). Interestingly, the combined loss of *Spry1* and *Spry2* results in defects in lung morphogenesis,

resembling the effect of oncogenic *Kras*. Furthermore, the defects in lung morphogenesis caused by the loss of *Spry1* and *Spry2* are rescued both with MAPK signalling cascade effector MEK1/2 inhibitor treatment and partial loss of *Fgf10* expression (Tang et al., 2011). Taken together, these results indicate a dynamic control as well as a need for accurately localised, timed or dosed EGFR, RAS-MAPK and FGF signalling to achieve homeostasis in the growing epithelial lung.

2.1.2.2 Development of the pulmonary mesenchyme and vasculature

As described above, lung morphogenesis is dependent on paracrine signalling between the branching endoderm and the surrounding mesoderm. Contrary to the extensive knowledge of the origins of epithelial cell lineages, little is known about the pulmonary mesodermal cells and their origins. Only recently have lineage-tracing assays begun to explore these cells and shed light on their mesenchyml origin. . Multipotent cardiopulmonary mesoderm progenitors (CPPs) that express *Wnt2*, *Gli1* and *Isl1*, function as progenitors of both cardiac and lung mesodermal cells (Peng et al., 2013). CPPs, which are located in the posterior pole of the heart, can generate pulmonary vascular and airway smooth muscle, as well as pericyte-like cells. Furthermore, the *Fgf10* expressing embryonic lung mesenchymal cells are reported to function as progenitors of several cell types in the embryonic and postnatal lung mesenchyme including vascular smooth muscle cells and lipofibroblasts (El Agha *et al.*, 2014).

The generation of a capillary network surrounding the distal epithelial structures of the lung is crucial for the exchange of gases, i.e. to provide oxygen to the tissues and for the removal of carbon dioxide. During the development of the pulmonary vascular network, precursor cells of the network undergo cellular maturation and patterning to form a vascular entity connecting airways and linking to the arterial and venous poles of the heart. Pulmonary endothelial cells are formed by two co-existing processes, namely vasculogenic and angiogenic process (Peng and Morrisey, 2013). Vasculogenesis is a *de novo* process of blood capillary formation, whereas angiogenesis is a process of formation of blood capillaries from the existing ones (deMello et al., 1997). The *Wnt2*, *Gli1* and *Isl1*-expressing multipotent CPPs function as vasculogenic progenitors of the proximal veins in the developing murine lung (Peng et al., 2013). The vascular endothelial (VE) cadherin-expressing endothelial progenitors, which exist already at E8.5, act as the angiogenic source of the distal alveolar capillaries (Peng et al., 2013). Vascular endothelial growth factor-A (encoded by *Vegfa*) is an important signalling molecule both in vasculogenesis and angiogenesis. Overexpression of *Vegfa* in the distal lung epithelium of the mouse lung leads to increased vascular density visualised at E17 with the expression of platelet endothelial cell adhesion molecule (PECAM1, also known as CD31). VEGFA and its receptor kinase insert domain receptor (encoded by *Kdr* also known as VEGFR2)-mediated epithelial-to-endothelial crosstalk in branching morphogenesis has been evidenced using an embryonic lung *ex vivo* culture system (Del Moral et al., 2006b).

Taken together, pulmonary mesenchyme acts as an important signalling centre during lung morphogenesis and functions as an essential source of non-epithelial pulmonary cells. However, more work is needed characterize the various mesodermal cell linages and their contribution to tissue homeostasis.

2.2 Lung cancer

Lung cancer is the leading cause of cancer deaths worldwide with 1,82 million new cases diagnosed and 1,6 million deaths annually (Figure 4) (Ferlay et al., 2015). Due to the asymptomatic disease progression and lack of systematic screening programs, lung cancer is typically diagnosed at a late and advanced stage of disease (Gridelli et al., 2015). The late diagnosis as well as the high level of heterogeneity within and between lung tumours caused by exposure to damaging agents, such as tobacco smoke, pollution, and micro-organisms, make the treatment of lung cancer challenging. Intratumour heterogeneity (ITH) rises during tumour progression via an evolutionary process where cancer cells with different fitness levels are subjected to selection, resulting in clonal evolution (Gerlinger et al., 2014). Clonal populations are thought to cooperate with one another, influencing cancer progression (Tabassum and Polyak, 2015). Recent advances in the generation of targeted therapies, which are designed to hit specific genetic drivers, have taken lung cancer diagnostics closer to a personalized level of treatment (Gridelli et al., 2015). Nevertheless, the inherent propensity of cancers toward clonal evolution may be one of the mechanisms cancers use to acquire drug resistance. Such resistance to treatment leads to disease relapse as has been observed in lung adenocarcinomas (ACs) (Zhang et al., 2014).

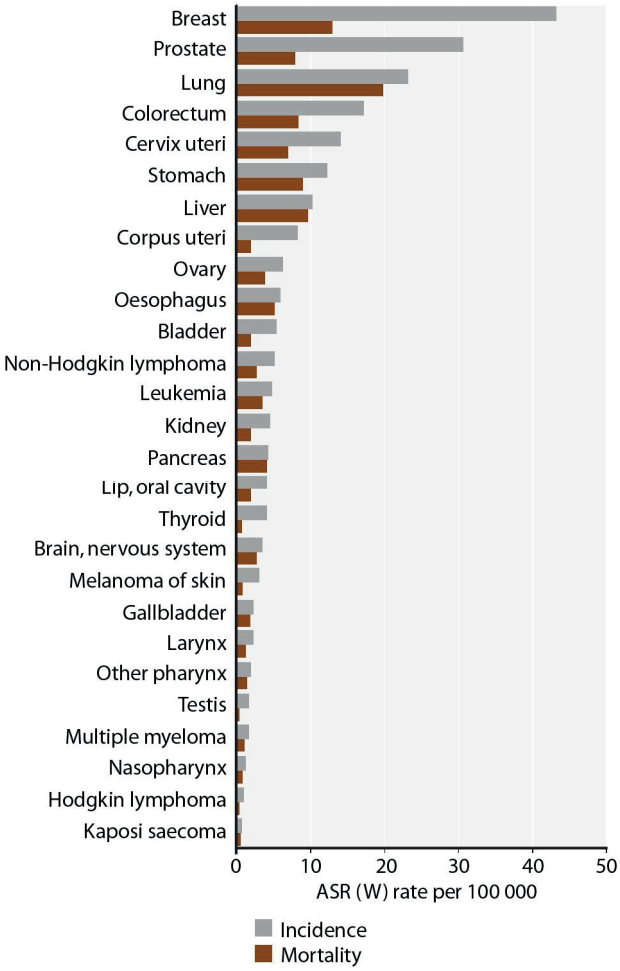

Figure 4. Worldwide incidences and mortalities of 27 major cancers in both sexes combined. An age-standardised rate (ASR) is a weighted mean of the age-specific rates per 100 000 per year. Data from GLOBOCAN 2012 (Ferlay *et al.*, 2015) (http://globocan.iarc.fr/Default.aspx).

Heterogeneity does not apply only to cancer cells. It is also seen within the tumour microenvironment, which is composed of extracellular matrix (ECM), vasculature, fibroblasts, and infiltrating immune cells. The reciprocal interaction between the tumour and its surrounding stroma modulates tumour progression (Hanahan and Coussens, 2012). Recently, specific interest has been given to the immune microenvironment as a possible target in cancer treatment. Clinical trials have shown promising results with drugs targeting the mechanisms by which cancer cells evade immune responses. One example is programmed death 1 (PD-1) antibody treatment. PD-1 and its ligands, PD-L1 and PD-L2, mediate inhibitory signals which protect normal peripheral tissues from the adaptive immune system, including the regulation of T-cell activation (Keir et al., 2008).

By expressing PD-1 or PD-L1, cancer cells escape immune attack. Blocking the PD-1-PD-L1 interaction with PD-1 antibody results in measurable responses in 20-25% of patients with advanced NSCLC (Topalian et al., 2012). Thus, use of the patient's own immune system to attack cancer cells is one possible way to circumvent the inherent heterogeneity of tumours.

2.2.1 Epidemiology

Lung cancer is the most common cancer in the world, both in terms of new cases as well as deaths (Figures 4 & 5) (Ferlay et al., 2015). Women in less developed countries are exception to the worldwide statistics and among whom lung cancer is the third most lethal cancer after breast, cervix, and uterine cancers (Ferlay et al., 2015). The low numbers of lung cancer deaths in Africa is probably a consequence of under-reporting, rather than an actual low incidence of deaths (Figure 5) (Ferlay et al., 2015). Interestingly, during the last 30 years there has been a shift in the incidence of specific lung tumour histopathologies, with an increase in adenocarcinoma diagnoses compared with squamous cell carcinoma. This difference is most likely due to the change in smoking behaviours and cigarette manufacture, as filter and light cigarettes have enabled a deeper aspiration resulting in an exposure of deeper parts of the bronchi and alveoli to the carcinogens in cigarette smoke (Gridelli et al., 2015).

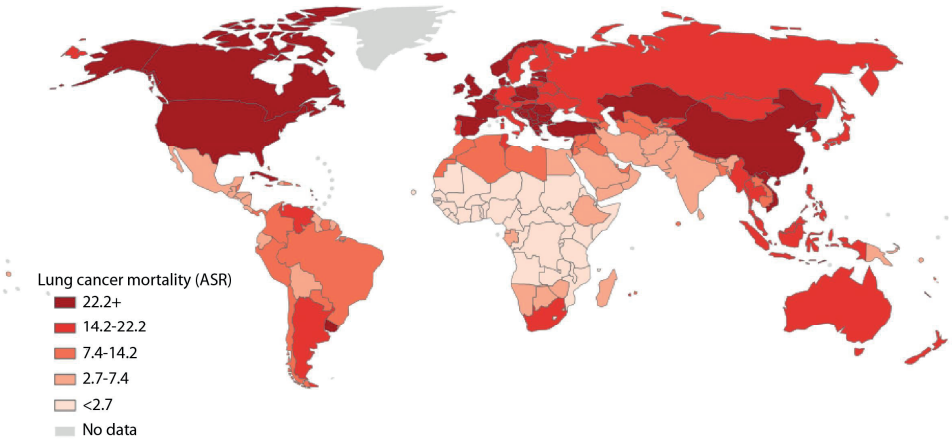

Figure 5. Mortality rates due to lung cancer in both sexes combined. An age-standardised rate (ASR) is a weighted mean of the age-specific rates per 100 000 per year. Data from GLOBOCAN 2012 (Ferlay *et al.*, 2015) (http://globocan.iarc.fr/Default.aspx).

2.2.2 Diagnosis

Lung cancer is diagnosed based on clinical symptoms, such as cough, chest pain, and dyspnoea and chest radiography and/or a contrast-enhanced computed tomography (CT) scan, after which pathological diagnosis and identification of genetic alterations are performed to guide treatment (Gridelli *et al.*, 2015). Cancer stage is determined by assessment of anatomical extent in three tumour components: the primary tumour (T), the lymph nodes (N), and the metastases (M). This system is called the Tumour-Node-Metastasis (TNM) classification (Travis et al., 2015). Pathological diagnosis of lung tumours is performed using resection samples or small biopsies, both of which have their own guidelines for classification (Travis et al., 2013).

The two main histopathological classes of lung cancer are non-small-cell lung cancer (NSCLC), which represents approximately 85% of diagnosed lung cancer cases, and small-cell lung cancer (SCLC), which constitute the remaining 15%. NSCLC is further separated into three main histopathologies, namely adenocarcinoma (AC; ~60% of NSCLC), squamous cell carcinoma (SCC; ~30% of NSCLC) and large cell carcinoma (LCC; ~10% of NSCLC) (Gridelli et al., 2015). Additional histopathology classes include adenosquamous carcinoma (ASC; 0,4-4%) and pleiomorphic carcinoma (~2-

3%), which are both rare but aggressive cancers with poor prognosis (Travis et al., 2015).

The adenocarcinoma pathological classification system was updated in 2011 by a multidisciplinary effort that emphasized correlations between pathological, clinical, radiologic, and molecular characteristics of AC tumours (the IASLC/ATS/ERS classification) (Travis et al., 2011). Pre-invasive adenocarcinoma *in situ* (AIS) shows a hyperproliferative growth pattern, but does not invade the normal alveolar structures. Invasive ACs, in which invasion of normal tissue structures is seen, are characterised by glandular differentiation, mucin production, and/or pneumocyte marker expression. Distinct growth patterns, namely lepidic, acinar, papillary, micropapillary, and solid can be identified. Classifications are determined according to the predominant subtype after comprehensive histological subtyping by semiquantitative estimation.

Immunohistochemical (IHC) workups, which guide the pathological diagnoses are used in everyday clinics to confirm the pathological classifications. The same IHC-based classification is used in the profiling of lung cancer mouse models (Figure 7 and section 2.3.1.3). Currently used AC markers are NKX2-1 and napsin-A. Both appear to give comparable sensitivities, although napsin-A has been suggested to better differentiate SCC from AC (Travis et al., 2015). Mucinous AC phenotype is confirmed with polysaccharide detecting periodic acid Schiff's (PAS) staining.

SCCs are characterised by p63 expression, specifically the DNp63 isoform, which contains an alternative transcriptionally inactive 'DN' domain, being preferred over p63, in up to 30% of ACs express p63 (Bishop et al., 2012). Cytokeratin-5, (CK5, official gene name type II cytoskeletal keratin 5, *KRT5*) alone, or in combination with cytokeratin-6 (CK6, official gene name type II keratin 6A/B, *KRT6A/B*) is used to confirm the squamous phenotype and classification (Travis et al., 2015).

SCLCs are distinguished from NSCLCs by their typical small cell morphology characterised by a smaller cytoplasm and poorly defined cell borders, as well as dispersed granular nuclear chromatin and absent or indistinguishable nucleoli (Travis et al., 2015). IHC markers such as a cytokeratin cocktail detecting multiple keratins (AE1/AE3 cocktail) and neural cell adhesion molecule 1 (NCAM1, also known as CD56) are used to confirm the epithelial and neuroendocrine nature of the SCLC tumours. Large cell carcinoma (LCC) is an undifferentiated NSCLC that lacks the typical characters of SCLC, AC and SCC. Only tumours that are either negative or show unclear patterns of common IHC markers are considered to be LCC (Travis et al., 2015). ASC is characterised by both AC and SCC components, each constituting at least 10% of the tumour. Typical AC and SCC markers, NKX2-1 and napsin-A and p63 and CK5/6 respectively, are used to classify ASCs. Pleiomorphic carcinomas are NSCLCs that contain at least 10% of spindle and/or giant cells that are diagnosed based on morphology (Travis et al., 2015).

For all lung cancer cases the prognosis is determined by the TNM classification and the patient's performance status. Furthermore, histological analysis and molecular profiling are used to predict treatment outcomes in a personalized manner (Travis et al., 2015) (for genetic profiling and targeted treatments see section 2.2.3). SCLCs have

generally poor prognosis with only 12,7 months of median overall survival time (Planchard and Le Pechoux, 2011), whereas NSCLCs have a variety of prognoses depending on the patient's performance score and the clinical and tumour stage. Pleiomorphic carcinomas have poor prognosis even in an early stage of the disease. Similarly, ASCs are reported to have a poorer prognosis when compared to other NSCLCs (Nakagawa *et al.*, 2003).

The cellular origin of human lung tumours is determined by the location and expression profiles of the specific tumour histopathology types. SCLCs with clear expression profiles of NE cells are considered to be developed from NE cells. ACs with alveolar cell (pneumocyte) expression are considered to have risen from the peripheral parts of the lungs whereas SCCs with basal cell marker expression are thought to have developed from airway basal cells (Chen *et al.*, 2014; Travis *et al.*, 2015). Studies on *in vivo* murine lung cancer models support these conclusions (Sutherland *et al.*, 2011; Sutherland *et al.*, 2014) and are discussed in more detail in section 2.3.1.3.

2.2.3 Genetic alterations and targeted treatments

At the genetic level every lung tumour is different. Nevertheless, as a result of recent major lung cancer sequencing efforts of the most common types of lung cancer, namely AC, SCC and SCLC, (Cancer Genome Atlas Research, 2012, 2014; George *et al.*, 2015; Peifer *et al.*, 2012) clear genetic commonalities within the lung tumour histopathology groups have been identified (Gridelli et al., 2015) (Table 1). Mutations in *TP53* are common in all lung cancer histopathology types, however the incidence is higher in SCLCs and SCCs than in ACs. (Gridelli *et al.*, 2015). To date, only the genetic profiling results from lung ACs, the most common and extensively studied lung cancer, are applied in clinics. Mutations in epidermal growth factor receptor (*EGFR*) or translocations of the anaplastic lymphoma kinase (*ALK*) gene can be treated with specific inhibitors (Gridelli et al., 2015) (Table 1). The following sections describe common lung cancer genetic alterations, approved targeted therapies, as well as selected therapies under development in lung ACs, SCCs, SCLCs and ASCs.

Table 1. Selected genetic alterations and available targeted treatments for common types of lung cancer. Adapted from Chen et al. 2014. Additional and updated information taken from Cancer Genome Atlas Research, 2012, 2014; George et al., 2015, Tochigi et al., 2011, and Vassella et al., 2015.

Gene	Status*	Freq. AC (%)	Freq. SCC (%)	Freq. SCLC (%)	Freq. ASC (%)	Approved first line targeted therapies
EGFR	M, C	17-18	9	3,6	13-31	Erlotinib, gefitinib
ALK	F	3-5	<1	N/A	0	Crizotinib
ROS1	F	1-2	N/A	N/A	0	Crizotinib
TP53	M	52	91	92	38	N/A
KRAS	M, C	30-37	4	N/A	13 (M)	N/A
STK11	M	15-21	2	1	6-22	N/A
PIK3CA	M, C	0,5-9	48	3	19 (M)	N/A
CDKN2A	M, C	14-24	44	2 (M)	13 (M)	N/A
FGFR1	M, C	6	18	1 (M)	0	N/A
PTEN	M, C	2-3	11	6	6	N/A
ERBB2	M, C	2-5	5	1	0	N/A
RB1	M, C	4-7	7	75	13 (M)	N/A
EPHA3	M, C	6-17	12	3	N/A	N/A

*Status: mutation (M), copy number alteration (C) or fusion (F); N/A, not available

2.2.3.1 Genetic alterations and targeted treatments in AC

Common lung cancer mutations in *EGFR*, which are mainly found in lung ACs (10,4-18,4%) (Cancer Genome Atlas Research, 2014; Cerami et al., 2012; Ding et al., 2008; Imielinski et al., 2012), include small in-frame deletions and missense substitutions in exons 18, 19, and 21. The mutations cluster around the active site of the receptor kinase domain (Lynch et al., 2004; Paez et al., 2004) causing activation of signalling pathways, including serine-threonine protein kinase AKT and signal transduction and activator of transcription (STAT) (Sordella et al., 2004). Due to the clear association between the sensitivity to the EGFR tyrosine kinase inhibitor (TKI), gefitinib (Iressa) and *EGFR* mutation status in AC cases (Lynch et al., 2004; Paez et al., 2004; Pao et al., 2004), gefitinib is now approved as a targeted first-line monotherapy for the treatment of patients with advanced or metastatic EGFR mutation-positive NSCLC. Another inhibitor, erlotinib, also targeting *EGFR* mutant NSCLC (Pao et al., 2004), is also approved as a first-line treatment for *EGFR* mutation-positive NSCLC following a phase-III clinical trial in European lung cancer patients (Rosell et al., 2012).

Small inversions in chromosome 2p resulting in the formation of a fusion gene of the echinoderm microtubule-associated protein-like 4 (*EML4*) and *ALK* genes were first identified in NSCLC patient tumours, at an incidence of approximately 7% (Soda et al., 2007). Since the identification of the *EML4-ALK* fusion gene, multiple variants have been found, and their incidence appears to be mainly restricted to ACs (Sasaki et al., 2010). The small-molecule inhibitor PF-2341066, which was developed to inhibit ALK and hepatocyte growth factor receptor encoded by MET proto-oncogene (*MET*) (Zou et al., 2007), has been further developed as the targeted therapy crizotinib (Cui et al., 2011). Crizotinib is currently approved for treatment of *EML4-ALK* positive NSCLC based on clinical trial studies (Kwak et al., 2010). Recently, crizotinib was shown to also target rearrangements of the receptor tyrosine kinase ROS proto-oncogene 1 (*ROS1*). The kinase domain of ROS1 shows 77% amino acid identity with ALK, and crizotinib is now assigned as a potential treatment of patients with rearrangements (Shaw et al., 2014b).

Interestingly, NSCLC patients with exon 20 insertions in *EGFR* do not respond to EGFR inhibition, indicating heterogeneity in the cellular sensitivity to the targeted therapies caused by the specific mutation types (Oxnard et al., 2013). Moreover, *EGFR* mutation positive tumours, responsive to targeted therapies, acquire resistance by mechanisms including secondary mutations in *EGFR,* such as the gatekeeper mutation T790M, responsible for about half of the acquired resistance cases (Arcila et al., 2011; Choi et al., 2010; Kobayashi et al., 2005). Furthermore, activation of other kinases such as MET, insulin-like growth factor 1 receptor (IGF1R), serine/threonine-protein kinase B-raf (BRAF) or downstream pathway signalling molecules such as mitogen-activated protein kinases (ERK1/2) have been shown to mediate resistance to EGFR inhibition (Cortot et al., 2013; Engelman et al., 2007; Ercan et al., 2012; Ohashi et al., 2012). Novel irreversible EGFR inhibitors including AZD9291 developed by AstraZeneca and WZ4002 developed by Jänne and colleagues can target the gatekeeper mutation

(T790M)- harbouring lung tumours (Cross et al., 2014; Finlay et al., 2014; Zhou et al., 2009). 50% of patients with tumours harboring EGFR T790M mutation were shown to respond to AZD9291 treatment in a phase-I clinical trial (Jänne et al., 2014). Moreover, targeting the downstream signalling pathways reactivated due to the targeted treatment appears effective, as combined inhibition of ERK1/2 by the MEK inhibitor trametinib and EGFR TKI WZ4002 can prevent both T790M- and non–T790M-mediated drug resistance (Tricker et al., 2015). Similarly, NSCLC patients with disease progression after initial treatment with crizotinib have shown good response to a more specific ALK inhibitor LDK378 (ceritinib), which is now approved as a treatment for NSCLC (Friboulet et al., 2014; Shaw et al., 2014a).

One potentially targetable lung cancer gene is *KRAS*, in which the first lung cancer mutations were identified in 1984 (Santos et al., 1984). With a mutation incidence up to 37% in lung ACs, *KRAS* is one of the most mutated genes in lung cancers (Pao and Hutchinson, 2012). However, no direct inhibitors of RAS oncoproteins have yet been applied in the clinic (Cox et al., 2014). Nevertheless, recent progress in mutant-specific inhibitor development has shown promising results, for example with a covalently-binding inhibitor developed against the KRAS G12C mutation (Ostrem et al., 2013). In addition to direct RAS inhibitors, other approaches such as blocking the membrane association, targeting of downstream effector signalling, finding synthetic lethal interactors with mutant RAS, and targeting of RAS-mediated changes in cell metabolism are all being investigated (Cox et al., 2014).

2.2.3.2 Genetic alterations in SCC and SCLC

Genetic profiling has also identified potent targets in SCC and SCLC, the second most common types of lung cancers. Members of the erythroblastic leukaemia viral oncogene homologues (ERBBs), fibroblast growth factor receptors (FGFRs) and Janus kinases (JAKs) were found to be genetically altered in 64% of 178 lung SCCs studied in the The Cancer Genome Atlas research network sequencing effort (Cancer Genome Atlas Research, 2012). Furthermore, therapeutically targetable cellular pathways, including members of phosphatidylinositol-3-OH kinase (PI3K)/AKT, receptor tyrosine kinase (RTK) and RAS pathways were found to be altered in 69% of the 178 cases (Cancer Genome Atlas Research, 2012). Targeted therapies against these alterations are under development.

Loss of *TP53* encoding p53 transcription factor and *RB1* encoding retinoblastoma-associated protein, a negative regulator of cell cycle, are frequent events in SCLCs. Recent comprehensive genetic profiling of SCLC manifested the loss of *TP53* and *RB1* as an obligatory event in SCLC (George *et al.*, 2015). Thus far, therapies restoring these master regulators have not been translated to clinics even though preclinical evidence suggests stage-specific effects. Restoration of *Trp53* (mouse ortholog for *TP53*) expression in latent mutant *Kras* driven adenocarcinoma mouse model showed clear

reduction in tumour progression accompanied with signs of cellular senescence (Feldser et al., 2010).

2.2.3.3 Genetic alterations and targeted treatments in ASC

Microdissection-based molecular profiling of lung ASCs analysing the AC and SCC components separately has identified *EGFR* mutations in ASCs with frequencies ranging from 13% to 31% (Tochigi et al., 2011; Vassella et al., 2015). The detected *EGFR* mutations are trunk mutations, as they are found in both the AC and SCC components. This finding corroborates clinical evidence that EGFR TKIs gefitinib and erlotinib are as effective in ASCs as in lung ACs (Song et al., 2013). Mutations in *KRAS* are found less frequently in ASCs than in ACs (up to 13%), and these appear to be trunk mutations (Tochigi et al., 2011). In support of ASC clonal tumour evolution, branch mutations have been detected in these tumours, separating the AC and SCC components. A targeted next-generation sequencing analysis of frequently mutated human cancer genes in 16 microdissected ASCs identified branch mutations in *TP53, CDKN2A*, *PIK3CA*, *RB1*, and *PTEN*. Of the mutations affecting the PI3K pathway, only one *PIK3CA* trunk mutations was identified. Two other *PIK3CA* mutations and one mutation in *PTEN*, a regulator of PI3K pathway, were branch mutations in the SCC component (Vassella et al., 2015). Interestingly, even though *PIK3CA* mutations in lung SCCs are as common as in ACs (10,1% and 6,1% respectively) the *PIK3CA* gene amplifications are much more frequent in SCCs than in ACs (44,9% and 1,7% respectively) (Cancer Genome Atlas Research, 2012, 2014; Cerami et al., 2012), indicating a possible role for PI3K pathway activation in the SCC component of ASCs. Mutations in *LKB1* (*STK11*), *APC*, *JAK3*, *TP53*, *RB1* and *KIT* were found in both the AC and SCC components, suggesting their founder role (Vassella et al., 2015).

Genetic landscapes of lung tumours can predict response to targeted therapies. Nevertheless, genetic ITH created by tumour evolution leading to clones with common early (trunk) and distinct late (branch) mutations has been suggested to affect treatment outcomes. De Bruin and colleagues sequenced altogether 25 spatially different regions from seven NSCLC tumours including four AC, one SCC, one ASC, and one undifferentiated NSCLC tumour and found evidence of branched evolution within the tumours (de Bruin et al., 2014). Similarly, whole-exome sequencing of 11 localized lung ACs identified clear ITH and possible association with increased likelihood of postsurgical relapse (Zhang et al., 2014).

A deeper understanding of the genetic factors and their role in specific lung cancer histopathologies and interaction with the tumour microenvironment are important for the design of individualized treatment options. Furthermore, understanding of the normal physiological functions of these factors is prerequisite for discerning their roles in cancer. The following sections describe four such factors, and their functions, relevant to this thesis work.

2.2.3.4 *KRAS*

KRAS belongs to the large Ras superfamily of small guanosine triphosphatases (GTPases) which, with its 150 members, regulate processes including cell cycle progression, cell survival, actin cytoskeletal organisation, cell polarity and movement, and vesicular and nuclear transport (Wennerberg et al., 2005). RAS oncogenes were first identified in retroviruses of leukemic rats, which were able to induce tumours in newborn rodents (Harvey, 1964; Kirsten and Mayer, 1967). Later, three separate studies discovered that the genes in Kirsten and Harvey sarcoma viruses had human homologues found in cancer cell lines, and capable of transforming mouse embryonic fibroblast NIH/3T3 cells (Der et al., 1982; Parada et al., 1982; Santos et al., 1982).

The name RAS comes from the ability of the first two identified members of the super family, *HRAS* and *KRAS*, to cause rat sarcomas. These two members are distinguished by the names of their discoverers Harvey and Kirsten (Cox and Der, 2010). The third member of the Ras family was identified in neuroblastoma-derived DNA, and therefore named *NRAS* (Hall et al., 1983). The molecular basis underlying RAS oncogenic functions were shown to be single point mutations detected in both the cancer cell lines and the viruses (Capon et al., 1983; Reddy et al., 1982; Tabin et al., 1982; Taparowsky et al., 1982). The three founding members of the Ras superfamily, namely *HRAS*, *KRAS*, and *NRAS* together comprise one of the most frequently mutated oncogene families in human cancers, and interestingly show tissue specificity in the distribution of distinct RAS gene mutations (Cox et al., 2014).

Interestingly, only *KRAS* has been shown to be essential for embryonic development. *Kras*-null mouse embryos die before birth due to defects in developing heart myocardial cell proliferation and increased neuronal programmed cell death, whereas *Hras* and *Nras* embryos develop normally (Koera et al., 1997).

2.2.3.4.1 RAS signalling

The members of the Ras superfamily of GTPases are divided into five major families on the basis of their sequence and functional similarities. These families are Ras, Rho, Rab, Ran, and Arf (Colicelli, 2004; Wennerberg et al., 2005).

The activity of GTPases depends on their GTP-bound state, which is modulated by two classes of regulatory proteins, guanine nucleotide exchange factors (GEFs) that stimulate the exchange of GDP to GTP and GTPase-activating proteins (GAPs) that terminate the active state by stimulating GTP hydrolysis (Bos et al., 2007; Wennerberg et al., 2005). Once activated, Ras family proteins interact with multiple distinct downstream signalling effectors. The best characterised Ras signalling cascade is the pathway initiated by EGFR activation that leads to Ras activation and subsequent activation of mitogen-activated protein kinase (MAPK) signalling: RAF, MEK1/2 and ERK1/2, finally leading to phosphorylation of Ets transcription factors (Wennerberg et al., 2005). Ets transcription factors regulate expression of genes involved in cell differentiation, proliferation, apoptosis, and tissue remodelling (Kar and Gutierrez-Hartmann, 2013). The link between EGFR and RAS was first noted following EGFR-

induced increases in Ras-GTP binding (Kamata and Feramisco, 1984). Almost a decade later, the connection to the MAPK-pathway was discovered in a study using immunoprecipitates of MAP kinase from the rat brain in a kinase assay which used immobilized Ras bound to the non-hydrolyzable GTP analog GMP-PNP (Moodie et al., 1993).

During the last 20 years, multiple other downstream effectors of RAS have been identified, including the class I phosphoinositide 3‑kinases (PI3Ks) (Rodriguez-Viciana et al., 1994) and the Ral guanine nucleotide-dissociation stimulator (RalGDS) and RalGDS-like protein (RGL) GEFs for the Ras-like small GTPases RalA and RalB (Karnoub and Weinberg, 2008; Spaargaren and Bischoff, 1994). Consistent with the functions of RAS, RalA and RalB GTPases regulate cellular proliferation as well as apoptosis (Chien and White, 2003). Early studies showed PI3K-dependent activation of AKT and protection from programmed cell death (Khwaja et al., 1997). Later, the more precise molecular mechanism of AKT activation was shown to require both translocation to the plasma membrane and phosphorylation at sites Thr308 and Ser473 (Vivanco and Sawyers, 2002). PI3K-AKT activation regulates multiple hallmarks of tumourigenesis, including cell proliferation by preventing cyclin D1 degradation (Diehl et al., 1998) and cell growth by targeting the mammalian target of rapamycin (mTOR) (Nave et al., 1999), and protection from apoptosis (Khwaja et al., 1997). Taken together, RAS acts as a signalling centre by switching its form between the GDP- and GTP-bound stages in response to cellular stimuli and thus mediates several signals, which regulate multiple cellular processes including growth and movement.

2.2.3.4.2 *KRAS* and lung cancer

The human *KRAS* gene at chromosome location 12p12.1 is mutated in up to 37% of lung ACs. In contract, *KRAS* mutations in SCCs and SCLCs are rare (0,6-1,1%, 3,6% respectively; Table 1 and Figure 6) (Cancer Genome Atlas Research, 2012, 2014; Cerami et al., 2012; Ding et al., 2008; Imielinski et al., 2012; Peifer et al., 2012; Rudin et al., 2012). Interestingly, lung cancer mutations are mainly found in *KRAS*, but not *HRAS* or *NRAS* isoforms (incidence <1%) (Cox et al., 2014).

The majority of mutations in *KRAS* observed in lung cancer result in a single amino acid missense mutation at residue glycine (G) 12, G13, or glutamine (Q) 61, of which G12 is the most frequent mutation. The amino G12 residue is observed most frequently changed to cysteine (G12C), but also valine (G12V) or aspartic acid (G12D) (Cox et al., 2014). Point mutation in RAS proteins impair intrinsic GTP hydrolysis and render them GAP insensitive, and thus continuously GTP-bound and active. Thus, this results an uncoupling of downstream signalling from activation by upstream regulators (Baines et al., 2011; Karnoub and Weinberg, 2008).

Downstream RAS effectors are also mutated in lung cancers, supporting RAS-dependent signalling in tumour growth. *PIK3CA*, which encodes one of the PI3Ks, is mutated in all three main lung cancer subclasses AC (0,6-6,1%), SCC (6,1%) and SCLC (4,8%). Interestingly, gene amplifications of *PIK3CA* are detected more often in SCCs (32,6-44,9%) than for example in ACs (1,1-2,2%), suggesting histopathology-specific

functions. Similar mutation patterns are seen in the phosphatase and tensin homologue (*PTEN*) tumour suppressor gene, a negative regulator of AKT kinase, for which mutations are more frequently detected in lung SCCs (7,9%) and SCLCs (4,8-13,8%) compared to lung ACs (1,3-2,2%) (Cancer Genome Atlas Research, 2012, 2014; Ding et al., 2008; Imielinski et al., 2012; Peifer et al., 2012; Rudin et al., 2012).

Activation of the most common lung cancer mutations in KRAS, G12C, G12V and G12D, have all been shown to initiate lung tumourigenesis in mice, leading to development of ACs (Fisher et al., 2001; Floyd et al., 2005; Jackson et al., 2001; Mainardi et al., 2014; Meuwissen et al., 2001). Of these, the most studied is the G12D mutation.

2.2.3.5 *TP53*

The transcription factor (TF) p53, encoded by the *TP53* gene (*Trp53* gene in mouse), belongs to a gene family that also includes *TP63* and *TP73*, encoding the p63 and p73 transcription factors (Nedelcu and Tan, 2007). The p63 and p73 TFs share similar but not identical structures with p53, and interestingly, whereas mice deficient for *Trp53* are developmentally normal, loss of *Trp63* and *Trp73* (mouse orthologs of *TP63* and *TP73*) results in embryonic lethality (Donehower et al., 1992; Mills et al., 1999; Yang et al., 2000). *Trp53*-null mice develop spontaneous tumours, primarily lymphomas (Donehower et al., 1992), highlighting the role of p53 in tumourigenesis. P53 was initially identified in simian virus (SV40)-induced tumours in hamsters as a cellular protein binding to SV40 large T antigen. It was found to accumulate in the nuclei of cancer cells (Linzer and Levine, 1979), and thus initially thought to function as an oncogene. However, the later finding that only the mutated, not the wild-type form of p53, cooperates with RAS in cellular transformation established a tumour suppressive role for the protein (Finlay et al., 1989; Hinds et al., 1989). Furthermore, it was found that p53 forms tetramers, which recognise specific responsive elements in the DNA, and that mutant forms of p53 are able to act in a dominant negative fashion to inhibit the function of the wild-type protein (Friedman *et al.*, 1993; Lane, 1992; Riley *et al.*, 2008; Wagner *et al.*, 1991).

2.2.3.5.1 Cellular functions of p53

P53 is a cellular stress sensor that is activated by multiple types of cellular stress, including DNA damage, hypoxia, oncogene expression, nutrient deprivation, and ribosome dysfunction (Bieging et al., 2014; Hu et al., 2012). Functionally, p53 has been linked to cell cycle arrest, senescence, apoptosis, DNA repair, autophagy, metabolic reprogramming, cellular stem-ness as well as to tumour invasion and metastasis (Bieging et al., 2014). The mechanisms of action of p53 include transcriptional activation, transcriptional repression, regulation of translation, and homologous recombination

(Bertrand et al., 2004; Ewen and Miller, 1996; Harris, 1996; Ho and Benchimol, 2003; Lane, 1992).

The classical cellular functions regulated by p53, cell cycle arrest, senescence, and apoptosis are mediated through p53-dependent transcriptional activation of specific genes. The transcriptional coactivator function of p53 is indeed the best-characterised function of p53 (Beckerman and Prives, 2010; Bieging et al., 2014). In adult cells not facing stress, p53 is kept inactive through MDM2, an E3 ubiquitin ligase that binds to p53 and targets it for proteosomal degradation. When cells face stress, the inhibition is released, and p53 target gene expression is activated. The p53 pathway is regulated by the activities of other signal transduction pathways, which define the outcome of p53 activation. For example, introduction of oncogenic RAS in normal cells leads to p53-mediated senescence (Yang et al., 2006). This observation has been further validated *in vivo* in an oncogenic BRAF-driven lung cancer mouse model, where deletion of p53 together with expression of $BRAF^{V600E}$ led to progression of benign lung lesions to lung AC (Dankort et al., 2007).

2.2.3.5.2 *TP53* and lung cancer

The human *TP53* gene at chromosomal location 17p13.1 is the most commonly mutated gene in human lung cancers. Its mutational incidence in the main histopathological subclasses of lung cancers ranges from 50% in lung ACs to nearly 100% in SCLC (Figure 6) (Cancer Genome Atlas Research, 2012, 2014; Cerami et al., 2012; Ding et al., 2008; Imielinski et al., 2012; Peifer et al., 2012; Rudin et al., 2012). The majority of lung cancer mutations in p53 are found within the DNA binding domain (Olivier et al., 2002).

Conditional loss of *Trp53* (mouse ortholog for *TP53*) expression in mouse lungs results in AC development with a long latency (350–530 days) (Meuwissen et al., 2003). *Trp53*-loss together with oncogenic *Kras* expression in mouse lung (referred to as KP from now on) results in ACs with a shorter latency and accelerates malignant progression when compared to *Trp53*-loss or oncogenic *Kras* expression alone (Jackson et al., 2005). Interestingly, the combined loss of *Rb1* together with *Trp53* gene expression results in development of SCLC (Meuwissen et al., 2003). Thus, co-occuring mutations with *Trp53*-loss define the murine lung tumour histopathology accurately correlating with the mutational spectrum detected in human cancers. Mutations in *TP53* are common in both lung ACs and SCLCs, but *KRAS* mutations are almost exclusively detected in lung ACs (up to 37%), while *RB1* mutations are common in SCLCs (45,2-65,5%) but not in ACs (Cancer Genome Atlas Research, 2012, 2014; Cerami et al., 2012; Ding et al., 2008; Imielinski et al., 2012; Peifer et al., 2012; Rudin et al., 2012). *In vivo* studies have also investigated the effect of p53 point mutations on lung tumourigenesis. The contact mutation $p53^{R270H}$ (homologous to human p53 R273H mutation) and structural mutation $p53^{R172H}$ (homologous to human p53 R175H mutation) combined with activation of oncogenic *Kras* accelerates malignant progression similar to total loss of p53. Interestingly, only the contact mutation $p53^{R270H}$ showed a dominant-negative effect in heterozygous mice (Jackson et al., 2005).

2.2.3.6 *LKB1/ STK11*

The liver kinase B1 (*LKB1*, official gene name serine/threonine kinase 11, *STK11*) is a serine/threonine kinase with tumour suppressor functions in a variety of cancers (Alessi et al., 2006; Vaahtomeri and Makela, 2011). The *LKB1* gene was initially identified in a search for causative germline mutations for Peutz-Jeghers syndrome (PJS) (Hemminki et al., 1998; Jenne et al., 1998). PJS (OMIM:175200) is an autosomal dominant disorder characterised by intestinal polyps classified as hamartomas concurrent with pigmented macules on the skin and mouth (Hemminki, 1999). PJS patients have a significantly increased risk of developing cancer (Giardiello et al., 1987; Hearle et al., 2006). The functional role of LKB1 in PJS has been further supported by the phenotypic similarity of *Lkb1*-null mice with PJS patients (Wei et al., 2005). The incidence of *LKB1* mutations in sporadic cancers is most frequent in NSCLC tumours and cervical cancers (Sanchez-Cespedes et al., 2002; Wingo et al., 2009).

2.2.3.6.1 LKB1 signalling

The LKB1 kinase has been indicated to regulate cell polarity, metabolism, cell differentiation, and proliferation via its at least 14 downstream kinases (Vaahtomeri and Makela, 2011). Activation of LKB1 occurs via heterotrimerisation with pseudokinase ste20-related adaptor protein (STRAD) and calcium-binding protein 39 (CAB39, also known as mouse protein 25, MO25) (Baas et al., 2003; Boudeau et al., 2003). The formation of the heterotrimer regulates LKB1 stability and cellular localisation (Boudeau et al., 2003; Dorfman and Macara, 2008).

One of the most studied LKB1 substrate kinases is AMP-activated protein kinase (AMPK), which is the master regulator of cellular and organismal metabolism and acts as a cellular energy sensor (Alexander and Walker, 2011). The catalytic subunit AMPKα and the two regulatory subunits AMPKβ and AMPKγ form a heterotrimer which is activated when the cellular AMP:ATP ratio rises, resulting in allosteric binding of AMP to the AMPKγ subunit (Alexander and Walker, 2011). AMPK activation also requires phosphorylation of AMPKα by LKB1 or calcium/calmodulin-dependent protein kinase kinase 2 (CAMKK) (Alexander and Walker, 2011). To adjust the cellular conditions to the reduction in ATP, AMPK inhibits protein synthesis by inhibiting mTOR signalling. mTOR inhibition occurs via AMPK-mediated phosphorylation of the tuberculosis sclerosis (TSC2/TSC1) complex and raptor, a component of the mTORC1 complex (Gwinn et al., 2008; Inoki et al., 2003).

The role of LKB1 in regulation of cell polarity has been evidenced in *C. elegans*, *Drosophila* as well as in mammalian cells. PAR-4, the C. elegans orthologue of LKB1, is required for anterior-posterior polarity of *C. elegans* embryo (Kemphues et al., 1988). In *Drosophila* oocytes, LKB1 loss leads to disruption of anterior-posterior cell polarity (Martin and St Johnston, 2003). LKB1 is also linked to regulation of cell polarity in mammalian cells, including intestinal epithelial and pancreatic acinar cells (Baas et al., 2004; Hezel et al., 2008). Interestingly, the LKB1-dependent regulation of cell polarity

has also been linked to its role in AMPK-mediated energy sensing. In Drosophila, both *Lkb1*- and AMPK-null mutants showed disruption of apico-basal cell polarity when the cells were exposed to sugar deprivation (Mirouse et al., 2007). The LKB1-dependent regulation of cell polarity is also mediated by additional LKB1 targets, AMPK-related kinases, namely microtube affinity-regulating kinases (MARK1-MARK4) and synapses of the amphid-defective kinases (SAD-A and SAD-B) (Hezel and Bardeesy, 2008).

2.2.3.6.2 *LKB1* and lung cancer

The human *LKB1* gene at chromosomal location 19p13.3 is among the most frequently mutated genes in lung ACs and ASCs (6-22%), whereas in lung SCCs the mutations are rare (1,7-3,9%) and in SCLCs absent (Table 1 and Figure 6) (Cancer Genome Atlas Research, 2012, 2014; Cerami *et al.*, 2012; Ding *et al.*, 2008; Imielinski *et al.*, 2012; Ji *et al.*, 2007a; Koivunen *et al.*, 2008; Peifer *et al.*, 2012; Rudin *et al.*, 2012; Sanchez-Cespedes *et al.*, 2002; Vassella *et al.*, 2015). Lung cancer mutations in LKB1 are distributed mainly along the kinase domain of the protein. Multiple types of somatic lung cancer mutations in *LKB1* have been identified, including nonsense, indel frameshift mutations, large deletions, and intronic mutations in splicing conserved sites. A large proportion of the mutations lead to protein truncations and thus inactive LKB1 (Sanchez-Cespedes, 2007). Interestingly, loss of LKB1 has been found to co-occur with *KRAS* mutations in NSCLC with an overall incidence of 30%. Moreover, the combined loss of LKB1 and mutation in *KRAS* was shown to be associated with a poorer prognosis in advanced NSCLC (Calles et al., 2015).

Mouse lung-specific *Lkb1* deletion on its own does not lead to a discernible phenotype (Ji et al., 2007a). However, the combined loss of *Lkb1* with expression of oncogenic $BRAF^{V600E}$ bypasses induction of $BRAF^{V600E}$-induced cellular senescence in mouse lung, promoting malignant carcinomas (Gonzalez-Sanchez et al., 2013). In addition, combined conditional loss of *Lkb1* with expression of oncogenic *Kras* exacerbates lung tumour progression, switches tumour histopathologies from AC to a mixed spectrum of three main NSCLC histopathologies including the more rare ASC, and promotes metastasis in 61% of $Kras^{LSL\text{-}G12D/+}$; $Lkb1^{fl/fl}$ or $Kras^{LSL\text{-}G12D/+}$; $Lkb1^{fl/-}$ (from here on referred to as KL) (Ji et al., 2007a). Mechanistically, the *Lkb1* mediated lung tumour suppression in the KL model is linked to reduction of AMPK activation. Whereas $Kras^{LSL\text{-}G12D/+}$ ACs are positive for phosphorylated AMPK and acetyl-CoA carboxylase (ACC), an enzyme functioning in the biosynthesis and oxidation of fatty acids, the KL ACs show clear reduction in both phospho-AMPK and phospho-ACC (Ji et al., 2007a). Interestingly, metastases in KL mice were reported to be AC-like and SCC-like metastases were not detected. Moreover, the KL ACs but not SCCs showed elevated expression of angiogenesis and/or metastasis genes, such as *Nedd9*, *Vegfc*, *Loxl1*, *Pdgf* receptor and *Mmp2*, suggesting that the metastases detected in the KL model are primarily disseminated from ACs (Ji et al., 2007a).

Subsequent studies have suggested that KL ACs transdifferentiate via an ASC intermediate to SCCs. Expression of lysyl oxidase (*Lox*) and the Hippo pathway transcriptional coactivator YAP1 where shown to maintain the KL AC histopathology,

concomitant with their reduction in KL SCCs. Furthermore, pharmacological LOX inhibition or genetic *Yap1* ablation promoted the transdifferentiation detected as an increased number of SCC lesions (Gao et al., 2014; Han et al., 2014). These studies linked the AC-ASC-SCC transdifferentiation to collagen disposition and ECM remodelling, as well as regulation of cell growth and apoptosis. In addition, also reactive oxygen species (ROS) accumulation was shown to modulate transdifferentiation, with KL ACs showing higher amounts of ROS, and treatments with the ROS scavenger N-acetyl cysteine reducing the amount of SCCs (Li et al., 2015). Lentiviral introduction of a constitutively active AMPK mutant (caAMPK) in KL mice decreased the amount of ROS in ACs and reduced SCC numbers, thus directly linking the AMPK pathway to both regulation of ROS and transdifferentiation. Moreover, pentose phosphate pathway (PPP) deregulation and impaired fatty acid oxidation were both shown to affect ROS and transdifferentiation. Specifically, glucose-6-phosphate dehydrogenase (G6PD), a regulator of PPP activity, showed lower enzymatic activity and protein expression in KL ACs compared with SCCs, and *in vivo G6pd* shRNA treatment increased the incidence of ACs (Li et al., 2015). Interestingly, conditional lung-specific *Lkb1*-loss in combination with *Pten*-loss or overexpression of *Sox2* leads to generation of pure lung SCCs without apparent transdifferentiation from AC (Mukhopadhyay et al., 2014; Xu et al., 2014a). Taken together, these results indicate that the loss of *Lkb1* contributes to SCC development, either during the process of tumour progression or directly triggering squamous differentiation upon tumour initiation.

2.2.3.7 *EPHA3*

The EPH receptor tyrosine kinase A3 (EPHA3) is a member of the EPH receptor tyrosine kinase (RTK) family, which is the largest family of RTKs, containing altogether 14 members in humans (Gucciardo et al., 2014; Pasquale, 2008). The name EPH is derived from the erythropoietin-producing hepatocellular carcinoma cell line from which the first member of the family, *EPHA1*, was cloned (Hirai et al., 1987). EPHA3 was identified on the cell surface of a pre-B acute lymphoblastic leukemia cell line, LK63, using the IIIA4 monoclonal antibody (Boyd et al., 1992).

In vivo studies have indicated a crucial role for *EphA3* in embryonic heart development. The null mouse model of *EphA3* was initially generated to study the potential functional role of *EphA3* in the developing medial motor column. Contrary to the hypothesis, derived from its expression pattern, no effect on motor axon direction to muscle targets was detected in *EphA3*-null mice (Vaidya et al., 2003). Instead, 75% of the *EphA3*-null mice died at birth due to cardiac abnormalities including defects in the development of their atrial septa and atrioventricular endocardial cushions. These defects were caused by defective endothelial-to-mesenchymal transition (EndMT), a specific form of mesenchymal conversion that generates progenitors of the atrioventricular valves. Endocardial cushion explants from E10.5 wt and *EphA3*-null embryos showed

fewer migrating cushion cells in a type I collagen matrix, indicating that this specific type of EMT process is altered in *EphA3*-null embryos (Stephen et al., 2007).

2.2.3.7.1 EPH/EPHA3 signalling

EPH receptor-mediated signalling has been shown to regulate cellular processes including modulation of the actin cytoskeleton, cell-substrate adhesion, intercellular junctions, cell shape and movement, as well as cell proliferation, survival, differentiation, and secretion (Gucciardo et al., 2014; Pasquale, 2008). EPH receptor signalling typically functions in cell sorting and tissue patterning, primarily during embryogenesis, through mechanisms linked to cell attraction and repulsion (Nievergall et al., 2012; Pasquale, 2005).

The EPHs are transmembrane proteins which interact with their ligands via an extracellular ligand-binding domain (LBD) in cell-cell contacts. EPH receptor ligands, the ephrins, are classified into two subgroups, class A and B, based on their sequence similarities and affinities. The EPHA receptors typically interact with ephrin-A ligands, while EPHB receptors interact with ephrin-B ligands, although exceptions have been found (Grunwald et al., 2004; Himanen et al., 2004; Qin et al., 2010; Smith et al., 1997). A ligand for EPHA3, ephrin-A5, was purified using a biosensor-based affinity detection approach (Lackmann et al., 1996) and later shown to be one of the preferred ligands for EPHA3 (Lackmann et al., 1997). In addition to ephrin-A5, also ephrin-A1 (encoded by *Efna1* gene) is indicated as a ligand for EPHA3, as it is expressed in the endothelial lining adjacent to the *EphA3*-positive endocardial cushions in the developing heart (Stephen et al., 2007). Interestingly, *Efna1*-null mice exhibit impaired cardiac function with increase in the amount of atrioventricular endocardial cushions indicating excess in the amount of cell which undergo EndMT during heart valve development (Frieden *et al.*, 2010). Unlike *EphA3*-null mice, *Efna1*-null mice do not die prenatally, suggesting additional and possibly compensating mechanisms for ephrin-A1 function. Indeed, ephrin-B2 is expressed in the epithelial layer of the developing heart valve leaflets and mice homozygous for a carboxy-terminal cytoplasmic domain mutant of ephrin-B2 show thickened cardiac valves similar to *Efna1*-null mice (Cowan *et al.*, 2004). These results suggest that multiple ephrin ligands function together with EPHA3 in a context and tissue dependent manner.

Unlike RTK signalling in general, EPH receptor and ephrin ligand signalling occurs in a bidirectional manner, both in the receptor-expressing cell (forward signalling) and in the ligand-expressing cell (reverse signalling) (Pasquale, 2008). As a consequence of ligand binding, the EPH receptors are autophosphorylated at two tyrosine residues within the juxtamembrane domain and one tyrosine residue within the activation segment of the kinase domain. The conformational changes resulting from autophosphorylation release the inhibition of the receptor kinase domain, triggering downstream signalling. The glycosylphosphatidylinositol (GPI)-linked ephrin-As use lipid raft-mediated interaction with transmembrane protein complexes and recruit signalling adaptor molecules such as the Src family kinase Fyn (Davy et al., 1999).

The EPH-ephrin interaction generally results in activation of downstream signalling pathways including the PI3K-AKT, RAS-MAPK, Janus kinase/Signal transducer and activator of transcription (JAK-STAT), as well as the focal adhesion kinase (FAK) and SRC kinase-mediated RhoA signalling. Also EPHA3 has been shown to signal through some of these pathways. Ephrin-A5-induced EPHA3 signalling can lead to changes in cell adhesion mediated by RhoA signalling in human epithelial kidney 293T, melanoma, and rhabdomyosarcoma cells (Clifford et al., 2008; Lawrenson et al., 2002). In addition, overexpression of wild-type EPHA3 in the human lung cancer cell line H1299 leads to both ephrin-A5- and ephrin-A1-induced reduction of phospho-AKT levels (Zhuang et al., 2012). Similarly, EPHA2 has been shown to function via a feedback loop to regulate Ras-Raf-MAPK (Macrae et al., 2005) and Ras–PI3K–AKT (Menges and McCance, 2008) pathways.

In addition to the traditional receptor-ligand interaction in cell-cell contacts, ephrin ligands interact with EPH receptors also laterally, in cis in the same cell. This interaction occurs independently of the N-terminal LBD of the receptor and inhibits the activation of the receptor by the trans-expressed ephrins (Carvalho et al., 2006; Falivelli et al., 2013). Additionally, the actual levels of EPH receptor expression can regulate their activity. Clusters formed by the EPH receptors within the cell membrane, induced by high abundance of the receptors rather than ligand interaction, lead to activation of the receptors (Wimmer-Kleikamp et al., 2004). Another mode of EPH receptor regulation was evidenced for *EPHA7*. The truncated form of EPHA7, encoded by an alternative splice variant of *EPHA7*, was shown to suppress tyrosine phosphorylation of the full-length EPHA7 (Holmberg et al., 2000). This shorter soluble form of EPHA7 was later shown to act as a tumour suppressor in follicular lymphoma by binding to EPHA2, thereby inhibiting oncogenic signals including ERK and SRC kinases (Oricchio et al., 2011). Moreover, an increasing number of studies reveal new mechanisms explaining regulation of EPH-ephrin signalling. Disintegrin and metalloprotease 10 (ADAM10)-mediated cleavage of membrane-bound ephrin-A5 ligand interacting with EPHA3 has been shown to lead to Eph-ephrin internalisation into the EPH expressing cell (Janes et al., 2005). Additionally, membrane type-1 matrix metalloproteinase (MT1-MMP)-mediated cleavage of EPHA2 has been shown to occur subsequently to ephrin binding. EPHA2 cleaved by MT1-MMP at the fibronectin type-III domain in cis translocates inside the cell, leading to SRC activation as well as an increase in RhoA activity and cell junction disassembly (Sugiyama et al., 2013).

2.2.3.7.2 *EPHA3* and cancer

The human *EPHA3* gene at chromosomal location 3p11.2 is a putative lung cancer gene, mutated in 6-16% of lung ACs, approximately 6% of lung SCCs and in 2-3% of SCLCs. Both deletions and amplifications in the genetic locus of *EPHA3* are found, respectively in 0,5% and 2% of ACs, or 2% and 4% of SCCs. (Table 1 and Figure 6) (Cancer Genome Atlas Research, 2012, 2014; Cerami et al., 2012; Ding et al., 2008; Imielinski et al., 2012; Peifer et al., 2012; Rudin et al., 2012). The lung cancer mutations in EPHA3 are located along the protein and they are mostly composed of missense

mutations. The effect of the mutations has been studied *in vitro* using transient transfection and *in vitro* kinase assay methods using 293T cells. Selected cancer point mutations in the extracellular domains of EPHA3 can affect ephrin ligand binding and/or the level of receptor cell surface localization, and selected kinase domain mutations impair the kinase activity of EPHA3 (Lisabeth et al., 2012).

One of the reported mechanisms of EPHA3 tumour suppression is its ephrin-A5- or ephrin-A1-induced activation of cellular apoptosis via reduction of phospho-AKT, and subsequent reduced phosphorylation of FOXO3A. These signaing activities are specific to wildtype EPHA3, as overexpression of EPHA3 G187R or G766E cancer mutation variants do not trigger a similar effect. Moreover, EPHA3 cancer mutations leading to receptor inactivation were shown to act in a dominant negative manner via inhibiting the activity of the wildtype receptor (Zhuang et al., 2012).

In addition to tumour-suppressing effects, EPHA3 has been indicated to possess tumour-promoting functions. EPHA3 is highly expressed in the most aggressive mesenchymal subtype of glioblastoma, where its expression is particularly detected in undifferentiated, tumour-initiating cells. shRNA- mediated downregulation of EPHA3 leads to increased ERK/MAPK pathway activation, increased cell differentiation and reduced capacity of sphere formation in primary glioblastoma cell cultures (Day et al., 2013). EPHA3-mediated control of the ERK/MAPK pathway has also been shown in neural precursor cells, where ephrin-A1 stimulation leads to ERK activation and increased neurogenesis, and therefore increased differentiation (Aoki et al., 2004). Interestingly, glioblastoma primary cell cultures expressing high levels of EPHA3 show low levels of EPHA3 kinase activity (Day et al., 2013). Activation of EPHA3 with a monoclonal antibody in the EPHA3 positive glioblastoma cell line U251 leads to rapid EPHA3 activation and reduction of cell proliferation (Day et al., 2013). These results suggest that high expression of EPHA3 in glioblastoma cells maintains the undifferentiated status of the cells, but in a kinase-independent fashion via control of ERK/MAPK pathway. Interestingly, normal physiological function of *EphA3* is also linked to mesenchymal cell identity in mice as loss of *EphA3* leads to reduced endothelial-to-mesenchymal transition during heart development (Stephen et al., 2007).

In a recent study, activation of EPHA3 has also been linked to tumour suppression, via disruption of the tumour microenvironment (TME) (Vail et al., 2014). This study reported EPHA3 overexpression in the microenvironment of a range of human cancers and mouse tumour xenografts. EPHA3 expression was detected in mouse bone marrow–derived cells with mesenchymal and myeloid phenotypes. Activation of mesenchymal–stromal/stem cells (MSCs) with EPHA3 agonist led to MSC contraction, and apoptosis *in vitro*, and disruption of the stromal tumour architecture leading to tumour growth inhibition *in vivo* (Vail et al., 2014). Together, these studies indicate both tumour suppressing, as well as tumour promoting, roles for EPHA3. However, thus far no studies have addressed the *in vivo* functional role of *EphA3* using murine genetically engineered models.

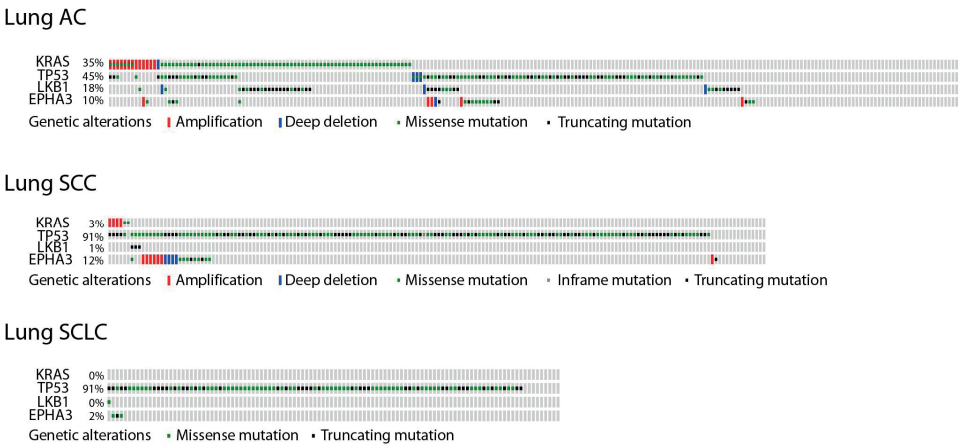

Figure 6. Genetic alterations of *KRAS*, *TP53*, *LKB1* (*STK11*) and *EPHA3* in the three main lung cancer histopathologies adenocarcinoma (AC), squamous cell carcinoma (SCC), and small-cell lung cancer (SCLC). Data exported from cBioportal and based on results from TCGA (Cancer Genome Atlas Research, 2012, 2014) and George et al., 2015.

2.3 Modelling lung cancer

Lung tumourigenesis is a multifactorial process, which over time creates tumours consisting of subclones of regionally-separated genetic alterations and different levels of genomic instability (de Bruin et al., 2014). Models that mimic the biological, genetic, etiological, immunological, and therapeutic properties of human lung cancer are a prerequisite for understanding the determinants of its biology, and for predictive testing of new therapeutic molecules.

Currently, the best characterised and most frequently used platform for preclinical testing of cancer therapeutics is the US National Cancer Institute 60 human tumour cell line panel (NCI-60), used for *in vitro* drug screening and development (Abaan et al., 2013). These cell lines have been valuable for early discoveries in cancer research. Examples start from the discovery of oncogenes, such as RAS (Der et al., 1982), and continue to the development of targeted therapies which block cell-autonomous pathways such as EGFR activation (Wakeling et al., 2002). Yet, the *in vitro* and *in vivo* (xenograft) testing of these cell lines, when compared with results from phase II trials, has shown good predictability only of compounds with anti-proliferative activity (Johnson *et al.*, 2001a). Moreover, it has been shown that their continued cultivation facilitated their adaptation to two dimensional (2D) conditions. Additionally, all cell lines showed a higher resemblance to each other, regardless of the tissue-of-origin, than to their clinical source samples, likely due to culture-acquired properties such as gain or loss of genetic information, alterations in growth and invasion, and/or selective loss of cell populations (Gillet et al., 2011).

The interest in developing and using more sophisticated preclinical models has led to the creation of more advanced models, such as patient derived xenografts (PDX) and genetically engineered mouse models (GEMMs). PDX models have been shown to recapitulate the heterogeneity and intrinsic properties of human primary tumours (Hidalgo et al., 2014). Moreover, lung cancer PDX models have shown molecular characteristics of the primary tumours and correlation with clinical response to cytotoxic agents (Fichtner et al., 2008; Fiebig et al., 1985). GEMMs, on the other hand, are particularly useful if tumour-stromal interactions are taken into account. A study using a mouse model of Burkitt's lymphoma showed that paracrine factors in the tumour microenvironment can affect lymphoma cell survival after genotoxic chemotherapy administration (Gilbert and Hemann, 2010) showing the importance of the physiological tumour microenvironment in cancer treatment testing. Moreover, more and more studies have reported on the role of the tumour immune microenvironment in cancer progression. For example, in a breast cancer mouse model driven by conditional loss of *Cdh1* and *Trp53*, tumour expressed IL1B was shown to induce expression of IL17 in gamma delta (γδ) T-cells, which induced granulocyte colony-stimulating factor (G-CSF)-dependent infiltration of myeloid derived suppressor cells (MDSCs) to the tumour site. The infiltration of the MDSCs was shown to suppress $CD8^+$ T-cells and promote metastasis (Coffelt et al., 2015).

Additionally, a recent study underlined the importance of carcinogen-induced models in the study of lung tumourigenesis. Murine lung tumours, initiated either by carcinogens or transgene expression, resulted in different cancer genomic landscapes. Methyl-nitrosourea (MNU) carcinogen-induced lung tumours carried numerous non-synonymous point mutations in contrast to the tumours induced by genetic activation of mutant *Kras*, which were enriched with copy number alterations (Westcott et al., 2015). Thus, the researchers concluded that these two models recapitulate genetic versus epigenetic features of cancers, predominantly representing mutations or copy number changes (Ciriello et al., 2013).

The following sections describe lung cancer GEMMs with specific concentration on genetic alterations, tumour histopathologies, cell-of-origin, and immune cell contexts relevant to this thesis work.

2.3.1 Genetically engineered mouse models of lung cancer

Genetic engineering of the murine genome is a powerful tool to address the functional importance of lung cancer genes in disease initiation and progression (Kwon and Berns, 2013). Genetic engineering started with traditional knock-out technology with microinjection of embryonic stem cells with vectors executing target genome homologous recombination (Capecchi, 2005; Schwartzberg et al., 1989). Tumour studies using full knock out mice have often been limited by the embryonic lethality of the mice due to the importance in embryonic development of the genes studied (Jacks et al., 1992; Koera et al., 1997). Use of conditional allelic systems, such as Cre–loxP or Flp–FRT, have permitted modulation of genetic loci in tissue and time-specific manners and have thus enabled *in vivo* study of cancer genes in a way which mimics the sporadic human cancer genetic alterations (Jackson et al., 2001; Meuwissen et al., 2003; Sadowski, 1995; Sauer and Henderson, 1988; Sternberg and Hamilton, 1981). Moreover, new state-of-the-art technologies including the use of the prokaryotic type II CRISPR- (clustered regularly interspaced short palindromic repeats) Cas9- (CRISPR-associated protein-9 nuclease) system, which enables simultaneous introduction of genetic alterations in single embryonic cells, is accelerating the process of *in vivo* genetic manipulation to functionally test single or combined genetic alterations (Sanchez-Rivera and Jacks, 2015; Sanchez-Rivera et al., 2014).

2.3.1.1 Genetic mutations

The first generations of lung cancer GEMMs used overexpression of putative oncogenes such as *c-Myc* or *EGF*, leading to the development of ACs (Ehrhardt et al., 2001). One of the earliest studies used expression of simian virus large T-antigen (SV40 Tag) under an SPC-promoter. The SV40 Tag binds to both p53 and RB1 in an inhibitory

manner, resulting in uncontrolled cellular proliferation. In contrast to results showing that combined loss of *Trp53* and *Rb1* drives development of SCLC (Meuwissen et al., 2003), SV40 Tag- induced tumours were classified as adenocarcinomas with papillary and lepidic growth (Wikenheiser et al., 1992), suggesting differences between SV40 Tag and direct mutation-mediated suppression of p53 and RB1.

A number of studies have generated *in vivo* evidence for the cancer driver roles of the most common genetic alterations of lung cancer, including mutant *EGFR* and *EML4-ALK* translocations. Expression of conditional human *EGFR* exon 19 deletion and exon 21 L858R mutation in mouse lung CC10-expressing cells leads to ACs with local invasion (Ji et al., 2006; Politi et al., 2006). Similarly, expression of the human *EML4-ALK* fusion gene in SPC^{+} cells leads to hundreds of adenocarcinoma nodules within only a few weeks after birth (Soda et al., 2008). Most recently, CRISPR-Cas9-mediated engineering of the mouse endogenous *Eml4-Alk* rearrangement resulted in development of lung tumours resembling human *ALK*-rearrangement positive NSCLC (Maddaloni et al., 2015; Soda et al., 2008).

Several GEMM studies have investigated the functional role and possible targetable features of oncogenic *Kras* and loss of *Trp53* and *Lkb1* in lung tumourigenesis. Three studies in year 2001 reported a mouse model carrying *Kras* G12D mutation, all resulting in development of lung ACs. Jacks and colleagues created mouse strains carrying oncogenic *Kras* G12D activated by a spontaneous recombination event (*Kras* latent allele, $Kras^{LA}$). These mice were highly predisposed to a range of tumour types, predominantly early onset lung tumours (Johnson et al., 2001b). Two inducible *Kras* G12D mouse strains were also created: one with reverse tetracycline-controlled transactivator (rtTA) controlled *Kras* G12D (Fisher et al., 2001) and one with Cre-loxP sites flanking a stop codon prior to the G12D mutation ($Kras^{LSL\text{-}G12D/+}$) (Jackson et al., 2001). All of these models have been combined with several other genetic modifications in studies exploring the effect of co-occurring mutations on lung tumourigenesis. These studies have clearly shown how loss of a tumour suppressor accelerates tumour progression initiated by activation of an oncogene. Table 2 lists selected models which used the conditional $Kras^{LSL\text{-}G12D/+}$ model (Jackson et al., 2001) in combination with other genetic alterations. These include genes involved in cell cycle regulation and sensing of oncogenic and genotoxic stress, such as *Trp53*, *Rb1*, *Rbl2*, and *Map2k7*; genes in the control of cellular metabolism, such as *Lkb1*; and genes acting downstream of Ras, such as *Pten* (references listed in the table 2). Loss of the transcription factor *Nkx2-1*, which has a role in cell differentiation during lung development, accelerates lung tumourigenesis (Snyder et al., 2013). This acceleration coincides with the conversion of the cellular transcription profile to a gastric lineage, as well as the development of mucinous ACs, a histopathology not detected in oncogenic *Kras*-induced tumours (Snyder et al., 2013). In addition, loss of the hypoxia-inducible transcriptional regulator *Hif2a* as well as *Notch2*, a gene controlling cell fate decisions during embryonic development, accelerates oncogenic *Kras*-driven AC formation (Baumgart et al., 2015; Mazumdar et al., 2010). Interestingly, in contrast to loss of *Notch2*, *Notch1*-loss reduces the oncogenic *Kras*-driven AC burden (Baumgart et al., 2015), indicating differential

roles for the members of the same signalling pathway. Conditional expression of an activated form of NOTCH1/2 (the NOTCH1/2 intracellular domain, N1/2ICD) in combination with oncogenic *Kras* promotes papillary AC formation in $CC10^{+}$ airway cells (Xu et al., 2014b), indicating that *Notch2*-mediated tumour suppression is dependent on the function of the full length protein. Furthermore, expression of a dominant negative form of mastermind-like protein (DNMaml1), inhibiting the transcriptional activation of Notch targets, interferes with oncogenic *Kras*-driven lung ACs from $CC10^{+}$ cells (Xu et al., 2014b). Deletion of RAS downstream effectors such as *Rac1* and *Pik3r2* together with *Pik3r1* inhibits oncogenic *Kras*-driven AC development (Engelman et al., 2008; Kissil et al., 2007). Together, these results indicate a clear cooperation between Ras and other pathways during lung tumourigenesis. Moreover, the results highlight the power of mouse models to confirm functional cooperation between pathways suspected to be key or even essential drivers of human lung cancer.

Table 2. Selected *Kras* G12D lung cancer mouse models. Change in tumour burden and tumourigenesis as compared to *Kras*$^{LSL\text{-}G12D/+}$.

Genetic modifications	Activation method	Histopathology	Reference
Kras$^{LSL\text{-}G12D/+}$	Ad5-CMV-Cre	AC spectrum*	(Jackson *et al.*, 2001)
Kras$^{LSL\text{-}G12D/+}$;*Spry2*$^{fl/fl}$	Ad5-CMV-Cre	Increased AC burden	(Shaw *et al.*, 2007)
Kras$^{LSL\text{-}G12D/+}$;*Dicer*$^{fl/fl}$	Ad5-CMV-Cre	Increased AC burden	(Kumar *et al.*, 2007)
Kras$^{LSL\text{-}G12D/+}$;*Trp53*$^{fl/fl}$	Ad5-CMV-Cre	Progressed AC with lymph node metastases	(Jackson *et al.*, 2005)
Kras$^{LSL\text{-}G12D/+}$;*Trp53*$^{LSL\text{-}R172H/-}$	Ad5-CMV-Cre	Progressed AC with lymph node metastases	(Jackson *et al.*, 2005)
Kras$^{LSL\text{-}G12D/+}$;*Trp53*$^{LSL\text{-}R270H/-}$	Ad5-CMV-Cre	Progressed AC with lymph node metastases	(Jackson *et al.*, 2005)
Kras$^{LSL\text{-}G12D/+}$;*Lkb1*$^{fl/fl}$	Ad5-CMV-Cre	Progressed tumourigenesis with broadened tumour histopathology spectrum (AC, ASC, SCC and LCC) and metastasis	(Ji *et al.*, 2007a)
Kras$^{LSL\text{-}G12D/+}$;*Pten*$^{fl/fl}$	CC10-Cre	Progressed AC	(Iwanaga *et al.*, 2008)
Kras$^{LSL\text{-}G12D/+}$;*Rb1*$^{fl/fl}$	Ad5-CMV-Cre	Increased AC burden	(Ho *et al.*, 2009)
Kras$^{LSL\text{-}G12D/+}$;*Rbl2*$^{fl/fl}$	Ad5-CMV-Cre	Increased AC burden	(Ho *et al.*, 2009)
Kras$^{LSL\text{-}G12D/+}$;tetO-*Yap*^{S127A}	Ad5-CMV-Cre + rtTA	Increased AC burden and progressed tumourigenesis	(Lau *et al.*, 2014)
Kras$^{LSL\text{-}G12D/+}$;*Nkx2-1*$^{fl/fl}$	Ad5-CMV-Cre	Increased AC burden and additional mucinous AC	(Snyder *et al.*, 2013)
Kras$^{LSL\text{-}G12D/+}$;*Hif2a*$^{fl/fl}$	Ad5-CMV-Cre	Increased AC burden	(Mazumdar *et al.*, 2010)
Kras$^{LSL\text{-}G12D/+}$;*Map2k7*$^{fl/\Delta}$	Ad5-CMV-Cre	Increased AC burden	(Schramek *et al.*, 2011)
Kras$^{LSL\text{-}G12D/+}$;*Notch2*$^{fl/fl}$	Ad5-CMV-Cre	Increased AC burden	(Baumgart *et al.*, 2015)
Kras$^{LSL\text{-}G12D/+}$;Rosa26-NotchICD-GFP**	CC10-CreER	Increased AC burden in airways	(Xu *et al.*, 2014b)
Kras$^{LSL\text{-}G12D/+}$;*Tgfbr2*$^{fl/fl}$	K5-CrePR	Increased AC burden	(Malkoski *et al.*, 2012)
Kras$^{LSL\text{-}G12D/+}$;*Rac1*$^{fl/fl}$	Ad5-CMV-Cre	Decreased AC burden	(Kissil *et al.*, 2007)
Kras$^{LSL\text{-}G12D/+}$;*Pik3r2*$^{-/-}$; *Pik3r1*$^{fl/fl}$	Ad5-CMV-Cre	Decreased AC burden	(Engelman *et al.*, 2008)
Kras$^{LSL\text{-}G12D/+}$;*Notch1*$^{fl/fl}$	Ad5-CMV-Cre	Decreased AC burden	(Baumgart *et al.*, 2015)
Kras$^{LSL\text{-}G12D/+}$;Rosa26-DNMaml1-GFP***	CC10-CreER	Decreased AC burden	(Xu *et al.*, 2014b)

*Epithelial hyperplasia of bronchioles, adenomatous hyperplasia, adenomas, both solid and papillary adenocarcinomas **Cell-autonomous and ligand-independent Notch activation by the intracellular domain (ICD) of Notch1. ***Notch inhibition by dominant-negative Mastermind-like protein (DNMaml1).

The functional consequence of *Trp53*-loss in lung cancer progression has been studied in combination with several other genetic alterations (listed in Table 3). In addition to the cooperation of oncogenic *Kras* and *Trp53*-loss, accelerating progression

of lung ACs (Jackson et al., 2005), the loss of *Trp53* cooperates with the loss of *Rb1* in the development of lung SCLCs (Meuwissen et al., 2003). Furthermore, *Trp53*- and *Rb1*-loss-driven SCLC development is accelerated when *Rbl2* (also known as p130), a cell cycle inhibitor related to RB1, is also deleted (Schaffer et al., 2010). Moreover, in contrast to results from oncogenic *Kras*-driven ACs, loss of both *Notch1* and *Notch2* inhibits SCLC development driven by loss of *Trp53*, *Rb1* and *Rbl2* (George *et al.*, 2015), indicating that Notch pathway activation is a key factor driving SCLC progression.

Table 3. Selected *Trp53*$^{fl/fl}$ lung cancer mouse models.

Genetic modifications	Activation method	Histopathology	Reference
Trp53$^{fl/fl}$	Ad5-CMV-Cre	AC	(Meuwissen *et al.*, 2003)
Trp53$^{fl/fl}$;*Rb1*$^{fl/fl}$	Ad5-CMV-Cre	NE hyperplasia and SCLC with metastases	(Meuwissen *et al.*, 2003)
Trp53$^{fl/fl}$;*Rb1*$^{fl/fl}$;*Rbl2*$^{fl/fl}$	Ad5-CMV-Cre	Increased SCLC burden when compared to Trp53$^{fl/fl}$; Rb1$^{fl/fl}$	(Schaffer *et al.*, 2010)
Trp53$^{fl/fl}$;*Rb1*$^{fl/fl}$;*Rbl2*$^{fl/fl}$; Rosa26-*Notch2ICD*-GFP*	Ad5-CMV-Cre	Decreased SCLC burden when compared to Trp53$^{fl/fl}$; Rb1$^{fl/fl}$; Rbl2$^{fl/fl}$	(George *et al.*, 2015)
Trp53$^{fl/fl}$;*Rb1*$^{fl/fl}$;*Rbl2*$^{fl/fl}$; Rosa26-*Notch1ICD*-GFP*	Ad5-CMV-Cre	Decreased SCLC burden when compared to Trp53$^{fl/fl}$; Rb1$^{fl/fl}$; Rbl2$^{fl/fl}$	(George *et al.*, 2015)
Trp53$^{fl/fl}$;*Braf*$^{CA/+}$	Ad5-CMV-Cre	Increased AC burden and progressed tumourigenesis when compared to Braf$^{CA/+}$	(Dankort *et al.*, 2007)

* Conditional expression of an activated form of NOTCH1/2 (NOTCH1/2 intracellular domain, N1/2ICD)

In addition, the functional role of *Lkb1*-loss in lung cancer progression has been studied in combination with several other genetic alterations. Table 4 lists selected mouse models that have used the conditional loss of *Lkb1* (Bardeesy et al., 2002) to study lung cancer. Loss of *Lkb1* accelerates lung tumourigenesis driven by oncogenic *Kras* and *Braf* (Gonzalez-Sanchez et al., 2013; Ji et al., 2007a; Mukhopadhyay et al., 2014). Interestingly, rather than merely affecting the tumour progression, *Lkb1*-loss switches the tumour histopathology development towards SCC (Ji et al., 2007a; Mukhopadhyay et al., 2014; Xu et al., 2014a). Lung specific loss of *Pten* alone leads to lung hyperplasia or to rare ACs, depending on the used method (Liu et al., 2015; Malkoski et al., 2014). Similarly, overexpression of *Sox2* in the lung promotes hyperplasia and AC tumourigenesis accompanied with expression of squamous markers (Lu et al., 2010). Lung specific loss of *Lkb1* combined with both *Pten*-loss and overexpression of *Sox2* leads to an increase in tumour progression and a switch to SCC development (Mukhopadhyay et al., 2014; Xu et al., 2014a). Nevertheless, *LKB1* mutations are rare in human lung SCCs (1,7-3,9%), and it remains to be elucidated if the molecular events linked to *Lkb1*-loss in SCC development are different in mice. Another possibility is that *LKB1* loss constitutes only a rare event in human SCC, defining a small subset of this histopathology.

Table 4. Selected $Lkb1^{fl/fl}$ lung cancer mouse models.

Genetic modifications	Activation method	Histopathology	Reference
$Lkb1^{fl/fl}$	Ad5-CMV-Cre	No tumour formation	(Ji *et al.*, 2007a)
$Lkb1^{fl/fl}$;$Braf^{CA/CA}$	Tyr::CreERT2 + Ad5-CMV-Cre	AC, Lkb1-loss bypasses senescence	(Gonzalez-Sanchez *et al.*, 2013)
$Lkb1^{fl/fl}$;$Pten^{fl/fl}$	Ad5-CMV-Cre	SCC	(Xu *et al.*, 2014a)
$Lkb1^{fl/fl}$	Lenti-Sox2-CMV-Cre	SCC with rare AC	(Mukhopadhyay *et al.*, 2014)
$Kras^{LSL\text{-}G12D/+}$;$Lkb1^{fl/fl}$	Ad5-CMV-Cre	Progressed tumourigenesis with broadened tumour histopathology spectrum (AC, ASC, SCC and LCC) and frequent metastases when compared to $Kras^{LSL\text{-}G12D/+}$	(Ji *et al.*, 2007a)
$Kras^{LSL\text{-}G12D/+}$;$Lkb1^{fl/fl}$; $SPC\text{-}YAP^{S127A}$	Ad5-CMV-Cre	Decreased incidence of SCC when compared to $Kras^{LSL\text{-}G12D/+}$; $Lkb1^{fl/fl}$	(Gao *et al.*, 2014)

2.3.1.2 Histopathology

The histopathological analysis of lung tumour samples is a standard procedure of lung cancer diagnosis, and is used to guide treatment decisions. In the case of murine lung cancer models, an accurate and comparative histopathology analysis can help to stratify models to mimic specific subsets of cancer patients (Figure 7). Several GEMMs expressing known human lung AC gene alterations develop a disease similar to that of humans, thus validating the use of mouse models in the study of human disease. These include models conferring expression of mutated *EGFR* (Ji et al., 2006), mutant *Kras* (Jackson et al., 2001), loss of *Trp53* (Meuwissen et al., 2003) or *Eml4-Alk* rearrangement (Maddaloni et al., 2015; Soda et al., 2008). Moreover, expression of mutated Ras effectors such as BRAF and PIK3CA also drive lung ACs (Engelman et al., 2008; Ji et al., 2007b), further supporting the role of Ras activation in lung AC development. Interestingly, loss of the transcription factor *Nkx2-1* in combination with oncogenic *Kras*, results in development of mucinous ACs, a tumour histopathology not detected in mice with activation of oncogenic *Kras* alone (Snyder et al., 2013). Loss of *Nkx2-1* alters differentiation and promotes the metastatic potential of KP ACs which is mechanistically linked to activation of high mobility group AT-hook 2 (Hmga2) expression (Winslow et al., 2011). Thus, loss of *Nkx2-1* is linked to lung tumours with a lower differentiation status and increased metastatic potential, such as that seen in some cases of mucinous AC histopathology.

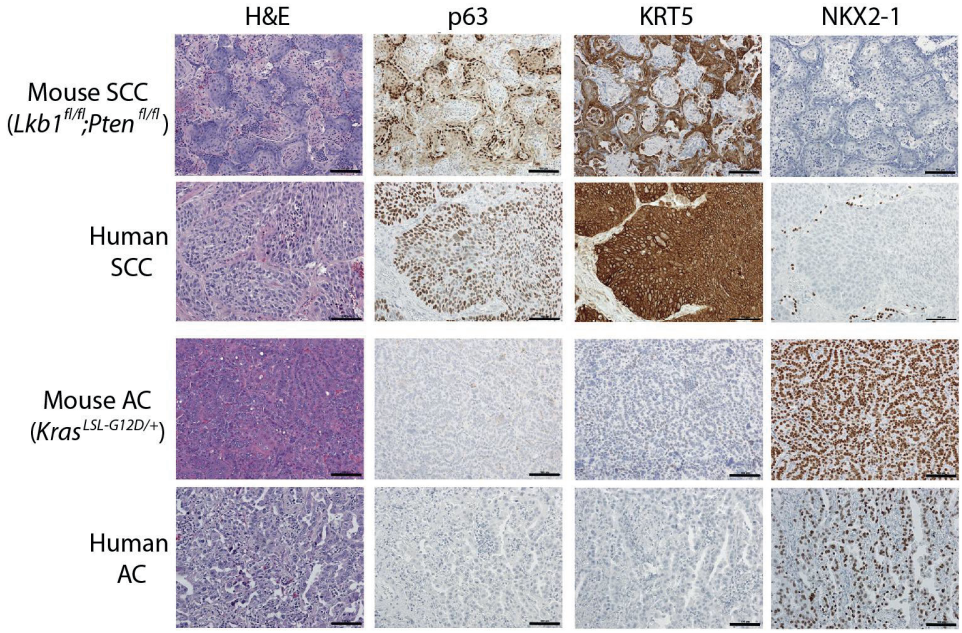

Figure 7. Immunohistochemistry-based characterisation is utilised to stratify mouse lung tumours to show their similarity to human disease. Both human and mouse SCC tumours are positive for p63 and KRT5 SCC markers and negative for NKX2-1 AC marker. Scale bars 100 mm. Adapted from Xu et al. 20014a.

Table 5 lists selected lung SCC and ASC GEMMs. The development of murine squamous cell carcinomas is triggered by lung specific expression of oncogenic *Kras* G12D in combination with loss of *Lkb1* or *Tgfbr2* (Ji et al., 2007a; Malkoski et al., 2012). As discussed earlier, also conditional loss of *Lkb1* in combination with loss of *Pten* (Xu et al., 2014a) (Figure 7) or overexpression of *Sox2* (Mukhopadhyay et al., 2014) leads to the development of lung SCCs. The *Lkb1* loss is required for these tumours to develop as SCCs since the conditional loss of *Pten* or expression of *Sox2* alone only results in lung hyperplasias or ACs (Liu *et al.*, 2015; Lu *et al.*, 2010; Malkoski *et al.*, 2014). Interestingly, expression of a kinase-inactive IKKα, a subunit of the IKK complex regulating NF-κB activation, leads to development of spontaneous SCCs, which show significantly decreased protein levels of LKB1 expression (Xiao et al., 2013). Moreover, these SCC tumours are characterised by infiltration of $F4/80^{+}$ tumour-associated macrophages (TAMs), and depletion of TAMs with liposome treatment prevents SCC formation (Xiao et al., 2013). Also, the combined loss of *Pten* and *Tgfrb2* results in SCCs with low incidence (Malkoski et al., 2014). Also Notch signalling is linked to squamous differentiation. Inhibition of Notch with DNMaml1 expression blocks oncogenic *Kras*-driven ACs and induces development of $SOX2^{+}$, $KRT5^{+}$, and $p63^{+}$ squamous hyperplasia from lung alveolar cells (Xu et al., 2014b). Finally, overexpression of human CK14 in $CC10^{+}$ progenitor cells leads to hyperplasia with squamous differentiation and occasional squamous metaplasia (Dakir et al., 2008).

Currently no targeted inhibitors are available for lung SCCs highlighting the importance of the development of preclinical models for this lung tumour histopathology.

ASC histopathology tumours are seen following 1) expression of oncogenic *Kras* G12D in combination with loss of *Lkb1* (Ji et al., 2007a), 2) expression of an in-frame M774 AYVM insertion of HER2 (Perera et al., 2009), or 3) combined loss of *Smad4* and *Pten* (Liu et al., 2015). ASCs, a relatively rare histopathology in humans, exhibit a mutational spectrum similar to lung ACs. As presented previously, studies using the KL mouse model have shown evidence for ASC being an intermediate histopathology stage between AC and SCC (Han et al., 2014).

Table 5. Selected lung ASC and SCC mouse models.

Genetic modifications	Activation method	Histopathology	Reference
CC10-*hK14* *		Hyperplasia with SC differentiation and rare SC metaplasia	(Dakir *et al.*, 2008)
Ikka$^{KA/KA}$**		Spontaneous SCC (LKB1 levels significantly decreased)	(Xiao *et al.*, 2013)
hHER2^{YVMA}	CC10-rtTA	ASCs with few ACs	(Perera *et al.*, 2009)
Kras$^{LSL\text{-}G12D/+}$;*Lkb1*$^{fl/fl}$	Ad5-CMV-Cre	AC, ASC, SCC, and LCC	(Ji *et al.*, 2007a)
Kras$^{LSL\text{-}G12D/+}$;*Tgfbr2*$^{fl/fl}$	K5-CrePR	AC with rare SCC	(Malkoski *et al.*, 2012)
Pten$^{fl/fl}$;*Smad4*$^{fl/fl}$	CCSPiCre	ASC	(Liu *et al.*, 2015)
Tgfbr2$^{fl/fl}$;*Pten*$^{fl/fl}$	K5-CrePR	AC with rare SCC	(Malkoski *et al.*, 2014)
Lkb1$^{fl/fl}$;*Pten*$^{fl/fl}$	Ad5-CMV-Cre	SCC	(Xu *et al.*, 2014a)
Lkb1$^{fl/fl}$	Lenti-Sox2-CMV-Cre	SCC with rare AC	(Mukhopadhyay *et al.*, 2014)

*Human CK14 under CC10 promoter, ** Dominant negative, kinase-dead IKKα

Alterations leading to loss of of *RB1* and *TP53* in human SCLC are obligatory events for this tumour histopathology (George *et al.*, 2015). Similarly, the loss of *Rb1* and *Trp53* appears to be a prerequisite also for murine SCLC development, as no SCLC develops from NE cells with ectopic expression of *Hras*, even following carcinogen nitrosamine treatment (Sunday et al., 1999).

2.3.1.3 Cell-of-origin

As introduced earlier, multiple lung epithelial progenitor cells have been identified based on their capacity to self-renew and/or differentiate into other lung epithelial cells (section 2.1.1). These progenitor cell types include basal cells, Clara cells, BASCs and AT2 cells (Leeman et al., 2014). Interestingly, recent studies comparing tumour

initiation, progression, and histopathology distribution of murine lung tumours derived from different cells-of-origin have shown that the site of the oncogenic event impacts on tumourigenesis, thus affecting tumour heterogeneity (Sutherland et al., 2011; Sutherland et al., 2014; Xu et al., 2014b; Xu et al., 2012).

Past lung GEMM research mostly utilised specific promoters to drive genetic alterations in distinct lung epithelial cells. Only recently, these cell sites have been compared with an aim to identify the relative effect of the cell-of-origin on lung tumourigenesis (Table 6). Specifically, these studies used promoters including CC10, SPC or CGRP to drive expression of Cre-recombinase in Clara, AT2 or NE cells, respectively. In the case of the CC10 promoter, Cre-mediated recombination is not detected in alveolar cells when adenovirus-mediated delivery is used (Sutherland et al., 2011). On the other hand, use of the CreER strain achieves Cre-mediated recombination in alveolar AT2 cells following multiple doses of tamoxifen (Rawlins *et al.*, 2009b), indicating a low level of CC10 expression in a subset of AT2 cells.

The progenitor-specific etiologies of lung ACs are relatively well described. Lung ACs driven by activation of oncogenic *Kras* with or without *Trp53*-loss can originate from Clara cells, AT2 cells, and BASCs (Kim et al., 2005; Sutherland et al., 2014; Xu et al., 2012). However, the role of BASCs as a cell-of-origin for murine lung ACs at the BADJ region is still under debate. Ad5-CMV-Cre-induced oncogenic *Kras* G12D expression increased the number of BASCs (Kim et al., 2005), but Ad5-SPC-Cre-infected $Kras^{LSL\text{-}G12D/+}$ mice failed to develop cellular proliferative abnormalities at the BADJ, accompanied by lack of an increase in the number of CC10/SPC double-positive cells (Sutherland et al., 2014). Two possible explanations have been suggested; either expression of SPC promoter-driven Cre via Ad5-SPC-Cre in CC10/SPC double-positive cells is too low to activate the conditional $Kras^{LSL\text{-}G12D/+}$ allele, or the CC10/SPC cells are not the cell-of-origin of these lesions (Sutherland et al., 2014).

Interestingly, also the role of $CC10^{+}$ lung epithelial cells as a cell-of-origin for murine lung ACs has been shown to be context dependent (Figure 8). The $CC10^{+}$ lung airway cells are sensitive to adenovirus-mediated inflammatory responses, which can accelerate tumour formation (Mainardi et al., 2014). When comparing Cre-ER- and Ad-CMV-Cre-mediated expression of $Kras^{G12V}$, Barbacid and colleagues showed that the microenvironmental inflammatory response in bronchial cells caused by Ad-Cre supported the progression of lung epithelial hyperplasias to low-grade adenomas, but not to high grade ACs. The progression of lung epithelial hyperplasias to low-grade adenomas was not seen following Cre-ER-mediated expression of $Kras^{G12V}$ (Mainardi et al., 2014). Similar findings were reported combining CC10-CreER and SPC-CreER strains with the $Kras^{LSL\text{-}G12D/+}$;$Trp53^{+/fl}$ model (Xu et al., 2012). Specifically, Hogan and colleagues showed that expression of oncogenic $Kras^{LSL\text{-}G12D/+}$ in combination with heterozygous loss of *Trp53* in $CC10^{+}$ airway cells did not lead to tumourigenesis, whereas SPC^{+} cells with identical genetic alterations formed ACs in the alveoli (Xu et al., 2012). Consistent with these results, adenovirus-mediated cell type-specific expression of Cre resulted in oncogenic *Kras*-induced tumourigenesis from CC10-expressing airway cells when compared to SPC-expressing cells (Sutherland et al.,

2014). As discussed by Barbacid and colleagues, the inflammatory response caused by the adenovirus infection may alter the differentiation status of the $CC10^{+}$ airway cells, sensitising cells to oncogenic *Kras*-induced transformation. Alternatively, and as observed in pancreatic acinar cells, the inflammatory response may inhibit OIS (Guerra et al., 2011). Indeed, $Kras^{G12V}$-induced early lesions have been shown to exhibit clear marks of OIS using markers such as senescence-associated β-galactosidase (SA-β-gal) and $p16^{INK4A}$, and this OIS was bypassed in fully developed ACs (Collado et al., 2005). It is not yet known if OIS explains why $CC10^{+}$ airway cells fail to progress to tumours in the case of the CreER models. Either way, the inflammation-promoting microenvironment might well recapitulate conditions seen in physiological lung airways.

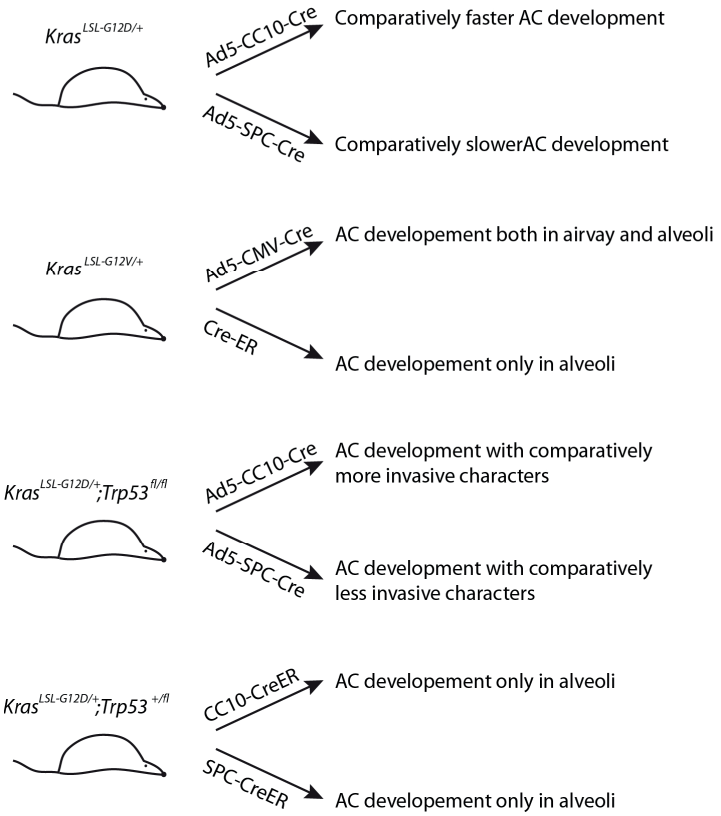

Figure 8. $CC10^{+}$ lung epithelial cells show a context-dependent propensity to develop into murine lung ACs. The models presented are based on results reported by Sutherland et al. 2014, Mainardi et al. 2014, and Xu et al. 2012.

The role of the cell-of-origin has also been shown to affect loss of *Trp53*- and *Rb1*-driven murine SCLC development. Sutherland and colleagues studied the effect of the cell-of-origin in murine SCLC using cell type-specific adenoviruses driving Cre-

mediated recombination in CC10-, SPC- or CGRP-expressing epithelial cells (Sutherland *et al.*, 2011). While $CGRP^+$ cells were shown to initiate $NCAM1^+$ NE tumours in 25 out of 30 mice, almost no SCLCs developed from CC10-expressing cells. Interestingly, also SPC^+ cells were shown to initiate development of SCLC (Sutherland *et al.*, 2011).

Taken together, these results indicate variation in the propensity of different lung epithelial cells to give rise to lung tumours driven by specific genetic alterations. Moreover, the sensitivity of airway $CC10^+$ cells to inflammation exacerbated tumourigenesis, implying intricate cooperation between oncogenic events, cellular identity and microenvironmental factors such as inflammation-inducing pathogens during lung tumourigenesis.

Table 6. Selected lung cancer mouse models addressing the role of the cell-of-origin during tumourigenesis.

Genetic modifications	Activation method	Histopathology	Reference
$Kras^{LSL\text{-}G12D/+}$	Ad5-CC10-Cre	AC spectrum with more high grade tumours than in Ad5-SPC-Cre induced	(Sutherland *et al.*, 2014)
$Kras^{LSL\text{-}G12D/+}$	Ad5-SPC-Cre	AC spectrum	(Sutherland *et al.*, 2014)
$Trp53^{fl/fl};Rb^{fl/fl}$	Ad5-CGRP-Cre	SCLC	(Sutherland *et al.*, 2011)
$Trp53^{fl/fl};Rb^{fl/fl}$	Ad5-CC10-Cre	Bronchiolar hyperplasia, and rare SCLC	(Sutherland *et al.*, 2011)
$Trp53^{fl/fl};Rb^{fl/fl}$	Ad5-SPC-Cre	SCLC with lower frequency than in Ad5-CGRP-Cre-induced	(Sutherland *et al.*, 2011)
$Kras^{LSL\text{-}G12D/+};Trp53^{fl/fl}$	Ad5-CC10-Cre	Progressive AC with more high grade tumours than in Ad5-SPC-Cre induced	(Sutherland *et al.*, 2014)
$Kras^{LSL\text{-}G12D/+};Trp53^{fl/fl}$	Ad5-SPC-Cre	Progressive AC	(Sutherland *et al.*, 2014)
$Kras^{LSL\text{-}G12D/+};Trp53^{+/fl}$	CC10-CreER	AC spectrum in the alveoli	(Xu *et al.*, 2012)
$Kras^{LSL\text{-}G12D/+};Trp53^{+/fl}$	SPC-CreER	AC spectrum in the alveoli	(Xu *et al.*, 2012)
$Kras^{LSL\text{-}G12D/+};Lkb1^{fl/fl}$	SPC-CreER	NSCLC histopathology spectrum with AC, ASC, SCC and LCC	(Han *et al.*, 2014)
$Kras^{LSL\text{-}G12D/+};Lkb1^{fl/fl}$	Ad5-SPC-Cre	NSCLC histopathology spectrum with AC, ASC, SCC and LCC	(Li *et al.*, 2015)

2.3.1.4 Modelling lung cancer immune contexture

Tumour immune contexture refers to the population of different tumour-infiltrating immune cell types, each conferring different effects on tumour progression (Fridman et al., 2012). The cells in the tumour microenvironment are part of the cancer immunoediting process that modulates cancer progression. The concept of immunoediting is used to describe three phases by which immunity controls and shapes

cancer (Dunn et al., 2002). These phases are (1) elimination (also called cancer immunosurveillance), describing the capacity of the immune system to remove benign lesions (2) equilibrium, characterised by dormant poorly proliferating cancer cells maintained by the immune system, and (3) escape, in which cancer cells have acquired a weakened immunogenicity or capacity to attenuate immune responses (e.g. immune tolerance via PD1, PD-L1 and/or CTLA-4) and therefore can grow to malignant disease, a phase when the cancer is usually diagnosed (Fridman et al., 2012; Koebel et al., 2007).

Analyses of the amount, location, and density of immune cell populations can assist in determining prognosis (Dieu-Nosjean et al., 2008; Halama et al., 2011). Specific lymphocyte infiltrations in lung NSCLC have been suggested to have positive prognostic value (Al-Shibli et al., 2008; Dieu-Nosjean et al., 2008; Donnem et al., 2010), clearly showing a correlation between the presence of $CD3^+CD4^+$ T-helper cells or $CD3^+CD8^+$ cytotoxic T-cells and good prognosis. In addition, analysis of neutrophil counts and the neutrophil-to-lymphocyte ratio has indicated an association between accumulation of neutrophils and poor disease prognosis in NSCLC (Sarraf et al., 2009; Teramukai et al., 2009). Moreover, a heterogeneous population of cells with myeloid origin and immunosuppressive activity, known as myeloid-derived suppressor cells (MDSCs), is shown to contribute to the suppression lymphocyte-mediated immunosurveillance (Gabrilovich and Nagaraj, 2009). MDSCs are a heterogeneous population of activated immature myeloid cells (IMCs), which in normal conditions function as progenitor cells for mature granulocytes, macrophages, or dendritic cells. MDSCs show the morphology of granulocytes or monocytes, which have been suggested to have different roles in cancer immunoediting, with granulocytic MDSCs showing more substantial expansion than the monocytic subset in tumour models (Gabrilovich and Nagaraj, 2009; Youn et al., 2008). Quantification of MDSCs characterised by CD11b, CD15, and CD33 expression from peripheral blood of lung cancer patients has implied a positive correlation between the abundance of MDSCs and poor prognosis (Liu et al., 2010). Additionally, a negative correlation has been found between the abundance of MDSCs and $CD3^+CD8^+$ cytotoxic T-cells, suggesting that active MDSC-mediated immunosuppression may contribute to the poor prognosis of lung cancer patients (Liu et al., 2010).

In mice, MDSCs characterised based on positive expression of CD11b (integrin alpha M) and Gr-1 antigen. Monoclonal Gr-1 antibody also recognises epitopes in lymphocyte antigen 6 complex, locus G and C (LY6G and LY6C) with preference to LY6G (Fleming et al., 1993). Epitope-specific antibodies against LY6G and LY6C have led to the identification of two mouse MDSC subsets, namely granulocytic MDSCs characterised as $CD11b^+LY6G^+LY6C^{low}$, and monocytic MDSCs characterised as $CD11b^+LY6G^-LY6C^{hi}$ (Youn et al., 2008).

In vivo studies using pancreatic cancer GEMMs have shown that MDSCs create a favourable environment for tumour growth and metastasis by secreting molecules which modulate the extracellular matrix, including matrix metalloproteinase 9 (MMP9) and cathepsin B (Shchors et al., 2013). The immunosuppressive characteristics of MDSCs, seen as a negative correlation between the presence of MSDCs and $CD3^+CD8^+$ T-cells, is

mechanistically linked to expression of L-arginase (*Arg1*) by MDSCs (Gabrilovich and Nagaraj, 2009). Elevated *Arg1* expression by tumour-associated myeloid cells leads to reduced availability of the amino-acid L-arginine, and therefore decreased proliferation and/or inhibition of T-cell function in an orthotopic murine lung AC model (Rodriguez et al., 2004). This observation is supported by human studies showing the amount of MDSCs, specifically expressing *ARG1*, to correlate with immunouppressive characteristics, namely reduced abundance and proliferation of lymphocytes (Liu et al., 2010; Munder et al., 2006).

The recruitment of MDSCs to tumour sites is linked to several protein factors that are released by tumour cells, including cytokines. The pro-inflammatory cytokine interleukin-1b (encoded by *Il1b*) can mobilise and recruit MDSCs to the stomach, sensitising the organ for gastric inflammation and carcinoma (Tu et al., 2008). In a murine breast cancer model, IL-1B has also been linked to the recruitment of MDSCs to tumour sites. Importantly, antibody-mediated inhibition of IL-1B can inhibit the recruitment of $CD11b^{+}Ly6G^{+}Ly6C^{+}$ MDSCs in a syngeneic murine breast carcinoma model; depletion of MDSCs with anti-Ly6G antibody reduced the amount of early metastases to the lungs, which was mechanistically linked to suppression of $CD8^{+}$ T-cell activation as also $CD8^{+}$ T-cell depletion facilitated metastasis (Coffelt et al., 2015).

GEMMs have also been used to study the lung cancer lymphocyte contexture. Using the CC10-TAg lung adenocarcinoma model, Coussens and colleagues reported that $CD4^{+}$ T-lymphocytes comprise the major population of lung adenocarcinoma $CD45^{+}$ immune cells, and when compared with normal lung tissue, an increased proportion of $CD4^{+}FOXP3^{+}$ regulatory T-cell (Treg) in the total $CD4^{+}$ population was detected (Ganesan et al., 2013). Their hypothesis that $FOXP3^{+}$ Tregs might be enriched within tumours that suppress $CD8^{+}$ T-cell responses was confirmed with anti-CD25–depleting mAb, which reduces the major subset of CD25-expressing $Foxp3^{+}$ Tregs. This reduction resulted in an increased infiltration of $CD8^{+}$ T-cells in the lung parenchyma, and tumour cell death. Interestingly, also lung squamous cell carcinomas, driven by loss of *Pten* and *Lkb1,* display marks of immunosuppression by expressing PD-L1, and show increased G-MDSC and $FOXP3^{+}$ T-cell infiltration (Xu et al., 2014a). Moreover, a mouse model expressing kinase-dead IKKα, a subunit of the IKK complex, develops spontaneous lung SCCs accompanied by pulmonary inflammation. Interestingly, SCC tumours in the latter model also showed a reduction in somatic LKB1 protein expression, further linking the loss of *Lkb1* to both SCC development and tumour inflammation (Xiao et al., 2013).

The present knowledge of the epidemiological, pathological, molecular, and microenvironmental details of lung cancer is greater than it has ever been. Simultaneously, development of sophisticated *in vitro* and *in vivo* methodologies has enabled functional research on the factors contributing to lung tumourigenesis. Combining this information to the growing amount of knowledge on the regulators of normal tissue homeostasis and embryonic development, will help to create a better understanding of lung tumourigenesis and assist its translation to individualized treatment options.

3 Aims of the study

Treatment of lung cancer is challenged by a high level of intra- and intertumour genomic, molecular, and microenvironmental heterogeneity. Despite extensive knowledge on molecular profiles of lung tumours, validation of their functional importance is needed to translate this information into the clinic. The first aim of this thesis work was to validate the functional importance of the putative tumour suppressor gene *EPHA3,* which is commonly mutated in human lung cancers and was identified as a hit in a high-content cellular senescence tumour suppressor screen. Furthermore, this thesis work aimed to uncover the role of specific progenitor cells in defining the murine lung tumour spectrum, both with respect to tumour growth and histopathology as well as immune microenvironments. This aim was performed by using a murine NSCLC model driven by two known lung cancer genetic alterations, oncogenic *Kras* and loss of the tumour suppressor *Lkb1,* with no prior knowledge on the lung niche specific contribution to histopathology or immune microenvironment heterogeneity.

To address these aims, the following specific questions were asked:

1. Does *EPHA3*, a gene commonly mutated in cancers, show characteristics of a tumour suppressor (Study I)?
2. Does *EphA3* demonstrate a tumour suppressive role in murine embryonic lungs and NSCLC (Study II)?
3. Does the cell-of-origin impact murine NSCLC development and lesion-specific immune microenvironments (Study III)?

4 Materials and methods

4.1 Materials

The following materials were used in this thesis work.

4.1.1 Cell lines

Cell line	Description	Source or reference	Study
293T Flp-In T-REx	Human embryonic kidney epithelial cell line containing a single stably integrated FRT site.	Life Technologies (Invitrogen)	I
hTERT-RPE1	hTERT immortalised human retinal pigmented epithelial cell line, converted also to a Flp-In cell line by inserting of a FRT site.	Clontech	I, II

4.1.2 Plasmids

Plasmid	Description	Vector	Tag	Source	Study
pgLAP5	Destination vector	pgLAP5	CT-GFP-LAP	Addgene	I
hEPHA3 wt	Expression vector	pgLAP5	CT-GFP-LAP	Verschuren laboratory *	I
hEPHA3 497C-A	Expression vector	pgLAP5	CT-GFP-LAP	Verschuren laboratory *	I
hEPHA3 807G-A	Expression vector	pgLAP5	CT-GFP-LAP	Verschuren laboratory *	I
hEPHA3 1137T-G	Expression vector	pgLAP5	CT-GFP-LAP	Verschuren laboratory *	I
hEPHA3 1336G-T	Expression vector	pgLAP5	CT-GFP-LAP	Verschuren laboratory *	I
hEPHA3 2183G-T	Expression vector	pgLAP5	CT-GFP-LAP	Verschuren laboratory *	I
hEPHA3 2283G-T	Expression vector	pgLAP5	CT-GFP-LAP	Verschuren laboratory *	I
hEPHA3 2416G-T	Expression vector	pgLAP5	CT-GFP-LAP	Verschuren laboratory *	I
hEPHA3 2798C-T	Expression vector	pgLAP5	CT-GFP-LAP	Verschuren laboratory *	I
hEPHA3 2297G-A	Expression vector	pgLAP5	CT-GFP-LAP	Verschuren laboratory *	I
pgLAP5/puro	Destination vector	pgLAP5/puro	CT-GFP-LAP	Addgene	I
hEPHA3 wt	Expression vector	pgLAP5/puro	CT-GFP-LAP	Verschuren laboratory	I
hEPHA3 497C-A	Expression vector	pgLAP5/puro	CT-GFP-LAP	Verschuren laboratory	I
hEPHA3 807G-A	Expression vector	pgLAP5/puro	CT-GFP-LAP	Verschuren laboratory	I
hEPHA3 1137T-G	Expression vector	pgLAP5/puro	CT-GFP-LAP	Verschuren laboratory	I

hEPHA3 1336G-T	Expression vector	pgLAP5/puro	CT-GFP-LAP	Verschuren laboratory	I
hEPHA3 2183G-T	Expression vector	pgLAP5/puro	CT-GFP-LAP	Verschuren laboratory	I
hEPHA3 2283G-T	Expression vector	pgLAP5/puro	CT-GFP-LAP	Verschuren laboratory	I
hEPHA3 2416G-T	Expression vector	pgLAP5/puro	CT-GFP-LAP	Verschuren laboratory	I
hEPHA3 2798C-T	Expression vector	pgLAP5/puro	CT-GFP-LAP	Verschuren laboratory	I
hEPHA3 2297G-A	Expression vector	pgLAP5/puro	CT-GFP-LAP	Verschuren laboratory	I
pEGFP-H2B-N1	Human H2B plasmid		CT-EGFP	Dr. Matt Summers	I
pDONR221	Gateway entry vector			Invitrogen	I
pOG44	Flp-recombinase plasmid			Invitrogen	I

* Used but not cloned by the author.

4.1.3 siRNAs

siRNA	Catalogue no.	Source or reference	Study
Human *EPHA1*	J-003115-10	GE Healthcare Dharmacon Inc.	I
Human *EPHA2*	J-003116-09	GE Healthcare Dharmacon Inc.	I
Human *EPHA3*	M-003117-03	GE Healthcare Dharmacon Inc.	I, II
Human *EPHA4*	J-003118-09	GE Healthcare Dharmacon Inc.	I
Human *EPHA5*	J-005315-08	GE Healthcare Dharmacon Inc.	I
Human *CDKN2A (p16^{INK4})*	M-011007-03	GE Healthcare Dharmacon Inc.	I
Human *EMI1* (*FBXO5*)	L-012434-00	GE Healthcare Dharmacon Inc.	I
Human *TP53*	SI02655170	Qiagen	I
siCONTROL	D-001810-10-20	GE Healthcare Dharmacon Inc.	I, II

4.1.4 Quantitative PCR (Q-PCR) probes and primers

Q-PCR probe	Catalogue no.	Source or reference	Study
Human *RPL19*	Hs02338565_gH	Life Technologies	I, II
Human *EPHA3*	Hs00739096_m1	Life Technologies	I, II
Human *CDKN2A (p16^{INK4})*	Hs00923894_m1	Life Technologies	I
Human *EPHA1*	Hs00178313_m1	Life Technologies	I
Human *EPHA2*	Hs00171656_m1	Life Technologies	I
Human *EPHA4*	Hs00177874_m1	Life Technologies	I
Human *EPHA5*	Hs00300724_m1	Life Technologies	I

Q-PCR primer	Nucleotide sequence	Source or reference	Study
Human *EPHA3* fwd	5'GCAGACAAAGACCCTCCAT3'	Verschuren laboratory	I
Human *EPHA3* rev	5'GTAACATCTTTCCGGCCTC3'	Verschuren laboratory	I
Human *CDKN2A (p16^{INK4})* fwd	5'CCCAACGCACCGAATAGTTAC3'	Verschuren laboratory	I
Human *CDKN2A (p16^{INK4})* rev	5'CCAGCGTGTCCAGGAAG3'	Verschuren laboratory	I
Human *TP53* fwd	5'GTCCCTTCCCAGAAAACCTA3'	Dr. Sergey Kuznetsov	I
Human *TP53* rev	5'CTCGGATAAGATGCTGAGGA3'	Dr. Sergey Kuznetsov	I
Human *RPL19* fwd	5'ACCCCAATGAGACCAATGAA3'	Verschuren laboratory	I
Human *RPL19* rev	5'CGCAAAATCCTCATTCTCCT3'	Verschuren laboratory	I
Mouse *EphA1* fwd	5'CAAGATTGCAAGACTGTGGC3'	(Abdul-Aziz *et al.*, 2009)	II
Mouse *EphA1* rev	5'CCTCCCACATTACAATCCCA3'	(Abdul-Aziz *et al.*, 2009)	II
Mouse *EphA2* fwd	5'GTCTATAAAGGGACGCTGAAGG3'	Verschuren laboratory	II
Mouse *EphA2* rev	5'CGCTCCATTCTCCATGTACTC3'	Verschuren laboratory	II
Mouse *EphA3* fwd	5'GAGACAGTATGCCGCAGTCA3'	Verschuren laboratory	II
Mouse *EphA3* rev	5'GCCTCTTGCTCTCAAAATGG3'	Verschuren laboratory	II
Mouse *EphA4* fwd	5'CCGAAGCAGCCTACACTACC3'	(Andersson *et al.*, 2011)	II
Mouse *EphA4* rev	5'GCCAGCAGTCCAGCATTAAC3'	(Andersson *et al.*, 2011)	II
Mouse *EphA5* fwd	5'AGTGACAGTGGGAGTCATCT3'	Verschuren laboratory	II
Mouse *EphA5* rev	5'GCAGTTTAATGTGCCCGTTATG3'	Verschuren laboratory	II
Mouse *EphA7* fwd	5'CAGCAGACGGGATTAGAGGA3'	Verschuren laboratory	II
Mouse *EphA7* rev	5'GATGACTCCATTGGGATGCT3'	Verschuren laboratory	II
Mouse *Efna1* fwd	5'CAGGAATCCCAGTGCTTGAA3'	Verschuren laboratory	II
Mouse *Efna1* rev	5'CAGCAGTGGTAGGAGCAATAC3'	Verschuren laboratory	II
Mouse *Efna5* fwd	5'GAGATGTTGACGCTGCTCTT3'	Verschuren laboratory	II
Mouse *Efna5* rev	5'TTCTGGGACAGAGTCCTCATAG3'	Verschuren laboratory	II
Mouse *Efnb2* fwd	5'CCAGACAAGAGCCATGAAGAT3'	Verschuren laboratory	II
Mouse *Efnb2* rev	5'TGCGATCCCTGCGAATAAG3'	Verschuren laboratory	II
Mouse *Fgf10* fwd	5'GCTGTTCTCCTTCACCAAGTA3'	Verschuren laboratory	II
Mouse *Fgf10* rev	5'ACTCCGATTTCCACTGATGTT3'	Verschuren laboratory	II
Mouse *Pecam1* fwd	5'GTGGTCATCGCCACCTTAATA3'	Verschuren laboratory	II
Mouse *Pecam1* rev	5'TTCTCGCTGTTGGAGTTCAG3'	Verschuren laboratory	II
Mouse *Nkx2-1* fwd	5'CTACTGCAACGGCAACCTG3'	Verschuren laboratory	II
Mouse *Nkx2-1* rev	5'CCATGCCACTCATATTCATGC3'	Verschuren laboratory	II
Mouse *Cdh1* fwd	5'CAGGTCTCCTCATGGCTTTGC3'	Verschuren laboratory	II
Mouse *Cdh1* rev	5'CTTCCGAAAAGAAGGCTGTCC3'	Verschuren laboratory	II
Mouse *Il1b* fwd	5'TGCCACCTTTTGACAGTGATGAGA 3'	Verschuren laboratory	III
Mouse *Il1b* rev	5'CCTGGAAGGTCCACGGGAA3'	Verschuren laboratory	III
Mouse *Arg1* fwd	5'TCGTGTACATTGGCTTGCGA3'	Verschuren laboratory	III
Mouse *Arg1* rev	5'GCCAATCCCCAGCTTGTCTA3'	Verschuren laboratory	III
Moue *H2-D1* fwd	5'CTGAAGAACGGGAACGCGAC3'	Verschuren laboratory	III
Moue *H2-D1* rev	5'TGTAAGAGTCAGTGGACGGAGG3'	Verschuren laboratory	III
Mouse *H2-M2* fwd	5'GTGCCTTGGATGGAACAGAT3'	Verschuren laboratory	III

Mouse *H2-M2* rev	5'CCAGTCATCCTTTGGATGGT3'	Verschuren laboratory	III
Mouse *Rpl19* fwd	5'CGGGAATCCAAGAAGATTGA3'	Verschuren laboratory	II, III
Mouse *Rpl19* rev	5'TTCAGCTTGTGGATGTGCTC3'	Verschuren laboratory	II, III

4.1.5 Mouse strains

Mouse strain	Description	Reference	Study
EphA3$^{-/-}$	*EphA3*-null mice lacking first exon of *EphA3*	(Stephen *et al.*, 2007; Vaidya *et al.*, 2003)	II
Kras$^{LSL-G12D/+}$	Mice carrying a conditional mutant allele of *Kras*	(Jackson *et al.*, 2001)	II, III
p53$^{fl/fl}$	Mice carrying a conditional loss-of-function allele of *Trp53*	(Marino *et al.*, 2000)	II, III
Lkb1$^{fl/fl}$	Mice carrying a conditional loss-of-function allele of *Lkb1 (Stk11)*	(Bardeesy *et al.*, 2002)	III
Rosa26$^{mT/mG}$	Membrane-Tomato/Membrane-GFP Cre-reporter mice	(Muzumdar *et al.*, 2007)	II, III

4.1.6 Probes for in situ hybridization

In situ hybridization probe	Fragment	Source or reference	Study
Mouse *EphA3*	Nucleotides 658-1474	Prof. Mark Krasnow	II
Mouse *Efna1*	Nucleotides 20-421	Prof. Mark Krasnow	II
Mouse *Fgf10*	Nucleotides 11-579	Prof. Irma Thesleff	II

4.1.7 Primary antibodies

Antibody (Cat. no.)	Description	Source or reference	Study
GFP	Rabbit polyclonal	Verschuren laboratory	I, II, III
GFP (A11122)	Rabbit polyclonal	Invitrogen	I
Phosphotyrosine 4G10 (05-321)	Mouse monoclonal	Millipore	I
EEA1 (610457)	Mouse monoclonal	BD Biosciences	I
β-actin (A1978)	Mouse monoclonal	Sigma-Aldrich	I, III

NKX2-1 (TTF1) (ab133638)	Rabbit monoclonal	Abcam	II, III
p63 (ab53039)	Rabbit polyclonal	Abcam	II, III
EPHA3 (34-8500)	Rabbit polyclonal	Invitrogen/Thermo Fisher Scientific	II
CD31 (PECAM1) (553370)	Rat monoclonal	Becton, Dickinson and Company	II
E-Cadherin (CST 3195)	Rabbit monoclonal	Cell Signaling Technology	II
BrdU		Cell Signaling Technology	II
Ki67 (RM-9106-S0)	Rabbit monoclonal	Thermo Fisher Scientific	III
Cytokeratin 5 (ab52635)	Rabbit monoclonal	Abcam	III
Gr-1 (Ly6G) (14-5931)	Rat monoclonal	E-Bioscience	III
CD11b (BSB6441)	Rabbit monoclonal	BioSB	III
CD3 (ab5690)	Rabbit polyclonal	Abcam	III
SOX2 (sc-17320)	Goat polyclonal	Santa Cruz Biotechnology	III
LKB1 (D60C5F10)	Rabbit monoclonal	Cell Signaling Technology	III

4.2 Methods

The following methods were used in this thesis work.

4.2.1 Cell culture and cell line generation (I)

hTERT immortalised human retinal pigmented epithelial cells (hTERT-RPE1, Clontech) were maintained in DMEM:F-12 (Invitrogen) containing 10% FBS (Gibco), 2mM L-Glutamine (Gibco) and 0,348% sodium bicarbonate (Gibco). Human embryonic kidney epithelial cells (293T) were maintained in DMEM (Lonza) containing 10% FBS (Gibco) and 2 mM L-Glutamine (Gibco). A stable H2B-GFP hTERT-RPE1 clonal cell line was generated by transfection with GFP-tagged human H2B plasmid (pEGFP-H2B-N1) followed by clonal selection using G418 (Roche). The 293T Flp-In T-Rex cell line was purchased from Invitrogen. The hTERT-RPE1 cell line was converted to a Flp-In cell line by the insertion of a FRT site. Stable cell lines were created as previously described (Torres et al., 2009). Briefly, human *EPHA3* cDNA and tumour variants were synthesised by DNA 2.0 into Gateway compatible pDONR221 entry vectors and cloned into appropriate pG-LAP5 or pG-LAP5/puro Gateway destination vectors using LR recombination technology (Invitrogen). pG-LAP constructs encoding proteins of interest were co-transfected with pOG44 plasmid encoding the Flp recombinase (Invitrogen) into Flp-In cell lines using Fugene 6 (Roche), followed by selection for stable integrants using Hygromycin B (pG-LAP5) or Puromycin (pG-LAP5/puro) selection. Pooled lines were used with 293T cells; clonal cell lines were used with hTERT-RPE1 cells.

4.2.2 siRNA transfections (I and II)

For gene expression silencing (knockdown), cells were treated with 50 nM pooled siRNA duplexes (GE Healthcare Dharmacon Inc.) or 30 nM for single siRNAs (Qiagen) using Oligofectamine reagent (Invitrogen) in 24-well plates.

4.2.3 Live cell imaging (I)

For live cell imaging hTERT-RPE1 cells expressing H2B-GFP protein were treated with 50 nM pooled siRNA using forward transfection with Oligofectamine reagent (Invitrogen) on 24-well plates. Transfections were carried out in replicates of four and imaging was performed using the IncuCyte™ FLR instrument (Essen BioScience) for five days. Cells from a duplicate plate were harvested at day three to confirm siRNA knockdown. Object analysis was performed with the IncuCyte default parameters.

4.2.4 Senescence-associated β-galactosidase (SA-β-gal) staining (I)

Cellular senescence was detected in cells transfected with siRNAs in 24-well plates (Corning), by staining for acidic β-galactosidase as described (Dimri *et al.*, 1995). Imaging of cells was performed with the Zeiss Axio light microscope and AxioCam MRc5 camera using Axio Vision Rel. 4.8 software.

4.2.5 Ligand treatment, *in vitro* kinase assay and immunoblotting (I)

For cellular activity measurements, 293T cells stably expressing LAP-tagged EPHA3 proteins were serum starved for 1 h, and then incubated with 1.5 µg/ml recombinant human ephrin-A5-Fc or IgG1-Fc proteins (R&D Systems), pre-clustered for 20 min with anti-human Fc antibody (Jackson ImmunoResearch) at 10:1 molar ratio. Cells were then lysed in RIPA buffer (50 mM Tris-HCl, pH 7.4, 1 mM EDTA, 150 mM NaCl, 0.1 % SDS, 1 % Triton X-100, 0.25 % Na-Deoxycholate, 100 mM β-glycerol-2-phophate, 15 mM sodiun fluoride, 2.5 mM orthovanadate) containing Protein Inhibitor Cocktail (Roche) and Phosphatase Inhibitor Cocktail (Roche), and 500 µg of protein lysate was rotated for 16h with 1 µg of anti-GFP antibody (Invitrogen). Antigen was captured using Protein G/A Sepharose beads (Sigma). Alternatively, specific antigen was captured using S-protein agarose beads (Novagen). Samples were immunoblotted using

anti-phosphotyrosine (PY 4G10; Upstate Biotechnology Inc.) or in-house affinity-purified anti-GFP antibodies.

For the *in vitro* kinase assay, 293T Flp-In T-Rex and hTERT-RPE1 Flp-In cells expressing LAP-tagged EPHA3 proteins were lysed in RIPA buffer containing protease inhibitors. 500 µg of total protein was incubated for 1h with 1 µg of GFP antibody (Invitrogen). Specific antigen was captured using Protein A/G Sepharose beads (Thermo Scientific), or, alternatively, with S-protein agarose beads (Novagen), and washed using RIPA and kinase buffer (50 mM NaCl, 20 mM Hepes pH 7.2, 10 mM $MgCl_2$, 2 mM EDTA, 0.02% Triton X-100). Beads were next incubated in kinase buffer supplemented with 20 µM adenosine 5'-triphosphate disodium salt hydrate (Sigma). Samples were immunoblotted using anti-phosphotyrosine or anti-GFP antibodies.

4.2.6 Immunostaining and fluorescence microscopy (I)

hTERT-RPE1 Flp-In cells stably expressing LAP-tagged EPHA3 proteins with or without ephrin-A5 treatment were fixed on coverslips and immunostained for GFP (EPHA3-LAP) and EEA1 early endosomal marker (BD Biosciences). Fluorescence microscopy imaging was performed with the Nikon 90i microscope using 60X objective. Image handling was done with Adobe Photoshop CS5 software.

4.2.7 Protein variant structural domain analysis (I)

For protein variant structural domain analysis, a PDB file with EPHA3 kinase and juxtamembrane domain structure information (2QOC) (Davis *et al.*, 2008) and the structural information of LKB1 tumour suppressor (2WTK) (Zeqiraj *et al.*, 2009) were downloaded from the RCSB (Research Collaboratory for Structural Bioinformatics) protein data bank (http://www.pdb.org/pdb/home/home.do). Mutation analysis, distance measurements, and alignment analysis were performed using the PyMOL molecular visualisation system.

4.2.8 RNA expression analysis (I-III)

Normal adult lung and tumour tissue was homogenised using a Precellys homogenisation kit (Bertin Technologies). Total RNA was extracted using NucleoSpin RNA II kit (MACHEREY-NAGEL) and quantified using NanoDrop 1000 (Thermo Fisher Scientific Inc.). Complementary DNA (cDNA) was synthesised from the extracted RNA using a High-capacity cDNA reverse transcription kit (Life

Technologies/Thermo Fisher Scientific Inc.). Quantitative PCR (qPCR) analysis was done for triplicate reactions using iQ™ SYBR® Green Supermix (Bio-Rad) or iQ™ Supermix (Bio-Rad) were run and analysed on a CFX384 TouchTM Real-Time PCR Detection System (Bio-Rad), using relative quantitation against the housekeeping *Rpl19* mRNA. Cycles started with three min. denaturation at 95 °C, followed by 40 cycles of 15 sec at 95°C, and 1 min at 60°C. A melting curve ranging from 57 °C to 95 °C was included in every analysis to confirm specific amplification. For *Arg1*, an annealing temperature of 58 °C was used. For the embryonic lung expression analysis, an exponential expression (ΔCq Expression) was obtained with formula ΔCq Expression=2–ΔCq, where ΔCq=Cq (target) – Cq (reference).

4.2.9 Mouse breeding and recombinant adenovirus administration (II and III)

All animal studies followed guidelines from the Finnish National Board of Animal Experimentation and were approved by the Experimental Animal Committee of the University of Helsinki and the State Provincial Office of Southern Finland (Licence number ESAVI-2010-04855/Ym-23). *EphA3*-null mice were bred with $Kras^{LSL\text{-}G12D/+}$ and $Trp53^{fl/fl}$ mice to generate the study cohorts and were maintained on a mixed genetic background using littermates as controls. $Kras^{LSL\text{-}G12D/+}$ mice were crossed with $Lkb1^{fl/fl}$ or $Trp53^{fl/fl}$ mice to generate $Kras^{LSL\text{-}G12D/+}$; $Lkb1^{fl/fl}$ (KL) or $Lkb1^{fl/fl}$; $Trp53^{fl/fl}$ (KP) mice on a mixed background. KL mice were crossed with $Rosa26^{mT/mG}$ Cre-reporter mice, resulting in mixed background cohorts. Six to ten wk old mice were intranasally or intratracheally administered with $3{,}3\times10^7$ or with $3{,}3\times10^8$ plaque-forming units (pfu) of Ad5-CMV-Cre (University of Turku, Finland), 1-20x10^7 pfu of Ad5-CC10-Cre or 2.5-7.5x10^9 pfu of Ad5-SPC-Cre viruses (Viral Vector Core Facility, University of Iowa, USA) under isoflurane anaesthesia.

4.2.10 Tissue preparation and immunohistochemistry (II and III)

Immunohistochemistry was performed for formalin fixed and paraffin embedded lungs that were sectioned (4-5 µm) from two distinct regions representing the surface and middle regions of the lungs. Sections were dehydrated and antigenic epitopes were exposed by heating in 10 mM citrate buffer, pH 6.0 (anti-GFP, anti-NKX2-1, anti-p63, anti-EPHA3, anti-E-Cadherin, anti-Ki67, anti-Cytokeratin 5, anti-CD11b, anti-CD3 and anti-SOX2) or by incubation in 0.05% trypsin at 37 °C (anti-CD31 and anti-Gr-1). Tissue sections were blocked with 1% BSA and 10% Normal Goat Serum in 1x PBS. Primary antibodies were detected using secondary antibody BrightVision poly-HRP anti-

rabbit (IL ImmunoLogic), or Peroxidase-Goat Anti-Rat IgG (H+L) (Invitrogen Corporation) for 30 min at ambient temperature. Detection was done with DAB (3,3'-diaminobenzidine, Bright DAB, IL ImmunoLogic). Immunohistologically stained lung sections were scanned with a Pannoramic 250 3DHISTECH (3DHISTECH Kft.) digital slide scanner using a 20x objective. Snapshots from the stained sections were taken with Pannoramic Viewer software (3DHISTECH Kft.).

4.2.11 Preparation of embryonic lung tissue (II)

For the embryonic lung epithelial and mesenchymal expression analysis, embryonic lungs were dissected and epithelial and mesenchymal cells separated using a previously described protocol (del Moral and Warburton, 2010) with minor modifications. Briefly, pregnant mice were sacrificed to harvest embryos at E11.5, E13.5 and E15.5 by CO_2 administration. Collected embryos were dissected under a stereoscopic microscope in a glass Petri dish immersed in PBS. Isolated lungs were transferred to 24-well plates containing CO_2-independent medium (Gibco by Life Technologies/Thermo Fisher Scientific Inc.). Epithelial and mesenchymal cells were separated by treating the lungs with 10 mg/ml collagenase (collagenase from Clostridium histolyticum, Sigma) in CO_2-independent medium at 37°C for 20 min. Enzymatic degradation was stopped by adding CO_2-independent medium supplemented with 5 U/ml RNase-free DNase (RQ1 RNase free DNase, M6101, Promega), after which mechanical cell separation was performed under a stereoscopic microscope. Mesenchymal and epithelial cells from one to five embryos were used to reach high enough RNA yields.

4.2.12 *In vivo* cell proliferation assay (II)

Cell proliferation in developing lung at E13.5 was assayed by detecting incorporation of 5-bromo-2-deoxyuridine (BrdU) in S phase of cell cycle. BrdU (Sigma) was injected into a timed pregnant mouse intraperitoneally. Mice were sacrificed and embryos were harvested four hours post injection. The embryos were fixed in formalin overnight and embedded in paraffin. BrdU positive cells were then detected using anti-BrdU antibody (Cell Signaling Technology).

4.2.13 Whole-mount immunohistochemistry and optical tomography scanning (II)

Sample processing and whole-mount immunohistochemistry of dissected embryonic lungs at E11.5-E15.5 were performed as described previously (Alanentalo *et al.*, 2007). Briefly, 4% paraformaldehyde fixed lungs were dehydrated with methanol followed by rehydration and processing to immunohistochemical staining. Localisation of anti-E-cadherin (Cell Signaling Technology) was detected either by fluorescently labelled secondary antibody conjugated to Alexa-Fluor-594-conjugated anti-rabbit IgG (Life Technologies/Thermo Fisher Scientific Inc.) or visualized by using the chromogenic DAB substrate (Immunologic) following the incubation with poly-HRP-conjugated anti-rabbit IgG antibody (Immunologic). Fluorescently labelled lungs were processed for optical projection tomography (OPT) scanning as described previously (Alanentalo *et al.*, 2007) including sample clearance with mixture of two parts of benzyl benzoate and one part benzyl alcohol, and scanned using a Bioptonics OPT 3001M Scanner. Chromogenically-stained samples were imaged using a Leica MZFLIII stereomicroscope (Leica) and Colorview camera (Software imaging system).

4.2.14 *In situ* hybridization (II)

The *in situ* hybridisation assay for the E14.5 embryonic sagittal paraffin sections was performed according to the standard protocol using probes labelled with 35[S]-UTP. The mouse *EphA3* probe covered an 817-bp fragment ranging from nucleotide 658 to 1474. The gene-specific fragment was inserted into pGEM-3Zf- vector. The mouse Efna1 probe covered a 402-bp fragment ranging from nucleotide 20 to 421 also inserted into pGEM-3Zf. After image acquisition dark-field images were inverted, linearly thresholded and combined with bright field images in Adobe Photoshop CS6 (Adobe Systems Software).

4.2.15 Image analysis (II, III)

All mouse lung tumour analyses were performed under the guidance of an expert pathologist. For the tumour burden analysis, whole slide scans of the H&E stained mouse lung sections were analysed using the structure based detection solution in Tissue Studio Image Analysis solution of the Definiens Developer XD 64 2.1 software (Definiens). For the quantitation of PAS or immunohistological stainings whole slide scans were analysed with marker or nuclear detection solution in the Tissue StudioTM image analysis solution of the Definiens Developer XD 64 2.1 software (Definiens). The three-dimensional (3D) visualization and branch end point analysis of the embryonic

mouse lungs was perfomed with Imaris 3D and 4D data software, using the Filament analysis function (Bitplane AG).

4.2.16 Comparative gene expression analysis (III)

Differentially expressed genes from the Illumina Mouse WT-6 version 2 expression array (Illumina, GEO, accession no. GSE69552) were compared with publically available gene expression data from NCBI-GEO (http://www.ncbi.nlm.nih.gov/geo/) database. $p < 0,01$ and $logFC > 1$ were used as cut-off values in the analysis. Venn diagrams comparing the lists of differentially expressed genes were generated with Venny 2.0.2 (http://bioinfogp.cnb.csic.es/tools/venny/) using ENSEMBL GENE IDs as gene identifiers.

4.2.17 Statistical analysis (I, II, III)

All numerical values are represented as mean +/- standard deviation (s.d.). Statistical significance was determined using two-tail student's t-test assuming equal variance between the datasets in all studies except in the survival curve analysis (study III), where a Gehan-Breslow-Wilcoxon Test was used.

5 Results and discussion

5.1 *EPHA3* has functions characteristic of a tumour suppressor (I)

As shown for the PTEN tumour suppressor, to prevent oncogenic transformation, nontransformed mammalian cells can activate in-built cellular checkpoints in response to loss of a tumour suppressor (Chen et al., 2005). This concept was used to identify putative, new tumour suppressors in an siRNA screen for cellular senescence. The screen utilised retinal pigmented epithelial cells (RPE) immortalised with human telomerase (hTERT). These cells model key aspects of nontransformed epithelial cells, including dormancy and normal expression of G0 markers, and the presence of primary cilia. hTERT-RPE1 cells were engineered to express a doxycycline-inducible *TP53* shRNA to identify proteins which specifically relied on the p53 pathway in their mechanism of action. The primary screen included 862 siRNA pools targeting kinases and proteins predicted to influence kinase signalling. Using proliferation marker Ki67, nuclei count, and size as readouts, the screen identified 16 primary candidates as regulators of cellular senescence (**I**, Fig. 1A & B).

A secondary screen using SA-β-gal as the readout confirmed 12 out of the initial 16 candidates (**I**, Fig. 1C). These 12 hits, namely *AURKA*, *CDK1*, *CSNK1A1*, *EPHA3*, *KSR2*, *LATS1*, *MAP2K3*, *MAP4K1*, *MYLK*, *NEK1*, *PIK3C2A*, and *SMG1* were studied further to determine the underlying senescence-associated pathways linked to their loss. The Arf-p53-p21 pathway was examined by measuring the levels of both p53 and p21 proteins subsequent to the siRNA-mediated gene expression knockdown of the senescence hits. Results indicated that the senescence phenotype detected after the silencing of the identified hits indeed correlated with p53-p21 activation (**I**, Fig. 2A). Dependency on p53 activation was further supported by the increased total cell numbers and percentages of proliferating cells after shRNA mediated *TP53* silencing in all 12 cases (**I**, Fig. 2B & C). In addition, DNA damage responses detected by γ-H2AX foci formation were seen in all cases but one (*PIK3C2A*) (**I**, Fig. S3). In the specific cases of *MYLK*, *MAP2K3*, *NEK1*, *EPHA3*, and *SMG1*, elevated levels of CDKI $p16^{INK4a}$ mRNA were also detected (**I**, Fig. 2D). Thus, the screen identified 12 putative tumour suppressors, of which loss-induced senescence was associated with activation of well-known cell cycle arrest pathways.

To further validate the tumour suppressive characteristics of the senescence hits, a genomic copy number analysis using SNP array-CGH from 53 panels of human tumours and cell lines was performed. The analysis identified significant loss in copy number in

the loci of the senescence hits throughout the studied data sets, thus supporting their tumour suppressive role (**I**, Fig. 3).

The senescence gene hits were grouped into three functional categories: (1) regulators of accurate mitotic cell cycle progression and cytokinesis, DNA damage signalling and the spindle assembly checkpoint: *AURKA*, *CDK1*, *CSNK1A1*, *LATS1*, *NEK1*, *SMG1*, (2) regulators of adhesion and migration: *EPHA3*, *MYLK*, *PIK3C2A*, and (3) regulators of growth factor-induced mitogenic signalling via p38 stress-activated protein kinases (SAPK) and jun amino-terminal kinases (JNK) pathways: *KSR2*, *MAP2K3*, *MAP4K1*.

An interesting hit in the senescence screen was *EPHA3*, a member of the large EPH RTK family generally known to control cell sorting and tissue patterning via cell attraction and repulsion (Pasquale, 2008). Several cancer sequencing studies have reported point mutations in *EPHA3*, with mutations particularly pronounced in lung and colorectal primary tumours (5,8% and 3% respectively, Catalogue of Somatic Mutations In Cancer). Thus, we decided to concentrate our studies on the functional validation of the tumour suppressive role of EPHA3.

5.1.1 Loss of EPHA3 receptor signalling confers p16^{INK4A}- and p53-dependent senescence

The human EPH receptor family includes nine EPHA receptor members (EPHA1–8 and EPHA10) (Gucciardo *et al.*, 2014). We first sought to determine if senescence induced by the loss of *EPHA3* was unique among the EPHA receptors expressed in hTERT-RPE1 cells, i.e *EPHA1*, *EPHA2*, *EPHA4*, and *EPHA5* in addition to *EPHA3*. One of the characteristics of senescent cells in 2D cell culture conditions is a flattened cell morphology and enlarged nuclear size (Mitsui and Schneider, 1976). We used hTERT-RPE1 cells stably expressing GFP-tagged histone H2B to monitor the number and size of the nuclei in 12 hours intervals for a total time of 132 hours. Both the nuclear size and the cell number after 132 hours of monitoring indicated cellular senescence in cells exposed to *EPHA3*, but not to *EPHA1*, *EPHA2*, *EPHA4*, or *EPHA5* silencing. This was further confirmed with SA-β-gal staining (**I**, Fig. S5A &B).

As *EPHA3* was among the putative tumour suppressor hits, the silencing of which led to regulation of p53 protein and p16^{INK4a} mRNA levels (**I**, Fig. 2A & D & S5C), we next asked if the senescence phenotype induced by *EPHA3*-loss was dependent on these senescence-regulating tumour suppressors. We used the same readout as for the EPHA receptor-associated senescence detection, namely nuclear count and size of hTERT-RPE1 cells stably expressing GFP histone H2B. The silencing of either *TP53* or *p16^{INK4a}* together with *EPHA3* resulted in partial rescue of the senescence phenotype indicating that *EPHA3*-loss induced senescence is dependent on both p53- and p16^{INK4a} -mediated signalling (**I**, Fig. 4A & B). This observation suggests that the putative tumour promoting effects of *EPHA3*-loss possibly require additional alterations in genes

functioning in these key senescence-inducing tumour suppressor pathways. Our initial search using the CONAN CGP copy number analysis tool (Sanger Institute) for co-occurrence of *p16^{INK4a}* mutations with *EPHA3* copy number loss, did not detect enrichment between these two genetic alterations. However, recent molecular profiling of lung ACs has delivered large amounts of new data, enabling deeper *in silico* analyses of genetic alterations and their co-occurrence {Cancer Genome Atlas Research, 2014 #165. Indeed, mutations in *TP53* showed statistically significant (p-value: 0,005, depicted from cBioportal) co-occurrence with genetic alterations (point mutations or copy number variation) in *EPHA3* (Cancer Genome Atlas Research, 2014; Cerami *et al.*, 2012). Taken together, these results established *EPHA3* as a regulator of cellular senescence in nontransformed epithelial cells and highlighted its role as a putative tumour suppressor. Moreover, the results clearly linked known senescence activators, p53 and p16^{INK4a}, to loss of *EPHA3*-induced senescence, suggesting possible interplay between these pathways during tumourigenesis (Figure 9A). However, the exact mechanism remains still to be elucidated.

5.1.2 EPHA3 cancer mutations cause loss of kinase function, supporting its tumour suppressive role

Our finding that *EPHA3*-loss confers p53- and p16^{INK4a}-dependent senescence led us to further investigate its tumour suppressive role. At this time in our study, several cancer sequencing studies had reported point mutations in EPHA3, with one of the highest incidence seen in lung ACs (up to 16%) (Cerami *et al.*, 2012; Imielinski *et al.*, 2012). In support of its tumour suppressive role, *EPHA3* mutations are spread along the protein rather than clustered in hot spots as seen in known oncogenes such as *KRAS*. Thus, we decided to study the effect of selected EPHA3 cancer point mutations. We hypothesised that reduced autophosphorylation activity of the receptor caused by the mutations would support a putative tumour suppressor function of *EPHA3*.

We selected nine EPHA3 cancer point mutations and created hTERT-RPE1 and 293T Flp-In cell lines stably expressing these variants tagged with a localisation and affinity purification (LAP)-tag. The selected mutations were located in different protein domains of EPHA3 (**I**, Fig. 5A). The mutations located in the extracellular part of EPHA3 included T166N situated in the LBD, M269I in the cysteine rich domain (CRD), and N379K and D446Y in the fibronectin-type-III repeats (FN-III 1 and FN-III 2). These mutations were detected in primary lung ACs (Ding *et al.*, 2008). Four mutations, R728L, K761N, G766E, D806N were located in the tyrosine kinase domain of EPHA3. Two of these, R728L and K761N, were reported in primary lung ACs (Ding *et al.*, 2008), G766E in a lung cancer cell line (Davies *et al.*, 2005) and D806N in colorectal cancer (Bardelli *et al.*, 2003). One mutation, T933M, located in the sterile α motif (SAM) of the intracellular part of EPHA3, and had been reported in lung cancer (Wood

et al., 2006) (see illustration of the selected mutations and their locations in EPHA3 protein in Figure 9B).

To study the cellular activation capacity of the selected EPHA3 mutation variants, we treated 293T cells expressing the tagged EPHA3 variants with pre-clustered recombinant ephrin-A5 protein. The autophosphorylation of EPH receptors is a prerequisite for their forward downstream signalling (Binns *et al.*, 2000). Thus, by monitoring the autophosphorylation status, we aimed to study the effect of the selected EPHA3 cancer variants on EPHA3 activity. As reported previously (Nievergall *et al.*, 2010), the activation status of EPHA3 detected by phosphotyrosine rose rapidly and was detected already 2 min after ephrin-A5 treatment. The activation level of wild-type (wt) EPHA3 peaked at 20 min after ephrin-A5 addition and decreased back to normal levels at 60 min. Two kinase domain mutation variants, G766E and D806N, showed a clear reduction in the ephrin-A5 induced activation status of EPHA3 (**I**, Fig. 5B).

To further confirm the effect of EPHA3 cancer mutations, we performed *in vitro* kinase assays in which tagged EPHA3 variants were incubated with excess of ATP to induce autophosphorylation. Again, kinase domain mutation variants G766E and D806N showed decreased activation (**I**, Fig. 5C). Additionally, one kinase domain mutation, R728L, showed a reduction in overall receptor levels (**I**, Fig. 5B & C, S6A, B & C). These results were in line with two other studies addressing the functional effect of EPHA3 cancer mutations (Lisabeth *et al.*, 2012; Zhuang *et al.*, 2012). The only exception was the EPHA3 kinase domain K761N mutation, as our results did not detect a decrease in its phosphorylation level, opposing results by Pasquale and colleagues (Lisabeth *et al.*, 2012). This difference may be a result of the methodologies used; we expressed variants from a single genome-integrated copy (Flp-In system) to more closely mimic endogenous receptor function.

The crystal structure of the juxtamembrane and kinase domain (JMKIN) of wild-type EPHA3 has been characterised (Davis *et al.*, 2008). This enabled us to analyse structural changes caused by the EPHA3 point mutations and find possible explanations for the decreased EPHA3 activity and expression levels. We found that mutation of arginine 728 to leucine shifts the surface charge of EPHA3 from positive to non-charged, possibly leading to altered protein-protein interactions and decreased expression level. Moreover, mutation of residue 806 from aspartic acid to asparagine suggested altered interaction with residues aspartic acid recidue 746 and histidine 744. These residues face the ATP binding pocket, thus possibly affecting EPHA3 receptor tyrosine kinase activity (**I**, Fig. 5D & E). The crystal structure surrounding G766 was disordered, impeding analyses of the effect of G766E mutation. Interestingly, structural alignment of the kinase domain of EPHA3 with the tumour suppressor LKB1 identified a common mutation site in these two kinases (D806 and D237, respectively). LKB1 D237Y mutation had been reported in primary AC (Ding *et al.*, 2008). We therefore analysed the kinase activity of the EPHA3 D806Y variant to mimic LKB1 D237Y, and showed that this lost its kinase activity (**I**, Fig. 5F & G). Taken together, our structural analysis suggested that the EPHA3 cancer mutations possibly alter protein-protein interactions and direct connections with kinase domain structural determinants.

The regulation of EPHA3 phosphorylation and endocytosis has been shown to be controlled by protein tyrosine phosphatase 1B (PTP1B). This was shown to be dependent on the EPHA3 kinase domain, as no interaction between EPHA3 and PTP1B was detected in cells expressing a kinase domain deletion mutant of EPHA3 (Nievergall *et al.*, 2010). However, we did not detect any defects in cellular internalisation upon ephrin-A5 activation of the studied EPHA3 cancer mutations (**I**, Fig. S7), indicating that the internalisation is independent on the autocatalytic capacity of EPHA3, and suggesting that PTP1B binds the full kinase domain. Indeed, only the EPHA3 mutants lacking the cytoplasmic domain or kinase domain showed absence of interaction with PTP1B, whereas EPHA3 mutated at the essential juxtamembrane and activation loop tyrosines showed marginal interaction with PTP1B (Nievergall *et al.*, 2010).

EPHA3 cancer mutation variants that failed to show a decrease in autophosphorylation or total receptor levels may still confer alternative EPHA3 inactivating effects, for example via altering ephrin binding or cellular trafficking. In support of these alternative mechanisms, a study by Pasquale and colleagues showed that two of the extracellular domain mutations situated in the LBD (T166N), and in CRD (M269I) decreased the ephrin-A5 binding capacity of EPHA3 (Lisabeth *et al.*, 2012). This was shown with ephrin-A5 Fc immobilised on sepharose beads. Moreover, the EPHA3 FN-III 2 lung cancer mutation G518L has been shown to enhance cis interaction of EPHA3 with co-expressed ephrin-A3, possibly inhibiting EPHA3 activation via decreasing its interaction with ephrins in trans (Falivelli *et al.*, 2013).

Together, these results indicate that EPHA3 cancer mutations confer loss of EPHA3 activity via multiple mechanisms, one of them being loss of the autocatalytic capacity (Figure 9B). Moreover, EPHA3 agonist or ligand-induced EPHA3 activation in glioblastoma, neural precursors or in lung cancer cell lines leads to reduced cell proliferation, increased cell differentiation, or apoptosis, respectively (Aoki *et al.*, 2004; Day *et al.*, 2013; Zhuang *et al.*, 2012). This further supports the tumour suppressive role of EPHA3. EPHA3 has also been shown to have kinase activity independent tumour promoting functions linked to maintenance of tumour cells in an undifferentiated and cancer stem cell-like state, as evidenced in glioblastoma (Day *et al.*, 2013). However, the dual functions of EPHA3 in tumour suppression and promotion do not prohibit targeting of EPHA3 as monoclonal antibody treatment shown to activate EPHA3 leads to apoptosis and prevents tumour cell proliferation in *in vitro* cultured glioblastoma cells or grafted tumours (Day *et al.*, 2013), suggesting that targeted EPHA3 treatment could be effective in cancer cases showing elevated EPHA3 levels, but absence of EPHA3 inactivating and dominant negative mutations.

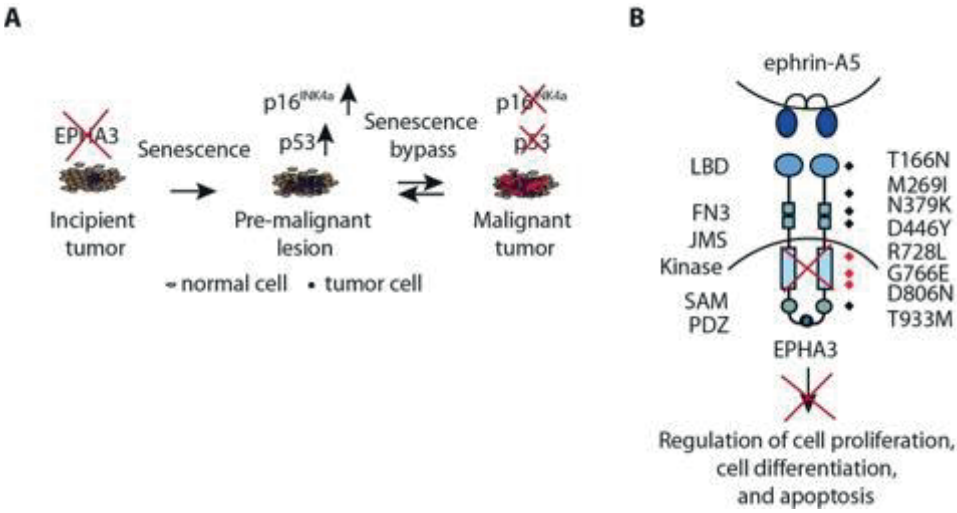

Figure 9. *EPHA3* demonstrates characters of a tumour suppressor (A) Proposed model for loss of *EPHA3* induced OIS. (B) Selected cancer point mutations of EPHA3 cause receptor inactivity possibly altering the tumour suppressive functions of the wild-type EPHA3. The EPHA3 protein contains an N-terminal ligand-binding domain (LBD), two fibronectin type-III repeats (FN3), a single-pass transmembrane domain (TM), an intracellular region containing a juxtamembrane region, a tyrosine kinase domain (Kinase), a sterile α motif (SAM), and a postsynaptic density protein PSD95, Drosophila disc large tumor suppressor DlgA, and zonula occludens-1 protein ZO-1 (PDZ)-binding motif.

5.2 EPHA3 fails to demonstrate a tumour suppressive role in the murine lung (II)

Our results from the cellular senescence screen and subsequent functional EPHA3 cancer mutation analysis indicated that *EPHA3* may act as a tumour suppressor. We therefore decided to investigate the *in vivo* tumour suppressive role of EPHA3 using a previously reported *EphA3* constitutive knock out model, with which a crucial role of *EphA3* in embryonic heart development has been established. 75% of the *EphA3*-null mice were reported to die at birth due to cardiac abnormalities including defects in the development of their atrial septa and atrioventricular endocardial cushions (Stephen *et al.*, 2007; Vaidya *et al.*, 2003). As *EPHA3* mutations are frequently found in lung cancers we decided to study the putative functional role of EPHA3 during murine lung tumourigenesis.

5.2.1 Constitutive loss of *EphA3* does not accelerate mutant *Kras*-driven lung tumourigenesis

To test the hypothesis that EPHA3 functions as a tumour suppressor in murine lung tumourigenesis, we used a constitutive knock out mouse model of *EphA3* generated by Brown and colleagues (Stephen *et al.*, 2007; Vaidya *et al.*, 2003). Monitoring of *EphA3*-heterozygous and -null mice for an approximate one year period showed no reduced survival due to lung tumour formation (data not shown), indicating that EPHA3-loss on its own does not initiate lung tumourigenesis. Similar results have been shown for the known lung tumour suppressors *LKB1* and *PTEN*, as their loss is not sufficient to initiate lung tumourigenesis in mice. However, conditional *Pten*- and *Lkb-1*-loss together with activation of oncogenic *Kras* in murine lungs accelerates *Kras*-driven lung tumourigenesis (Iwanaga *et al.*, 2008; Ji *et al.*, 2007a). We thus next asked if loss of *EPHA3* might modulate oncogene-induced lung tumourigenesis. Lung cancer mutations in *EPHA3* show an occasional, albeit not statistically significant co-occurrence with *KRAS* mutations (**II**, Fig. S1A) (Cancer Genome Atlas Research, 2014; Cerami *et al.*, 2012). We therefore crossed the *EphA3*-null mice with mice carrying a conditional G12D *Kras* mutation allele ($Kras^{LSL\text{-}G12D/+}$) (Jackson *et al.*, 2001). The activation of oncogenic *Kras* in epithelial cells was induced by intranasal delivery of adenovirus expressing Cre-recombinase (Ad5-CMV-Cre). The efficacy of each infection was monitored with a dual fluorescence $Rosa26^{mT/mG}$ Cre-reporter strain (**II**, Fig. S1B) (Muzumdar *et al.*, 2007). $Kras^{LSL\text{-}G12D/+}$;$EphA3^{+/+}$ (n=9), $Kras^{LSL\text{-}G12D/+}$;$EphA3^{+/-}$ (n=16), and $Kras^{LSL\text{-}G12D/+}$; $EphA3^{-/-}$ (n=8) mouse cohorts were monitored for 19 weeks, a time period which was selected based on initial condition monitoring of the mice. Tumour burden analysis was performed with H&E-stained lung paraffin sections representing two separate regions of the mouse lungs. This showed no difference between the $Kras^{LSL\text{-}}$

$^{G12D/+}$;*EphA3*$^{+/+}$, *Kras*$^{LSL\text{-}G12D/+}$;*EphA3*$^{+/-}$, and *Kras*$^{LSL\text{-}G12D/+}$;*EphA3*$^{-/-}$ cohorts (average tumour/lung ratio 19,7%, 16,1%, and 18,5%, respectively) (**II**, Fig. 1A & B, S1C). Furthermore, no shift in the tumour histopathology was detected, and all tumours were positive for the AC marker NKX2-1 and negative for the SCC marker p63 (**II**, Fig. 1C).

5.2.2 Constitutive loss of *EphA3* does not accelerate *Trp53*-loss-driven lung tumourigenesis

Our *in vitro* results showing loss of *EPHA3*-induced, and p53 and p16^{INK4a} dependent senescence (**I**, Fig. 4B), suggested possible cooperation between alterations in these genes during tumourigenesis. Mutations in *TP53* show statistically significant co-occurrence with genetic alterations (point mutations or copy number variation) in *EPHA3* in human lung ACs {Cerami, 2012 #168}(Cancer Genome Atlas Research, 2014). We therefore decided to test if loss of *EphA3* would alter loss of *Trp53*-driven lung tumourigenesis. As *Trp53*-loss on its own leads to lung tumourigenesis with a long latency (350–530 days) (Meuwissen *et al.*, 2003), we decided to monitor the *Trp53*$^{fl/fl}$;*EphA3*$^{+/+}$ (n=7), *Trp53*$^{fl/fl}$;*EphA3*$^{+/-}$ (n=11) and *Trp53*$^{fl/fl}$;*EphA3*$^{-/-}$ (n=13) cohorts for 15 months (450 days) following intranasal delivery of Ad5-CMV-Cre. At 15 months, three mice had died due to AC formation. These included two *Trp53*$^{fl/fl}$;*EphA3*$^{+/+}$ mice and one *Trp53*$^{fl/fl}$;*EphA3*$^{-/-}$ mouse. Analysis of the remaining mice without any signs of reduced condition in all three cohorts at 15 months post infection, showed absence of lung tumourigenesis. These results suggest that loss of *EphA3* does not cooperate with loss of *Trp53* in murine lung tumourigenesis (**II**, Fig. 1D).

Taken together, our results from the murine lung tumourigenesis studies showed that constitutive loss of *EphA3* does not alter oncogenic *Kras*- or *Trp53*-loss driven lung tumourigenesis. This might be due to compensating effects by the other lung expressed Eph receptors, thus distinguishing the used method of constitutive loss of *EphA3* from the sporadically occurring human lung cancer mutations. Alternatively, it is possible that other EPH receptors instead of *EphA3* are functionally important in murine lung tumourigenesis. Indeed, a recent study exploring genetic alterations in mouse SCLC driven by loss of *Trp53* and *Rb1* revealed recurrent somatically acquired *EphA5* and *EphA7* mutations (McFadden *et al.*, 2014). Furthermore, a recent *in vivo* shRNA screen identified *EphA2* as a tumour suppressor cooperating with oncogenic *Kras* in promoting murine lung AC (Yeddula *et al.*, 2015), suggesting that these Eph receptors, rather than *EphA3*, may modulate murine lung tumourigenesis (Figure 10).

The senescence induced by *EPHA3*-loss was dependent on both p53 and p16^{INK4a}. However, our study did not address the possible effect of *EphA3*-loss together with combined loss of *Trp53* and *p16*^{INK4a} shown to lead to low tumour multiplicity and high frequency of fatal pulmonary haemorrhage (Ji *et al.*, 2007a). Therefore, it remains

possible that loss of *EphA3* may accelerate *Trp53*- and $p16^{INK4a}$-loss induced lung tumourigenesis.

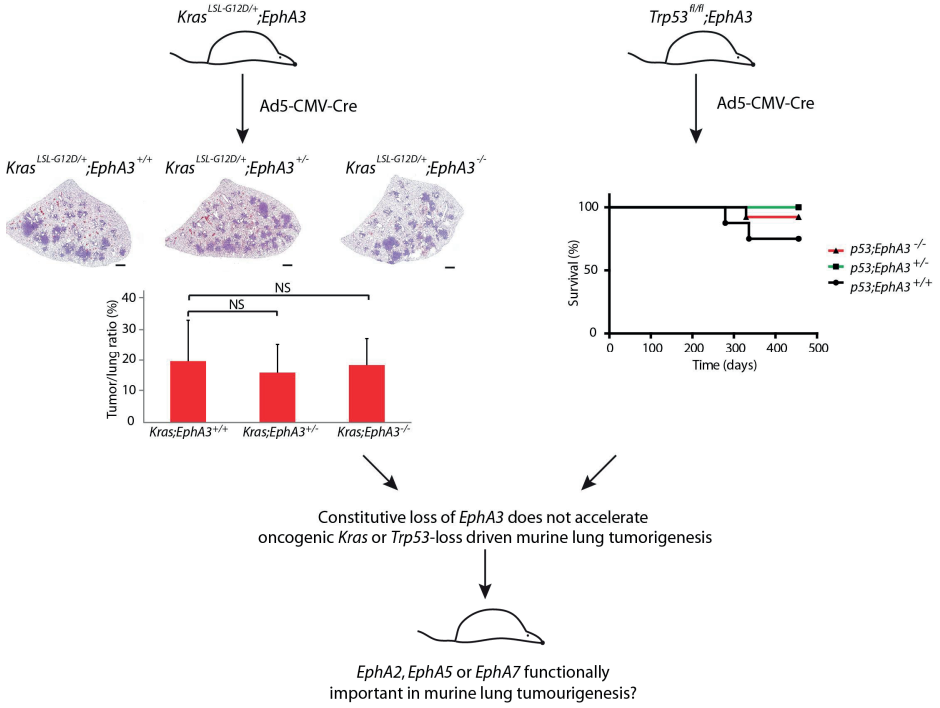

Figure 10. *EphA3* fails to demonstrate tumour suppressive role in murine lung tumourigenesis driven by oncogenic *Kras* and *Trp53*-loss. This suggests possible murine lung tumourigenesis specific functional importance of other Eph receptors such as *EphA5* and *EphA7*, which were recently found to be somatically mutated in murine SCLC (McFadden et al., 2014) or *EphA2* which was recently found to cooperate with oncogenic *Kras* in murine lung AC progression (Yeddula *et al.*, 2015).

5.3 The role of EPHA3 in lung morphogenesis (II)

EPH receptors play important roles in embryonic development, controlling tissue boundaries and patterning (Nievergall *et al.*, 2012). *EphA3* also plays a critical role in embryogenesis, with 75% of *EphA3*-null mice showing increased perinatal mortality due to defects in cardiogenesis. Perinatally mortal *EphA3*-null mice have enlarged, blood-filled atria and almost absent atrial septum. This is caused by hypoplastic endocardial cushions, a specific mesenchymal cell layer derived from endocardium via EndMT (Stephen *et al.*, 2007).

Despite the well-established role of EPHs and ephrins in embryonic development, still relatively little was known about their role in lung development. Ephrin-B2 is linked to alveolar epithelial and endothelial cell viability and vascular growth in hyperoxic rats (Vadivel *et al.*, 2012). shRNA-mediated *in vivo* silencing of *Efnb2* (coding ephrin-B2) during the postnatal stage of alveolar development in rats resulted in defects in alveolar and vascular growth. $Efnb2^{LacZ/6YFDV}$ mice, which expresses a truncated ephrin-B2 incapable of reverse signalling, showed reduced elastic properties of lungs indicating a link between ephrin-B2 and pulmonary compliance in mice (Bennett *et al.*, 2013). Important regulators of lung morphogenesis such as *Fgf9* and *Nkx2-1* have been functionally implicated in lung tumourigenesis. Thus, we decided to investigate the possible role of *EphA3* in murine lung development, aiming to elucidate functional mechanisms, which could be translated to lung tumourigenesis.

5.3.1 *EphA3* is expressed in the distal mesenchyme of the developing lung

To investigate the localisation of *EphA3* expression in embryonic lungs, we analysed the expression profile of *EphA3* mRNA and protein expression during the pseudoglandular stage of lung development. We first performed an *in situ* hybridisation analysis using radiolabeled probe against the *EphA3* nucleotide sequence ranging from 658 to 1474, on sagittal sections of wt and *EphA3*-null embryos at E14.5. This revealed a distal mesenchymal expression pattern of *EphA3* mRNA in wt embryos confirmed by the absence of the signal in *EphA3*-null embryos (**II**, Fig. 2A). We then analysed the EPHA3 protein expression using a commercial polyclonal rabbit anti-EPHA3 antibody, at three different time points of the pseudoglandular stage, E11.5, E13.5, and E15.5. In all time points, EPHA3 was detected in the distal mesenchyme of the embryonic lungs (**II**, Fig. 2B & S1D). This was further confirmed by a Q-PCR-based expression analysis of dissected embryonic lung epithelium and mesenchyme, interestingly showing highest expression at E13.5 (**II**, Fig. 2C & 3A). The expression of *EphA3* correlated with the known mesenchymal expression pattern of *Fgf10* and *Cd31* (official gene symbol

Pecam1), and opposed the epithelial expression of *Cdh1* and *Nkx2-1* in the epithelium- and mesenchyme-specific Q-PCR expression analysis (**II**, Fig. 3B & S2A).

We next asked if the expression of *EphA3* in the developing lung mesenchyme was unique among other Eph receptors. We analysed the expression patterns of selected EphA receptors, namely *EphA1*-*EphA5* and *EphA7*, as well as selected ephrins at E11.5, E13.5, and E15.5. Our Q-PCR expression analysis at E13.5 and E15.5 confirmed the reported epithelial expression of *Efnb2* encoded ephrin-B2 (data not shown) (Bennett *et al.*, 2013). *EphA1* and *EphA5* were absent in both epithelium and mesenchyme at all three time points whereas *EphA2*, *EphA4*, and *EphA7* showed a low to medium level of expression in the epithelium. *EphA4* showed a low and *EphA7* a medium level of expression in the mesenchyme, but *EphA3* was the only Eph receptor with restrictive expression in the embryonic lung mesenchyme. Of note, no change in the expression of *EphA7* was detected in *EphA3*-heterozygous or -null lungs (**II**, Fig. S2B). When we compared the expression levels of adult mouse lung to embryonic lung mesenchyme at E13.5, only expression of *EphA2* and *EphA4* was detected in the adult lung. This may suggest a negligible role for *EphA3* in postnatal lung homeostasis, and may thus explain the absence of the discernible effect of EphA3 on murine lung tumorigenesis (**II**, Fig. S3A & B). *Efna1* (encoding ephrin-A1) and *Efna5* (endoding ephrin-A5) showed medium and very low expression in the development lung epithelium, respectively, suggesting that ephrin-A1 is the primary ligand for EPHA3 in the developing lung (**II**, Fig. 3B). Epithelial expression of *Efna1* was confirmed by *in situ* hybridisation assay using a probe against the Efna1 nucleotide sequence ranging from 20 to 421 (**II**, Fig. S2C).

Together, these results showed, for the first time, the expression of *EphA3* in the developing lung and its expression restricted to the lung mesenchyme was a unique expression patter among the studied EphA receptors. Since the expression was found specifically during the pseudoglandular stage, during which the epithelial branching takes place, we hypothesised that EPHA3 may play role in this process. Alternatively, given that the pulmonary vasculature develops in parallel to the branching epithelia and one of the well-established roles of EPHs is control of vascular development (Gerety and Anderson, 2002; Nievergall *et al.*, 2012) we hypothesised that EPHA3 may control development of the pulmonary vasculature.

5.3.2 *EphA3* loss is associated with altered expression of branching morphogenesis and vasculogenesis genes

To first investigate if expression of epithelial or mesenchymal genes are altered due to the loss of *EphA3*, we measured the mRNA expression levels of known regulators of lung morphogenesis in these two tissue compartments. This was done with epithelial and mesenchymal cells dissected from the lungs of wt, *EphA3*-heterozygous and -null embryos, at E11.5, E13.5, and E15.5 (**II**, Fig. 3A). Q-PCR-based expression analyses

showed a small but statistically significant increase in the expression of *Nkx2-1* in the epithelium of the *EphA3*-heterozygous embryonic lungs at E13.5 when compared with wild-type tissue. This was accompanied with a similar increase in endothelial *Cd31* and mesenchymal *Fgf10* measured from the mesenchymal cell fraction of E13.5 *EphA3*-heterozygous embryonic lungs (**II**, Fig. 3C). Both *Nkx2-1* and *Fgf10* are key regulators of lung morphogenesis. *Nkx2-1* deletion in mice leads to unbranched lungs, causing prenatal mortality of the embryos (Kimura *et al.*, 1996) and *Fgf10*-null embryos display complete absence of lungs (Min *et al.*, 1998; Sekine *et al.*, 1999). Furthermore, the ectopic expression of *Fgf10* in lung development has been linked to prevention of proximal cell differentiation and promotion of basal cell fate (Volckaert *et al.*, 2013). Opposing expression patterns of epithelial *Nkx2-1* and mesenchymal *Fgf10* are detected early in lung development and interestingly, ectopic *Fgf10* expression is shown to induce ectopic expression of *Nkx2-1* in chicken embryonic lungs resulting (Sakiyama *et al.*, 2003). Thus, our observation that a small but significant change was detected in the expression of these two key regulators of lung morphogenesis suggested a possible role for *EphA3* in lung development. Additionally, the altered *Cd31* expression levels in endothelial cells of the developing mesenchyme suggested a possible effect on the development of pulmonary vasculature. Of note, we did not detect similar expression changes in the lungs of *EphA3*-heterozygous and -null embryos with age E15.5, indicating a dynamic role for *EphA3* in the possible regulation of these genes (**II**, Fig. S3C).

5.3.3 Constitutive loss of *EphA3* does not overtly affect murine lung morphogenesis

Our finding that *EphA3*-reduction has a small but significant effect on the expression levels of epithelial *Nkx2-1* and endothelial and mesenchymal *Cd31* and *Fgf10*, respectively, suggested a possible role for *EphA3* in lung morphogenesis and/or development of the pulmonary vasculature. To investigate if constitutive loss of *EphA3* affects lung branching morphogenesis, we analysed the branch end-points of the embryonic lungs at E13.5 by E-cadherin whole-mount immunohistochemistry staining and optical projection tomography (OPT). 3D image analysis-based branch end-point counting showed no difference between the wt (average 108), *EphA3*-heterozygous (average 113), and *EphA3*-null embryonic lungs (**II**, Fig. 4A & B). We also performed whole mount staining for E-Cadherin on lungs of embryos aged E11.5 and E15.5. Qualitative analysis of these embryonic lungs further confirmed that constitutive loss of *EphA3* does not lead to defects in lung branching morphogenesis (**II**, Fig. S3C).

Proliferation and differentiation of the pulmonary mesenchyme is coordinated by reciprocal signalling between the growing epithelia and the surrounding mesenchyme (Morrisey and Hogan, 2010). Therefore, we hypothesised that *EphA3*-loss could impair this interplay and possibly affect mesenchymal cell proliferation. We investigated the

effect of *EphA3*-loss on embryonic lung cellular proliferation of the distal mesenchyme at E13.5. We measured the percentage of distal mesenchymal cells in the S phase of the cell cycle by BrdU incorporation. No statistically significant change was measured in the amount of mesenchymal cells in S phase between wt (26%), *EphA3*-heterozygous (36%) or *EphA3*-null lungs (26%) (**II**, Fig. 4C).

Previous studies have established a role for EPHB4-ephrin-B2 signalling in vasculogenic development. *Efnb2* (gene encoding ephrin-B2) is expressed in arterial but not venous endothelial cells, whereas *EphB4* expression is detected in veins but not arteries. *Efnb2*-null embryos exhibit defects both in arteries and veins of the head and yolk sac, as well as in myocardial trabeculation (Wang *et al.*, 1998). Supporting the role of EPHB4 as a specific receptor for ephrin-B2 in vascular endothelial cells, mice carrying a mutation of *EphB4* have a similar phenotype as *Efnb2* null mice (Gerety *et al.*, 1999). Both EPHB4 and ephrin-B2 are also expressed in pulmonary arterial and venous vessels during the pseudoglandular stage of lung development (Schwarz *et al.*, 2009). As *EphA3* was expressed in the distal mesenchyme of the developing lung, we hypothesised that its loss may affect pulmonary vasculogenesis, as evidenced with both ephrin-B2 and EphB4 loss. To test this, we qualitatively analysed CD31 positive pulmonary endothelial cells at E13,5. Again, no difference in the amount nor in the localisation of CD31 positive endothelia was detected when comparing wt, *EphA3*-heterozygous or *EphA3*-null lungs (**II**, Fig. 4D).

Taken together, our study identified *EphA3* expression to be restricted to the mesenchyme, a unique pattern for the developing lung-expressed Eph receptors (Figure 11A). However, in contrary to our hypothesis based on the small but significant expression changes in epithelial *Nkx2-1*, mesenchymal *Fgf10* and endothelial *Cd31* in *EphA3*-heterozygous embryonic lungs, *EphA3* failed to demonstrate a critical role in lung epithelial branching, mesenchymal cell proliferation, or in the abundance and localization of CD31 positive endothelia. This can be explained by at least two phenomenon. First, partial penetrance of the *EphA3*-null genotype reported in the original analysis of *EphA3*-null mice (Vaidya *et al.*, 2003), which we confirmed by monitoring the viability of *EphA3*-null pups and subsequent macroscopic inspection, could explain why no overt difference was detected in the comparison between the wt and *EphA3*-null embryos at the studied time points. Secondly, functional redundancy between lung-expressed EphA receptors could explain the negative results observed in the lung morphogenesis analysis of *EphA3*-heterozygous and –null embryonic lungs (Figure 11B). Indeed, a recent study suggested possible functional compensation between *EphA3*, *EphA4*, and *EphA7*, all co-expressed during embryonic palate development in mice (Agrawal *et al.*, 2014). Compound homozygous *EphA3*- and *EphA4*-loss did not lead to defective midfacial development, suggesting a possible functional compensation by *EphA7*. However, we did not detect any misexpression of mesenchymal *EphA7* at the studied time points (**II**, Fig. S2B), which indicates that possible *EphA3*-loss induced compensation by *EphA7* would not be mediated by transcriptional upregulation. *EphA3*, *EphA4*, and *EphA7* were still the EphA receptors

we observed to be coexpressed in the embryonic lung mesenchyme, though *EphA4* at very low levels, and EPHA4 functions as a receptor for ephrin-A1 (Jellinghaus *et al.*, 2013). In the future, *EphA3-Efna1* double knock out mouse model could elucidate the role of the EPHA3-ephrin-A1 axis in the lung morphogenesis. However, it is also possible that mesenchymal *Fgf10*, which expression was elevated in *EphA3*-heterozygous lung mesenchyme at E13,5, would compensate the loss of *EphA3*.

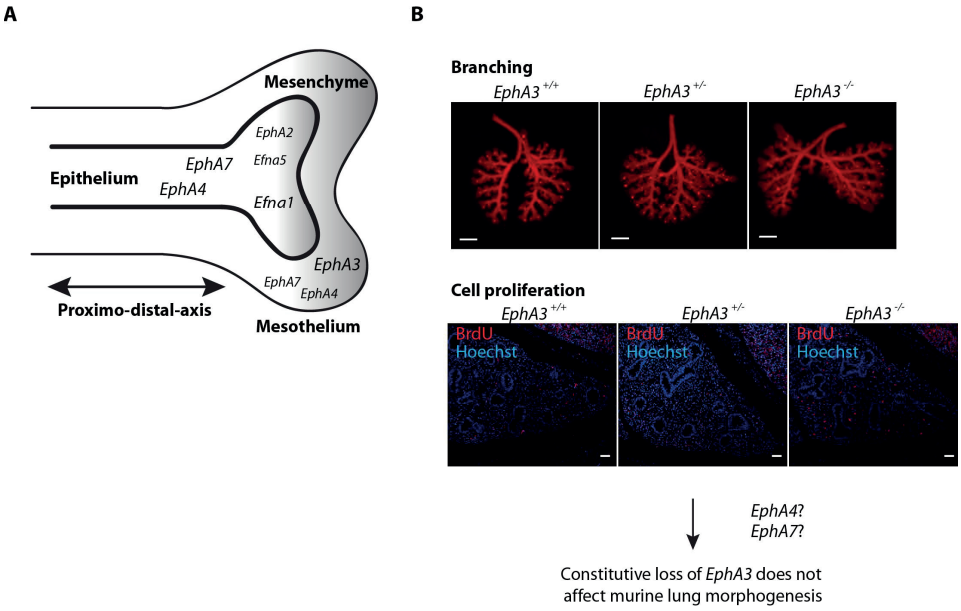

Figure 11. *EphA3* in murine lung development. (A) Ephs and ephrins found to be expressed during the pseudoglandular phase of murine lung development. Size of the text refers to the level of observed expression. (B) Constitutive loss of *EphA3* does not overtly affect murine lung morphogenesis. Despite the embryonic lung mesenchymal expression of *EphA3*, no alterations are seen in lung branching morphogenesis or cell proliferation of *EphA3* heterozygous or homozygous embryos at E13.5. This suggests possible redundancy between the lung-expressed Eph receptors including *EphA4* and *EphA7*. Scale bars 300 µm in E-cadherin whole-mount images and 100 µm in BrdU images.

5.4 Cell-of-origin links histopathology spectrum and immune microenvironment in mutant *Kras* and loss of *Lkb1* driven NSCLC (III)

NSCLC comprises a heterogeneous group of lung cancers, with a variety of prognostic and predictive characteristics including patient's performance score, clinical stage, and tumour histopathology. The three main tumour histopathology subclasses of NSCLC, namely AC, SCC, and LCC, all have been detected in murine GEMMs modelling human NSCLC. These studies have confirmed and revealed insights in human lung tumourigenesis, and have functionally connected the underlying genetic driver events to the development of specific histopathologies (Chen et al., 2014). Activation of oncogenic *Kras* (G12D) in $CC10^+$ airway cells, SPC^+ alveolar cells or BASCs positive for both CC10 and SPC and located at the BADJ, can induce lung ACs (Kim et al., 2005; Sutherland et al., 2014). However, the role of BASCs as cell-of-origin for oncogenic *Kras* driven ACs is somewhat controversial and would need further investigation (Kim et al., 2005; Sutherland et al., 2014). Similarly, contradictory results have been gained in studies initiating *Kras*-driven tumourigenesis from $CC10^+$ cells. Adenovirus mediated inflammation has been suggested to promote oncogenic *Kras*-driven tumourigenesis from $CC10^+$ cells (Mainardi et al., 2014). Also, whereas the CC10-CreER mediated induction of oncogenic *Kras* combined with heterozygous loss of *Trp53* in mouse lungs fails to lead to tumourigenesis (Xu et al., 2012), adenovirus mediated induction of the same genetic alterations in $CC10^+$ cells results not only tumourigenesis but also ACs with increased invasive and metastatic characters when compared to ACs derived from SPC^+ cells (Sutherland et al., 2014). Thus, these results suggest progenitor- or niche-specific dependency on microenvironmental factors during lung tumourigenesis.

While the progenitor-specific aetiologies for lung ACs are relatively well described, the influence of the cell-of-origin for SCC or more rare ASC histopathology is less clear. Airway basal cells have been proposed to act as SCC progenitors following loss of *Pten* with *Tgfbr2* or *Lkb1* (Malkoski et al., 2014; Xu et al., 2014a). Moreover, SPC^+ alveolar cells are shown to initiate ACs which transdifferentiate to SCCs via an ASC intermediate (Han et al., 2014). However, it is not yet known if the $CC10^+$ airway cells and SPC^+ alveolar cells exhibit differential propensities to originate SCCs or ASCs.

Lung cancer *in vivo* studies have revealed a critical role for *Lkb1*-loss in promoting oncogenic *Kras*-driven lung tumourigenesis towards more rapid tumour development (shorter latency), and generation of a wider spectrum of tumour histopathologies accompanied with frequent metastasis (Ji et al., 2007a). The transdifferentiation from ACs to SCCs during $Kras^{LSL\text{-}G12D/+}$;$Lkb1^{fl/fl}$ (KL) tumourigenesis, which has been mechanistically linked to modulation of tumour ECM and regulation of cell growth and apoptosis, as well as ROS and metabolic adaptation (Gao et al., 2014; Han et al., 2014; Li et al., 2015), possibly partly explains the wide spectrum of tumour histopathologies. The KL model is a particularly interesting model to study the role of cell-of-origin, because it develops a large variety of NSCLC histopathologies and therefore permits one

to ask if the role of *Lkb1*-loss differentially modulates oncogenic *Kras*-driven tumourigenesis depending on the progenitor. Thus, we decided to investigate if the cell-of-origin could contribute to the development of divergent histopathologies initiated by the expression of oncogenic *Kras* and *Lkb1*-loss.

5.4.1 Cell-of-origin defines survival and histopathology spectrum in NSCLC driven by mutant *Kras* and *Lkb1*-loss

To test how the cell-of-origin influences tumourigenesis driven by mutant *Kras* and *Lkb1*-loss, we analysed cohorts of KL mice (n=9) intranasally infected with adenoviruses expressing Cre-recombinase in a progenitor-restrictive manner, either under a CC10 or SPC promoter (Ad5-CC10-Cre and Ad5-SPC-Cre respectively). Crossing the KL mice to the Rosa26$^{mT/mG}$ strain (Muzumdar et al., 2007) enabled us to monitor the Cre expression activation in the lung epithelial cells. Analysis of the mGFP signal at 2-4 weeks post infection showed accurate bronchiolar and alveolar mGFP signal, respectively, correlating with previous findings (Sutherland et al., 2011) (**III**, Fig. S1A). The amount of Ad5-CC10-Cre (1x10^7 pfu) and Ad5-SPC-Cre (2.5x10^9 pfu) was adjusted based on their ability to achieve comparable infection rates. We followed both Ad5-CC10-Cre and Ad5-SPC-Cre infected KL mice until they showed signs of illness (breathing abnormalities and weight loss), at which time they were sacrificed. Interestingly, we observed a clear difference in the survival of mice in these two cohorts. Ad5-CC10-Cre infected KL mice showed a statistically significant (Kaplan-Meier survival analysis, p=0,0125, Gehan-Breslow-Wilcoxon test) shorter latency when compared to Ad5-SPC-Cre infected KL mice (median survival 79 and 120 days respectively) (**III**, Fig. 1A). This suggested that lung tumours which originate from CC10$^+$ lung epithelial cells grow and/or progress faster.

To address if the cell-of-origin defines the generation of tumour histopathology spectra in KL mice, we analysed Ad5-CC10-Cre and Ad5-SPC-Cre infected KL mice (n=5 in both cohorts) and quantitatively assessed the amount of each lesion type from full lung lobe sets of individual mice. Immunohistological staining for NKX2-1 and p63 was used to guide the histopathology classification (**III**, Fig. 1B). Of note, the KL ASCs in our mouse cohorts showed clear positivity for CK5 in the SCC component, whereas contrary to previously reported results on KL SCCs (Han et al., 2014), no SOX2 positivity was detected in the SCC component of ASCs (**III**, Fig. S1D). When the lung lesions were normalised against the total lesion count in each lung, clear differences in the predominant lesion type were observed. The Ad5-CC10-Cre infected KL mice had ASC tumours as the predominant lesion type (average 51%), whereas the invasive AC (characterised with a lepidic growth pattern at the lesion border) and papillary ACs (PACs) comprised the major part of Ad5-SPC-Cre induced lesions (average 66% and 17%, respectively). Moreover, the Ad5-CC10-Cre induced tumours included invasive

ACs classified as acinar (average 3%) and mucinous ACs (average 9%), two invasive AC growth patterns which were not detected among the Ad5-SPC-Cre induced lesions in this cohort. ASCs were rarely detected in Ad5-SPC-Cre mice (3%). These results suggested that the Ad5-CC10-Cre-specific histopathology spectrum could explain the difference seen in the survival of Ad5-CC10-Cre and Ad5-SPC-Cre mice (**III**, Fig. 1B & C). Luminal papillary hyperplasias or AIS were detected at 6 weeks following Ad5-CC10-Cre or Ad5-SPC-Cre infection of KL mice, respectively, indicating that these could represent precursors for the detected late-stage tumours (**III**, Fig. S1G). Of note, only one pure SCC lesion was detected at 9 weeks post infection (**III**, Fig. S1G).

To strengthen our hypothesis that the Ad5-CC10-Cre specific histopathology spectrum could explain the reduced survival of Ad5-CC10-Cre infected KL mice, we assessed the proliferation status and size of both Ad5-CC10-Cre and Ad5-SPC-Cre induced lesions. We found that Ad5-CC10-Cre infected mice had more proliferating cells, detected with Ki67 proliferation marker, in common invasive ACs, namely invasive ACs and papillary ACs as well as AIS (**III**, Fig. 1D & S2A). Of these, the difference between AISs and papillary ACs was statistically significant. We did not observe any size difference between the lesions in Ad5-CC10-Cre and Ad5-SPC-Cre KL mice. However, the size of the ASCs was substantially bigger than the size of the other lesions, often occupying the whole lung lobe, suggesting that they grew faster (**III**, Fig. 1E). Mucin production was assessed with periodic acid Schiff's (PAS) staining, and it was detected in mucinous invasive ACs and ASCs (**III**, Fig. 1F). To assess the differentiation status of the lesions, we performed a quantitative analysis of NKX2-1 positive cells for the Ad5-CC10-Cre-induced lesions, which represented a broader lesion spectrum than the Ad5-SPC-Cre-induced lesions. The amount of NKX2-1 positive cells was lower in acinar and mucinous invasive ACs, as well as in ASCs when compared to PACs (**III**, Fig. 1G). Moreover, unlike the other lesions, the ASCs were homogenously expressing the high mobility group AT-hook 2 (HMGA2) transcription factor. Expression of HMGA2 is commonly detected in more poorly differentiated and invasive tumours such as oncogenic *Kras* and *Trp53*- or *Nkx2-1*-loss driven lung tumours (Snyder et al., 2013; Sutherland et al., 2014; Winslow et al., 2011) (**III**, Fig. S2B). Taken together, our results indicate that the lung lesions derived from the $CC10^{+}$ cells grow faster, and show decreased differentiation.

Our results thus show an increased incidence of ASCs as well as other less differentiated acinar and mucinous invasive ACs in Ad5–CC10–Cre cohorts, and suggest that CC10 progenitors may have an increased propensity to initiate faster growing lung tumours. This corroborates previous results in $Kras^{LSL\text{-}G12D/+}$ and $Kras^{LSL\text{-}G12D/+};Trp53^{fl/fl}$ (KP) models which also showed ACs with increased invasive and metastatic characters, possibly indicating faster tumour progression, upon Ad5-CC10-Cre-mediated tumour initiation (Sutherland et al., 2014). Interestingly, studies in human lung tissue have indicated LKB1 expression to be restricted to airway cells (Ghaffar et al., 2003). This suggests a possible lung airway epithelium- restricted role for LKB1 in the normal lung, potentially explaining the different effects of *Lkb1* deletion in $CC10^{+}$ and SPC^{+} epithelial progenitors.

Our results further suggest that oncogenic *Kras* activation combined with *Lkb1*-loss in SPC^+ alveolar cells predominantly initiates lung ACs (specifically, invasive AC and PACs), recapitulating lung tumour phenotype initiated by oncogenic *Kras* only (Johnson *et al.*, 2001b). This is in line with previous studies showing oncogenic *Kras*-driven AC formation originating from alveolar regions (Mainardi et al., 2014; Sutherland et al., 2014; Xu et al., 2012). We however also observed a small percentage of ASCs in Ad5–SPC–Cre infected KL mice, supporting the previously reported AC-ASC transdifferentiation of lesions derived from SPC^+ alveolar cells (Han et al., 2014; Li et al., 2015).

5.4.2 NSCLC driven by mutant *Kras* and *Lkb*- loss shows histotype-specific gene expression signatures

To gain insights in the biological differences between the predominant Ad5-CC10-Cre- and Ad5-SPC-Cre-induced lung tumour histopathologies, we performed transcriptional profiling of Ad5-CC10-Cre-induced ASCs and Ad5-SPC-Cre-induced PACs collected at the end-stage of the tumour bearing mice. PACs were the second most frequently detected lesion type in Ad5-SPC-Cre infected mice (17%, **III**, Fig. 1C), and because it represents a progressive invasive AC subtype with a substantially larger size than invasive ACs, they were selected for transcriptional profiling. Two tumours per mouse from three Ad5-CC10-Cre- or three Ad5-SPC-Cre-infected mice were harvested and processed for RNA extraction, protein lysates and histological examination (**III**, Fig. S3A). The ASC histopathology was confirmed by western blot analysis using anti-p63 antibody (**III**, Fig. S3B). Unsupervised hierarchical clustering of 340 genes that were differentially expressed between ASCs and PACs (cut-off adjusted p-value<0,01 LogFC>1) revealed distinct clustering of ASC and papillary AC tumours (**III**, Fig. 2A). To characterise the data, we performed a comparative gene expression analysis using a Venn diagram generation tool and ENSEMBL GENE IDs as gene identifiers. The Venn diagram generation tool identifies commonalities in the studied data sets. The datasets we used for the comparison were a comparison of human SCC and AC (Kuner et al., 2009), and a comparison of murine SCC and AC (*Lkb1*- and Pten-loss driven SCC, called LP, and $Kras^{LSL\text{-}G12D/+}$ driven ACs) (Xu et al., 2014a) expression profiles. Altogether 40 (29 upregulated and 11 downregulated) commonly differentially altered genes were found between these data sets (**III**, Fig. 2B). This set of 40 genes was enriched for increased expression of squamous markers, such as *Trp63*, *Krt5* and multiple other cytokeratins. Downregulated genes included the recently described AC marker napsin A (*Napsa*) (Turner et al., 2012) (**III**, Fig. 2C).

Together, these results underlined previously reported results of an ASC-specific squamous expression profile (Ji et al., 2007a), and further identified Napsa expression in the KL PACs. Our expression profiling therefore underscores a predominant squamous component in ASC tumours driven by oncogenic *Kras* and *Lkb1*-loss.

We further compared the set of genes that were differentially expressed between KL ASCs and PACs to genes expressed differentially in wt murine basal cells (Griffonia simplicifolia isolectin A3B, GSI-A3B$^+$ and KRT5$^+$) versus non-basal cells (GSI-A3B$^-$ and KRT5$^-$) (Rock et al., 2009). This revealed 108 commonly up- or downregulated genes in these two data sets (**III**, Fig. S3C). This included up regulation of known basal and squamous epithelial marker genes *Trp63*, snail family zinc finger 2 (*Snai2*), basonuclin (*Bnc1*), stratifin (*Sfn*), and cytokeratins. We also found common enrichment of the pro-inflammatory cytokine interleukin 1β (*Il1b*) and its type II interleukin 1 receptor (*Il1r2*). As expected, the AC biomarker SPC was downregulated in both airway basal cells and ASC (**III**, Table S1). As the analysed ASCs originated from CC10$^+$ airway cells, the enrichment for genes typically expressed in basal cells suggests a transcriptional switch of transformed CC10$^+$ cells to more basal-like expression during ASC development. Our last comparison was with the published KL data, in which transcriptional profiles of Ad5-CMV-Cre induced ACs and ASCs were compared (Ji et al., 2007a). We found 23 commonly enriched genes, including SCC signature genes *Trp63* and cytokeratins (**III**, Fig. S3C & Table S1).

5.4.3 ASCs and PACs driven by mutant *Kras* and *Lkb1*-loss show histotype-specific expression of immune-related genes

To gain more in depth understanding of the possible mechanisms contributing to the two predominant lung tumour histopathologies, we analysed the 340 differentially expressed genes between KL ASCs and PACs using the Ingenuity Pathway Analysis (IPA) tool. Analysis identified enrichment in immune related canonical pathways including granulocyte adhesion and diapedesis (upregulated in ASCs: *Ngfr*, *Il1b*, *Hspb1*, *Il1r2*, *Cldn23*, *Ppbp*; downregulated in ASCs: *Cldn18*, *Cxcl15*, *Itga2*, *Ccl6*, *Ccl17*) and antigen presentation (downregulated in ASCs: *Cd74*, *Ciita*, *H2-D1*, *H2-DMa*, *H2-DMb1*), indicating possible differences in immune-related properties between ASCs and PACs (**III**, Fig. 3A).

We then asked if the observed histopathology-dependent immune-related gene expression patterns would exist independently of driver genotypes. Indeed, expression pattern analysis of selected immune related genes in KL ASCs and PACs together with KP Ad5-CC10-Cre- and Ad5-SPC-Cre-derived ACs, revealed histopathology-dependent expression differences (**III**, Fig. 3B). These included ASC-specific elevated expression of the pro-inflammatory cytokine *Il1b* and arginase 1 enzyme gene (*Arg1*), a key mediator of T-cell immunosuppression (Munder et al., 2006). Moreover, as partly identified with the IPA analysis, expression of class II major histocompatibility complex (MHC) genes (*H2-DMa*, *H2-Ab1*, *H2-DMb1*), and class II MHC associated gene *Cd74* as well as the chemokine *Cxcl15* and the lymphocyte and monocyte chemoattractant chemokines *Ccl17* and *Ccl6*, were significantly lower in ASCs than in ACs (**III**, Fig. 3B). Expression of class I MHC genes (*H2-M2*, *H2-D1*) was lower in KL ASCs when

compared to KL PACs, but showed variable expression in KP ACs. *Cxcl5*, a downstream chemokine target of *Il1b*, showed elevated levels in both KL ASCs and KP ACs, suggesting a possible association with tumour grade rather than histopathology (**III**, Fig. 3B). Interestingly, some of these immune-related genes were found to be commonly enriched between KL ASC-AC and the published mouse SCC-AC (LP vs $Kras^{LSL\text{-}G12D/+}$) comparison (Xu et al., 2014a). These included *Ciita*, *H2-DMa*, *Ngfr*, *Cldn23*, *Ppbp*, *Cldn18*, *Cxcl15*, *Cxcl5*, and *H2-Ab1* (**III**, Table S1). In addition, *Arg1* was commonly upregulated in both KL ASC and LP SCC, but was excluded from the comparison analysis because of the used cut-off values (cut-off 0,01, *Arg1* Adj.p-value: 0,012). Q-PCR-based validation of selected genes confirmed the KL ASC-specific upregulation of immune-related gene expression differences including *Il1b* and *Arg1* and the decreased expression of class I MHC genes (**III**, Fig. 3C).

In summary, these results indicated immune-related expression differences between the KL ASCs and PACs, possibly contributing to their differential tumourigenic growth. Moreover, the observation that both KL and KP ACs express very similar immune genes together with the overlap between the KL ASC-AC and LP SCC-$Kras^{LSL\text{-}G12D/+}$ AC expression profiles, suggested that tumour progression may coincide with immune modulation of the tumour microenvironment in a histopathology-specific manner and simultaneously excluded the effect of potential adenovirus-associated inflammatory response.

5.4.4 ASCs show recruitment of Gr-1$^+$CD11b$^+$myeloid cells with possible immune suppressive characteristics

Elevated *Il1b* expression has been linked to mobilisation and recruitment of neutrophils representing subpopulation of MDSCs in murine models of stomach and breast cancer (Coffelt et al., 2015; Tu et al., 2008). In the stomach, recruitment of MDSCs sensitises to gastric inflammation and carcinoma (Tu et al., 2008), whereas in breast cancer the tumour-infiltrated MDSCs suppress CD8$^+$ T-cell activation and facilitate lung metastasis (Coffelt et al., 2015). Additionally, *Arg1* expression by the MDSCs is linked to regulation of T-cell function. Thus, we reasoned that the observed immune-related gene expression profile of KL ASCs, particularly the elevated *Il1b* and *Arg1* and decreased MHC expression, may indicate a histotype-specific immune cell contexture.

To know if KL ASCs were enriched with myeloid cells expressing murine MDSC markers, namely Gr-1 and CD11b, we performed a quantitative IHC-based analysis of lesions from Ad5-CC10-Cre- and Ad5-SPC-Cre-infected KL lungs (n=5 in both cohorts). The amount of both Gr-1$^+$ and CD11b$^+$ immune cells was normalised against the total amount of cells in each lesion, enabling inspection of these cells relative to the size of the lesion. The analysis between the KL ASCs and KL PACs revealed a clear difference in the amount of Gr-1$^+$ (average 4,4% and 0,3% respectively) and CD11b$^+$

neutrophils (average 9,4% and 2% respectively) (**III**, Fig. 4A, 4B & S3E). Next we asked if the increased amount of Gr-1$^+$ and CD11b$^+$ neutrophils correlated with the number of infiltrating T-cells in these lesion types. Indeed, we found decreased numbers of CD3$^+$ T-cells in ASCs when compared to PACs (average 0,8% and 1,4% respectively), suggesting a negative correlation between the recruitment of MDSCs and the amount of T-cells (**III**, Fig. 4A & 4B). Double positivity of Gr-1$^+$ and CD11b$^+$ was confirmed by flow cytometry analysis, which further confirmed the increased number of neutrophils in ASCs when compared to PACs (average 15% and 0,3% of live cells, respectively) (**III**, Fig. 4C & 4D). Since *Il1b* and *Arg1* expression was significantly lower also in KP ACs when compared to ASCs **(III**, Fig. 3B), we analysed Gr-1$^+$, CD11b$^+$ and CD3$^+$ immune cells in KP tumours. Spleen-derived Ly6C^{hi}CD11b$^+$ monocytic and Ly6G^{hi}CD11b$^+$ granulocytic immune cells have been shown to promote tumourigenesis of KP ACs (Cortez-Retamozo et al., 2012). Our IHC-based quantitation of Gr-1$^+$, CD11b$^+$ and CD3$^+$ immune cells in KP ACs (n=2 in both Ad5-CC10-Cre and Ad5-SPC-Cre cohorts) indeed showed positive but also highly variable numbers of Gr-1$^+$ and CD11b$^+$ cells in both Ad5-CC10-Cre- and Ad5-SPC-Cre-induced KP tumours. Furthermore, the results suggested increased numbers of Gr-1$^+$ and CD11b$^+$ cells in the Ad5-CC10-Cre cohort (**III**, Fig. S3F & G), suggesting that neutrophil infiltration in the KP model may correlate with the tumour differentiation status.

Taken together, our results show a differential contribution of specific lung epithelial progenitors to oncogenic *Kras* and loss of *Lkb1* driven lung tumourigensis, detected as separate histopathology spectrums in Ad5-CC10-Cre- and Ad5-SPC-Cre-infected KL mice. Our results tentatively suggest that KL tumours derived from CC10$^+$ cells progress faster than those derived from SPC$^+$ cells (Figure 12). However, this was not absolute, since tumours with a higher differentiation status, namely AIS, invasive ACs and PACs, were also detected in Ad5-CC10-Cre cohorts, and more poorly differentiated ASCs were also detected in the Ad5-SPC-Cre cohorts. Thus, significant histotype heterogeneity is seen within each of the CC10$^+$- and SPC$^+$-derived lesions. Indeed, a specific naphthalene-resistant subpopulation of CC10$^+$ Clara cells in the NEB microenvironment argues that CC10$^+$ cellular subpopulations show varied stem cell-like regenerative properties (Hong et al., 2001). Similarly, some but not all AT2 cells express low levels of CC10, indicating heterogeneity among the alveolar SPC expressing AT2 cells as well (Rawlins *et al.*, 2009b).

Expression profiling of the two predominant tumour histopathology classes in Ad5-CC10-Cre and Ad5-SPC-Cre KL cohorts, ASCs and PACs respectively, underlined the squamous characteristics of ASCs. Furthermore, immune-related gene expression patterns separated these two predominant histopathology classes suggesting role for the tumour immune modulation in the progression of these lesion types. In support of this, we identified an ASC-specific enrichment of Gr-1$^+$ and CD11b$^+$ neutrophil infiltration and decrease in CD3$^+$ T-lymphocytes. Thus, our results suggest a tumour histotype-specific immune modulation of the tumour microenvironment leading to more rapid tumourigenesis.

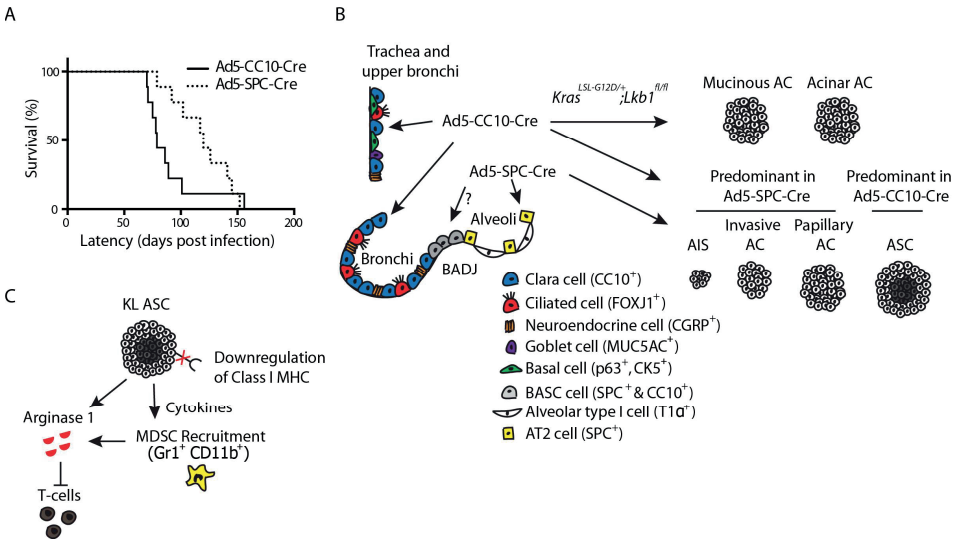

Figure 12. The niche specific effect of oncogenic *Kras* and *Lkb1*-loss on murine lung tumourigenesis. (A) Ad5-CC10-Cre infected KL mice show shorter latency when compared to Ad5-SPC-Cre infected KL mice (median survival 79 and 120 days respectively). (B) $CC10^{+}$ airway cells possess higher propensity to initiate faster growing and progressing lung tumours, namely ASCs, mucinous and acinar ACs. (C) ASCs are characterised by immunosuppressive microenvironment.

7 Concluding remarks and future prospects

As the molecular profiles of lung tumours are becoming more clear, validation of their functional importance is needed to translate this information into the clinic. The studies presented here extend from functional *in vitro* validation of a putative tumour suppressor gene *EPHA3* (I) to its *in vivo* validation in murine lung cancer (II), and further continue to the characterisation of progenitor cell-specific murine lung tumourigenesis driven by expression of oncogenic *Kras* and loss of the tumour suppressor *Lkb1* (III).

Our results, together with data published during the course of this work (Lisabeth et al., 2012; Zhuang et al., 2012), support the notion that *EPHA3* has tumour suppressor-like functions, which are specifically dependent on its kinase activity (I). An EPHA3 monoclonal agonistic antibody, mAb IIIA4, known to trigger kinase activity-dependent apoptosis *in vitro* and to prevent xenograft tumour formation *in vivo* (Day et al., 2013), now has a humanised therapeutic counterpart, named KB004. KB004 show promising tolerance and has shown evidence of clinical activity in phase I clinical trials of advanced hematologic malignancies (Swords et al., 2013). Our results show that inactivation of the EPHA3 kinase domain caused by the EPHA3 cancer mutations may imply that mutational testing prior to KB004 treatment of EPHA3-expressing solid cancers, such as NSCLC, may predict efficacy of the treatment. However, the suitability and efficacy of the KB004 for the treatment of solid cancers requires more testing and clinical trials.

Our attempt to model loss of EPHA3 function in murine lung AC using a constitutive knock out model of *EphA3* was challenged by biological complexity. Constitutive *EphA3*-loss in combination with two key genetic alterations of human lung cancer, namely oncogenic *Kras* or *Trp53*-loss, did not result in discernible changes in lung tumourigenesis. It is possible that other EPH receptors such as EphA5 or EphA7, recently found to be somatically mutated in murine SCLC (McFadden et al., 2014) or *EphA2* which loss cooperates with oncogenic *Kras* promoting murine lung AC (Yeddula *et al.*, 2015), may compensate for loss of *EphA3* function in murine lung tumourigenesis. Nevertheless, more sophisticated methods, such as genome editing by CRISPR-Cas9 to enable rapid *in vivo* generation of (combinatorial) genetic alterations (Sanchez-Rivera *et al.*, 2014), are required to validate the putative NSCLC-specific *in vivo* relevance of EPHA- loss of function.

Tumourigenesis often overthrows developmental regulatory mechanisms, underlining the importance of understanding the normal physiological function of genes. Interestingly, in our search for *EphA3* lung developmental functions, we found that *EphA3* expression was uniquely restricted to the developing lung mesenchyme.

However, we did not find any defects in lung morphogenesis due to *EphA3*-loss, though small changes in the expression of key lung morphogenesis regulators were detected. Our results highlight the complexity of multicellular signalling networks that inherently exhibit redundant mechanisms to overcome alterations in single molecules. Indeed, redundancy between Ephs and ephrins has been suggested. *EphA3*, *EphA4*, and *EphA7* have been suggested to redundantly function in cleft palate formation (Agrawal et al., 2014), and ephrin-B1 and ephrin-B2 are shown to function redundantly in thymocyte development, peripheral T cell differentiation, and antiviral immune responses (Luo et al., 2011).

The latter section of this thesis work concentrated on known lung cancer genes *KRAS* and *LKB1*, and their site-specific functional importance in murine lung tumourigenesis. Two questions were addressed: (1) Do cells in the proximal airways and distal alveolar space show differential propensities to transform and progress to specific lung tumour histopathologies driven by oncogenic *Kras* and *Lkb1*-loss, and (2) Do the growth, progression and histopathology of mutant *Kras*- and *Lkb1*-loss-driven lung tumours correlate with a specific, possibly immunosuppressive immune contexture.

In support of differential tumourigenic propensities between the cells in airways and alveoli, we found that $CC10^+$ lung epithelial cells, the majority of which are located in the airways (Rawlins *et al.*, 2009b), have an increased propensity to give rise to faster growing and progressing lung tumours, classified as acinar and mucinous ACs, and ASCs. Of these, the predominant histopathology class was ASC. SPC^+ alveolar cells predominantly gave rise to invasive ACs, with or without a papillary growth pattern, representing moderately or well differentiated lung histopathologies.

Lung ASCs represent a rare but aggressive type of NSCLC, representing 0,4-4% of diagnosed lung cancer cases (Travis et al., 2015). Its mutational spectrum resembles that of lung ACs, and harbour *EGFR* (13-31%), *KRAS* (13%) or *LKB1* (up to 22%) mutations (Koivunen et al., 2008; Tochigi et al., 2011; Vassella et al., 2015), all shown to be trunk mutations. In support of clonal evolution contributing to the different histopathological AC and SCC components, the SCC component is indicated to acquire branch mutations in genes functioning in the PI3K pathway (Vassella et al., 2015). Interestingly, both AKT activation and SCC transdifferentiation have been suggested as an acquired resistance mechanism following combination treatment with docetaxel and the MEK inhibitor selumetinib, or docetaxel in combination with the metabolic drug phenformin, respectively (Chen et al., 2012; Li et al., 2015). This suggests that the clonality of ASC provides resistance mechanism to this aggressive type of NSCLC. Our closer investigation of the transcriptional differences between KL ASCs and PACs led to identification of immune-related transcriptional profiles in these two murine lung tumour histopathologies. The elevated expression of cytokine *Il1b* and arginase 1 enzyme gene *Arg1* by the ASCs led us to study the immune contexture within the KL lung lesions. Correlating with the results from human lung cancer patients (Liu et al., 2010) we found increased infiltration of myeloid cells, representing a likely subpopulation of MDSCs, in the faster growing and more poorly differentiated KL ASCs when compared to slower growing and more differentiated KL PACs. We also detected a decreased number of

tumour-infiltrating T-cells in KL ASCs, further supporting the immunosuppressive microenvironment of ASCs. It remains to be seen if these findings correlate with the corresponding human lung tumour histopathologies exhibiting a similar differentiation status. If so, then the KL ASC model represents a relevant preclinical model for the study of MDSC-specific immune therapy in ASCs, a lung cancer type for which treatment is challenged by its clonal heterogeneity.

Taken together the results presented in this thesis work underline the importance of the niche specific investigation of molecular factors of lung cancer. Furthermore, the ASC specific immunosuppressive microenvironment highlights the necessity of pre-clinical models in future investigation of systemic lung cancer treatments such as modulation of the immune cell contexture.

Acknowledgements

This work was carried out in the Institute for Molecular Medicine Finland (FIMM) between the years 2009 and 2016. It has been a privilege to be part of FIMM community and see the growth of the institute during these years. Thus, I wish to thank the former director of FIMM Professor Olli Kallioniemi for creating an inspiring working environment and excellent research facilities. I also wish to thank the present director of FIMM, Professor Jaakko Kaprio for taking over the FIMM leadership. I'm grateful to all the FIMM administrative personnel, especially Susanna Rosas, Reetta Niemelä, Sanni Hyppönen, Heidi Alatalo, and Emilia Vanamo for providing their help. I also want to express my gratitude to Dr. Gretchen Repasky for her valuable work in FIMM specially in student related matters, and of course for proof-reading this thesis.

This thesis work was financially supported by the Doctoral School in Health Sciences (DSHealth) and the Doctoral Programme in Biomedicine (DPBM), The Finnish Cultural Foundation, and the K. Albin Johansson Foundation, which all are thanked for their support.

I wish to sincerely thank my supervisor Dr. Emmy Vershuren for giving me opportunity to do my Ph.D in FIMM and in her research group. It has been a colourful and exiting journey with a lot of challenges. Your strength and forward looking attitude have taken us through them. Docent Juha Klefström I wish to thank for supporting my thesis work and Dr. Sergey Kuznetsov for his support during my first year in FIMM.

I would like to thank the examiners of my thesis, Docent Satu kuure and Docent Cecilia Sahlgren for their excellent comments. I'm very grateful to my opponent Professor Anton Berns for accepting the invitation to be my Opponent and Professor Tomi Mäkelä for being the Custos. I also wish to acknowledge my thesis committee members Docent Päivi Ojala and Professor Johanna Ivaska for supporting my thesis work throughout these years.

This work could not have been completed without the exceptionally smart, supporting, and lively colleagues I have been privileged to work with during these years. First of all, Anna and Sonja, thank you for your patience and never ending capability to answer and meet all of my questions and requests. I have learned a great deal from both of you. Barun, without your contribution I would not have made it. Thank you for all the work you did, one could not wish for better colleague to share a project with. One of the most exciting time periods during my thesis work was spring 2015 when I had the opportunity to join the cell-of-origin and tumour heterogeneity project. Thank you Ashwini for all the great moments and excellent team work. I'm very thankful to all former and present members of the Verschuren group, especially Katja, Dat, Merja,

Sarang, and Jennifer for all their help and being great colleagues. FIMM is full of top class people with whom I have been privileged share thoughts and ideas during these years. All former and present members of the Kuznetsov and Kainov groups, especially Manu!!, Yuexi, Pauliina, Daria, and Masha I wish to thank for their excellent company and support. Susanne, Arjan, and Mamun, thank you for your friendship. Sami, Elina, Riku, Teijo, Margarita, Tiia, Guru, Meri, JP and many others who I'm most likely now forgetting to mention, thank you for great discussions and all your help. I thank my former colleagues Terhi, Mia, and Jenny for their friendship and running company. I also wish to thank my previous colleagues from THL, especially Jonna, for your support and friendship. And Krisse, thank you for the great company during the university years.

To keep in one's right mind one needs moments of laugh and joy. I truly have had those. For that I thank all my dear friends and the members of the Wasa chefen (WC) clan and its subgroups, Rotunaiset and Kulttuurikerho. My dear friends, with whom I have had the privilege to spend many happy moments, Anna, Sussu, Eikka, Niina H., Minna, Kaisa N., Kaisa P., Niina N., Sanna, Tiitu, and Laura, I wish to thank for their priceless friendship. And Sussu, thank you so much for making the cover for this thesis! I thank my sister Laura and brother Tuomo for just being there. I wish to express my greatest gratitude to my parents who have supported me throughout my life. One could not wish for better family. Lastly, I want to express my gratitude to my partner and friend Saku for being exceptionally patient and supportive throughout all these years. Thank you for being beside me.

Helsinki, January 2016
Jenni Lahtela

References

Abaan, O.D., Polley, E.C., Davis, S.R., Zhu, Y.J., Bilke, S., Walker, R.L., Pineda, M., Gindin, Y., Jiang, Y., Reinhold, W.C., Holbeck, S.L., Simon, R.M., Doroshow, J.H., Pommier, Y. and Meltzer, P.S., 2013. The exomes of the NCI-60 panel: a genomic resource for cancer biology and systems pharmacology. Cancer Res 73, 4372-4382.

Abdul-Aziz, N.M., Turmaine, M., Greene, N.D. and Copp, A.J., 2009. EphrinA-EphA receptor interactions in mouse spinal neurulation: implications for neural fold fusion. Int J Dev Biol 53, 559-568.

Agrawal, P., Wang, M., Kim, S., Lewis, A.E. and Bush, J.O., 2014. Embryonic expression of EphA receptor genes in mice supports their candidacy for involvement in cleft lip and palate. Dev Dyn 243, 1470-1476.

Al-Shibli, K.I., Donnem, T., Al-Saad, S., Persson, M., Bremnes, R.M. and Busund, L.T., 2008. Prognostic effect of epithelial and stromal lymphocyte infiltration in non-small cell lung cancer. Clin Cancer Res 14, 5220-5227.

Alanentalo, T., Asayesh, A., Morrison, H., Loren, C.E., Holmberg, D., Sharpe, J. and Ahlgren, U., 2007. Tomographic molecular imaging and 3D quantification within adult mouse organs. Nature Methods 4, 31-33.

Alessi, D.R., Sakamoto, K. and Bayascas, J.R., 2006. LKB1-dependent signaling pathways. Annu Rev Biochem 75, 137-163.

Alexander, A. and Walker, C.L., 2011. The role of LKB1 and AMPK in cellular responses to stress and damage. FEBS Lett 585, 952-957.

Andersson, L., Westerlund, J., Liang, S., Carlsson, T., Amendola, E., Fagman, H. and Nilsson, M., 2011. Role of EphA4 receptor signaling in thyroid development: regulation of folliculogenesis and propagation of the C-cell lineage. Endocrinology 152, 1154-1164.

Aoki, M., Yamashita, T. and Tohyama, M., 2004. EphA receptors direct the differentiation of mammalian neural precursor cells through a mitogen-activated protein kinase-dependent pathway. J Biol Chem 279, 32643-32650.

Arcila, M.E., Oxnard, G.R., Nafa, K., Riely, G.J., Solomon, S.B., Zakowski, M.F., Kris, M.G., Pao, W., Miller, V.A. and Ladanyi, M., 2011. Rebiopsy of lung cancer patients with acquired resistance to EGFR inhibitors and enhanced detection of the T790M mutation using a locked nucleic acid-based assay. Clin Cancer Res 17, 1169-1180.

Arman, E., Haffner-Krausz, R., Gorivodsky, M. and Lonai, P., 1999. Fgfr2 is required for limb outgrowth and lung-branching morphogenesis. P Natl Acad Sci USA 96, 11895-11899.

Baas, A.F., Boudeau, J., Sapkota, G.P., Smit, L., Medema, R., Morrice, N.A., Alessi, D.R. and Clevers, H.C., 2003. Activation of the tumour suppressor kinase LKB1 by the STE20-like pseudokinase STRAD. EMBO J 22, 3062-3072.

Baas, A.F., Kuipers, J., van der Wel, N.N., Batlle, E., Koerten, H.K., Peters, P.J. and Clevers, H.C., 2004. Complete polarization of single intestinal epithelial cells upon activation of LKB1 by STRAD. Cell 116, 457-466.

Baines, A.T., Xu, D. and Der, C.J., 2011. Inhibition of Ras for cancer treatment: the search continues. Future Med Chem 3, 1787-1808.

Bardeesy, N., Sinha, M., Hezel, A.F., Signoretti, S., Hathaway, N.A., Sharpless, N.E., Loda, M., Carrasco, D.R. and DePinho, R.A., 2002. Loss of the Lkb1 tumour suppressor provokes intestinal polyposis but resistance to transformation. Nature 419, 162-167.

Bardelli, A., Parsons, D.W., Silliman, N., Ptak, J., Szabo, S., Saha, S., Markowitz, S., Willson, J.K., Parmigiani, G., Kinzler, K.W., Vogelstein, B. and Velculescu, V.E., 2003. Mutational analysis of the tyrosine kinome in colorectal cancers. Science 300, 949.

Barkauskas, C.E., Cronce, M.J., Rackley, C.R., Bowie, E.J., Keene, D.R., Stripp, B.R., Randell, S.H., Noble, P.W. and Hogan, B.L., 2013. Type 2 alveolar cells are stem cells in adult lung. Journal of Clinical Investigation 123, 3025-3036.

Baumgart, A., Mazur, P.K., Anton, M., Rudelius, M., Schwamborn, K., Feuchtinger, A., Behnke, K., Walch, A., Braren, R., Peschel, C., Duyster, J., Siveke, J.T. and Dechow, T., 2015. Opposing role of Notch1 and Notch2 in a Kras(G12D)-driven murine non-small cell lung cancer model. Oncogene 34, 578-588.

Beckerman, R. and Prives, C., 2010. Transcriptional regulation by p53. Cold Spring Harb Perspect Biol 2, a000935.

Bellusci, S., Furuta, Y., Rush, M.G., Henderson, R., Winnier, G. and Hogan, B.L., 1997a. Involvement of Sonic hedgehog (Shh) in mouse embryonic lung growth and morphogenesis. Development 124, 53-63.

Bellusci, S., Grindley, J., Emoto, H., Itoh, N. and Hogan, B.L., 1997b. Fibroblast growth factor 10 (FGF10) and branching morphogenesis in the embryonic mouse lung. Development 124, 4867-4878.

Bellusci, S., Henderson, R., Winnier, G., Oikawa, T. and Hogan, B.L., 1996. Evidence from normal expression and targeted misexpression that bone morphogenetic protein (Bmp-4) plays a role in mouse embryonic lung morphogenesis. Development 122, 1693-1702.

Bennett, K.M., Afanador, M.D., Lal, C.V., Xu, H., Persad, E., Legan, S.K., Chenaux, G., Dellinger, M., Savani, R.C., Dravis, C., Henkemeyer, M. and Schwarz, M.A., 2013. Ephrin-B2 reverse signaling increases alpha5beta1 integrin-mediated fibronectin deposition and reduces distal lung compliance. Am J Respir Cell Mol Biol 49, 680-687.

Bertrand, P., Saintigny, Y. and Lopez, B.S., 2004. p53's double life: transactivation-independent repression of homologous recombination. Trends Genet 20, 235-243.

Bieging, K.T., Mello, S.S. and Attardi, L.D., 2014. Unravelling mechanisms of p53-mediated tumour suppression. Nat Rev Cancer 14, 359-370.

Binns, K.L., Taylor, P.P., Sicheri, F., Pawson, T. and Holland, S.J., 2000. Phosphorylation of tyrosine residues in the kinase domain and juxtamembrane region regulates the biological and catalytic activities of Eph receptors. Mol Cell Biol 20, 4791-4805.

Bishop, J.A., Teruya-Feldstein, J., Westra, W.H., Pelosi, G., Travis, W.D. and Rekhtman, N., 2012. p40 (DeltaNp63) is superior to p63 for the diagnosis of pulmonary squamous cell carcinoma. Mod Pathol 25, 405-415.

Bos, J.L., Rehmann, H. and Wittinghofer, A., 2007. GEFs and GAPs: critical elements in the control of small G proteins. Cell 129, 865-877.

Boudeau, J., Baas, A.F., Deak, M., Morrice, N.A., Kieloch, A., Schutkowski, M., Prescott, A.R., Clevers, H.C. and Alessi, D.R., 2003. MO25alpha/beta interact with STRADalpha/beta enhancing their ability to bind, activate and localize LKB1 in the cytoplasm. EMBO J 22, 5102-5114.

Boyd, A.W., Ward, L.D., Wicks, I.P., Simpson, R.J., Salvaris, E., Wilks, A., Welch, K., Loudovaris, M., Rockman, S. and Busmanis, I., 1992. Isolation and characterization of a novel receptor-type protein tyrosine kinase (hek) from a human pre-B cell line. J Biol Chem 267, 3262-3267.

Calles, A., Sholl, L.M., Rodig, S.J., Pelton, A.K., Hornick, J.L., Butaney, M., Lydon, C., Dahlberg, S.E., Oxnard, G.R., Jackman, D.M. and Janne, P.A., 2015. Immunohistochemical Loss of LKB1 Is a Biomarker for More Aggressive Biology in KRAS-Mutant Lung Adenocarcinoma. Clin Cancer Res 21, 2851-2860.

Campisi, J. and d'Adda di Fagagna, F., 2007. Cellular senescence: when bad things happen to good cells. Nat Rev Mol Cell Biol 8, 729-740.

Cancer Genome Atlas Research, N., 2012. Comprehensive genomic characterization of squamous cell lung cancers. Nature 489, 519-525.

Cancer Genome Atlas Research, N., 2014. Comprehensive molecular profiling of lung adenocarcinoma. Nature 511, 543-550.

Capecchi, M.R., 2005. Gene targeting in mice: functional analysis of the mammalian genome for the twenty-first century. Nat Rev Genet 6, 507-512.

Capon, D.J., Seeburg, P.H., McGrath, J.P., Hayflick, J.S., Edman, U., Levinson, A.D. and Goeddel, D.V., 1983. Activation of Ki-ras2 gene in human colon and lung carcinomas by two different point mutations. Nature 304, 507-513.

Carvalho, R.F., Beutler, M., Marler, K.J., Knoll, B., Becker-Barroso, E., Heintzmann, R., Ng, T. and Drescher, U., 2006. Silencing of EphA3 through a cis interaction with ephrinA5. Nat Neurosci 9, 322-330.

Cerami, E., Gao, J., Dogrusoz, U., Gross, B.E., Sumer, S.O., Aksoy, B.A., Jacobsen, A., Byrne, C.J., Heuer, M.L., Larsson, E., Antipin, Y., Reva, B., Goldberg, A.P., Sander, C. and Schultz, N., 2012. The cBio cancer genomics portal: an open platform for exploring multidimensional cancer genomics data. Cancer Discov 2, 401-404.

Chang, D.R., Martinez Alanis, D., Miller, R.K., Ji, H., Akiyama, H., McCrea, P.D. and Chen, J., 2013. Lung epithelial branching program antagonizes alveolar differentiation. P Natl Acad Sci USA 110, 18042-18051.

Chen, F., Desai, T.J., Qian, J., Niederreither, K., Lu, J. and Cardoso, W.V., 2007. Inhibition of Tgf beta signaling by endogenous retinoic acid is essential for primary lung bud induction. Development 134, 2969-2979.

Chen, G., Korfhagen, T.R., Xu, Y., Kitzmiller, J., Wert, S.E., Maeda, Y., Gregorieff, A., Clevers, H. and Whitsett, J.A., 2009. SPDEF is required for mouse pulmonary goblet cell differentiation and regulates a network of genes associated with mucus production. Journal of Clinical Investigation 119, 2914-2924.

Chen, Z., Cheng, K., Walton, Z., Wang, Y., Ebi, H., Shimamura, T., Liu, Y., Tupper, T., Ouyang, J., Li, J., Gao, P., Woo, M.S., Xu, C., Yanagita, M., Altabef, A., Wang, S., Lee, C., Nakada, Y., Pena, C.G., Sun, Y., Franchetti, Y., Yao, C., Saur, A., Cameron, M.D., Nishino, M., Hayes, D.N., Wilkerson, M.D., Roberts, P.J., Lee, C.B., Bardeesy, N., Butaney, M., Chirieac, L.R., Costa, D.B., Jackman, D., Sharpless, N.E., Castrillon, D.H., Demetri, G.D., Janne, P.A., Pandolfi, P.P., Cantley, L.C., Kung, A.L., Engelman, J.A. and Wong, K.K., 2012. A murine lung cancer co-clinical trial identifies genetic modifiers of therapeutic response. Nature 483, 613-617.

Chen, Z., Fillmore, C.M., Hammerman, P.S., Kim, C.F. and Wong, K.K., 2014. Non-small-cell lung cancers: a heterogeneous set of diseases. Nat Rev Cancer 14, 535-546.

Chen, Z., Trotman, L.C., Shaffer, D., Lin, H.K., Dotan, Z.A., Niki, M., Koutcher, J.A., Scher, H.I., Ludwig, T., Gerald, W., Cordon-Cardo, C. and Pandolfi, P.P., 2005. Crucial role of p53-dependent cellular senescence in suppression of Pten-deficient tumorigenesis. Nature 436, 725-730.

Chien, Y. and White, M.A., 2003. RAL GTPases are linchpin modulators of human tumour-cell proliferation and survival. EMBO Rep 4, 800-806.

Choi, Y.L., Soda, M., Yamashita, Y., Ueno, T., Takashima, J., Nakajima, T., Yatabe, Y., Takeuchi, K., Hamada, T., Haruta, H., Ishikawa, Y., Kimura, H., Mitsudomi, T., Tanio, Y., Mano, H. and Group, A.L.K.L.C.S., 2010. EML4-ALK mutations in lung cancer that confer resistance to ALK inhibitors. New Engl J Med 363, 1734-1739.

Ciriello, G., Miller, M.L., Aksoy, B.A., Senbabaoglu, Y., Schultz, N. and Sander, C., 2013. Emerging landscape of oncogenic signatures across human cancers. Nat Genet 45, 1127-1133.

Clifford, N., Smith, L.M., Powell, J., Gattenlohner, S., Marx, A. and O'Connor, R., 2008. The EphA3 receptor is expressed in a subset of rhabdomyosarcoma cell lines and suppresses cell adhesion and migration. J Cell Biochem 105, 1250-1259.

Coffelt, S.B., Kersten, K., Doornebal, C.W., Weiden, J., Vrijland, K., Hau, C.S., Verstegen, N.J., Ciampricotti, M., Hawinkels, L.J., Jonkers, J. and de Visser, K.E., 2015. IL-17-producing gammadelta T cells and neutrophils conspire to promote breast cancer metastasis. Nature 522, 345-348.

Colicelli, J., 2004. Human RAS superfamily proteins and related GTPases. Sci STKE 2004, RE13.

Collado, M., Gil, J., Efeyan, A., Guerra, C., Schuhmacher, A.J., Barradas, M., Benguria, A., Zaballos, A., Flores, J.M., Barbacid, M., Beach, D. and Serrano, M., 2005. Tumour biology: senescence in premalignant tumours. Nature 436, 642.

Colvin, J.S., Feldman, B., Nadeau, J.H., Goldfarb, M. and Ornitz, D.M., 1999. Genomic organization and embryonic expression of the mouse fibroblast growth factor 9 gene. Dev Dyn 216, 72-88.

Colvin, J.S., White, A.C., Pratt, S.J. and Ornitz, D.M., 2001. Lung hypoplasia and neonatal death in Fgf9-null mice identify this gene as an essential regulator of lung mesenchyme. Development 128, 2095-2106.

Cortez-Retamozo, V., Etzrodt, M., Newton, A., Rauch, P.J., Chudnovskiy, A., Berger, C., Ryan, R.J., Iwamoto, Y., Marinelli, B., Gorbatov, R., Forghani, R., Novobrantseva, T.I., Koteliansky, V., Figueiredo, J.L., Chen, J.W., Anderson, D.G., Nahrendorf, M., Swirski, F.K., Weissleder, R. and Pittet, M.J., 2012. Origins of tumor-associated macrophages and neutrophils. P Natl Acad Sci USA 109, 2491-2496.

Cortot, A.B., Repellin, C.E., Shimamura, T., Capelletti, M., Zejnullahu, K., Ercan, D., Christensen, J.G., Wong, K.K., Gray, N.S. and Janne, P.A., 2013. Resistance to irreversible EGF receptor tyrosine kinase inhibitors through a multistep mechanism involving the IGF1R pathway. Cancer Res 73, 834-843.

Cowan, C.A., Yokoyama, N., Saxena, A., Chumley, M.J., Silvany, R.E., Baker, L.A., Srivastava, D. and Henkemeyer, M., 2004. Ephrin-B2 reverse signaling is required for axon pathfinding and cardiac valve formation but not early vascular development. Dev Biol 271, 263-271.

Cox, A.D. and Der, C.J., 2010. Ras history: The saga continues. Small GTPases 1, 2-27.

Cox, A.D., Fesik, S.W., Kimmelman, A.C., Luo, J. and Der, C.J., 2014. Drugging the undruggable RAS: Mission possible? Nat Rev Drug Discov 13, 828-851.

Creelan, B.C., 2014. Update on immune checkpoint inhibitors in lung cancer. Cancer Control 21, 80-89.

Cross, D.A., Ashton, S.E., Ghiorghiu, S., Eberlein, C., Nebhan, C.A., Spitzler, P.J., Orme, J.P., Finlay, M.R., Ward, R.A., Mellor, M.J., Hughes, G., Rahi, A., Jacobs, V.N., Red Brewer, M., Ichihara, E., Sun, J., Jin, H., Ballard, P., Al-Kadhimi, K., Rowlinson, R., Klinowska, T., Richmond, G.H., Cantarini, M., Kim, D.W., Ranson, M.R. and Pao, W., 2014. AZD9291, an irreversible EGFR TKI, overcomes T790M-mediated resistance to EGFR inhibitors in lung cancer. Cancer Discov 4, 1046-1061.

Cui, J.J., Tran-Dube, M., Shen, H., Nambu, M., Kung, P.P., Pairish, M., Jia, L., Meng, J., Funk, L., Botrous, I., McTigue, M., Grodsky, N., Ryan, K., Padrique, E., Alton, G., Timofeevski, S., Yamazaki, S., Li, Q., Zou, H., Christensen, J., Mroczkowski, B., Bender, S., Kania, R.S. and Edwards, M.P., 2011. Structure based drug design of crizotinib (PF-02341066), a potent and selective dual inhibitor of mesenchymal-epithelial transition factor (c-MET) kinase and anaplastic lymphoma kinase (ALK). J Med Chem 54, 6342-6363.

Dakir, E.H., Feigenbaum, L. and Linnoila, R.I., 2008. Constitutive expression of human keratin 14 gene in mouse lung induces premalignant lesions and squamous differentiation. Carcinogenesis 29, 2377-2384.

Dankort, D., Filenova, E., Collado, M., Serrano, M., Jones, K. and McMahon, M., 2007. A new mouse model to explore the initiation, progression, and therapy of BRAFV600E-induced lung tumors. Genes Dev 21, 379-384.

Davies, H., Hunter, C., Smith, R., Stephens, P., Greenman, C., Bignell, G., Teague, J., Butler, A., Edkins, S., Stevens, C., Parker, A., O'Meara, S., Avis, T., Barthorpe, S., Brackenbury, L., Buck, G., Clements, J., Cole, J., Dicks, E., Edwards, K., Forbes, S., Gorton, M., Gray, K., Halliday, K., Harrison, R., Hills, K., Hinton, J., Jones, D., Kosmidou, V., Laman, R., Lugg, R., Menzies, A., Perry, J., Petty, R., Raine, K., Shepherd, R., Small, A., Solomon, H., Stephens, Y., Tofts, C., Varian, J., Webb, A., West, S., Widaa, S., Yates, A., Brasseur, F., Cooper, C.S., Flanagan, A.M., Green, A., Knowles, M., Leung, S.Y., Looijenga, L.H., Malkowicz, B., Pierotti, M.A., Teh, B.T., Yuen, S.T., Lakhani, S.R., Easton, D.F., Weber, B.L., Goldstraw, P., Nicholson, A.G., Wooster, R., Stratton, M.R. and Futreal, P.A., 2005. Somatic mutations of the protein kinase gene family in human lung cancer. Cancer Res 65, 7591-7595.

Davis, T.L., Walker, J.R., Loppnau, P., Butler-Cole, C., Allali-Hassani, A. and Dhe-Paganon, S., 2008. Autoregulation by the juxtamembrane region of the human ephrin receptor tyrosine kinase A3 (EphA3). Structure 16, 873-884.

Davy, A., Gale, N.W., Murray, E.W., Klinghoffer, R.A., Soriano, P., Feuerstein, C. and Robbins, S.M., 1999. Compartmentalized signaling by GPI-anchored ephrin-A5 requires the Fyn tyrosine kinase to regulate cellular adhesion. Genes Dev 13, 3125-3135.

Day, B.W., Stringer, B.W., Al-Ejeh, F., Ting, M.J., Wilson, J., Ensbey, K.S., Jamieson, P.R., Bruce, Z.C., Lim, Y.C., Offenhauser, C., Charmsaz, S., Cooper, L.T., Ellacott, J.K., Harding, A., Leveque, L., Inglis, P., Allan, S., Walker, D.G., Lackmann, M., Osborne, G., Khanna, K.K., Reynolds, B.A., Lickliter, J.D. and Boyd, A.W., 2013. EphA3 maintains tumorigenicity and is a therapeutic target in glioblastoma multiforme. Cancer Cell 23, 238-248.

de Bruin, E.C., McGranahan, N., Mitter, R., Salm, M., Wedge, D.C., Yates, L., Jamal-Hanjani, M., Shafi, S., Murugaesu, N., Rowan, A.J., Gronroos, E., Muhammad, M.A., Horswell, S., Gerlinger, M., Varela, I., Jones, D., Marshall, J., Voet, T., Van Loo, P., Rassl, D.M., Rintoul, R.C., Janes, S.M., Lee, S.M., Forster, M., Ahmad, T., Lawrence, D., Falzon, M., Capitanio, A., Harkins, T.T., Lee, C.C., Tom, W., Teefe, E., Chen, S.C., Begum, S., Rabinowitz, A., Phillimore, B., Spencer-Dene, B., Stamp, G., Szallasi, Z., Matthews, N., Stewart, A., Campbell, P. and Swanton, C., 2014. Spatial and temporal diversity in genomic instability processes defines lung cancer evolution. Science 346, 251-256.

De Moerlooze, L., Spencer-Dene, B., Revest, J.M., Hajihosseini, M., Rosewell, I. and Dickson, C., 2000. An important role for the IIIb isoform of fibroblast growth factor receptor 2 (FGFR2) in mesenchymal-epithelial signalling during mouse organogenesis. Development 127, 483-492.

de Visser, K.E., Eichten, A. and Coussens, L.M., 2006. Paradoxical roles of the immune system during cancer development. Nat Rev Cancer 6, 24-37.

del Moral, P.M., De Langhe, S.P., Sala, F.G., Veltmaat, J.M., Tefft, D., Wang, K., Warburton, D. and Bellusci, S., 2006a. Differential role of FGF9 on epithelium and mesenchyme in mouse embryonic lung. Dev Biol 293, 77-89.

Del Moral, P.M., Sala, F.G., Tefft, D., Shi, W., Keshet, E., Bellusci, S. and Warburton, D., 2006b. VEGF-A signaling through Flk-1 is a critical facilitator of early embryonic lung epithelial to endothelial crosstalk and branching morphogenesis. Dev Biol 290, 177-188.

del Moral, P.M. and Warburton, D., 2010. Explant Culture of Mouse Embryonic Whole Lung, Isolated Epithelium, or Mesenchyme Under Chemically Defined Conditions as a System to Evaluate the Molecular Mechanism of Branching Morphogenesis and Cellular Differentiation. Mouse Cell Culture: Methods and Protocols 633, 71-79.

deMello, D.E., Sawyer, D., Galvin, N. and Reid, L.M., 1997. Early fetal development of lung vasculature. Am J Respir Cell Mol Biol 16, 568-581.

Der, C.J., Krontiris, T.G. and Cooper, G.M., 1982. Transforming genes of human bladder and lung carcinoma cell lines are homologous to the ras genes of Harvey and Kirsten sarcoma viruses. P Natl Acad Sci USA 79, 3637-3640.

Desai, T.J., Brownfield, D.G. and Krasnow, M.A., 2014. Alveolar progenitor and stem cells in lung development, renewal and cancer. Nature 507, 190-194.

Desai, T.J., Malpel, S., Flentke, G.R., Smith, S.M. and Cardoso, W.V., 2004. Retinoic acid selectively regulates Fgf10 expression and maintains cell identity in the prospective lung field of the developing foregut. Dev Biol 273, 402-415.

Diehl, J.A., Cheng, M., Roussel, M.F. and Sherr, C.J., 1998. Glycogen synthase kinase-3beta regulates cyclin D1 proteolysis and subcellular localization. Genes Dev 12, 3499-3511.

Dieu-Nosjean, M.C., Antoine, M., Danel, C., Heudes, D., Wislez, M., Poulot, V., Rabbe, N., Laurans, L., Tartour, E., de Chaisemartin, L., Lebecque, S., Fridman, W.H. and Cadranel, J., 2008. Long-term survival for patients with non-small-cell lung cancer with intratumoral lymphoid structures. J Clin Oncol 26, 4410-4417.

Dimri, G.P., Lee, X., Basile, G., Acosta, M., Scott, G., Roskelley, C., Medrano, E.E., Linskens, M., Rubelj, I., Pereira-Smith, O. and et al., 1995. A biomarker that identifies senescent human cells in culture and in aging skin in vivo. P Natl Acad Sci USA 92, 9363-9367.

Ding, L., Getz, G., Wheeler, D.A., Mardis, E.R., McLellan, M.D., Cibulskis, K., Sougnez, C., Greulich, H., Muzny, D.M., Morgan, M.B., Fulton, L., Fulton, R.S., Zhang, Q., Wendl, M.C., Lawrence, M.S., Larson, D.E., Chen, K., Dooling, D.J., Sabo, A., Hawes, A.C., Shen, H., Jhangiani, S.N., Lewis, L.R., Hall, O., Zhu, Y., Mathew, T., Ren, Y., Yao, J., Scherer, S.E., Clerc, K., Metcalf, G.A., Ng, B., Milosavljevic, A., Gonzalez-Garay, M.L., Osborne, J.R., Meyer, R., Shi, X., Tang, Y., Koboldt, D.C., Lin, L., Abbott, R., Miner, T.L., Pohl, C., Fewell, G., Haipek, C., Schmidt, H., Dunford-Shore, B.H., Kraja, A., Crosby, S.D., Sawyer, C.S., Vickery, T., Sander, S., Robinson, J., Winckler, W., Baldwin, J., Chirieac, L.R., Dutt, A., Fennell, T., Hanna, M., Johnson, B.E., Onofrio, R.C., Thomas, R.K., Tonon, G., Weir, B.A., Zhao, X., Ziaugra, L., Zody, M.C., Giordano, T., Orringer, M.B., Roth, J.A., Spitz, M.R., Wistuba, II, Ozenberger, B., Good, P.J., Chang, A.C., Beer, D.G., Watson, M.A., Ladanyi, M., Broderick, S., Yoshizawa, A., Travis, W.D., Pao, W., Province, M.A., Weinstock, G.M., Varmus, H.E., Gabriel, S.B., Lander, E.S., Gibbs, R.A., Meyerson, M. and Wilson, R.K., 2008. Somatic mutations affect key pathways in lung adenocarcinoma. Nature 455, 1069-1075.

Dixit, R., Ai, X. and Fine, A., 2013. Derivation of lung mesenchymal lineages from the fetal mesothelium requires hedgehog signaling for mesothelial cell entry. Development 140, 4398-4406.

Donehower, L.A., Harvey, M., Slagle, B.L., McArthur, M.J., Montgomery, C.A., Jr., Butel, J.S. and Bradley, A., 1992. Mice deficient for p53 are developmentally normal but susceptible to spontaneous tumours. Nature 356, 215-221.

Donnem, T., Al-Shibli, K., Andersen, S., Al-Saad, S., Busund, L.T. and Bremnes, R.M., 2010. Combination of low vascular endothelial growth factor A (VEGF-A)/VEGF receptor 2 expression and high lymphocyte

infiltration is a strong and independent favorable prognostic factor in patients with nonsmall cell lung cancer. Cancer 116, 4318-4325.

Dorfman, J. and Macara, I.G., 2008. STRADalpha regulates LKB1 localization by blocking access to importin-alpha, and by association with Crm1 and exportin-7. Mol Biol Cell 19, 1614-1626.

Dunn, G.P., Bruce, A.T., Ikeda, H., Old, L.J. and Schreiber, R.D., 2002. Cancer immunoediting: from immunosurveillance to tumor escape. Nat Immunol 3, 991-998.

Ehrhardt, A., Bartels, T., Geick, A., Klocke, R., Paul, D. and Halter, R., 2001. Development of pulmonary bronchiolo-alveolar adenocarcinomas in transgenic mice overexpressing murine c-myc and epidermal growth factor in alveolar type II pneumocytes. Brit J Cancer 84, 813-818.

El Agha, E., Herold, S., Al Alam, D., Quantius, J., MacKenzie, B., Carraro, G., Moiseenko, A., Chao, C.M., Minoo, P., Seeger, W. and Bellusci, S., 2014. Fgf10-positive cells represent a progenitor cell population during lung development and postnatally. Development 141, 296-306.

Engelman, J.A., Chen, L., Tan, X., Crosby, K., Guimaraes, A.R., Upadhyay, R., Maira, M., McNamara, K., Perera, S.A., Song, Y., Chirieac, L.R., Kaur, R., Lightbown, A., Simendinger, J., Li, T., Padera, R.F., Garcia-Echeverria, C., Weissleder, R., Mahmood, U., Cantley, L.C. and Wong, K.K., 2008. Effective use of PI3K and MEK inhibitors to treat mutant Kras G12D and PIK3CA H1047R murine lung cancers. Nat Med 14, 1351-1356.

Engelman, J.A., Zejnullahu, K., Mitsudomi, T., Song, Y., Hyland, C., Park, J.O., Lindeman, N., Gale, C.M., Zhao, X., Christensen, J., Kosaka, T., Holmes, A.J., Rogers, A.M., Cappuzzo, F., Mok, T., Lee, C., Johnson, B.E., Cantley, L.C. and Janne, P.A., 2007. MET amplification leads to gefitinib resistance in lung cancer by activating ERBB3 signaling. Science 316, 1039-1043.

Ercan, D., Xu, C., Yanagita, M., Monast, C.S., Pratilas, C.A., Montero, J., Butaney, M., Shimamura, T., Sholl, L., Ivanova, E.V., Tadi, M., Rogers, A., Repellin, C., Capelletti, M., Maertens, O., Goetz, E.M., Letai, A., Garraway, L.A., Lazzara, M.J., Rosen, N., Gray, N.S., Wong, K.K. and Janne, P.A., 2012. Reactivation of ERK signaling causes resistance to EGFR kinase inhibitors. Cancer Discov 2, 934-947.

Evan, G.I. and d'Adda di Fagagna, F., 2009. Cellular senescence: hot or what? Curr Opin Genet Dev 19, 25-31.

Evans, M.J., Stephens, R.J., Cabral, L.J. and Freeman, G., 1972. Cell renewal in the lungs of rats exposed to low levels of NO2. Arch Environ Health 24, 180-188.

Ewen, M.E. and Miller, S.J., 1996. p53 and translational control. Biochim Biophys Acta 1242, 181-184.

Falivelli, G., Lisabeth, E.M., Rubio de la Torre, E., Perez-Tenorio, G., Tosato, G., Salvucci, O. and Pasquale, E.B., 2013. Attenuation of eph receptor kinase activation in cancer cells by coexpressed ephrin ligands. PLoS One 8, e81445.

Feldser, D.M., Kostova, K.K., Winslow, M.M., Taylor, S.E., Cashman, C., Whittaker, C.A., Sanchez-Rivera, F.J., Resnick, R., Bronson, R., Hemann, M.T. and Jacks, T., 2010. Stage-specific sensitivity to p53 restoration during lung cancer progression. Nature 468, 572-575.

Ferlay, J., Soerjomataram, I., Dikshit, R., Eser, S., Mathers, C., Rebelo, M., Parkin, D.M., Forman, D. and Bray, F., 2015. Cancer incidence and mortality worldwide: sources, methods and major patterns in GLOBOCAN 2012. Int J Cancer 136, E359-386.

Fichtner, I., Rolff, J., Soong, R., Hoffmann, J., Hammer, S., Sommer, A., Becker, M. and Merk, J., 2008. Establishment of patient-derived non-small cell lung cancer xenografts as models for the identification of predictive biomarkers. Clin Cancer Res 14, 6456-6468.

Fiebig, H.H., Neumann, H.A., Henss, H., Koch, H., Kaiser, D. and Arnold, H., 1985. Development of three human small cell lung cancer models in nude mice. Recent Results Cancer Res 97, 77-86.

Finlay, C.A., Hinds, P.W. and Levine, A.J., 1989. The p53 proto-oncogene can act as a suppressor of transformation. Cell 57, 1083-1093.

Finlay, M.R., Anderton, M., Ashton, S., Ballard, P., Bethel, P.A., Box, M.R., Bradbury, R.H., Brown, S.J., Butterworth, S., Campbell, A., Chorley, C., Colclough, N., Cross, D.A., Currie, G.S., Grist, M., Hassall, L., Hill, G.B., James, D., James, M., Kemmitt, P., Klinowska, T., Lamont, G., Lamont, S.G., Martin, N., McFarland, H.L., Mellor, M.J., Orme, J.P., Perkins, D., Perkins, P., Richmond, G., Smith, P., Ward, R.A., Waring, M.J., Whittaker, D., Wells, S. and Wrigley, G.L., 2014. Discovery of a potent and selective EGFR inhibitor (AZD9291) of both sensitizing and T790M resistance mutations that spares the wild type form of the receptor. J Med Chem 57, 8249-8267.

Fisher, G.H., Wellen, S.L., Klimstra, D., Lenczowski, J.M., Tichelaar, J.W., Lizak, M.J., Whitsett, J.A., Koretsky, A. and Varmus, H.E., 2001. Induction and apoptotic regression of lung adenocarcinomas by regulation of a K-Ras transgene in the presence and absence of tumor suppressor genes. Genes Dev 15, 3249-3262.

Fleming, T.J., Fleming, M.L. and Malek, T.R., 1993. Selective expression of Ly-6G on myeloid lineage cells in mouse bone marrow. RB6-8C5 mAb to granulocyte-differentiation antigen (Gr-1) detects members of the Ly-6 family. J Immunol 151, 2399-2408.

Floyd, H.S., Farnsworth, C.L., Kock, N.D., Mizesko, M.C., Little, J.L., Dance, S.T., Everitt, J., Tichelaar, J., Whitsett, J.A. and Miller, M.S., 2005. Conditional expression of the mutant Ki-rasG12C allele results in formation of benign lung adenomas: development of a novel mouse lung tumor model. Carcinogenesis 26, 2196-2206.

Friboulet, L., Li, N., Katayama, R., Lee, C.C., Gainor, J.F., Crystal, A.S., Michellys, P.Y., Awad, M.M., Yanagitani, N., Kim, S., Pferdekamper, A.C., Li, J., Kasibhatla, S., Sun, F., Sun, X., Hua, S., McNamara, P., Mahmood, S., Lockerman, E.L., Fujita, N., Nishio, M., Harris, J.L., Shaw, A.T. and Engelman, J.A., 2014. The ALK inhibitor ceritinib overcomes crizotinib resistance in non-small cell lung cancer. Cancer Discov 4, 662-673.

Fridman, W.H., Pages, F., Sautes-Fridman, C. and Galon, J., 2012. The immune contexture in human tumours: impact on clinical outcome. Nat Rev Cancer 12, 298-306.

Frieden, L.A., Townsend, T.A., Vaught, D.B., Delaughter, D.M., Hwang, Y., Barnett, J.V. and Chen, J., 2010. Regulation of heart valve morphogenesis by Eph receptor ligand, ephrin-A1. Dev Dyn 239, 3226-3234.

Friedman, P.N., Chen, X., Bargonetti, J. and Prives, C., 1993. The p53 protein is an unusually shaped tetramer that binds directly to DNA. P Natl Acad Sci USA 90, 3319-3323.

Fu, X.W., Nurse, C.A., Wong, V. and Cutz, E., 2002. Hypoxia-induced secretion of serotonin from intact pulmonary neuroepithelial bodies in neonatal rabbit. J Physiol 539, 503-510.

Gabrilovich, D.I. and Nagaraj, S., 2009. Myeloid-derived suppressor cells as regulators of the immune system. Nat Rev Immunol 9, 162-174.

Ganesan, A.P., Johansson, M., Ruffell, B., Yagui-Beltran, A., Lau, J., Jablons, D.M. and Coussens, L.M., 2013. Tumor-infiltrating regulatory T cells inhibit endogenous cytotoxic T cell responses to lung adenocarcinoma. J Immunol 191, 2009-2017.

Gao, Y., Zhang, W., Han, X., Li, F., Wang, X., Wang, R., Fang, Z., Tong, X., Yao, S., Li, F., Feng, Y., Sun, Y., Hou, Y., Yang, Z., Guan, K., Chen, H., Zhang, L. and Ji, H., 2014. YAP inhibits squamous transdifferentiation of Lkb1-deficient lung adenocarcinoma through ZEB2-dependent DNp63 repression. Nat Commun 5, 4629.

George, J., Lim, J.S., Jang, S.J., Cun, Y., Ozretic, L., Kong, G., Leenders, F., Lu, X., Fernandez-Cuesta, L., Bosco, G., Muller, C., Dahmen, I., Jahchan, N.S., Park, K.S., Yang, D., Karnezis, A.N., Vaka, D., Torres, A., Wang, M.S., Korbel, J.O., Menon, R., Chun, S.M., Kim, D., Wilkerson, M., Hayes, N., Engelmann, D., Putzer, B., Bos, M., Michels, S., Vlasic, I., Seidel, D., Pinther, B., Schaub, P., Becker, C., Altmuller, J., Yokota, J., Kohno, T., Iwakawa, R., Tsuta, K., Noguchi, M., Muley, T., Hoffmann, H., Schnabel, P.A., Petersen, I., Chen, Y., Soltermann, A., Tischler, V., Choi, C.M., Kim, Y.H., Massion, P.P., Zou, Y., Jovanovic, D., Kontic, M., Wright, G.M., Russell, P.A., Solomon, B., Koch, I., Lindner, M., Muscarella, L.A., la Torre, A., Field, J.K., Jakopovic, M., Knezevic, J., Castanos-Velez, E., Roz, L., Pastorino, U., Brustugun, O.T., Lund-Iversen, M., Thunnissen, E., Kohler, J., Schuler, M., Botling, J., Sandelin, M., Sanchez-Cespedes, M., Salvesen, H.B., Achter, V., Lang, U., Bogus, M., Schneider, P.M., Zander, T., Ansen, S., Hallek, M., Wolf, J., Vingron, M., Yatabe, Y., Travis, W.D., Nurnberg, P., Reinhardt, C., Perner, S., Heukamp, L., Buttner, R., Haas, S.A., Brambilla, E., Peifer, M., Sage, J. and Thomas, R.K., 2015. Comprehensive genomic profiles of small cell lung cancer. Nature 524, 47-53.

Gerety, S.S. and Anderson, D.J., 2002. Cardiovascular ephrinB2 function is essential for embryonic angiogenesis. Development 129, 1397-1410.

Gerety, S.S., Wang, H.U., Chen, Z.F. and Anderson, D.J., 1999. Symmetrical mutant phenotypes of the receptor EphB4 and its specific transmembrane ligand ephrin-B2 in cardiovascular development. Mol Cell 4, 403-414.

Gerlinger, M., McGranahan, N., Dewhurst, S.M., Burrell, R.A., Tomlinson, I. and Swanton, C., 2014. Cancer: evolution within a lifetime. Annu Rev Genet 48, 215-236.

Ghaffar, H., Sahin, F., Sanchez-Cepedes, M., Su, G.H., Zahurak, M., Sidransky, D. and Westra, W.H., 2003. LKB1 protein expression in the evolution of glandular neoplasia of the lung. Clin Cancer Res 9, 2998-3003.

Ghosh, M., Brechbuhl, H.M., Smith, R.W., Li, B., Hicks, D.A., Titchner, T., Runkle, C.M. and Reynolds, S.D., 2011. Context-dependent differentiation of multipotential keratin 14-expressing tracheal basal cells. Am J Respir Cell Mol Biol 45, 403-410.

Giardiello, F.M., Welsh, S.B., Hamilton, S.R., Offerhaus, G.J., Gittelsohn, A.M., Booker, S.V., Krush, A.J., Yardley, J.H. and Luk, G.D., 1987. Increased risk of cancer in the Peutz-Jeghers syndrome. New Engl J Med 316, 1511-1514.

Gilbert, L.A. and Hemann, M.T., 2010. DNA damage-mediated induction of a chemoresistant niche. Cell 143, 355-366.

Gillet, J.P., Calcagno, A.M., Varma, S., Marino, M., Green, L.J., Vora, M.I., Patel, C., Orina, J.N., Eliseeva, T.A., Singal, V., Padmanabhan, R., Davidson, B., Ganapathi, R., Sood, A.K., Rueda, B.R., Ambudkar, S.V. and Gottesman, M.M., 2011. Redefining the relevance of established cancer cell lines to the study of mechanisms of clinical anti-cancer drug resistance. P Natl Acad Sci USA 108, 18708-18713.

Gontan, C., de Munck, A., Vermeij, M., Grosveld, F., Tibboel, D. and Rottier, R., 2008. Sox2 is important for two crucial processes in lung development: branching morphogenesis and epithelial cell differentiation. Dev Biol 317, 296-309.

Gonzalez-Sanchez, E., Martin-Caballero, J., Flores, J.M., Hernandez-Losa, J., Ma Angeles, M., Cortes, J., Mares, R., Barbacid, M. and Recio, J.A., 2013. Lkb1 loss promotes tumor progression of BRAF(V600E)-induced lung adenomas. PLoS One 8, e66933.

Gridelli, C., Rossi, A., Carbone, D.P., Guarize, J., Karachaliou, N., Mok, T., Petrella, F., Spaggiari, L. and Rosell, R., 2015. Non-small-cell lung cancer. Nature Reviews Disease Primers 1, 16.

Grunwald, I.C., Korte, M., Adelmann, G., Plueck, A., Kullander, K., Adams, R.H., Frotscher, M., Bonhoeffer, T. and Klein, R., 2004. Hippocampal plasticity requires postsynaptic ephrinBs. Nat Neurosci 7, 33-40.

Gucciardo, E., Sugiyama, N. and Lehti, K., 2014. Eph- and ephrin-dependent mechanisms in tumor and stem cell dynamics. Cell Mol Life Sci 71, 3685-3710.

Guerra, C., Collado, M., Navas, C., Schuhmacher, A.J., Hernandez-Porras, I., Canamero, M., Rodriguez-Justo, M., Serrano, M. and Barbacid, M., 2011. Pancreatitis-induced inflammation contributes to pancreatic cancer by inhibiting oncogene-induced senescence. Cancer Cell 19, 728-739.

Gwinn, D.M., Shackelford, D.B., Egan, D.F., Mihaylova, M.M., Mery, A., Vasquez, D.S., Turk, B.E. and Shaw, R.J., 2008. AMPK phosphorylation of raptor mediates a metabolic checkpoint. Mol Cell 30, 214-226.

Halama, N., Michel, S., Kloor, M., Zoernig, I., Benner, A., Spille, A., Pommerencke, T., von Knebel, D.M., Folprecht, G., Luber, B., Feyen, N., Martens, U.M., Beckhove, P., Gnjatic, S., Schirmacher, P., Herpel, E., Weitz, J., Grabe, N. and Jaeger, D., 2011. Localization and density of immune cells in the invasive margin of human colorectal cancer liver metastases are prognostic for response to chemotherapy. Cancer Res 71, 5670-5677.

Hall, A., Marshall, C.J., Spurr, N.K. and Weiss, R.A., 1983. Identification of transforming gene in two human sarcoma cell lines as a new member of the ras gene family located on chromosome 1. Nature 303, 396-400.

Han, X., Li, F., Fang, Z., Gao, Y., Li, F., Fang, R., Yao, S., Sun, Y., Li, L., Zhang, W., Ma, H., Xiao, Q., Ge, G., Fang, J., Wang, H., Zhang, L., Wong, K.K., Chen, H., Hou, Y. and Ji, H., 2014. Transdifferentiation of lung adenocarcinoma in mice with Lkb1 deficiency to squamous cell carcinoma. Nat Commun 5, 3261.

Hanahan, D. and Coussens, L.M., 2012. Accessories to the crime: functions of cells recruited to the tumor microenvironment. Cancer Cell 21, 309-322.

Hanahan, D. and Weinberg, R.A., 2000. The hallmarks of cancer. Cell 100, 57-70.

Hanahan, D. and Weinberg, R.A., 2011. Hallmarks of cancer: the next generation. Cell 144, 646-674.

Harris, C.C., 1996. p53 tumor suppressor gene: from the basic research laboratory to the clinic--an abridged historical perspective. Carcinogenesis 17, 1187-1198.

Harrod, K.S., Mounday, A.D., Stripp, B.R. and Whitsett, J.A., 1998. Clara cell secretory protein decreases lung inflammation after acute virus infection. Am J Physiol 275, L924-930.

Harvey, J.J., 1964. An Unidentified Virus Which Causes the Rapid Production of Tumours in Mice. Nature 204, 1104-1105.

Hearle, N., Schumacher, V., Menko, F.H., Olschwang, S., Boardman, L.A., Gille, J.J., Keller, J.J., Westerman, A.M., Scott, R.J., Lim, W., Trimbath, J.D., Giardiello, F.M., Gruber, S.B., Offerhaus, G.J., de Rooij, F.W., Wilson, J.H., Hansmann, A., Moslein, G., Royer-Pokora, B., Vogel, T., Phillips, R.K., Spigelman, A.D. and Houlston, R.S., 2006. Frequency and spectrum of cancers in the Peutz-Jeghers syndrome. Clin Cancer Res 12, 3209-3215.

Hemminki, A., 1999. The molecular basis and clinical aspects of Peutz-Jeghers syndrome. Cell Mol Life Sci 55, 735-750.

Hemminki, A., Markie, D., Tomlinson, I., Avizienyte, E., Roth, S., Loukola, A., Bignell, G., Warren, W., Aminoff, M., Hoglund, P., Jarvinen, H., Kristo, P., Pelin, K., Ridanpaa, M., Salovaara, R., Toro, T., Bodmer, W., Olschwang, S., Olsen, A.S., Stratton, M.R., de la Chapelle, A. and Aaltonen, L.A., 1998. A serine/threonine kinase gene defective in Peutz-Jeghers syndrome. Nature 391, 184-187.

Hezel, A.F. and Bardeesy, N., 2008. LKB1; linking cell structure and tumor suppression. Oncogene 27, 6908-6919.

Hezel, A.F., Gurumurthy, S., Granot, Z., Swisa, A., Chu, G.C., Bailey, G., Dor, Y., Bardeesy, N. and Depinho, R.A., 2008. Pancreatic LKB1 deletion leads to acinar polarity defects and cystic neoplasms. Mol Cell Biol 28, 2414-2425.

Hidalgo, M., Amant, F., Biankin, A.V., Budinska, E., Byrne, A.T., Caldas, C., Clarke, R.B., de Jong, S., Jonkers, J., Maelandsmo, G.M., Roman-Roman, S., Seoane, J., Trusolino, L. and Villanueva, A., 2014. Patient-derived xenograft models: an emerging platform for translational cancer research. Cancer Discov 4, 998-1013.

Himanen, J.P., Chumley, M.J., Lackmann, M., Li, C., Barton, W.A., Jeffrey, P.D., Vearing, C., Geleick, D., Feldheim, D.A., Boyd, A.W., Henkemeyer, M. and Nikolov, D.B., 2004. Repelling class discrimination: ephrin-A5 binds to and activates EphB2 receptor signaling. Nat Neurosci 7, 501-509.

Hinds, P., Finlay, C. and Levine, A.J., 1989. Mutation is required to activate the p53 gene for cooperation with the ras oncogene and transformation. J Virol 63, 739-746.

Hirai, H., Maru, Y., Hagiwara, K., Nishida, J. and Takaku, F., 1987. A novel putative tyrosine kinase receptor encoded by the eph gene. Science 238, 1717-1720.

Ho, J. and Benchimol, S., 2003. Transcriptional repression mediated by the p53 tumour suppressor. Cell Death Differ 10, 404-408.

Ho, V.M., Schaffer, B.E., Karnezis, A.N., Park, K.S. and Sage, J., 2009. The retinoblastoma gene Rb and its family member p130 suppress lung adenocarcinoma induced by oncogenic K-Ras. Oncogene 28, 1393-1399.

Hogan, B.L., Barkauskas, C.E., Chapman, H.A., Epstein, J.A., Jain, R., Hsia, C.C., Niklason, L., Calle, E., Le, A., Randell, S.H., Rock, J., Snitow, M., Krummel, M., Stripp, B.R., Vu, T., White, E.S., Whitsett, J.A. and Morrisey, E.E., 2014. Repair and regeneration of the respiratory system: complexity, plasticity, and mechanisms of lung stem cell function. Cell Stem Cell 15, 123-138.

Holmberg, J., Clarke, D.L. and Frisen, J., 2000. Regulation of repulsion versus adhesion by different splice forms of an Eph receptor. Nature 408, 203-206.

Hong, K.U., Reynolds, S.D., Giangreco, A., Hurley, C.M. and Stripp, B.R., 2001. Clara cell secretory protein-expressing cells of the airway neuroepithelial body microenvironment include a label-retaining subset and are critical for epithelial renewal after progenitor cell depletion. Am J Resp Cell Mol 24, 671-681.

Hong, K.U., Reynolds, S.D., Watkins, S., Fuchs, E. and Stripp, B.R., 2004. In vivo differentiation potential of tracheal basal cells: evidence for multipotent and unipotent subpopulations. American Journal of Physiology-Lung Cellular and Molecular Physiology 286, L643-649.

Hu, W., Feng, Z. and Levine, A.J., 2012. The Regulation of Multiple p53 Stress Responses is Mediated through MDM2. Genes Cancer 3, 199-208.

Imielinski, M., Berger, A.H., Hammerman, P.S., Hernandez, B., Pugh, T.J., Hodis, E., Cho, J., Suh, J., Capelletti, M., Sivachenko, A., Sougnez, C., Auclair, D., Lawrence, M.S., Stojanov, P., Cibulskis, K., Choi, K., de Waal, L., Sharifnia, T., Brooks, A., Greulich, H., Banerji, S., Zander, T., Seidel, D., Leenders, F., Ansen, S., Ludwig, C., Engel-Riedel, W., Stoelben, E., Wolf, J., Goparju, C., Thompson, K., Winckler, W., Kwiatkowski, D., Johnson, B.E., Janne, P.A., Miller, V.A., Pao, W., Travis, W.D., Pass, H.I., Gabriel, S.B.,

Lander, E.S., Thomas, R.K., Garraway, L.A., Getz, G. and Meyerson, M., 2012. Mapping the hallmarks of lung adenocarcinoma with massively parallel sequencing. Cell 150, 1107-1120.

Inoki, K., Zhu, T. and Guan, K.L., 2003. TSC2 mediates cellular energy response to control cell growth and survival. Cell 115, 577-590.

Ishii, Y., Rex, M., Scotting, P.J. and Yasugi, S., 1998. Region-specific expression of chicken Sox2 in the developing gut and lung epithelium: regulation by epithelial-mesenchymal interactions. Dev Dyn 213, 464-475.

Iwanaga, K., Yang, Y., Raso, M.G., Ma, L., Hanna, A.E., Thilaganathan, N., Moghaddam, S., Evans, C.M., Li, H., Cai, W.W., Sato, M., Minna, J.D., Wu, H., Creighton, C.J., Demayo, F.J., Wistuba, II and Kurie, J.M., 2008. Pten inactivation accelerates oncogenic K-ras-initiated tumorigenesis in a mouse model of lung cancer. Cancer Res 68, 1119-1127.

Jacks, T., Fazeli, A., Schmitt, E.M., Bronson, R.T., Goodell, M.A. and Weinberg, R.A., 1992. Effects of an Rb mutation in the mouse. Nature 359, 295-300.

Jackson, E.L., Olive, K.P., Tuveson, D.A., Bronson, R., Crowley, D., Brown, M. and Jacks, T., 2005. The differential effects of mutant p53 alleles on advanced murine lung cancer. Cancer Res 65, 10280-10288.

Jackson, E.L., Willis, N., Mercer, K., Bronson, R.T., Crowley, D., Montoya, R., Jacks, T. and Tuveson, D.A., 2001. Analysis of lung tumor initiation and progression using conditional expression of oncogenic K-ras. Genes Dev 15, 3243-3248.

Janes, P.W., Saha, N., Barton, W.A., Kolev, M.V., Wimmer-Kleikamp, S.H., Nievergall, E., Blobel, C.P., Himanen, J.P., Lackmann, M. and Nikolov, D.B., 2005. Adam meets Eph: an ADAM substrate recognition module acts as a molecular switch for ephrin cleavage in trans. Cell 123, 291-304.

Jellinghaus, S., Poitz, D.M., Ende, G., Augstein, A., Weinert, S., Stutz, B., Braun-Dullaeus, R.C., Pasquale, E.B. and Strasser, R.H., 2013. Ephrin-A1/EphA4-mediated adhesion of monocytes to endothelial cells. Biochim Biophys Acta 1833, 2201-2211.

Jenne, D.E., Reimann, H., Nezu, J., Friedel, W., Loff, S., Jeschke, R., Muller, O., Back, W. and Zimmer, M., 1998. Peutz-Jeghers syndrome is caused by mutations in a novel serine threonine kinase. Nat Genet 18, 38-43.

Ji, H., Li, D., Chen, L., Shimamura, T., Kobayashi, S., McNamara, K., Mahmood, U., Mitchell, A., Sun, Y., Al-Hashem, R., Chirieac, L.R., Padera, R., Bronson, R.T., Kim, W., Janne, P.A., Shapiro, G.I., Tenen, D., Johnson, B.E., Weissleder, R., Sharpless, N.E. and Wong, K.K., 2006. The impact of human EGFR kinase domain mutations on lung tumorigenesis and in vivo sensitivity to EGFR-targeted therapies. Cancer Cell 9, 485-495.

Ji, H., Ramsey, M.R., Hayes, D.N., Fan, C., McNamara, K., Kozlowski, P., Torrice, C., Wu, M.C., Shimamura, T., Perera, S.A., Liang, M.C., Cai, D., Naumov, G.N., Bao, L., Contreras, C.M., Li, D., Chen, L., Krishnamurthy, J., Koivunen, J., Chirieac, L.R., Padera, R.F., Bronson, R.T., Lindeman, N.I., Christiani, D.C., Lin, X., Shapiro, G.I., Janne, P.A., Johnson, B.E., Meyerson, M., Kwiatkowski, D.J., Castrillon, D.H., Bardeesy, N., Sharpless, N.E. and Wong, K.K., 2007a. LKB1 modulates lung cancer differentiation and metastasis. Nature 448, 807-810.

Ji, H., Wang, Z., Perera, S.A., Li, D., Liang, M.C., Zaghlul, S., McNamara, K., Chen, L., Albert, M., Sun, Y., Al-Hashem, R., Chirieac, L.R., Padera, R., Bronson, R.T., Thomas, R.K., Garraway, L.A., Janne, P.A., Johnson, B.E., Chin, L. and Wong, K.K., 2007b. Mutations in BRAF and KRAS converge on activation of the mitogen-activated protein kinase pathway in lung cancer mouse models. Cancer Res 67, 4933-4939.

Johnson, J.I., Decker, S., Zaharevitz, D., Rubinstein, L.V., Venditti, J.M., Schepartz, S., Kalyandrug, S., Christian, M., Arbuck, S., Hollingshead, M. and Sausville, E.A., 2001a. Relationships between drug activity in NCI preclinical in vitro and in vivo models and early clinical trials. Brit J Cancer 84, 1424-1431.

Johnson, L., Mercer, K., Greenbaum, D., Bronson, R.T., Crowley, D., Tuveson, D.A. and Jacks, T., 2001b. Somatic activation of the K-ras oncogene causes early onset lung cancer in mice. Nature 410, 1111-1116.

Jänne, P.A., Ramalingam, S.S., Yang, J.C., Ahn, M.J., Kim, D., Kim, S., Planchard, D., Ohe, Y., Felip, E., Watkins, C., Cantarini, M., Ghiorghiu, S. and Ranson, M.R., 2014. Clinical activity of the mutant-selective EGFR inhibitor AZD9291 in patients (pts) with EGFR inhibitor–resistant non-small cell lung cancer (NSCLC). 2014 ASCO Annual Meeting.

Kamata, T. and Feramisco, J.R., 1984. Epidermal growth factor stimulates guanine nucleotide binding activity and phosphorylation of ras oncogene proteins. Nature 310, 147-150.

Kar, A. and Gutierrez-Hartmann, A., 2013. Molecular mechanisms of ETS transcription factor-mediated tumorigenesis. Crit Rev Biochem Mol Biol 48, 522-543.

Karnoub, A.E. and Weinberg, R.A., 2008. Ras oncogenes: split personalities. Nat Rev Mol Cell Biol 9, 517-531.

Keir, M.E., Butte, M.J., Freeman, G.J. and Sharpe, A.H., 2008. PD-1 and its ligands in tolerance and immunity. Annu Rev Immunol 26, 677-704.

Kemphues, K.J., Priess, J.R., Morton, D.G. and Cheng, N.S., 1988. Identification of genes required for cytoplasmic localization in early C. elegans embryos. Cell 52, 311-320.

Khwaja, A., Rodriguez-Viciana, P., Wennstrom, S., Warne, P.H. and Downward, J., 1997. Matrix adhesion and Ras transformation both activate a phosphoinositide 3-OH kinase and protein kinase B/Akt cellular survival pathway. EMBO J 16, 2783-2793.

Kim, C.F.B., Jackson, E.L., Woolfenden, A.E., Lawrence, S., Babar, I., Vogel, S., Crowley, D., Bronson, R.T. and Jacks, T., 2005. Identification of bronchioalveolar stem cells in normal lung and lung cancer. Cell 121, 823-835.

Kimura, S., Hara, Y., Pineau, T., Fernandez-Salguero, P., Fox, C.H., Ward, J.M. and Gonzalez, F.J., 1996. The T/ebp null mouse: thyroid-specific enhancer-binding protein is essential for the organogenesis of the thyroid, lung, ventral forebrain, and pituitary. Genes Dev 10, 60-69.

Kirsten, W.H. and Mayer, L.A., 1967. Morphologic responses to a murine erythroblastosis virus. J Natl Cancer I 39, 311-335.

Kissil, J.L., Walmsley, M.J., Hanlon, L., Haigis, K.M., Bender Kim, C.F., Sweet-Cordero, A., Eckman, M.S., Tuveson, D.A., Capobianco, A.J., Tybulewicz, V.L. and Jacks, T., 2007. Requirement for Rac1 in a K-ras induced lung cancer in the mouse. Cancer Res 67, 8089-8094.

Kobayashi, S., Boggon, T.J., Dayaram, T., Janne, P.A., Kocher, O., Meyerson, M., Johnson, B.E., Eck, M.J., Tenen, D.G. and Halmos, B., 2005. EGFR mutation and resistance of non-small-cell lung cancer to gefitinib. New Engl J Med 352, 786-792.

Koebel, C.M., Vermi, W., Swann, J.B., Zerafa, N., Rodig, S.J., Old, L.J., Smyth, M.J. and Schreiber, R.D., 2007. Adaptive immunity maintains occult cancer in an equilibrium state. Nature 450, 903-907.

Koera, K., Nakamura, K., Nakao, K., Miyoshi, J., Toyoshima, K., Hatta, T., Otani, H., Aiba, A. and Katsuki, M., 1997. K-ras is essential for the development of the mouse embryo. Oncogene 15, 1151-1159.

Koivunen, J.P., Kim, J., Lee, J., Rogers, A.M., Park, J.O., Zhao, X., Naoki, K., Okamoto, I., Nakagawa, K., Yeap, B.Y., Meyerson, M., Wong, K.K., Richards, W.G., Sugarbaker, D.J., Johnson, B.E. and Janne, P.A., 2008. Mutations in the LKB1 tumour suppressor are frequently detected in tumours from Caucasian but not Asian lung cancer patients. Brit J Cancer 99, 245-252.

Kumar, M.S., Lu, J., Mercer, K.L., Golub, T.R. and Jacks, T., 2007. Impaired microRNA processing enhances cellular transformation and tumorigenesis. Nat Genet 39, 673-677.

Kuner, R., Muley, T., Meister, M., Ruschhaupt, M., Buness, A., Xu, E.C., Schnabel, P., Warth, A., Poustka, A., Sultmann, H. and Hoffmann, H., 2009. Global gene expression analysis reveals specific patterns of cell junctions in non-small cell lung cancer subtypes. Lung Cancer 63, 32-38.

Kwak, E.L., Bang, Y.J., Camidge, D.R., Shaw, A.T., Solomon, B., Maki, R.G., Ou, S.H., Dezube, B.J., Janne, P.A., Costa, D.B., Varella-Garcia, M., Kim, W.H., Lynch, T.J., Fidias, P., Stubbs, H., Engelman, J.A., Sequist, L.V., Tan, W., Gandhi, L., Mino-Kenudson, M., Wei, G.C., Shreeve, S.M., Ratain, M.J., Settleman, J., Christensen, J.G., Haber, D.A., Wilner, K., Salgia, R., Shapiro, G.I., Clark, J.W. and Iafrate, A.J., 2010. Anaplastic lymphoma kinase inhibition in non-small-cell lung cancer. New Engl J Med 363, 1693-1703.

Kwon, M.C. and Berns, A., 2013. Mouse models for lung cancer. Mol Oncol 7, 165-177.

Lackmann, M., Bucci, T., Mann, R.J., Kravets, L.A., Viney, E., Smith, F., Moritz, R.L., Carter, W., Simpson, R.J., Nicola, N.A., Mackwell, K., Nice, E.C., Wilks, A.F. and Boyd, A.W., 1996. Purification of a ligand for the EPH-like receptor HEK using a biosensor-based affinity detection approach. P Natl Acad Sci USA 93, 2523-2527.

Lackmann, M., Mann, R.J., Kravets, L., Smith, F.M., Bucci, T.A., Maxwell, K.F., Howlett, G.J., Olsson, J.E., Vanden Bos, T., Cerretti, D.P. and Boyd, A.W., 1997. Ligand for EPH-related kinase (LERK) 7 is the preferred high affinity ligand for the HEK receptor. J Biol Chem 272, 16521-16530.

Lane, D.P., 1992. Cancer. p53, guardian of the genome. Nature 358, 15-16.

Lau, A.N., Curtis, S.J., Fillmore, C.M., Rowbotham, S.P., Mohseni, M., Wagner, D.E., Beede, A.M., Montoro, D.T., Sinkevicius, K.W., Walton, Z.E., Barrios, J., Weiss, D.J., Camargo, F.D., Wong, K.K. and Kim, C.F., 2014. Tumor-propagating cells and Yap/Taz activity contribute to lung tumor progression and metastasis. EMBO J 33, 468-481.

Lawrenson, I.D., Wimmer-Kleikamp, S.H., Lock, P., Schoenwaelder, S.M., Down, M., Boyd, A.W., Alewood, P.F. and Lackmann, M., 2002. Ephrin-A5 induces rounding, blebbing and de-adhesion of EphA3-expressing 293T and melanoma cells by CrkII and Rho-mediated signalling. J Cell Sci 115, 1059-1072.

Lazzaro, D., Price, M., de Felice, M. and Di Lauro, R., 1991. The transcription factor TTF-1 is expressed at the onset of thyroid and lung morphogenesis and in restricted regions of the foetal brain. Development 113, 1093-1104.

Leeman, K.T., Fillmore, C.M. and Kim, C.F., 2014. Lung Stem and Progenitor Cells in Tissue Homeostasis and Disease. Stem Cells in Development and Disease 107, 207-233.

Li, F., Han, X., Li, F., Wang, R., Wang, H., Gao, Y., Wang, X., Fang, Z., Zhang, W., Yao, S., Tong, X., Wang, Y., Feng, Y., Sun, Y., Li, Y., Wong, K.K., Zhai, Q., Chen, H. and Ji, H., 2015. LKB1 Inactivation Elicits a Redox Imbalance to Modulate Non-small Cell Lung Cancer Plasticity and Therapeutic Response. Cancer Cell 27, 698-711.

Linzer, D.I. and Levine, A.J., 1979. Characterization of a 54K dalton cellular SV40 tumor antigen present in SV40-transformed cells and uninfected embryonal carcinoma cells. Cell 17, 43-52.

Lisabeth, E.M., Fernandez, C. and Pasquale, E.B., 2012. Cancer somatic mutations disrupt functions of the EphA3 receptor tyrosine kinase through multiple mechanisms. Biochemistry 51, 1464-1475.

Liu, C.Y., Wang, Y.M., Wang, C.L., Feng, P.H., Ko, H.W., Liu, Y.H., Wu, Y.C., Chu, Y., Chung, F.T., Kuo, C.H., Lee, K.Y., Lin, S.M., Lin, H.C., Wang, C.H., Yu, C.T. and Kuo, H.P., 2010. Population alterations of L-arginase- and inducible nitric oxide synthase-expressed CD11b+/CD14(-)/CD15+/CD33+ myeloid-derived suppressor cells and CD8+ T lymphocytes in patients with advanced-stage non-small cell lung cancer. J Cancer Res Clin Oncol 136, 35-45.

Liu, J., Cho, S.N., Akkanti, B., Jin, N., Mao, J., Long, W., Chen, T., Zhang, Y., Tang, X., Wistub, II, Creighton, C.J., Kheradmand, F. and DeMayo, F.J., 2015. ErbB2 Pathway Activation upon Smad4 Loss Promotes Lung Tumor Growth and Metastasis. Cell Rep 10, 1599.

Lu, Y., Futtner, C., Rock, J.R., Xu, X., Whitworth, W., Hogan, B.L. and Onaitis, M.W., 2010. Evidence that SOX2 overexpression is oncogenic in the lung. PLoS One 5, e11022.

Luo, H., Charpentier, T., Wang, X., Qi, S., Han, B., Wu, T., Terra, R., Lamarre, A. and Wu, J., 2011. Efnb1 and Efnb2 proteins regulate thymocyte development, peripheral T cell differentiation, and antiviral immune responses and are essential for interleukin-6 (IL-6) signaling. J Biol Chem 286, 41135-41152.

Lynch, T.J., Bell, D.W., Sordella, R., Gurubhagavatula, S., Okimoto, R.A., Brannigan, B.W., Harris, P.L., Haserlat, S.M., Supko, J.G., Haluska, F.G., Louis, D.N., Christiani, D.C., Settleman, J. and Haber, D.A., 2004. Activating mutations in the epidermal growth factor receptor underlying responsiveness of non-small-cell lung cancer to gefitinib. New Engl J Med 350, 2129-2139.

Macrae, M., Neve, R.M., Rodriguez-Viciana, P., Haqq, C., Yeh, J., Chen, C., Gray, J.W. and McCormick, F., 2005. A conditional feedback loop regulates Ras activity through EphA2. Cancer Cell 8, 111-118.

Maddaloni, E., Sabatino, F., Del Toro, R., Crugliano, S., Grande, S., Lauria Pantano, A., Maurizi, A.R., Palermo, A., Bonini, S., Pozzilli, P. and Manfrini, S., 2015. In vivo corneal confocal microscopy as a novel non-invasive tool to investigate cardiac autonomic neuropathy in Type 1 diabetes. Diabetic Med 32, 262-266.

Mainardi, S., Mijimolle, N., Francoz, S., Vicente-Duenas, C., Sanchez-Garcia, I. and Barbacid, M., 2014. Identification of cancer initiating cells in K-Ras driven lung adenocarcinoma. P Natl Acad Sci USA 111, 255-260.

Malkoski, S.P., Cleaver, T.G., Thompson, J.J., Sutton, W.P., Haeger, S.M., Rodriguez, K.J., Lu, S.L., Merrick, D. and Wang, X.J., 2014. Role of PTEN in basal cell derived lung carcinogenesis. Mol Carcinogen 53, 841-846.

Malkoski, S.P., Haeger, S.M., Cleaver, T.G., Rodriguez, K.J., Li, H., Lu, S.L., Feser, W.J., Baron, A.E., Merrick, D., Lighthall, J.G., Ijichi, H., Franklin, W. and Wang, X.J., 2012. Loss of transforming growth factor

beta type II receptor increases aggressive tumor behavior and reduces survival in lung adenocarcinoma and squamous cell carcinoma. Clin Cancer Res 18, 2173-2183.

Marino, S., Vooijs, M., van Der Gulden, H., Jonkers, J. and Berns, A., 2000. Induction of medulloblastomas in p53-null mutant mice by somatic inactivation of Rb in the external granular layer cells of the cerebellum. Genes Dev 14, 994-1004.

Martin, S.G. and St Johnston, D., 2003. A role for Drosophila LKB1 in anterior-posterior axis formation and epithelial polarity. Nature 421, 379-384.

Mazumdar, J., Hickey, M.M., Pant, D.K., Durham, A.C., Sweet-Cordero, A., Vachani, A., Jacks, T., Chodosh, L.A., Kissil, J.L., Simon, M.C. and Keith, B., 2010. HIF-2alpha deletion promotes Kras-driven lung tumor development. P Natl Acad Sci USA 107, 14182-14187.

McFadden, D.G., Papagiannakopoulos, T., Taylor-Weiner, A., Stewart, C., Carter, S.L., Cibulskis, K., Bhutkar, A., McKenna, A., Dooley, A., Vernon, A., Sougnez, C., Malstrom, S., Heimann, M., Park, J., Chen, F., Farago, A.F., Dayton, T., Shefler, E., Gabriel, S., Getz, G. and Jacks, T., 2014. Genetic and clonal dissection of murine small cell lung carcinoma progression by genome sequencing. Cell 156, 1298-1311.

Menges, C.W. and McCance, D.J., 2008. Constitutive activation of the Raf-MAPK pathway causes negative feedback inhibition of Ras-PI3K-AKT and cellular arrest through the EphA2 receptor. Oncogene 27, 2934-2940.

Metzger, R.J., Klein, O.D., Martin, G.R. and Krasnow, M.A., 2008. The branching programme of mouse lung development. Nature 453, 745-750.

Meuwissen, R., Linn, S.C., Linnoila, R.I., Zevenhoven, J., Mooi, W.J. and Berns, A., 2003. Induction of small cell lung cancer by somatic inactivation of both Trp53 and Rb1 in a conditional mouse model. Cancer Cell 4, 181-189.

Meuwissen, R., Linn, S.C., van der Valk, M., Mooi, W.J. and Berns, A., 2001. Mouse model for lung tumorigenesis through Cre/lox controlled sporadic activation of the K-Ras oncogene. Oncogene 20, 6551-6558.

Miettinen, P.J., Warburton, D., Bu, D., Zhao, J.S., Berger, J.E., Minoo, P., Koivisto, T., Allen, L., Dobbs, L., Werb, Z. and Derynck, R., 1997. Impaired lung branching morphogenesis in the absence of functional EGF receptor. Dev Biol 186, 224-236.

Mills, A.A., Zheng, B., Wang, X.J., Vogel, H., Roop, D.R. and Bradley, A., 1999. p63 is a p53 homologue required for limb and epidermal morphogenesis. Nature 398, 708-713.

Min, H., Danilenko, D.M., Scully, S.A., Bolon, B., Ring, B.D., Tarpley, J.E., DeRose, M. and Simonet, W.S., 1998. Fgf-10 is required for both limb and lung development and exhibits striking functional similarity to Drosophila branchless. Genes Dev 12, 3156-3161.

Minoo, P., Su, G., Drum, H., Bringas, P. and Kimura, S., 1999. Defects in tracheoesophageal and lung morphogenesis in Nkx2.1(-/-) mouse embryos. Dev Biol 209, 60-71.

Mirouse, V., Swick, L.L., Kazgan, N., St Johnston, D. and Brenman, J.E., 2007. LKB1 and AMPK maintain epithelial cell polarity under energetic stress. J Cell Biol 177, 387-392.

Mitsui, Y. and Schneider, E.L., 1976. Increased nuclear sizes in senescent human diploid fibroblast cultures. Exp Cell Res 100, 147-152.

Moodie, S.A., Willumsen, B.M., Weber, M.J. and Wolfman, A., 1993. Complexes of Ras.GTP with Raf-1 and mitogen-activated protein kinase kinase. Science 260, 1658-1661.

Morrisey, E.E. and Hogan, B.L.M., 2010. Preparing for the First Breath: Genetic and Cellular Mechanisms in Lung Development. Developmental Cell 18, 8-23.

Mukhopadhyay, A., Berrett, K.C., Kc, U., Clair, P.M., Pop, S.M., Carr, S.R., Witt, B.L. and Oliver, T.G., 2014. Sox2 cooperates with Lkb1 loss in a mouse model of squamous cell lung cancer. Cell Rep 8, 40-49.

Munder, M., Schneider, H., Luckner, C., Giese, T., Langhans, C.D., Fuentes, J.M., Kropf, P., Mueller, I., Kolb, A., Modolell, M. and Ho, A.D., 2006. Suppression of T-cell functions by human granulocyte arginase. Blood 108, 1627-1634.

Munoz-Espin, D., Canamero, M., Maraver, A., Gomez-Lopez, G., Contreras, J., Murillo-Cuesta, S., Rodriguez-Baeza, A., Varela-Nieto, I., Ruberte, J., Collado, M. and Serrano, M., 2013. Programmed cell senescence during mammalian embryonic development. Cell 155, 1104-1118.

Munoz-Espin, D. and Serrano, M., 2014. Cellular senescence: from physiology to pathology. Nat Rev Mol Cell Biol 15, 482-496.

Muzumdar, M.D., Tasic, B., Miyamichi, K., Li, L. and Luo, L., 2007. A global double-fluorescent Cre reporter mouse. Genesis 45, 593-605.

Nakagawa, K., Yasumitu, T., Fukuhara, K., Shiono, H. and Kikui, M., 2003. Poor prognosis after lung resection for patients with adenosquamous carcinoma of the lung. Ann Thorac Surg 75, 1740-1744.

Nave, B.T., Ouwens, M., Withers, D.J., Alessi, D.R. and Shepherd, P.R., 1999. Mammalian target of rapamycin is a direct target for protein kinase B: identification of a convergence point for opposing effects of insulin and amino-acid deficiency on protein translation. Biochem J 344 Pt 2, 427-431.

Nedelcu, A.M. and Tan, C., 2007. Early diversification and complex evolutionary history of the p53 tumor suppressor gene family. Dev Genes Evol 217, 801-806.

Nievergall, E., Janes, P.W., Stegmayer, C., Vail, M.E., Haj, F.G., Teng, S.W., Neel, B.G., Bastiaens, P.I. and Lackmann, M., 2010. PTP1B regulates Eph receptor function and trafficking. J Cell Biol 191, 1189-1203.

Nievergall, E., Lackmann, M. and Janes, P.W., 2012. Eph-dependent cell-cell adhesion and segregation in development and cancer. Cell Mol Life Sci 69, 1813-1842.

Ohashi, K., Sequist, L.V., Arcila, M.E., Moran, T., Chmielecki, J., Lin, Y.L., Pan, Y., Wang, L., de Stanchina, E., Shien, K., Aoe, K., Toyooka, S., Kiura, K., Fernandez-Cuesta, L., Fidias, P., Yang, J.C., Miller, V.A., Riely, G.J., Kris, M.G., Engelman, J.A., Vnencak-Jones, C.L., Dias-Santagata, D., Ladanyi, M. and Pao, W., 2012. Lung cancers with acquired resistance to EGFR inhibitors occasionally harbor BRAF gene mutations but lack mutations in KRAS, NRAS, or MEK1. P Natl Acad Sci USA 109, E2127-2133.

Olivier, M., Eeles, R., Hollstein, M., Khan, M.A., Harris, C.C. and Hainaut, P., 2002. The IARC TP53 database: new online mutation analysis and recommendations to users. Hum Mutat 19, 607-614.

Oricchio, E., Nanjangud, G., Wolfe, A.L., Schatz, J.H., Mavrakis, K.J., Jiang, M., Liu, X., Bruno, J., Heguy, A., Olshen, A.B., Socci, N.D., Teruya-Feldstein, J., Weis-Garcia, F., Tam, W., Shaknovich, R., Melnick, A., Himanen, J.P., Chaganti, R.S. and Wendel, H.G., 2011. The Eph-receptor A7 is a soluble tumor suppressor for follicular lymphoma. Cell 147, 554-564.

Ostrem, J.M., Peters, U., Sos, M.L., Wells, J.A. and Shokat, K.M., 2013. K-Ras(G12C) inhibitors allosterically control GTP affinity and effector interactions. Nature 503, 548-551.

Oxnard, G.R., Lo, P.C., Nishino, M., Dahlberg, S.E., Lindeman, N.I., Butaney, M., Jackman, D.M., Johnson, B.E. and Janne, P.A., 2013. Natural history and molecular characteristics of lung cancers harboring EGFR exon 20 insertions. Journal of Thoracic Oncology 8, 179-184.

Paez, J.G., Janne, P.A., Lee, J.C., Tracy, S., Greulich, H., Gabriel, S., Herman, P., Kaye, F.J., Lindeman, N., Boggon, T.J., Naoki, K., Sasaki, H., Fujii, Y., Eck, M.J., Sellers, W.R., Johnson, B.E. and Meyerson, M., 2004. EGFR mutations in lung cancer: correlation with clinical response to gefitinib therapy. Science 304, 1497-1500.

Pao, W. and Hutchinson, K.E., 2012. Chipping away at the lung cancer genome. Nat Med 18, 349-351.

Pao, W., Miller, V., Zakowski, M., Doherty, J., Politi, K., Sarkaria, I., Singh, B., Heelan, R., Rusch, V., Fulton, L., Mardis, E., Kupfer, D., Wilson, R., Kris, M. and Varmus, H., 2004. EGF receptor gene mutations are common in lung cancers from "never smokers" and are associated with sensitivity of tumors to gefitinib and erlotinib. P Natl Acad Sci USA 101, 13306-13311.

Parada, L.F., Tabin, C.J., Shih, C. and Weinberg, R.A., 1982. Human EJ bladder carcinoma oncogene is homologue of Harvey sarcoma virus ras gene. Nature 297, 474-478.

Pasquale, E.B., 2005. Eph receptor signalling casts a wide net on cell behaviour. Nat Rev Mol Cell Biol 6, 462-475.

Pasquale, E.B., 2008. Eph-ephrin bidirectional signaling in physiology and disease. Cell 133, 38-52.

Peifer, M., Fernandez-Cuesta, L., Sos, M.L., George, J., Seidel, D., Kasper, L.H., Plenker, D., Leenders, F., Sun, R., Zander, T., Menon, R., Koker, M., Dahmen, I., Muller, C., Di Cerbo, V., Schildhaus, H.U., Altmuller, J., Baessmann, I., Becker, C., de Wilde, B., Vandesompele, J., Bohm, D., Ansen, S., Gabler, F., Wilkening, I., Heynck, S., Heuckmann, J.M., Lu, X., Carter, S.L., Cibulskis, K., Banerji, S., Getz, G., Park, K.S., Rauh, D., Grutter, C., Fischer, M., Pasqualucci, L., Wright, G., Wainer, Z., Russell, P., Petersen, I., Chen, Y., Stoelben, E., Ludwig, C., Schnabel, P., Hoffmann, H., Muley, T., Brockmann, M., Engel-Riedel, W., Muscarella, L.A.,

Fazio, V.M., Groen, H., Timens, W., Sietsma, H., Thunnissen, E., Smit, E., Heideman, D.A., Snijders, P.J., Cappuzzo, F., Ligorio, C., Damiani, S., Field, J., Solberg, S., Brustugun, O.T., Lund-Iversen, M., Sanger, J., Clement, J.H., Soltermann, A., Moch, H., Weder, W., Solomon, B., Soria, J.C., Validire, P., Besse, B., Brambilla, E., Brambilla, C., Lantuejoul, S., Lorimier, P., Schneider, P.M., Hallek, M., Pao, W., Meyerson, M., Sage, J., Shendure, J., Schneider, R., Buttner, R., Wolf, J., Nurnberg, P., Perner, S., Heukamp, L.C., Brindle, P.K., Haas, S. and Thomas, R.K., 2012. Integrative genome analyses identify key somatic driver mutations of small-cell lung cancer. Nat Genet 44, 1104-1110.

Peng, T. and Morrisey, E.E., 2013. Development of the pulmonary vasculature: Current understanding and concepts for the future. Pulm Circ 3, 176-178.

Peng, T., Tian, Y., Boogerd, C.J., Lu, M.M., Kadzik, R.S., Stewart, K.M., Evans, S.M. and Morrisey, E.E., 2013. Coordination of heart and lung co-development by a multipotent cardiopulmonary progenitor. Nature 500, 589-592.

Pepicelli, C.V., Lewis, P.M. and McMahon, A.P., 1998. Sonic hedgehog regulates branching morphogenesis in the mammalian lung. Curr Biol 8, 1083-1086.

Perera, S.A., Li, D., Shimamura, T., Raso, M.G., Ji, H., Chen, L., Borgman, C.L., Zaghlul, S., Brandstetter, K.A., Kubo, S., Takahashi, M., Chirieac, L.R., Padera, R.F., Bronson, R.T., Shapiro, G.I., Greulich, H., Meyerson, M., Guertler, U., Chesa, P.G., Solca, F., Wistuba, II and Wong, K.K., 2009. HER2YVMA drives rapid development of adenosquamous lung tumors in mice that are sensitive to BIBW2992 and rapamycin combination therapy. P Natl Acad Sci USA 106, 474-479.

Planchard, D. and Le Pechoux, C., 2011. Small cell lung cancer: new clinical recommendations and current status of biomarker assessment. Eur J Cancer 47 Suppl 3, S272-283.

Politi, K., Zakowski, M.F., Fan, P.D., Schonfeld, E.A., Pao, W. and Varmus, H.E., 2006. Lung adenocarcinomas induced in mice by mutant EGF receptors found in human lung cancers respond to a tyrosine kinase inhibitor or to down-regulation of the receptors. Genes Dev 20, 1496-1510.

Qin, H., Noberini, R., Huan, X., Shi, J., Pasquale, E.B. and Song, J., 2010. Structural characterization of the EphA4-Ephrin-B2 complex reveals new features enabling Eph-ephrin binding promiscuity. J Biol Chem 285, 644-654.

Que, J., Luo, X., Schwartz, R.J. and Hogan, B.L., 2009. Multiple roles for Sox2 in the developing and adult mouse trachea. Development 136, 1899-1907.

Rawlins, E.L., Clark, C.P., Xue, Y. and Hogan, B.L., 2009a. The Id2+ distal tip lung epithelium contains individual multipotent embryonic progenitor cells. Development 136, 3741-3745.

Rawlins, E.L., Okubo, T., Xue, Y., Brass, D.M., Auten, R.L., Hasegawa, H., Wang, F. and Hogan, B.L., 2009b. The role of Scgb1a1+ Clara cells in the long-term maintenance and repair of lung airway, but not alveolar, epithelium. Cell Stem Cell 4, 525-534.

Rawlins, E.L., Ostrowski, L.E., Randell, S.H. and Hogan, B.L., 2007. Lung development and repair: contribution of the ciliated lineage. P Natl Acad Sci USA 104, 410-417.

Reddy, E.P., Reynolds, R.K., Santos, E. and Barbacid, M., 1982. A point mutation is responsible for the acquisition of transforming properties by the T24 human bladder carcinoma oncogene. Nature 300, 149-152.

Riley, T., Sontag, E., Chen, P. and Levine, A., 2008. Transcriptional control of human p53-regulated genes. Nat Rev Mol Cell Biol 9, 402-412.

Rock, J.R., Onaitis, M.W., Rawlins, E.L., Lu, Y., Clark, C.P., Xue, Y., Randell, S.H. and Hogan, B.L., 2009. Basal cells as stem cells of the mouse trachea and human airway epithelium. P Natl Acad Sci USA 106, 12771-12775.

Rock, J.R., Randell, S.H. and Hogan, B.L.M., 2010. Airway basal stem cells: a perspective on their roles in epithelial homeostasis and remodeling. Disease Models & Mechanisms 3, 545-556.

Rodier, F. and Campisi, J., 2011. Four faces of cellular senescence. J Cell Biol 192, 547-556.

Rodriguez-Viciana, P., Warne, P.H., Dhand, R., Vanhaesebroeck, B., Gout, I., Fry, M.J., Waterfield, M.D. and Downward, J., 1994. Phosphatidylinositol-3-OH kinase as a direct target of Ras. Nature 370, 527-532.

Rodriguez, P.C., Quiceno, D.G., Zabaleta, J., Ortiz, B., Zea, A.H., Piazuelo, M.B., Delgado, A., Correa, P., Brayer, J., Sotomayor, E.M., Antonia, S., Ochoa, J.B. and Ochoa, A.C., 2004. Arginase I production in the

tumor microenvironment by mature myeloid cells inhibits T-cell receptor expression and antigen-specific T-cell responses. Cancer Res 64, 5839-5849.

Rosell, R., Carcereny, E., Gervais, R., Vergnenegre, A., Massuti, B., Felip, E., Palmero, R., Garcia-Gomez, R., Pallares, C., Sanchez, J.M., Porta, R., Cobo, M., Garrido, P., Longo, F., Moran, T., Insa, A., De Marinis, F., Corre, R., Bover, I., Illiano, A., Dansin, E., de Castro, J., Milella, M., Reguart, N., Altavilla, G., Jimenez, U., Provencio, M., Moreno, M.A., Terrasa, J., Munoz-Langa, J., Valdivia, J., Isla, D., Domine, M., Molinier, O., Mazieres, J., Baize, N., Garcia-Campelo, R., Robinet, G., Rodriguez-Abreu, D., Lopez-Vivanco, G., Gebbia, V., Ferrera-Delgado, L., Bombaron, P., Bernabe, R., Bearz, A., Artal, A., Cortesi, E., Rolfo, C., Sanchez-Ronco, M., Drozdowskyj, A., Queralt, C., de Aguirre, I., Ramirez, J.L., Sanchez, J.J., Molina, M.A., Taron, M., Paz-Ares, L., Spanish Lung Cancer Group in collaboration with Groupe Francais de, P.-C. and Associazione Italiana Oncologia, T., 2012. Erlotinib versus standard chemotherapy as first-line treatment for European patients with advanced EGFR mutation-positive non-small-cell lung cancer (EURTAC): a multicentre, open-label, randomised phase 3 trial. Lancet Oncol 13, 239-246.

Rudin, C.M., Durinck, S., Stawiski, E.W., Poirier, J.T., Modrusan, Z., Shames, D.S., Bergbower, E.A., Guan, Y., Shin, J., Guillory, J., Rivers, C.S., Foo, C.K., Bhatt, D., Stinson, J., Gnad, F., Haverty, P.M., Gentleman, R., Chaudhuri, S., Janakiraman, V., Jaiswal, B.S., Parikh, C., Yuan, W., Zhang, Z., Koeppen, H., Wu, T.D., Stern, H.M., Yauch, R.L., Huffman, K.E., Paskulin, D.D., Illei, P.B., Varella-Garcia, M., Gazdar, A.F., de Sauvage, F.J., Bourgon, R., Minna, J.D., Brock, M.V. and Seshagiri, S., 2012. Comprehensive genomic analysis identifies SOX2 as a frequently amplified gene in small-cell lung cancer. Nat Genet 44, 1111-1116.

Sadowski, P.D., 1995. The Flp recombinase of the 2-microns plasmid of Saccharomyces cerevisiae. Prog Nucleic Acid Res Mol Biol 51, 53-91.

Sakiyama, J., Yamagishi, A. and Kuroiwa, A., 2003. Tbx4-Fgf10 system controls lung bud formation during chicken embryonic development. Development 130, 1225-1234.

Sanchez-Cespedes, M., 2007. A role for LKB1 gene in human cancer beyond the Peutz-Jeghers syndrome. Oncogene 26, 7825-7832.

Sanchez-Cespedes, M., Parrella, P., Esteller, M., Nomoto, S., Trink, B., Engles, J.M., Westra, W.H., Herman, J.G. and Sidransky, D., 2002. Inactivation of LKB1/STK11 is a common event in adenocarcinomas of the lung. Cancer Res 62, 3659-3662.

Sanchez-Rivera, F.J. and Jacks, T., 2015. Applications of the CRISPR-Cas9 system in cancer biology. Nat Rev Cancer 15, 387-395.

Sanchez-Rivera, F.J., Papagiannakopoulos, T., Romero, R., Tammela, T., Bauer, M.R., Bhutkar, A., Joshi, N.S., Subbaraj, L., Bronson, R.T., Xue, W. and Jacks, T., 2014. Rapid modelling of cooperating genetic events in cancer through somatic genome editing. Nature 516, 428-431.

Santos, E., Martin-Zanca, D., Reddy, E.P., Pierotti, M.A., Della Porta, G. and Barbacid, M., 1984. Malignant activation of a K-ras oncogene in lung carcinoma but not in normal tissue of the same patient. Science 223, 661-664.

Santos, E., Tronick, S.R., Aaronson, S.A., Pulciani, S. and Barbacid, M., 1982. T24 human bladder carcinoma oncogene is an activated form of the normal human homologue of BALB- and Harvey-MSV transforming genes. Nature 298, 343-347.

Sarraf, K.M., Belcher, E., Raevsky, E., Nicholson, A.G., Goldstraw, P. and Lim, E., 2009. Neutrophil/lymphocyte ratio and its association with survival after complete resection in non-small cell lung cancer. J Thorac Cardiovasc Surg 137, 425-428.

Sasaki, T., Rodig, S.J., Chirieac, L.R. and Janne, P.A., 2010. The biology and treatment of EML4-ALK non-small cell lung cancer. Eur J Cancer 46, 1773-1780.

Sauer, B. and Henderson, N., 1988. Site-specific DNA recombination in mammalian cells by the Cre recombinase of bacteriophage P1. P Natl Acad Sci USA 85, 5166-5170.

Schaffer, B.E., Park, K.S., Yiu, G., Conklin, J.F., Lin, C., Burkhart, D.L., Karnezis, A.N., Sweet-Cordero, E.A. and Sage, J., 2010. Loss of p130 accelerates tumor development in a mouse model for human small-cell lung carcinoma. Cancer Res 70, 3877-3883.

Schramek, D., Kotsinas, A., Meixner, A., Wada, T., Elling, U., Pospisilik, J.A., Neely, G.G., Zwick, R.H., Sigl, V., Forni, G., Serrano, M., Gorgoulis, V.G. and Penninger, J.M., 2011. The stress kinase MKK7 couples oncogenic stress to p53 stability and tumor suppression. Nat Genet 43, 212-219.

Schuller, H.M., Plummer, H.K., 3rd and Jull, B.A., 2003. Receptor-mediated effects of nicotine and its nitrosated derivative NNK on pulmonary neuroendocrine cells. Anat Rec A Discov Mol Cell Evol Biol 270, 51-58.

Schwartzberg, P.L., Goff, S.P. and Robertson, E.J., 1989. Germ-line transmission of a c-abl mutation produced by targeted gene disruption in ES cells. Science 246, 799-803.

Schwarz, M.A., Caldwell, L., Cafasso, D. and Zheng, H., 2009. Emerging pulmonary vasculature lacks fate specification. Am J Physiol Lung Cell Mol Physiol 296, L71-81.

Sekine, K., Ohuchi, H., Fujiwara, M., Yamasaki, M., Yoshizawa, T., Sato, T., Yagishita, N., Matsui, D., Koga, Y., Itoh, N. and Kato, S., 1999. Fgf10 is essential for limb and lung formation. Nat Genet 21, 138-141.

Serrano, M., Lin, A.W., McCurrach, M.E., Beach, D. and Lowe, S.W., 1997. Oncogenic ras provokes premature cell senescence associated with accumulation of p53 and p16INK4a. Cell 88, 593-602.

Shaw, A.T., Kim, D.W., Mehra, R., Tan, D.S., Felip, E., Chow, L.Q., Camidge, D.R., Vansteenkiste, J., Sharma, S., De Pas, T., Riely, G.J., Solomon, B.J., Wolf, J., Thomas, M., Schuler, M., Liu, G., Santoro, A., Lau, Y.Y., Goldwasser, M., Boral, A.L. and Engelman, J.A., 2014a. Ceritinib in ALK-rearranged non-small-cell lung cancer. New Engl J Med 370, 1189-1197.

Shaw, A.T., Meissner, A., Dowdle, J.A., Crowley, D., Magendantz, M., Ouyang, C., Parisi, T., Rajagopal, J., Blank, L.J., Bronson, R.T., Stone, J.R., Tuveson, D.A., Jaenisch, R. and Jacks, T., 2007. Sprouty-2 regulates oncogenic K-ras in lung development and tumorigenesis. Genes Dev 21, 694-707.

Shaw, A.T., Ou, S.H., Bang, Y.J., Camidge, D.R., Solomon, B.J., Salgia, R., Riely, G.J., Varella-Garcia, M., Shapiro, G.I., Costa, D.B., Doebele, R.C., Le, L.P., Zheng, Z., Tan, W., Stephenson, P., Shreeve, S.M., Tye, L.M., Christensen, J.G., Wilner, K.D., Clark, J.W. and Iafrate, A.J., 2014b. Crizotinib in ROS1-rearranged non-small-cell lung cancer. New Engl J Med 371, 1963-1971.

Shchors, K., Nozawa, H., Xu, J., Rostker, F., Swigart-Brown, L., Evan, G. and Hanahan, D., 2013. Increased invasiveness of MMP-9-deficient tumors in two mouse models of neuroendocrine tumorigenesis. Oncogene 32, 502-513.

Smith, A., Robinson, V., Patel, K. and Wilkinson, D.G., 1997. The EphA4 and EphB1 receptor tyrosine kinases and ephrin-B2 ligand regulate targeted migration of branchial neural crest cells. Curr Biol 7, 561-570.

Snyder, E.L., Watanabe, H., Magendantz, M., Hoersch, S., Chen, T.A., Wang, D.G., Crowley, D., Whittaker, C.A., Meyerson, M., Kimura, S. and Jacks, T., 2013. Nkx2-1 represses a latent gastric differentiation program in lung adenocarcinoma. Mol Cell 50, 185-199.

Snyder, J.C., Reynolds, S.D., Hollingsworth, J.W., Li, Z., Kaminski, N. and Stripp, B.R., 2010. Clara cells attenuate the inflammatory response through regulation of macrophage behavior. Am J Respir Cell Mol Biol 42, 161-171.

Soda, M., Choi, Y.L., Enomoto, M., Takada, S., Yamashita, Y., Ishikawa, S., Fujiwara, S., Watanabe, H., Kurashina, K., Hatanaka, H., Bando, M., Ohno, S., Ishikawa, Y., Aburatani, H., Niki, T., Sohara, Y., Sugiyama, Y. and Mano, H., 2007. Identification of the transforming EML4-ALK fusion gene in non-small-cell lung cancer. Nature 448, 561-566.

Soda, M., Takada, S., Takeuchi, K., Choi, Y.L., Enomoto, M., Ueno, T., Haruta, H., Hamada, T., Yamashita, Y., Ishikawa, Y., Sugiyama, Y. and Mano, H., 2008. A mouse model for EML4-ALK-positive lung cancer. P Natl Acad Sci USA 105, 19893-19897.

Song, Z., Lin, B., Shao, L. and Zhang, Y., 2013. Therapeutic efficacy of gefitinib and erlotinib in patients with advanced lung adenosquamous carcinoma. J Chin Med Assoc 76, 481-485.

Sordella, R., Bell, D.W., Haber, D.A. and Settleman, J., 2004. Gefitinib-sensitizing EGFR mutations in lung cancer activate anti-apoptotic pathways. Science 305, 1163-1167.

Spaargaren, M. and Bischoff, J.R., 1994. Identification of the guanine nucleotide dissociation stimulator for Ral as a putative effector molecule of R-ras, H-ras, K-ras, and Rap. P Natl Acad Sci USA 91, 12609-12613.

Stephen, L.J., Fawkes, A.L., Verhoeve, A., Lemke, G. and Brown, A., 2007. A critical role for the EphA3 receptor tyrosine kinase in heart development. Dev Biol 302, 66-79.

Sternberg, N. and Hamilton, D., 1981. Bacteriophage P1 site-specific recombination. I. Recombination between loxP sites. J Mol Biol 150, 467-486.

Stewart, B.W., Wild, C., International Agency for Research on Cancer and World Health Organization, 2014. World cancer report 2014. International Agency for Research on Cancer WHO Press, Lyon, France.

Storer, M., Mas, A., Robert-Moreno, A., Pecoraro, M., Ortells, M.C., Di Giacomo, V., Yosef, R., Pilpel, N., Krizhanovsky, V., Sharpe, J. and Keyes, W.M., 2013. Senescence is a developmental mechanism that contributes to embryonic growth and patterning. Cell 155, 1119-1130.

Sugiyama, N., Gucciardo, E., Tatti, O., Varjosalo, M., Hyytiainen, M., Gstaiger, M. and Lehti, K., 2013. EphA2 cleavage by MT1-MMP triggers single cancer cell invasion via homotypic cell repulsion. J Cell Biol 201, 467-484.

Sunday, M.E., Haley, K.J., Sikorski, K., Graham, S.A., Emanuel, R.L., Zhang, F., Mu, Q., Shahsafaei, A. and Hatzis, D., 1999. Calcitonin driven v-Ha-ras induces multilineage pulmonary epithelial hyperplasias and neoplasms. Oncogene 18, 4336-4347.

Sutherland, K.D. and Berns, A., 2010. Cell of origin of lung cancer. Mol Oncol 4, 397-403.

Sutherland, K.D., Proost, N., Brouns, I., Adriaensen, D., Song, J.Y. and Berns, A., 2011. Cell of origin of small cell lung cancer: inactivation of Trp53 and Rb1 in distinct cell types of adult mouse lung. Cancer Cell 19, 754-764.

Sutherland, K.D., Song, J.Y., Kwon, M.C., Proost, N., Zevenhoven, J. and Berns, A., 2014. Multiple cells-of-origin of mutant K-Ras-induced mouse lung adenocarcinoma. P Natl Acad Sci USA 111, 4952-4957.

Swords, R.T., Wei, A.H., Durrant, S., Advani, A.S., Hertzberg, M.S., Lewis, I.D., Greenberg, P.L., Cortes, J., Yarranton, G.T., Walling, J.M. and Lancet, J.E., 2013. KB004, a Novel Non-Fucosylated Humaneered® Antibody, Targeting EphA3, Is Active and Well Tolerated in a Phase I/II Study of Advanced Hematologic Malignancies 55th ASH Annual Meeting and Exposition, New Orleans, LA. Washington, DC.

Tabassum, D.P. and Polyak, K., 2015. Tumorigenesis: it takes a village. Nat Rev Cancer 15, 473-483.

Tabin, C.J., Bradley, S.M., Bargmann, C.I., Weinberg, R.A., Papageorge, A.G., Scolnick, E.M., Dhar, R., Lowy, D.R. and Chang, E.H., 1982. Mechanism of activation of a human oncogene. Nature 300, 143-149.

Tang, N., Marshall, W.F., McMahon, M., Metzger, R.J. and Martin, G.R., 2011. Control of mitotic spindle angle by the RAS-regulated ERK1/2 pathway determines lung tube shape. Science 333, 342-345.

Taparowsky, E., Suard, Y., Fasano, O., Shimizu, K., Goldfarb, M. and Wigler, M., 1982. Activation of the T24 bladder carcinoma transforming gene is linked to a single amino acid change. Nature 300, 762-765.

Teramukai, S., Kitano, T., Kishida, Y., Kawahara, M., Kubota, K., Komuta, K., Minato, K., Mio, T., Fujita, Y., Yonei, T., Nakano, K., Tsuboi, M., Shibata, K., Furuse, K. and Fukushima, M., 2009. Pretreatment neutrophil count as an independent prognostic factor in advanced non-small-cell lung cancer: an analysis of Japan Multinational Trial Organisation LC00-03. Eur J Cancer 45, 1950-1958.

Tochigi, N., Dacic, S., Nikiforova, M., Cieply, K.M. and Yousem, S.A., 2011. Adenosquamous carcinoma of the lung: a microdissection study of KRAS and EGFR mutational and amplification status in a western patient population. Am J Clin Pathol 135, 783-789.

Topalian, S.L., Hodi, F.S., Brahmer, J.R., Gettinger, S.N., Smith, D.C., McDermott, D.F., Powderly, J.D., Carvajal, R.D., Sosman, J.A., Atkins, M.B., Leming, P.D., Spigel, D.R., Antonia, S.J., Horn, L., Drake, C.G., Pardoll, D.M., Chen, L., Sharfman, W.H., Anders, R.A., Taube, J.M., McMiller, T.L., Xu, H., Korman, A.J., Jure-Kunkel, M., Agrawal, S., McDonald, D., Kollia, G.D., Gupta, A., Wigginton, J.M. and Sznol, M., 2012. Safety, activity, and immune correlates of anti-PD-1 antibody in cancer. New Engl J Med 366, 2443-2454.

Torres, J.Z., Miller, J.J. and Jackson, P.K., 2009. High-throughput generation of tagged stable cell lines for proteomic analysis. Proteomics 9, 2888-2891.

Travis, W.D., Brambilla, E., Burke, A.P., Marx, A. and Nicholson, A.G., 2015. WHO Classification of Tumors of the Lung, Pleura, Thymus and Heart, 4th ed. International Agency for Research on Cancer.

Travis, W.D., Brambilla, E., Noguchi, M., Nicholson, A.G., Geisinger, K.R., Yatabe, Y., Beer, D.G., Powell, C.A., Riely, G.J., Van Schil, P.E., Garg, K., Austin, J.H., Asamura, H., Rusch, V.W., Hirsch, F.R., Scagliotti, G., Mitsudomi, T., Huber, R.M., Ishikawa, Y., Jett, J., Sanchez-Cespedes, M., Sculier, J.P., Takahashi, T., Tsuboi, M., Vansteenkiste, J., Wistuba, I., Yang, P.C., Aberle, D., Brambilla, C., Flieder, D., Franklin, W., Gazdar, A., Gould, M., Hasleton, P., Henderson, D., Johnson, B., Johnson, D., Kerr, K., Kuriyama, K., Lee, J.S., Miller, V.A., Petersen, I., Roggli, V., Rosell, R., Saijo, N., Thunnissen, E., Tsao, M. and Yankelewitz, D., 2011. International association for the study of lung cancer/american thoracic society/european respiratory

society international multidisciplinary classification of lung adenocarcinoma. Journal of Thoracic Oncology 6, 244-285.

Travis, W.D., Brambilla, E. and Riely, G.J., 2013. New pathologic classification of lung cancer: relevance for clinical practice and clinical trials. J Clin Oncol 31, 992-1001.

Treutlein, B., Brownfield, D.G., Wu, A.R., Neff, N.F., Mantalas, G.L., Espinoza, F.H., Desai, T.J., Krasnow, M.A. and Quake, S.R., 2014. Reconstructing lineage hierarchies of the distal lung epithelium using single-cell RNA-seq. Nature 509, 371-375.

Tricker, E.M., Xu, C., Uddin, S., Capelletti, M., Ercan, D., Ogino, A., Pratilas, C.A., Rosen, N., Gray, N.S., Wong, K.K. and Janne, P.A., 2015. Combined EGFR/MEK Inhibition Prevents the Emergence of Resistance in EGFR-Mutant Lung Cancer. Cancer Discov.

Tsao, P.N., Vasconcelos, M., Izvolsky, K.I., Qian, J., Lu, J. and Cardoso, W.V., 2009. Notch signaling controls the balance of ciliated and secretory cell fates in developing airways. Development 136, 2297-2307.

Tu, S., Bhagat, G., Cui, G., Takaishi, S., Kurt-Jones, E.A., Rickman, B., Betz, K.S., Penz-Oesterreicher, M., Bjorkdahl, O., Fox, J.G. and Wang, T.C., 2008. Overexpression of interleukin-1beta induces gastric inflammation and cancer and mobilizes myeloid-derived suppressor cells in mice. Cancer Cell 14, 408-419.

Turner, B.M., Cagle, P.T., Sainz, I.M., Fukuoka, J., Shen, S.S. and Jagirdar, J., 2012. Napsin A, a new marker for lung adenocarcinoma, is complementary and more sensitive and specific than thyroid transcription factor 1 in the differential diagnosis of primary pulmonary carcinoma: evaluation of 1674 cases by tissue microarray. Arch Pathol Lab Med 136, 163-171.

Vaahtomeri, K. and Makela, T.P., 2011. Molecular mechanisms of tumor suppression by LKB1. FEBS Lett 585, 944-951.

Vadivel, A., van Haaften, T., Alphonse, R.S., Rey-Parra, G.J., Ionescu, L., Haromy, A., Eaton, F., Michelakis, E. and Thebaud, B., 2012. Critical role of the axonal guidance cue EphrinB2 in lung growth, angiogenesis, and repair. Am J Respir Crit Care Med 185, 564-574.

Wagner, P., Simanis, V., Maimets, T., Keenan, E., Addison, C., Brain, R., Grimaldi, M., Sturzbecher, H.W. and Jenkins, J., 1991. A human tumour-derived mutant p53 protein induces a p34cdc2 reversible growth arrest in fission yeast. Oncogene 6, 1539-1547.

Vaidya, A., Pniak, A., Lemke, G. and Brown, A., 2003. EphA3 null mutants do not demonstrate motor axon guidance defects. Mol Cell Biol 23, 8092-8098.

Vail, M.E., Murone, C., Tan, A., Hii, L., Abebe, D., Janes, P.W., Lee, F.T., Baer, M., Palath, V., Bebbington, C., Yarranton, G., Llerena, C., Garic, S., Abramson, D., Cartwright, G., Scott, A.M. and Lackmann, M., 2014. Targeting EphA3 inhibits cancer growth by disrupting the tumor stromal microenvironment. Cancer Res 74, 4470-4481.

Wakeling, A.E., Guy, S.P., Woodburn, J.R., Ashton, S.E., Curry, B.J., Barker, A.J. and Gibson, K.H., 2002. ZD1839 (Iressa): an orally active inhibitor of epidermal growth factor signaling with potential for cancer therapy. Cancer Res 62, 5749-5754.

Wang, H.U., Chen, Z.F. and Anderson, D.J., 1998. Molecular distinction and angiogenic interaction between embryonic arteries and veins revealed by ephrin-B2 and its receptor Eph-B4. Cell 93, 741-753.

Vassella, E., Langsch, S., Dettmer, M.S., Schlup, C., Neuenschwander, M., Frattini, M., Gugger, M. and Schafer, S.C., 2015. Molecular profiling of lung adenosquamous carcinoma: hybrid or genuine type? Oncotarget 6, 23905-23916.

Watson, J.K., Rulands, S., Wilkinson, A.C., Wuidart, A., Ousset, M., Van Keymeulen, A., Gottgens, B., Blanpain, C., Simons, B.D. and Rawlins, E.L., 2015. Clonal Dynamics Reveal Two Distinct Populations of Basal Cells in Slow-Turnover Airway Epithelium. Cell Rep 12, 90-101.

Weaver, M., Dunn, N.R. and Hogan, B.L., 2000. Bmp4 and Fgf10 play opposing roles during lung bud morphogenesis. Development 127, 2695-2704.

Wei, C., Amos, C.I., Stephens, L.C., Campos, I., Deng, J.M., Behringer, R.R., Rashid, A. and Frazier, M.L., 2005. Mutation of Lkb1 and p53 genes exert a cooperative effect on tumorigenesis. Cancer Res 65, 11297-11303.

Wennerberg, K., Rossman, K.L. and Der, C.J., 2005. The Ras superfamily at a glance. J Cell Sci 118, 843-846.

Westcott, P.M., Halliwill, K.D., To, M.D., Rashid, M., Rust, A.G., Keane, T.M., Delrosario, R., Jen, K.Y., Gurley, K.E., Kemp, C.J., Fredlund, E., Quigley, D.A., Adams, D.J. and Balmain, A., 2015. The mutational landscapes of genetic and chemical models of Kras-driven lung cancer. Nature 517, 489-492.

Wikenheiser, K.A., Clark, J.C., Linnoila, R.I., Stahlman, M.T. and Whitsett, J.A., 1992. Simian virus 40 large T antigen directed by transcriptional elements of the human surfactant protein C gene produces pulmonary adenocarcinomas in transgenic mice. Cancer Res 52, 5342-5352.

Wimmer-Kleikamp, S.H., Janes, P.W., Squire, A., Bastiaens, P.I. and Lackmann, M., 2004. Recruitment of Eph receptors into signaling clusters does not require ephrin contact. J Cell Biol 164, 661-666.

Wingo, S.N., Gallardo, T.D., Akbay, E.A., Liang, M.C., Contreras, C.M., Boren, T., Shimamura, T., Miller, D.S., Sharpless, N.E., Bardeesy, N., Kwiatkowski, D.J., Schorge, J.O., Wong, K.K. and Castrillon, D.H., 2009. Somatic LKB1 mutations promote cervical cancer progression. PLoS One 4, e5137.

Winslow, M.M., Dayton, T.L., Verhaak, R.G., Kim-Kiselak, C., Snyder, E.L., Feldser, D.M., Hubbard, D.D., DuPage, M.J., Whittaker, C.A., Hoersch, S., Yoon, S., Crowley, D., Bronson, R.T., Chiang, D.Y., Meyerson, M. and Jacks, T., 2011. Suppression of lung adenocarcinoma progression by Nkx2-1. Nature 473, 101-104.

Vivanco, I. and Sawyers, C.L., 2002. The phosphatidylinositol 3-Kinase AKT pathway in human cancer. Nat Rev Cancer 2, 489-501.

Wolchok, J.D. and Chan, T.A., 2014. Cancer: Antitumour immunity gets a boost. Nature 515, 496-498.

Volckaert, T., Campbell, A., Dill, E., Li, C., Minoo, P. and De Langhe, S., 2013. Localized Fgf10 expression is not required for lung branching morphogenesis but prevents differentiation of epithelial progenitors. Development 140, 3731-3742.

Wood, L.D., Calhoun, E.S., Silliman, N., Ptak, J., Szabo, S., Powell, S.M., Riggins, G.J., Wang, T.L., Yan, H., Gazdar, A., Kern, S.E., Pennacchio, L., Kinzler, K.W., Vogelstein, B. and Velculescu, V.E., 2006. Somatic mutations of GUCY2F, EPHA3, and NTRK3 in human cancers. Hum Mutat 27, 1060-1061.

Xiao, Z., Jiang, Q., Willette-Brown, J., Xi, S., Zhu, F., Burkett, S., Back, T., Song, N.Y., Datla, M., Sun, Z., Goldszmid, R., Lin, F., Cohoon, T., Pike, K., Wu, X., Schrump, D.S., Wong, K.K., Young, H.A., Trinchieri, G., Wiltrout, R.H. and Hu, Y., 2013. The pivotal role of IKKalpha in the development of spontaneous lung squamous cell carcinomas. Cancer Cell 23, 527-540.

Xu, C., Fillmore, C.M., Koyama, S., Wu, H., Zhao, Y., Chen, Z., Herter-Sprie, G.S., Akbay, E.A., Tchaicha, J.H., Altabef, A., Reibel, J.B., Walton, Z., Ji, H., Watanabe, H., Janne, P.A., Castrillon, D.H., Rustgi, A.K., Bass, A.J., Freeman, G.J., Padera, R.F., Dranoff, G., Hammerman, P.S., Kim, C.F. and Wong, K.K., 2014a. Loss of Lkb1 and Pten leads to lung squamous cell carcinoma with elevated PD-L1 expression. Cancer Cell 25, 590-604.

Xu, X., Huang, L., Futtner, C., Schwab, B., Rampersad, R.R., Lu, Y., Sporn, T.A., Hogan, B.L. and Onaitis, M.W., 2014b. The cell of origin and subtype of K-Ras-induced lung tumors are modified by Notch and Sox2. Genes Dev 28, 1929-1939.

Xu, X., Rock, J.R., Lu, Y., Futtner, C., Schwab, B., Guinney, J., Hogan, B.L. and Onaitis, M.W., 2012. Evidence for type II cells as cells of origin of K-Ras-induced distal lung adenocarcinoma. P Natl Acad Sci USA 109, 4910-4915.

Yang, A., Walker, N., Bronson, R., Kaghad, M., Oosterwegel, M., Bonnin, J., Vagner, C., Bonnet, H., Dikkes, P., Sharpe, A., McKeon, F. and Caput, D., 2000. p73-deficient mice have neurological, pheromonal and inflammatory defects but lack spontaneous tumours. Nature 404, 99-103.

Yang, G., Rosen, D.G., Zhang, Z., Bast, R.C., Jr., Mills, G.B., Colacino, J.A., Mercado-Uribe, I. and Liu, J., 2006. The chemokine growth-regulated oncogene 1 (Gro-1) links RAS signaling to the senescence of stromal fibroblasts and ovarian tumorigenesis. P Natl Acad Sci USA 103, 16472-16477.

Yeddula, N., Xia, Y., Ke, E., Beumer, J. and Verma, I.M., 2015. Screening for tumor suppressors: Loss of ephrin receptor A2 cooperates with oncogenic KRas in promoting lung adenocarcinoma. P Natl Acad Sci USA.

Youn, J.I., Nagaraj, S., Collazo, M. and Gabrilovich, D.I., 2008. Subsets of myeloid-derived suppressor cells in tumor-bearing mice. J Immunol 181, 5791-5802.

Zeqiraj, E., Filippi, B.M., Deak, M., Alessi, D.R. and van Aalten, D.M., 2009. Structure of the LKB1-STRAD-MO25 complex reveals an allosteric mechanism of kinase activation. Science 326, 1707-1711.

Zhang, J., Fujimoto, J., Zhang, J., Wedge, D.C., Song, X., Zhang, J., Seth, S., Chow, C.W., Cao, Y., Gumbs, C., Gold, K.A., Kalhor, N., Little, L., Mahadeshwar, H., Moran, C., Protopopov, A., Sun, H., Tang, J., Wu, X., Ye, Y., William, W.N., Lee, J.J., Heymach, J.V., Hong, W.K., Swisher, S., Wistuba, II and Futreal, P.A., 2014. Intratumor heterogeneity in localized lung adenocarcinomas delineated by multiregion sequencing. Science 346, 256-259.

Zhou, W., Ercan, D., Chen, L., Yun, C.H., Li, D., Capelletti, M., Cortot, A.B., Chirieac, L., Iacob, R.E., Padera, R., Engen, J.R., Wong, K.K., Eck, M.J., Gray, N.S. and Janne, P.A., 2009. Novel mutant-selective EGFR kinase inhibitors against EGFR T790M. Nature 462, 1070-1074.

Zhuang, G., Song, W., Amato, K., Hwang, Y., Lee, K., Boothby, M., Ye, F., Guo, Y., Shyr, Y., Lin, L., Carbone, D.P., Brantley-Sieders, D.M. and Chen, J., 2012. Effects of cancer-associated EPHA3 mutations on lung cancer. J Natl Cancer I 104, 1182-1197.

Zou, H.Y., Li, Q., Lee, J.H., Arango, M.E., McDonnell, S.R., Yamazaki, S., Koudriakova, T.B., Alton, G., Cui, J.J., Kung, P.P., Nambu, M.D., Los, G., Bender, S.L., Mroczkowski, B. and Christensen, J.G., 2007. An orally available small-molecule inhibitor of c-Met, PF-2341066, exhibits cytoreductive antitumor efficacy through antiproliferative and antiangiogenic mechanisms. Cancer Res 67, 4408-4417.

I

REPORT

Cell Cycle 12:4, 625–634; February 15, 2013; © 2013 Landes Bioscience

A high-content cellular senescence screen identifies candidate tumor suppressors, including EPHA3

Jenni Lahtela,[1] Laura B. Corson,[2] Annabrita Hemmes,[1] Matthew J. Brauer,[2] Sonja Koopal,[1] James Lee,[2] Thomas L. Hunsaker,[2] Peter K. Jackson[2,†] and Emmy W. Verschuren[1,†,*]

[1]Institute for Molecular Medicine Finland (FIMM); University of Helsinki; Helsinki, Finland; [2]Genentech Inc.; South San Francisco, CA USA

[†]These authors share co-senior authorship.

Keywords: senescence, DDR, p53, p16^{INK4a}, tumor suppressor, EPHA3, RTK

Abbreviations: DDR, DNA damage response; SA-β-Gal, senescence associated-β-galactosidase; CGH, comparative genomic hybridization; EPHA3, EPH receptor A3; RTK, receptor tyrosine kinase

Activation of a cellular senescence program is a common response to prolonged oncogene activation or tumor suppressor loss, providing a physiological mechanism for tumor suppression in premalignant cells. The link between senescence and tumor suppression supports the hypothesis that a loss-of-function screen measuring bona fide senescence marker activation should identify candidate tumor suppressors. Using a high-content siRNA screening assay for cell morphology and proliferation measures, we identify 12 senescence-regulating kinases and determine their senescence marker signatures, including elevation of senescence-associated β-galactosidase, DNA damage and p53 or p16^{INK4a} expression. Consistent with our hypothesis, SNP array CGH data supports loss of gene copy number of five senescence-suppressing genes across multiple tumor samples. One such candidate is the *EPHA3* receptor tyrosine kinase, a gene commonly mutated in human cancer. We demonstrate that selected intracellular EPHA3 tumor-associated point mutations decrease receptor expression level and/or receptor tyrosine kinase (RTK) activity. Our study therefore describes a new strategy to mine for novel candidate tumor suppressors and provides compelling evidence that EPHA3 mutations may promote tumorigenesis only when key senescence-inducing pathways have been inactivated.

Introduction

Cancer genomic profiling studies have revealed that the majority of drivers for malignant tumor progression are mutations in tumor suppressors,[1,2] illustrating the need to accurately catalog cancer-specific tumor suppressors and their impact on treatment efficacy. Reverse genomics approaches using RNA interference (RNAi) libraries allow for rapid identification of novel gene functions and ideally, monitor cellular parameters tightly linked to the function in question. Common to many potent oncogenic signals is the activation of built-in checkpoint mechanisms that halt aberrant proliferation, instead triggering irreversible cellular fates, including apoptosis and senescence.[3] It is well-established that senescence can result not only from prolonged oncogene activation (e.g., oncogenic Ras, cyclin E), but also loss of tumor suppression (e.g., loss of PTEN, VHL or NF1 genes).[4] A physiological role for senescence in suppressing malignant progression is supported by its in vivo detection during early stages cancer development.[5,6]

The program of cellular senescence comprises permanent cell cycle arrest associated with cell morphological changes, notably cell and nuclear flattening and an increase in senescence-associated β-galactosidase (SA-β-Gal) activity.[7] Senescence in vitro and in vivo coincides with the occurrence of ATM/ATR and p53/p21^{Cip1} DNA damage response (DDR) pathways, and previous research, including our own, suggests this to be a consequence of unbalanced DNA replication vs. mitotic cell cycle stages.[8-10] Senescence is also commonly triggered by activation of the Ets/p16^{INK4a}/Rb tumor suppressor pathway. Although the role of DDR and p16^{INK4a} pathways in mediating senescence is well established, their relative contributions remain ill-defined and multiple pathways may act cooperatively.[4]

Since senescence is commonly detected in cells containing intact cellular DDR and p16^{INK4a} pathways, we reasoned that a siRNA screen in untransformed cells would potentially identify putative tumor suppressor genes. Our screen contrasts with previous studies, which focused on senescence bypass events, and biased for discovery of genes intrinsically linked to or required for the specific arrest pathway.[11-13] Furthermore, the proposed pro-tumorigenic effect of a senescence-associated inflammatory response[14] warrants a closer study to assess whether senescence can

*Correspondence to: Emmy W. Verschuren; Email: emmy.verschuren@helsinki.fi
Submitted: 11/16/12; Accepted: 01/06/13
http://dx.doi.org/10.4161/cc.23515

be induced upon loss of relevant gene function. Here we identify 12 kinases as newly identified regulators of cellular senescence using quantitative senescence β-galactosidase staining, and show that senescence frequently correlates with DNA damage induction and is mostly p53- and sometimes $p16^{INK4A}$-dependent. In support of our hypothesis to reveal candidate tumor suppressor genes, analysis of SNP aCGH data showed that a significant number of candidate genes displayed gene copy loss in sets of tumor samples.

Interestingly, one novel senescence regulator, the *EPHA3* receptor tyrosine kinase (RTK) gene, is among the most frequently mutated genes in human lung adenocarcinomas and colorectal cancers.[15-18] EPHA receptors have traditionally been assigned oncogenic roles due to their overexpression in a variety of cancers including carcinomas, melanoma and gliomas.[19,20] However, in support of additional tumor suppressor functions, certain ephrin-EPHs are suggested to show temporally bi-phasic roles during tumor progression,[21] and EPHA7 receptor was recently shown to act as a tumor suppressor in follicular lymphoma.[22] We here show that senescence upon loss of EPHA3 is regulated by $p16^{INK4a}$ and p53 and, in agreement with recent data from the Pasquale and Zhuang labs,[23,24] show that selected EPHA3 tumor-associated mutations decrease receptor expression levels and overall kinase activity. Our results suggests that concomitant loss of EPHA3 and key senescence-inducing tumor suppressor functions may cooperatively stimulate tumorigenesis, and conclude that our senescence screen successfully identified strong candidates for tumor suppressor genes.

Results

Identification of senescence-inducing kinase siRNAs. We utilized a cell-based screen to identify regulators of premature senescence in untransformed cells, hypothesizing that a loss-of-function screen may identify new tumor suppressor genes. We chose to screen the hTERT-immortalized retinal pigmented epithelial line hTERT-RPE1, because it models key aspects of untransformed cells, including quiescence with a high efficiency of G_0 markers, notably the presence of primary cilia.[25] Unlike quiescent cells, senescent cells exhibit an irreversible proliferative arrest, followed by formation of enlarged nuclei and a flattened cytoplasmic morphology, with rare exceptions.[4] These features were used to analyze a multiparametric HCS siRNA screen of hTERT-RPE1 cells engineered to express a doxycycline-inducible p53 shRNA (from here on called hTERT-RPE1 p53shRNA), designed to identify proteins that impinge on the p53 pathway (Corson LB, et al., manuscript in preparation). Our analysis focused on loss of the proliferation marker Ki67 and decreased nuclei counts, combined with an average increase in nuclear size (**Fig. 1A**). This approach identified a group of 16 kinase siRNAs, which we labeled as "senescence-like" (**Fig. 1B**).

We next tested hits as bona fide senescence regulators in a secondary screen detecting the widely studied SA-β-Gal senescence biomarker, on parallel transfections using siRNA pools plus the four individual siRNAs per gene. Knockdown of Emi1, previously reported to elicit pronounced DNA damage-induced senescence in hTERT-RPE1 cells, was included as a positive control[8] (**Fig. S1A**). Normalized senescence scores were calculated by quantitation of the staining intensities per single oligonucleotide or pool (**Fig. S1B and Table S2**). To correlate the phenotype with knockdown efficiency, we performed TaqMan RNA expression analysis (**Fig. S2**). Genuine hits were assigned if both the siRNA pool, plus at least two oligonuceotides conferring > 50% knockdown efficiency, scored positive (**Table S3**). This approach validated 12 of 16 senescence-like kinome siRNAs as genuine senescence hits (**Fig. 1C**).

Delineation of senescence signatures. Activation of a p53-dependent DNA damage response (DDR) and increased $p16^{INK4a}$ CKI expression have been causally linked to senescence. hTERT-RPE1 cells contain an intact p53 checkpoint, and p53 stabilization and nuclear accumulation are seen upon sustained damage signaling.[8,26] A two- to 4-fold increase in cells expressing threshold p53 and $p21^{CIP1}$ protein levels was measured in the HCS analysis (**Fig. 2A**). In all cases, total cell numbers and percentages of proliferating cells were significantly increased in p53 knockdown cells compared with p53+ cells (**Fig. 2B**; **Fig. S3A**), suggesting a p53-dependent growth arrest. Furthermore, we measured increased DNA damage by γ-H2AX foci formation upon senescence induction in all but one case (PIK3C2A), with strongest hits showing foci in 40–50% of cells (**Fig. S3B**). Finally, a decreased senescence score was measured after transfection of six of 12 senescence hit siRNAs in p53 knockdown cells (**Fig. 2C**), implying that senescence typically required activation of a p53-dependent DDR.

Next, we assessed activation of the $p16^{INK4a}$ tumor suppressor pathway following senescence suppressor siRNA transfection. In hTERT-RPE1 cells, classic senescence induction following oncogenic RAS expression did not result in a significant increase in $p16^{INK4a}$ mRNA (data not shown). Contrary to p53 pathway activation, significant increases in $p16^{INK4a}$ mRNA expression were less frequently detected upon senescence hit siRNA transfection, and most clearly upon knockdown of MYLK, MAP2K3, NEK1, EPHA3 and SMG1 (**Fig. 2D**). We conclude that in a majority of cases senescence induction is associated with activation of well-known cell cycle arrest pathways, schematically summarized in **Figure 2E**. As expected, this corresponds to a delayed cell cycle progression, as measured by DNA replication analysis in synchronized cells (**Fig. S4**).

Genome copy number and mutational analysis to appoint putative tumor suppressors. To establish whether senescence hits encompass tumor suppressors, we combined a cancer genomic analysis approach with cancer mutation and literature surveys. Validating our hypothesis, three hits identified have previously been shown to display bona fide tumor suppressor functions in murine models (**Fig. 1C**). Specifically, *AurkA* heterozygous mice present haploinsufficient tumor suppression with increased incidence of lymphoma, lung and liver tumors;[27] conditional *Csnk1a1* ablation triggers colorectal carcinogenesis and LOH;[28] and *Lats1*-deficient mice develop soft tissue sarcoma and ovarian tumors.[29] Interestingly, all three models exhibit signs of chromosomal instability or DDR activation, and a p53-dependent DDR-senescence response is proposed to halt carcinogenesis in the *Csnk1a1*-null or heterozygous animals.[28] This verifies that

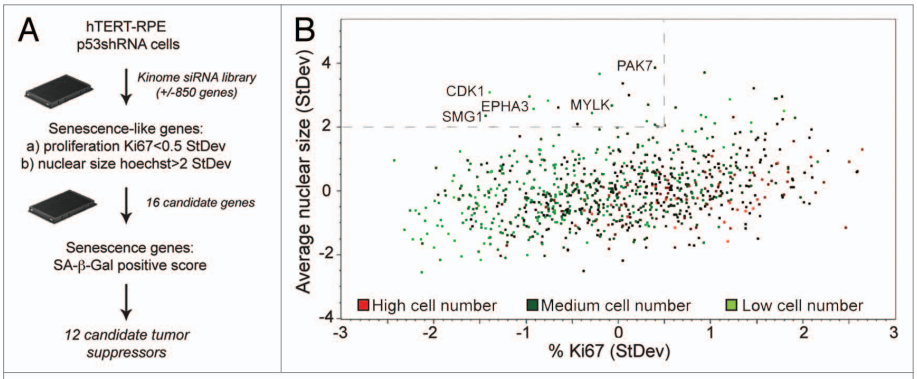

C

Gene	Name	Score	*Hs*	*Mm*	Ref.
1. AURKA	aurora kinase A	75.3		✓	(26)
2. CDK1	cyclin-dependent kinase 1	36.5			
3. CSNK1A1	casein kinase 1, alpha 1	16.1		✓	(27)
4. EPHA3	EPH receptor A3	11.8			
5. KSR2	kinase suppressor of ras 2	19.7			
6. LATS1	large tumor suppressor, homolog 1	11.7	✓	✓	(28, 29)
7. MAP2K3	mitogen-activated protein kinase kinase 3	12.6			
8. MAP4K1	mitogen-activated protein kinase kinase kinase kinase 1	37.1			
9. MYLK	myosin light chain kinase	18.7			
10. NEK1	NIMA (never in mitosis gene a)-related kinase 1	11.1			
11. PIK3C2A	phosphoinositide-3-kinase, class 2, alpha polypeptide	36.5			
12. SMG1	smg-1 homolog, phosphatidylinositol 3-kinase-related kinase	34.1			
+FBXO5		**17.5**			
-siCTRL		**3.5**			

Figure 1. Identification of senescence-inducing kinase siRNAs. (**A**) Schematic overview of the high-content senescence screen. (**B**) Scatterplot analysis of data from the kinome HCS screen in p53+ cells. Cells were stained for Ki67, p53, p21^{CIP1} and Hoechst at day 3, and multiparametric analysis was performed to determine siRNAs displaying decreased proliferation (< 0.5 StDev Ki67%) and an increased nuclear size (> 2.0 StDev Hoechst mean area). High, medium and low cell number indicators are assigned as the third parameter. (**C**) Senescence scores per gene are the sum of the senescence scores of its siRNA pool and the four individual siRNAs, omitting siRNAs conferring less than 50% specific gene knockdown. Scoring details are depicted in **Table S2**. References to studies establishing bona fide tumor suppressor functions for human (*Hs*) or mouse (*Mm*) genes are indicated.

individual findings from our in vitro study have a capacity to broaden our knowledge of physiological disease progression.

Among the candidates, only *LATS1* is suggested to act as a tumor suppressor in human disease, supported by its conserved role in growth control from flies to man[30] (**Fig. 1C**). We therefore next asked if we could observe an increased propensity for genome copy number loss of our senescence genes in human tumor samples. Validating our strategy, loci encompassing known tumor suppressors showed significant copy number loss across data sets, defining a "tumor suppressor copy number signature."Importantly, clustering analysis of this signature identified a set of five screen candidates with a similar genomic profile, namely *LATS1*, *CDK1*, *EPHA3*, *NEK1* and *MAP2K3* (**Fig. 3**). Locus inspection showed none to be in the vicinity of known tumor suppressors, supporting the deduction that these constitute candidate tumor suppressor genes.

As a final in silico approach, we surveyed the increasing collection of cancer-specific mutations as reported in the COSMIC database. Indeed, out of the 12 genes, seven genes were mutated in 1–4% of tumors. Of outstanding interest, with a reported mutation frequency of 4–6%, the *EPHA3* RTK gene was shown to be among the most frequently mutated genes in human colorectal, lung and ovarian carcinomas.[15-18,31] Furthermore, EPHA RTK family kinases have pleiotropic functions and *EPHA3* was originally assigned oncogenic properties in lymphomas.[21,32] We thus decided to key in on a putative new role for *EPHA3* as a tumor suppressor.

Loss of EPHA3 receptor signaling confers p16^{INK4A} and p53-dependent senescence. Since the EPHA RTK family consists of nine members, we first asked if EPHA3 uniquely induced cellular senescence using SA-β-Gal staining upon siRNA transfection of additional EPHA receptors expressed in hTERT-RPE1 (*EPHA1*, *A2*, *A4*, and *A5* mRNAs, data not shown). Knockdown of Emi1 was included as a positive control.[8] Our results showed that senescence was uniquely detected after knockdown of EPHA3 and not measurably apparent after knockdown of other EPHA RTKs expressed in hTERT-RPE1 cells (**Fig. S5**).

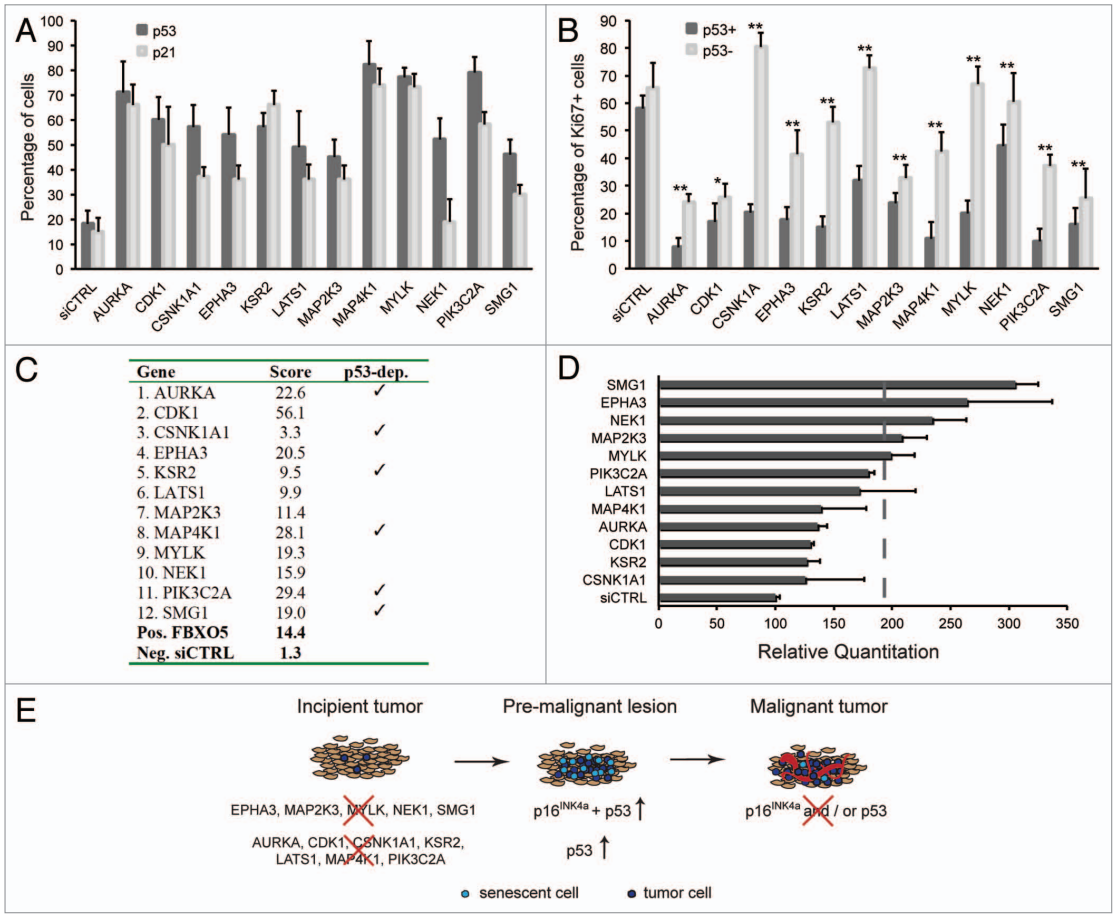

Gene	Score	p53-dep.
1. AURKA	22.6	✓
2. CDK1	56.1	
3. CSNK1A1	3.3	✓
4. EPHA3	20.5	
5. KSR2	9.5	✓
6. LATS1	9.9	
7. MAP2K3	11.4	
8. MAP4K1	28.1	✓
9. MYLK	19.3	
10. NEK1	15.9	
11. PIK3C2A	29.4	✓
12. SMG1	19.0	✓
Pos. FBXO5	**14.4**	
Neg. siCTRL	**1.3**	

Figure 2. Delineation of senescence signatures. (**A**) hTERT-RPE1 p53 shRNA cells were transfected with kinome siRNAs in the absence of doxycycline and immunostained for p53 and $p21^{CIP1}$ following 72 h culture. Percentages of cells expressing p53, $p21^{CIP1}$ above threshold levels were calculated, and averages from four 384 wells are shown. (**B**) hTERT-RPE1 p53 shRNA cells were transfected with kinome siRNAs in the absence or presence of doxycycline and immunostained for Ki67. Percentages of cells expressing Ki67 protein above threshold levels were calculated, and averages from four 384 wells are shown. * indicates $p \leq 0.05$ and ** indicates $p \leq 0.01$. (**C**) Senescence scores per gene are the sum of the senescence scores of the siRNA pool plus four individual siRNAs, omitting siRNAs conferring less than 50% knockdown. Detailed scoring information is depicted in **Table S3**. (**D**) Quantitative $p16^{INK4A}$ mRNA expression analyses during senescence induction. hTERT-RPE1 p53 shRNA cells were transfected with pooled siRNAs in the absence of doxycycline. RNA expression was quantitated using TaqMan analyses after 3 days of transfection. (**E**) Schematic model summarizing kinome screen data, using data depicted in (**A**) and (**D**). In an incipient tumor, modeled by hTERT-RPE1 cells, loss of selected tumor suppressors activates p53- and/or $p16^{INK4A}$-dependent senescence, and overt DNA damage. In a premalignant tumor, senescence may serve as a cell-intrinsic tumor suppressor mechanism to subvert oncogenic transformation. Loss of $p16^{INK4A}$ and/or p53 promotes malignancy.

Characterization of the senescence signature showed that siRNA-mediated knockdown of EPHA3 leads to increased $p16^{INK4a}$ and p53 expression (**Fig. 2A and D**). We next asked if the senescence phenotype was mediated by $p16^{INK4a}$ or p53 activation using in vivo imaging. Time-lapse imaging of siRNA-treated hTERT-RPE1 cells stably expressing GFP-tagged H2B protein showed a rescue of EPHA3 knockdown-induced senescence when $p16^{INK4a}$ (**Fig. 4A**; **Fig. S5E**) or p53 (**Fig. 4B**; **Fig. S5F**) were co-depleted. A rescue of senescence was both measured by an increase in total cell number, as well as a decrease in average nuclear size. We therefore conclude that EPHA3 knockdown-induced senescence requires $p16^{INK4a}$ and p53.

Selected EPHA3 gene mutations confer loss of kinase function. Similar to other EPHA RTKs, activation of EPHA3 occurs via autophosphorylation of conserved tyrosine residues[33] and ephrin ligand binding triggers receptor oligomerisation and consequent receptor activation.[34] To find how tumor-associated EPHA3 point mutations affect receptor activity we assayed for kinase activity monitoring autophosphorylation. HEK 293T and hTERT-RPE1 cells expressing a select set of EPHA3-LAP

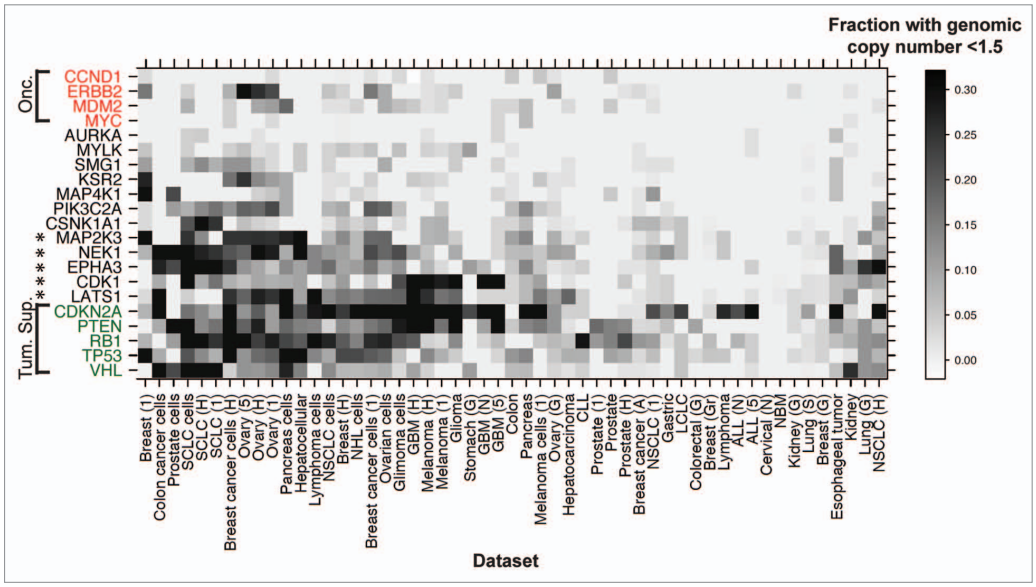

Figure 3. Senescence gene loss evidenced by genomic copy number analysis. Heatmap clustering analysis of SNP array-CGH data from 2654 samples from 53 panels of human tumors and cell lines, to identify sets with a genome copy number lower than 1.5. A sliding scale density gradient was applied. Loci encompassing tumor suppressors *CDKN2A*, *RB1*, *TP53* and *VHL* were included as positive controls and oncogenes *CCND1*, *ERBB2*, *MDM2* and *MYC* as negative controls. Stars indicate genes closely resembling the tumor suppressor signature.

tumor-associated mutation variants were generated to assess relative cellular receptor activities (**Fig. 5A**; **Fig. S6A and B**). As expected, ephrin-A5 ligand activation leads to receptor internalisation and trafficking via the early endosomal compartment labeled with EEA1[35] (**Fig. S7**). Of note, a decreased steady-state expression of the R728L variant was detected in both cell lines, and the T933M variant in hTERT-RPE1 cells (**Fig. S6A and B**).

Wild type EPHA3 shows a transient activation curve following ephrin-A5 ligand-induced activation, peaking at 20 min (**Fig. 5B**), consistent with published data.[35] Decreased normalized cellular kinase activities were detected for two receptor variants mutated in the cytoplasmic region (G766E and D806N) and one variant mutated in the cytoplasmic region showed a decrease in overall receptor level (R728L) (**Fig. 5B**). We next asked how point mutations affected absolute kinase activity using in vitro immunoprecipitation kinase assays. In this assay, EPHA3 variants G766E and D806N showed a clear loss of kinase activity (**Fig. 5C**; **Fig. S6C**). We conclude that selected intracellular EPHA3 tumor-associated point mutations lead to a decrease in receptor expression level and/or normalized tyrosine kinase activity.

Structural analysis of EPHA3 kinase domain cancer point mutations. Next, we examined the crystal structure of the juxtamembrane and kinase domain (JMKIN) of wild type EPHA3[34] to explain possible functional deficiencies of the tumor-associated mutations. The mutated residues K761, G766 and D806 are situated within the kinase domain, while R728 is situated on the surface area between two α-helices (**Fig. S6D**). We were unable to assess the G766 variant as the crystal structure surrounding this residue is disordered. Arginine 728 to Leucine alteration causes a shift in the surface charge from positive to non-charged (**Fig. 5D**), which may affect the steady-state expression level of the receptor via altered protein-protein interactions and/or increased receptor degradation, explaining its reduced expression level (**Fig. 5B**; **Fig. S6A and B**). Mutation of residue 806 from aspartic acid to asparagine may alter the interaction between residues aspartic acid 746 and histidine 744, which face the ATP binding pocket and may therefore directly affect the EPHA3 catalytic activity (**Fig. 5E**).

Interestingly, structural alignment of EPHA3 JMKIN with the tumor suppressor LKB1 kinase domain showed that LKB1 lung cancer-associated point mutation D237Y is homologous to mutated residue D806 in EPHA3.[15] We therefore tested EPHA3 D806Y mutation for kinase activity, and show that this mutant is kinase-defective (**Fig. 5F and G**). We conclude that selected cancer-associated point mutations appear to affect EPHA3 kinase activity either through altering protein-protein interactions, or through direct effects on kinase domain structural determinants, decreasing EPHA3 receptor tyrosine kinase activity. This supports our hypothesis that *EPHA3* acts as a tumor suppressor gene.

Discussion

Cancer genomics initiatives have identified numerous often low-frequency mutations that can prove predictive for clinical response to targeted therapy, creating new opportunities for personalized cancer care and biomarker discovery. Not surprisingly, clinical response and therapy resistance can be critically modified by the

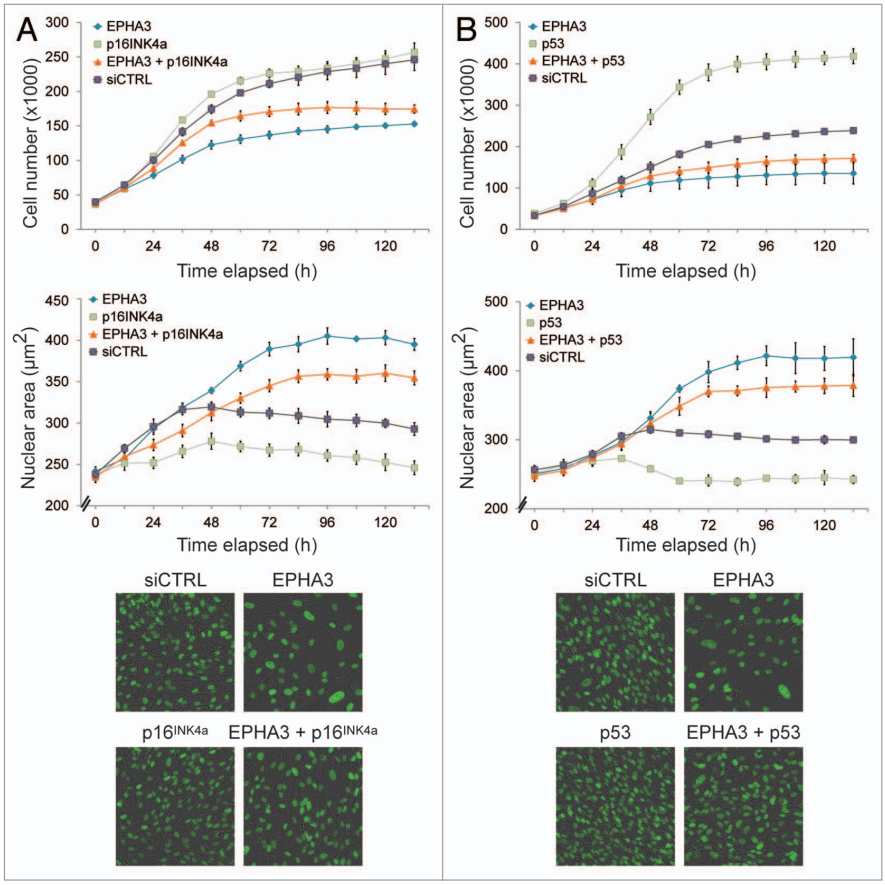

Figure 4. Loss of EPHA3 confers p16^{INK4A}- and p53-dependent senescence. Live cell analysis of (**A**) EPHA3 plus p16^{INK4a} siRNA-treated and (**B**) EPHA3 plus p53 siRNA-treated hTERT-RPE1 cells. The average nuclear area off all cells per image is shown. Representative 20× images from each condition are shown in the lower panels.

landscape of tumor suppressor mutations,[36] which constitute in fact the majority of cancer drivers.[1] Yet, the detailed consequences of tumor suppressor mutations are often unknown. We developed a "bottom-up" senescence-based strategy to functionally identify tumor suppressor candidates. Validating our approach, we identified three genes with known tumor suppressor function in human or mouse (*AURKA*, *CSNK1A1* and *LATS1*), and SNP aCGH data showed that half of the candidates displayed increased genome copy loss in tumor sample sets (**Fig. 3**). Clearly, our study is not exhaustive and would be enhanced by parallel assessment of DNA methylation and gene expression changes. Nonetheless, it illustrates the power of combining functional genomics with delineation of somatic mutations. We propose that detection of senescence in cells harbouring intact damage checkpoint pathways, such as hTERT-RPE1, can be employed as a shortcut to identify cancer-promoting events.

Our senescence gene hits can readily be grouped in three functional categories: (1) regulators of accurate mitotic cell cycle progression and cytokinesis, DNA damage signaling and the spindle assembly checkpoint (SAC): AURKA, CDK1, CSNK1A1, LATS1, NEK1, SMG1; (2) regulators of adhesion and migration: EPHA3, MYLK, PIK3C2A; and (3) regulators of growth factor-induced mitogenic signaling via p38 SAPK and JNK: KSR2, MAP2K3, MAP4K1. Hence, a compendium of genes that intersect on accurate spindle assembly checkpoint control and fine-tuning of cell adhesion as well as cytokinesis machineries describe a likely set of candidate tumor suppressors. This is further supported by recent sequencing efforts that reveal frequent mutations in mitotic kinases including Aurora, Polo and LATS kinases as well as Nek family kinases.[17,37] Although conceptually perhaps unsurprising, functional data mining also reveals unexpected dual functions for previously established oncogenic proteins, as exemplified by the *AURKA* oncogene, which indeed was shown to be haploinsufficient for tumor suppression in mice.[27]

Senescence can be viewed as a cell-intrinsic fail-safe response to overt oncogenic proliferative signals,[3] a key effector of cancer

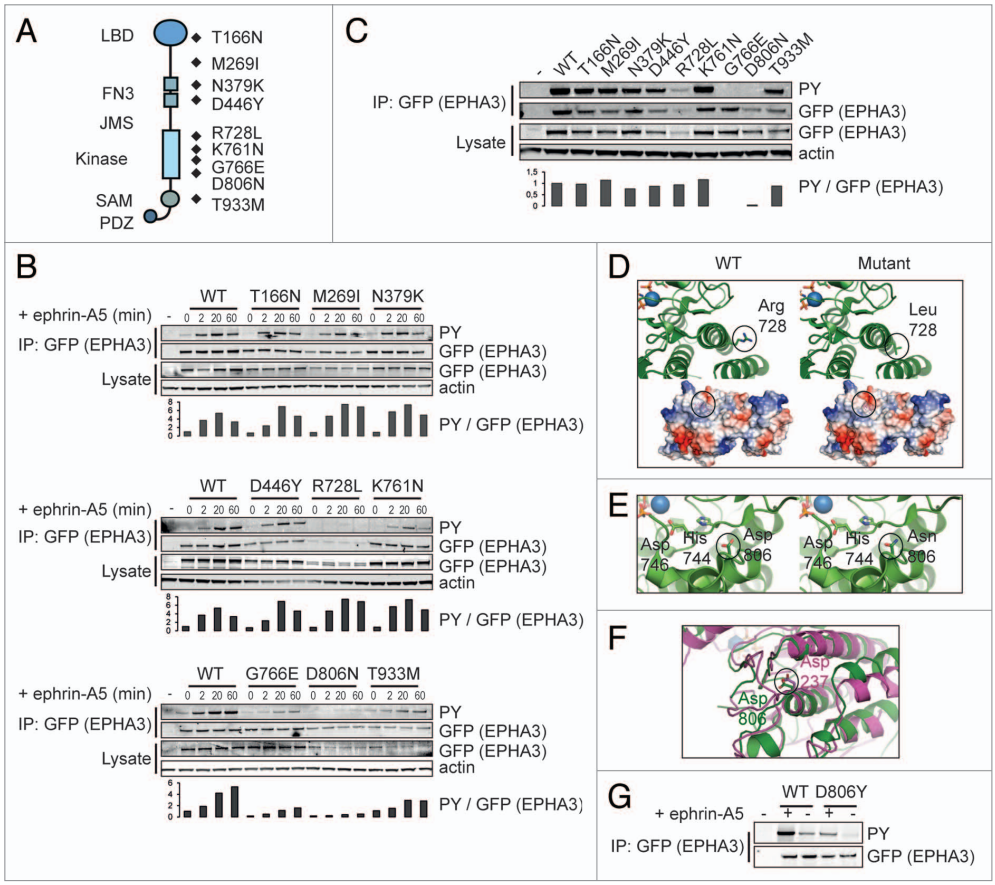

Figure 5. Selected EPHA3 cancer gene mutations confer decreased kinase function. (**A**) Schematic representation of EPHA3 protein domains and selected cancer point mutations pertinent to this study. (**B**) Cellular kinase activities of selected EPHA3 tumor variants. 293T cells expressing EPHA3-LAP variants were treated with preclustered ephrin-A5 and immunoprecipitates were immunoblotted. Anti-GFP was used to detect EPHA3-LAP. Relative cellular kinase activities were determined by normalization of the PY (phosphotyrosine) against the EPHA3 signal, and normalized values relative to WT are shown in arbitrary units. (**C**) In vitro kinase assays of selected EPHA3 tumor variants. Immunoprecipitates from kinase assays or input lysate samples from 293T EPHA3-LAP lines were immunoblotted with indicated antibodies, and normalized values were calculated as in (**B**). (**D–F**) Structural analyses of EPHA3 tumor variants R728L and D806N and structural alignment of the EPHA3 and LKB1 kinase domains. PDB structure files were analyzed using the PyMOL molecular visualization package. Notable alterations are encircled. (**G**) In vitro kinase assay of EPHA3 D806Y variant. 293T cells expressing EPHA3-LAP proteins or control lysate were treated with preclustered ephrin-A5. GFP immunoprecipitates from kinase assays were immunoblotted with the indicated antibodies.

chemotherapy response,[38,39] or a barrier to tumor initiation in incipient human tumors.[4,5] Contrary to such anti-proliferative responses, senescence in the stromal microenvironment may also promote paracrine epithelial tumor growth via secretion of inflammatory molecules, akin to a tissue repair response.[40] Furthermore, an elegant recent study suggested that inflammatory signals themselves can subvert a senescence barrier.[41] Its precise physiological role thus is likely complex and possibly context-dependent, yet common to a multi-step carcinogenesis paradigm wherein loss of p53 and/or $p16^{INK4a}$ affords proliferation of damaged cells. We confirm that senescence correlates with activation of a pronounced p53-dependent DDR, consistent with previous studies describing p53 activation and/or senescence upon loss or inhibition of AURKA,[42] CDK1,[43] CSNK1A1,[28] LATS1,[44] MAP2K3[45] and SMG1.[46] This further illustrates the importance of perturbations in both surveillance systems and checkpoint response pathways as a frequent driver of tumor progression.

Contrary to p53 activation, significant increases in $p16^{INK4a}$ mRNA expression were less frequently detected upon senescence hit siRNA transfection, and most clearly upon loss of MYLK, MAP2K3, SMG1, NEK1 and EPHA3 (**Fig. 2D**). None of these genes were previously known to activate the $p16^{INK4A}$-dependent senescence program. Of the candidate tumor suppressors, the *EPHA3* RTK gene was shown to be frequently mutated in human

lung adenocarcinomas and colorectal cancers.[15-18] Consistent with its candidacy as a tumor suppressor, array CGH data showed frequent loss of the chromosome 3 arm encoding *EPHA3* in the lung cancer data set in particular. This is confirmed by recent data reporting a striking loss of the *EPHA3* gene in 42% of primary lung adenocarcinomas.[24] We found that senescence upon EPHA3 loss is partially rescued by concomitant $p16^{INK4a}$ or p53 depletion, and that this is a function unique to EPHA3. Our data therefore suggests that loss of EPHA3 activity may promote tumorigenesis only when key senescence-inducing tumor suppressor pathways are absent. We however did not detect an enrichment for $p16^{INK4a}$ mutations in lung cancer samples that display *EPHA3* copy number loss, using the CONAN CGP copy number analysis tool available via the Sanger Institute. The in vivo functional cooperation of EPHA3 and $p16^{INK4a}$ loss of function is, however, unlikely straightforward and uniform, warranting closer inspection of their co-dependencies during tumorigenesis.

Previous EPH receptor studies have revealed dual opposing roles during tumor initiation vs progression,[47,48] and EPHA3 has been ascribed both oncogenic[49,50] and tumor-suppressive functions.[51] In support of its role as a tumor suppressor, EPHA3 gene mutations are distributed along the gene rather than clustered in hot spots. Importantly, we show that cancer-associated point mutations G766E and D806N are kinase-defective, as well as a mutation analogous to D237Y in the well-established LKB1 tumor suppressor. Furthermore, we show that the R728L variant decreases overall receptor levels and cellular receptor activity. Our results agree with recent reports by Lisabeth and Zhuang and colleagues that describe a disruption of RTK functions for selected EPHA3 tumor variants,[23,24] likely acting to decrease apoptotic susceptibility in a dominant-negative fashion.[24] In conclusion, our results strengthen evidence for a role for *EPHA3* as a candidate tumor suppressor gene.

It is well-established that the interplay between different EPH receptors influences their signaling outcome.[22] Furthermore, EPH receptors cross signal to other tyrosine kinase families, with evidence for negative regulation of c-MET by EPHA signaling.[52] Interestingly, a secreted form of EPHA7 was recently shown to act as a tumor suppressor in follicular lymphoma via inhibition of EPHA2 in a dominant-negative fashion.[22] Since also *EPHA3* is expressed as an alternative isoform, it will be interesting to study how it may influence the EPH-RTK signaling network. Furthermore, while no increased tumor growth is detected in a constitutive EPHA3 murine-null model,[53,54] our study warrants further comprehensive in vivo loss-of-function analyses. Taken together, we developed a successful cell-based strategy to functionally mine for novel candidate tumor suppressors, and provide compelling evidence that loss-of-function EPHA3 variants may promote tumorigenesis when common senescence-inducing pathways are inactive.

Materials and Methods

Cell lines, culture and treatment. hTERT-RPE1 cells (Clontech) were maintained in DMEM:F-12 (Invitrogen) containing 10% FBS, 2mM L-Glutamine and 0.348% sodium bicarbonate, following manufacturer recommendations. 293T cells were maintained in DMEM (Lonza) containing 10% FBS and 2 mM L-Glutamine, following manufacturer recommendations. Inducible p53 shRNA hTERT-RPE1 cells were constructed using the pHUSH tetracycline-inducible retrovirus gene transfer vector[55] with a previously described p53 shRNA,[56] and labeled hTERT-RPE1 p53 shRNA. Knockdown in the selected subclone was validated by absence of p53 and p21 induction upon etoposide treatment, and p53 protein was absent after 72h treatment with 1 μg/ml doxycycline. A stable H2B-GFP hTERT-RPE1 clonal cell line was generated by transfection with GFP-tagged human H2B plasmid (pEGFP-H2B-N1) followed by clonal selection using G418 (Roche).

High-content kinase siRNA screen. hTERT-RPE1 p53 shRNA cells were treated +/– 1 μg/ml doxycycline for three days prior to transfection, also called "p53+" or "p53–" cells. A Dharmacon siGENOME library, composed of 862 siRNA pools targeting kinases and proteins predicted to influence kinase signaling was used (**Table S1**; Corson et al. manuscript in preparation). Following three days of culture, cells were fixed with 4% paraformaldehyde, permeabilized with 0.2% Triton X-100 and blocked in 5% fish gelatin (Sigma). Cells were immunostained with primary antibodies in 5% fish gelatin during overnight incubation at 4°C and incubated with secondary antibodies for 1 h at ambient temperature. Primary antibodies were rabbit anti-p53 (Cell Signaling 928; 1:1,500), goat anti-p21 (R&D Systems AF1047; 1:20,000) and mouse-anti-Ki67 (BD PharMingen 55600; 1:1,500). Secondary antibodies were Cy5 anti-mouse (Jackson 715-495-150), Cy3 anti-rabbit (Jackson 711-165-152), and AF488 anti-goat (Invitrogen A11055). Hoechst 33342 was used at 1:50,000. For primary screen data analysis depicted in **Figure 1B**, the data set in which p53 was functional (p53+) was used.

HCS imaging, quantitation and statistics. 384 Multiwell plates were imaged with a 10× objective and 2× binning on the ImageXpress Micro high content imaging system (Molecular Devices). Four sites were acquired per well with duplicate wells for every condition. Analysis using MetaXpress Cell Scoring and Multiwavelength Modules included: (1) total number of nuclei; (2) percentage cells positive for p53, p21 and Ki67; and (3) average nuclear size. An image analysis example is shown in **Figure S1C**. Data was collected in an Oracle database managed through Molecular Devices MDCStore. Images, measurements, annotations, normalizations, and statistical analysis were managed through AcuityXpress software.

Senescence-associated β-galactosidase (SA-β-gal) staining and quantitation. Cellular senescence was detected in cells transfected in 96-well cellBIND plates (Corning), by staining for acidic β-galactosidase as described,[7] followed by DNA counterstaining with Hoechst 33342. Cells were imaged on a Nikon Eclipse Ti microscope equipped with a monochrome camera, applying a DAPI scan and sequential brightfield RGB images. Composite color images were generated using a NIS Elements AR (Nikon) colorcombine journal. Image analysis was performed using a MetaMorph journal (Molecular Devices) following a scoring system detailed in the **Supplemental Materials and Methods**.

SNP array-CGH tumor sample analysis. SNP/CHIP array-CGH data available at Genentech (CARFOG, June 2009) for 2654 samples from 53 human tumor and cell line panels was mined using the "genoset" package from Bioconductor[57] and plotted as a heatmap to show the fraction of samples per data set containing a genome locus copy number lower than 1.5 copies. For visualization, the scale was trimmed at a value of 0.3: data sets with this value or greater were shown with the maximum density of the scale.

Immunoprecipitation and western blotting. Cells expressing stable LAP-tagged EPHA3 proteins were serum starved for 1 h, and then incubation with 1.5 μg/ml recombinant human ephrin-A5-Fc or IgG1-Fc proteins (R&D Systems) pre-clustered for 20 min with anti-human Fc antibody (Jackson ImmunoResearch) at 10:1 molar ratio. Ligand-activated 293T cells expressing LAP-tagged EPHA3 proteins were lysed in RIPA buffer containing Protein Inhibitor Cocktail (Roche) and Phosphatase Inhibitor Cocktail (Roche). 500 μg of protein was rotated for 16h with 1 μg of anti-GFP antibody (Invitrogen). Antigen was captured using Protein G/A Sepharose beads (Sigma). Alternatively, specific antigen was captured using S-protein agarose beads (Novagen). Samples were immunoblotted using anti-phosphotyrosine (PY 4G10; Upstate Biotechnology Inc.) or in-house affinity-purified anti-GFP antibodies.

In vitro kinase assay. 293T and hTERT-RPE1 cells expressing LAP-tagged EPHA3 proteins were lysed in RIPA buffer containing protease inhibitors. 500 μg of total protein was incubated for 1h with 1 μg of antibodies to GFP (Invitrogen). Specific antigen was captured using Protein A/G Sepharose beads (Thermo Scientific), or, alternatively, with S-protein agarose beads (Novagen), and washed using RIPA and kinase buffer (50 mM NaCl, 20 mM Hepes pH 7.2, 10 mM $MgCl_2$, 2 mM EDTA, 0.02% Triton X-100). Beads were next incubated in kinase buffer supplemented with 20 μM Adenosine 5'-triphosphate disodium salt hydrate (Sigma). Samples were immunoblotting using anti-phosphotyrosine or anti-GFP antibodies.

Live cell imaging. hTERT-RPE1 cells expressing H2B-GFP protein were treated with 50 nM pooled siRNA using forward transfection with Oligofectamine reagent (Invitrogen) on 24-well plates. Transfections were in replicates of four and imaging was performed using the IncuCyte™ FLR instrument (Essen BioScience) for five days. A duplicate plate was harvested at day three to confirm siRNA knockdown. IncuCyte object analysis was performed with default parameters.

Disclosure of Potential Conflicts of Interest

The authors disclose no potential conflicts of interest.

Acknowledgments

We wish to acknowledge Alex Loktev, Mindan Sfakianos, Chris Westlake, David Davis and Seija Hackl for providing expert advice and technical support. We are grateful to Meredith Sagolla and Jeff Eastham-Anderson for advanced light microscopy support, Denis Kainov for structural analysis support and thank members of the Jackson and Verschuren labs for discussions. pEGFP-H2B-N1 was a gift from Jorge Torres (UCLA).

Author Contributions

J.L., L.B.C., A.H., S.K., T.L.H. and E.W.V. conducted aspects of the experimental design, performed experiments, and data interpretation. James L. managed the siRNA library and M.J.B. performed statistical data analysis. P.K.J., L.B.C., J.L. and E.W.V. interpreted results, and J.L. and E.W.V. wrote the manuscript.

Financial Disclosures

Research was supported by an EU-FP7 Marie Curie Grant PIRG06-GA-2009-256485 (E.W.V.), the Sigrid Juselius and Orion-Farmos Foundations (E.W.V.), and a Graduate Program scholarship to J.L.

Supplemental Materials

Supplemental materials may be found here:
www.landesbioscience.com/journals/cc/article/23515

References

1. Bozic I, Antal T, Ohtsuki H, Carter H, Kim D, Chen S, et al. Accumulation of driver and passenger mutations during tumor progression. Proc Natl Acad Sci U S A 2010; 107:18545-50; PMID:20876136; http://dx.doi.org/10.1073/pnas.1010978107
2. Forbes SA, Bindal N, Bamford S, Cole C, Kok CY, Beare D, et al. COSMIC: mining complete cancer genomes in the Catalogue of Somatic Mutations in Cancer. Nucleic Acids Res 2011; 39(Database issue):D945-50; PMID:20952405; http://dx.doi.org/10.1093/nar/gkq929
3. Lowe SW, Cepero E, Evan G. Intrinsic tumour suppression. Nature 2004; 432:307-15; PMID:15549092; http://dx.doi.org/10.1038/nature03098
4. Kuilman T, Michaloglou C, Mooi WJ, Peeper DS. The essence of senescence. Genes Dev 2010; 24:2463-79; PMID:21078816; http://dx.doi.org/10.1101/gad.1971610
5. Collado M, Serrano M. Senescence in tumours: evidence from mice and humans. Nat Rev Cancer 2010; 10:51-7; PMID:20029423; http://dx.doi.org/10.1038/nrc2772
6. Ohtani N, Mann DJ, Hara E. Cellular senescence: its role in tumor suppression and aging. Cancer Sci 2009; 100:792-7; PMID:19302284; http://dx.doi.org/10.1111/j.1349-7006.2009.01123.x
7. Dimri GP, Lee X, Basile G, Acosta M, Scott G, Roskelley C, et al. A biomarker that identifies senescent human cells in culture and in aging skin in vivo. Proc Natl Acad Sci U S A 1995; 92:9363-7; PMID:7568133; http://dx.doi.org/10.1073/pnas.92.20.9363
8. Verschuren EW, Ban KH, Masek MA, Lehman NL, Jackson PK. Loss of Emi1-dependent APC/C inhibition deregulates E2F target expression and elicits DNA damage-induced senescence. Mol Cell Biol 2007; 27:7955-65; PMID:17875940; http://dx.doi.org/10.1128/MCB.00908-07
9. Bartkova J, Rezaei N, Liontos M, Karakaidos P, Kletsas D, Issaeva N, et al. Oncogene-induced senescence is part of the tumorigenesis barrier imposed by DNA damage checkpoints. Nature 2006; 444:633-7; PMID:17136093; http://dx.doi.org/10.1038/nature05268
10. Di Micco R, Fumagalli M, Cicalese A, Piccinin S, Gasparini P, Luise C, et al. Oncogene-induced senescence is a DNA damage response triggered by DNA hyper-replication. Nature 2006; 444:638-42; PMID:17136094; http://dx.doi.org/10.1038/nature05327
11. Berns K, Hijmans EM, Mullenders J, Brummelkamp TR, Velds A, Heimerikx M, et al. A large-scale RNAi screen in human cells identifies new components of the p53 pathway. Nature 2004; 428:431-7; PMID:15042092; http://dx.doi.org/10.1038/nature02371
12. Mullenders J, Fabius AW, Madiredjo M, Bernards R, Beijersbergen RL. A large scale shRNA barcode screen identifies the circadian clock component ARNTL as putative regulator of the p53 tumor suppressor pathway. PLoS One 2009; 4:e4798; PMID:19277210; http://dx.doi.org/10.1371/journal.pone.0004798
13. Rovillain E, Mansfield L, Lord CJ, Ashworth A, Jat PS. An RNA interference screen for identifying downstream effectors of the p53 and pRB tumour suppressor pathways involved in senescence. BMC Genomics 2011; 12:355; PMID:21740549; http://dx.doi.org/10.1186/1471-2164-12-355
14. Campisi J. Cellular senescence: putting the paradoxes in perspective. Curr Opin Genet Dev 2011; 21:107-12; PMID:21093253; http://dx.doi.org/10.1016/j.gde.2010.10.005

15. Ding L, Getz G, Wheeler DA, Mardis ER, McLellan MD, Cibulskis K, et al. Somatic mutations affect key pathways in lung adenocarcinoma. Nature 2008; 455:1069-75; PMID:18948947; http://dx.doi.org/10.1038/nature07423
16. Wood LD, Calhoun ES, Silliman N, Ptak J, Szabo S, Powell SM, et al. Somatic mutations of GUCY2F, EPHA3, and NTRK3 in human cancers. Hum Mutat 2006; 27:1060-1; PMID:16941478; http://dx.doi.org/10.1002/humu.9452
17. Greenman C, Stephens P, Smith R, Dalgliesh GL, Hunter C, Bignell G, et al. Patterns of somatic mutation in human cancer genomes. Nature 2007; 446:153-8; PMID:17344846; http://dx.doi.org/10.1038/nature05610
18. Bardelli A, Parsons DW, Silliman N, Ptak J, Szabo S, Saha S, et al. Mutational analysis of the tyrosine kinome in colorectal cancers. Science 2003; 300:949; PMID:12738854; http://dx.doi.org/10.1126/science.1082596
19. Easty DJ, Bennett DC. Protein tyrosine kinases in malignant melanoma. Melanoma Res 2000; 10:401-11; PMID:11095400; http://dx.doi.org/10.1097/00008390-200010000-00001
20. Wykosky J, Debinski W. The EphA2 receptor and ephrinA1 ligand in solid tumors: function and therapeutic targeting. Mol Cancer Res 2008; 6:1795-806; PMID:19074825; http://dx.doi.org/10.1158/1541-7786.MCR-08-0244
21. Lackmann M, Boyd AW. Eph, a protein family coming of age: more confusion, insight, or complexity? Sci Signal 2008; 1:re2; PMID:18413883; http://dx.doi.org/10.1126/stke.115re2
22. Oricchio E, Nanjangud G, Wolfe AL, Schatz JH, Mavrakis KJ, Jiang M, et al. The Eph-receptor A7 is a soluble tumor suppressor for follicular lymphoma. Cell 2011; 147:554-64; PMID:22036564; http://dx.doi.org/10.1016/j.cell.2011.09.035
23. Lisabeth EM, Fernandez C, Pasquale EB. Cancer somatic mutations disrupt functions of the EphA3 receptor tyrosine kinase through multiple mechanisms. Biochemistry 2012; 51:1464-75; PMID:22242939; http://dx.doi.org/10.1021/bi2014079
24. Zhuang G, Song W, Amato K, Hwang Y, Lee K, Boothby M, et al. Effects of cancer-associated EPHA3 mutations on lung cancer. J Natl Cancer Inst 2012; 104:1182-97; PMID:22829656; http://dx.doi.org/10.1093/jnci/djs297
25. Nachury MV, Loktev AV, Zhang Q, Westlake CJ, Peränen J, Merdes A, et al. A core complex of BBS proteins cooperates with the GTPase Rab8 to promote ciliary membrane biogenesis. Cell 2007; 129:1201-13; PMID:17574030; http://dx.doi.org/10.1016/j.cell.2007.03.053
26. Loewer A, Batchelor E, Gaglia G, Lahav G. Basal dynamics of p53 reveal transcriptionally attenuated pulses in cycling cells. Cell 2010; 142:89-100; PMID:20598361; http://dx.doi.org/10.1016/j.cell.2010.05.031
27. Lu LY, Wood JL, Ye L, Minter-Dykhouse K, Saunders TL, Yu X, et al. Aurora A is essential for early embryonic development and tumor suppression. J Biol Chem 2008; 283:31785-90; PMID:18801727; http://dx.doi.org/10.1074/jbc.M805880200
28. Elyada E, Pribluda A, Goldstein RE, Morgenstern Y, Brachya G, Cojocaru G, et al. CKIα ablation highlights a critical role for p53 in invasiveness control. Nature 2011; 470:409-13; PMID:21331045; http://dx.doi.org/10.1038/nature09673
29. St John MA, Tao W, Fei X, Fukumoto R, Carcangiu ML, Brownstein DG, et al. Mice deficient of Lats1 develop soft-tissue sarcomas, ovarian tumours and pituitary dysfunction. Nat Genet 1999; 21:182-6; PMID:9988269; http://dx.doi.org/10.1038/5965
30. Pan D. The hippo signaling pathway in development and cancer. Dev Cell 2010; 19:491-505; PMID:20951342; http://dx.doi.org/10.1016/j.devcel.2010.09.011
31. Cancer Genome Atlas Research Network. Integrated genomic analyses of ovarian carcinoma. Nature 2011; 474:609-15; PMID:21720365; http://dx.doi.org/10.1038/nature10166
32. Janes PW, Adikari S, Lackmann M. Eph/ephrin signalling and function in oncogenesis: lessons from embryonic development. Curr Cancer Drug Targets 2008; 8:473-9; PMID:18781894; http://dx.doi.org/10.2174/156800908785699315
33. Binns KL, Taylor PP, Sicheri F, Pawson T, Holland SJ. Phosphorylation of tyrosine residues in the kinase domain and juxtamembrane region regulates the biological and catalytic activities of Eph receptors. Mol Cell Biol 2000; 20:4791-805; PMID:10848605; http://dx.doi.org/10.1128/MCB.20.13.4791-4805.2000
34. Davis TL, Walker JR, Loppnau P, Butler-Cole C, Allali-Hassani A, Dhe-Paganon S. Autoregulation by the juxtamembrane region of the human ephrin receptor tyrosine kinase A3 (EphA3). Structure 2008; 16:873-84; PMID:18547520; http://dx.doi.org/10.1016/j.str.2008.03.008
35. Nievergall E, Janes PW, Stegmayer C, Vail ME, Haj FG, Teng SW, et al. PTP1B regulates Eph receptor function and trafficking. J Cell Biol 2010; 191:1189-203; PMID:21135139; http://dx.doi.org/10.1083/jcb.201005035
36. Chen Z, Cheng K, Walton Z, Wang Y, Ebi H, Shimamura T, et al. A murine lung cancer co-clinical trial identifies genetic modifiers of therapeutic response. Nature 2012; 483:613-7; PMID:22425996; http://dx.doi.org/10.1038/nature10937
37. Malumbres M, Barbacid M. Cell cycle, CDKs and cancer: a changing paradigm. Nat Rev Cancer 2009; 9:153-66; PMID:19238148; http://dx.doi.org/10.1038/nrc2602
38. Chien Y, Scuoppo C, Wang X, Fang X, Balgley B, Bolden JE, et al. Control of the senescence-associated secretory phenotype by NF-κB promotes senescence and enhances chemosensitivity. Genes Dev 2011; 25:2125-36; PMID:21979375; http://dx.doi.org/10.1101/gad.17276711
39. Schmitt CA, Fridman JS, Yang M, Lee S, Baranov E, Hoffman RM, et al. A senescence program controlled by p53 and p16INK4a contributes to the outcome of cancer therapy. Cell 2002; 109:335-46; PMID:12015983; http://dx.doi.org/10.1016/S0092-8674(02)00734-1
40. Salminen A, Kauppinen A, Kaarniranta K. Emerging role of NF-κB signaling in the induction of senescence-associated secretory phenotype (SASP). Cell Signal 2012; 24:835-45; PMID:22182507; http://dx.doi.org/10.1016/j.cellsig.2011.12.006
41. Guerra C, Collado M, Navas C, Schuhmacher AJ, Hernández-Porras I, Cañamero M, et al. Pancreatitis-induced inflammation contributes to pancreatic cancer by inhibiting oncogene-induced senescence. Cancer Cell 2011; 19:728-39; PMID:21665147; http://dx.doi.org/10.1016/j.ccr.2011.05.011
42. Huck JJ, Zhang M, McDonald A, Bowman D, Hoar KM, Stringer B, et al. MLN8054, an inhibitor of Aurora A kinase, induces senescence in human tumor cells both in vitro and in vivo. Mol Cancer Res 2010; 8:373-84; PMID:20197380; http://dx.doi.org/10.1158/1541-7786.MCR-09-0300
43. Zhang W, Peng G, Lin SY, Zhang P. DNA damage response is suppressed by the high cyclin-dependent kinase 1 activity in mitotic mammalian cells. J Biol Chem 2011; 286:35899-905; PMID:21878640; http://dx.doi.org/10.1074/jbc.M111.267690
44. Takahashi A, Ohtani N, Yamakoshi K, Iida S, Tahara H, Nakayama K, et al. Mitogenic signalling and the p16INK4a-Rb pathway cooperate to enforce irreversible cellular senescence. Nat Cell Biol 2006; 8:1291-7; PMID:17028578; http://dx.doi.org/10.1038/ncb1491
45. Jia M, Souchelnytskyi N, Hellman U, O'Hare M, Jat PS, Souchelnytskyi S. Proteome profiling of immortalization-to-senescence transition of human breast epithelial cells identified MAP2K3 as a senescence-promoting protein which is downregulated in human breast cancer. Proteomics Clin Appl 2010; 4:816-28; PMID:21137025; http://dx.doi.org/10.1002/prca.201000006
46. Brumbaugh KM, Otterness DM, Geisen C, Oliveira V, Brognard J, Li X, et al. The mRNA surveillance protein hSMG-1 functions in genotoxic stress response pathways in mammalian cells. Mol Cell 2004; 14:585-98; PMID:15175154; http://dx.doi.org/10.1016/j.molcel.2004.05.005
47. Nievergall E, Lackmann M, Janes PW. Eph-dependent cell-cell adhesion and segregation in development and cancer. Cell Mol Life Sci 2012; 69:1813-42; PMID:22204021; http://dx.doi.org/10.1007/s00018-011-0900-6
48. Pasquale EB. Eph receptors and ephrins in cancer: bidirectional signalling and beyond. Nat Rev Cancer 2010; 10:165-80; PMID:20179713; http://dx.doi.org/10.1038/nrc2806
49. Vecchi M, Confalonieri S, Nuciforo P, Viganò MA, Capra M, Bianchi M, et al. Breast cancer metastases are molecularly distinct from their primary tumors. Oncogene 2008; 27:2148-58; PMID:17952122; http://dx.doi.org/10.1038/sj.onc.1210858
50. Xi HQ, Wu XS, Wei B, Chen L. Aberrant expression of EphA3 in gastric carcinoma: correlation with tumor angiogenesis and survival. J Gastroenterol 2012; 47:785-94; PMID:22350700; http://dx.doi.org/10.1007/s00535-012-0549-4
51. Guan M, Liu L, Zhao X, Wu Q, Yu B, Shao Y, et al. Copy number variations of EphA3 are associated with multiple types of hematologic malignancies. Clin Lymphoma Myeloma Leuk 2011; 11:50-3; PMID:21454190; http://dx.doi.org/10.3816/CLML.2011.n.006
52. Miao H, Nickel CH, Cantley LG, Bruggeman LA, Bennardo LN, Wang B. EphA kinase activation regulates HGF-induced epithelial branching morphogenesis. J Cell Biol 2003; 162:1281-92; PMID:14517207; http://dx.doi.org/10.1083/jcb.200304018
53. Vaidya A, Pniak A, Lemke G, Brown A. EphA3 null mutants do not demonstrate motor axon guidance defects. Mol Cell Biol 2003; 23:8092-8; PMID:14585969; http://dx.doi.org/10.1128/MCB.23.22.8092-8098.2003
54. Stephen LJ, Fawkes AL, Verhoeve A, Lemke G, Brown A. A critical role for the EphA3 receptor tyrosine kinase in heart development. Dev Biol 2007; 302:66-79; PMID:17046737; http://dx.doi.org/10.1016/j.ydbio.2006.08.058
55. Gray DC, Hoeflich KP, Peng L, Gu Z, Gogineni A, Murray LJ, et al. pHUSH: a single vector system for conditional gene expression. BMC Biotechnol 2007; 7:61; PMID:17897455; http://dx.doi.org/10.1186/1472-6750-7-61
56. Brummelkamp TR, Bernards R, Agami R. A system for stable expression of short interfering RNAs in mammalian cells. Science 2002; 296:550-3; PMID:11910072; http://dx.doi.org/10.1126/science.1068999
57. Haverty PM. genoset: Provides classes similar to ExpressionSet for copy number analysis. R package version 1.2.0. http://www.bioconductor.org. 2011

Landes Bioscience

www.landesbioscience.com

Supplemental Material to:

Jenni Lahtela, Laura B. Corson, Annabrita Hemmes, Matthew J. Brauer, Sonja Koopal, James Lee, Thomas L. Hunsaker, Peter K. Jackson and Emmy W. Verschuren

A high-content cellular senescence screen identifies candidate tumor suppressors, including EPHA3

2013; 12(4)

http://dx.doi.org/10.4161/cc.23515

http://www.landesbioscience.com/journals/cc/article/23515/

Supplementary Information Lahtela et al.

Supplementary Materials and Methods

Generation of EPHA3-LAP variant cell lines

The 293T Flp-In T-REx cell line was purchased from Invitrogen. The hTERT-RPE1 cell line was converted to a Flp-In cell line by the insertion of a FRT site. Stable cell lines were created as previously described [1]. Briefly, human EPHA3 cDNA and tumor variants were synthesised by DNA 2.0 into Gateway compatible pDONR221 entry vectors and cloned into appropriate pG-LAP5 or pG-LAP5/puro Gateway destination vectors using LR recombination technology (Invitrogen). pG-LAP constructs encoding proteins of interest were co-transfected with pOG44 plasmid encoding the Flp recombinase (Invitrogen) into Flp-In cell lines using Fugene 6 (Roche), followed by selection for stable integrants using Hygromycin B (pG-LAP5) or Puromycin (pG-LAP5/puro) selection. Pooled lines were used for 293T cell, clonal cell lines were used for hTERT-RPE1 cells.

Cell transfections

For gene knockdown, cells were treated with 50 nM pooled siRNA duplexes or 12.5 nM single siRNAs using reverse transfection with Dharmafect #2 reagent (Dharmacon) in 384 well CellBIND Surface polystyrene plates (Corning), or with Oligofectamine reagent (Invitrogen) in 96 well plates for forward transfections. Dharmacon pools comprising the siGENOME kinase pool library are listed in the Supplementary Table 1, and Dharmacon siGENOME SMARTpool siRNAs used in follow up studies were: CDK1 M-003224-03; CSNK1A M-003957-03; EPHA3 M-003117-03; KSR2 M-005322-03; LATS1 M-004632-03; MAP2K3 M-003509-03; MAP4K1 M-003586-03; MYLK M-005351-03; NEK1 M-004864-03; PAK7 M-003973-03; PASK M-005018-03; PIK3C2A M-006771-03; PIP5K1A M-

004780-03; RPS6KA1 M-004663-03; SMG1 M-005033-03; AURKA M-003545-03; p16INK4 M-011007-03; siCONTROL non-targeting siRNA #3 (siCtrl) D-001210-03. Dharmacon ON-TARGET*Plus* SMARTpool siRNAs were: EMI1 (FBXO5) L-012434-00; siCONTROL non-targeting siRNA pool #1 (siCtrl) D-001206-13 or non-targeting pool (siCTRL) D-001810-10.

RNA expression analysis

For quantitative real-time RT-PCR analysis, total RNA was prepared using the RNeasy Mini kit (QIAGEN). RNA (100 ng) was used for qRT-PCR reactions using TaqMan One-step RT-PCR Master Mix kit and primers (450 nM) plus MGB probe (125 nM) supplied in TaqMan® Gene Expression Assays (Applied Biosystems), using probes listed below. Triplicate reactions were run and analysed on an ABI 7500 thermocycler, using relative quantitation against housekeeping RPL19 mRNA. Alternatively, total RNA was prepared using NucleoSpin RNA II (Macherey-Nagel). cDNA synthesis was performed from 750 ng of total RNA using High Capacity cDNA Reverse Transcription Kit (Applied Biosystems) which was used for quantitative PCR analysis with iQ Supermix (BIO-RAD) reagent. The following TaqMan® probes were used: CDK1 Hs00364293_m1; CSNK1A; Hs00740463_m1; EPHA3 Hs00739096_m1; KSR2 Hs00543274_m1; LATS1 Hs00177987_m1; MAP2K3 Hs00177127_m1; MAP4K1 Hs00179345_m1; MYLK Hs00364926_m1; NEK1 Hs00404339_m1; PAK7 Hs00379321_m1; PASK Hs00209470_m1; PIK3C2A Hs00153223_m1; PIP5K1A Hs00801004_s1; RPS6KA1 Hs00179731_m1; SMG1 Hs00247891_m1; AURKA Hs00269212_m1; RPL19 Hs02338565_gH; INK4a Hs00923894_m1; EPHA1 Hs00178313_m1; EPHA2 Hs00171656_m1; EPHA3 Hs00739096_m1; EPHA4 Hs00177874_m1; EPHA5 Hs00300724_m1;RPL19 Hs02338565_gH. Triplicate reactions were run and analysed on a Biorad CFX384

thermocycler, using relative quantitation against housekeeping RPL19 mRNA expression. For RNA expression analysis using SYBR Green (BioRad) reagent, the following TaqMan® probes were used: INK4a Hs00923894_m1; EPHA3 Hs00739096_m1; RPL19 Hs02338565_gH with the following primers: EPHA3 fwd 5'GCAGACAAAGACCCTCCAT3' rev 5'GTAACATCTTTCCGGCCTC3'; $p16^{INK4a}$ fwd 5'CCCAACGCACCGAATAGTTAC3' rev 5'CCAGCGTGTCCAGGAAG3'; p53 fwd 5'GTCCCTTCCCAGAAAACCTA3' rev 5'CTCGGATAAGATGCTGAGGA3' RPL19 fwd 5'ACCCCAATGAGACCAATGAA3' rev 5'CGCAAAATCCTCATTCTCCT3'.

Senescence-associated β-galactosidase quantitation

A color threshold was assigned to RGB images of SA-βGal staining to remove background signal, followed by binarisation and smoothening to remove pixels <5 or >5000. The number of nuclei per image was calculated, followed by image binarisation, dilation of nuclear objects by 15 pixels, and drawing of a region limit. DNA regions were overlaid onto the binarised RGB images, followed by quantitation of the percentage of SA-β-Gal positive pixels per region. A macro was run to bin cells according to their average staining intensity (intensity/cell/image in bins of 0, 0-10%, 11-20% etc.). The senescence score per siRNA (pools or singles) was calculated as the sum of the staining intensities normalised against the total cell number per bin: $\sum$ [(normalised #cells * maximum bin intensity)].

DNA damage measurements

hTERT-RPE1 p53 shRNA cells growing on coverslips were transfected with siRNAs, and at 96h fixed in 4% paraformaldehyde, permeabilised with 0.2% Triton X-100, followed by immunostaining using 0.4-2 μg/mL primary phospho-Histone H2A.X Ser139 (Upstate) antibody and Alexa Fluor 488 secondary antibody (Molecular Probes). DNA was

counterstained with Hoechst 33342 dye and image analysis was performed using a Zeiss AX10 microscope and Slidebook4.1 software.

Protein variant structural domain analysis

A PDB file with EPHA3 kinase and juxtamembrane domain structure information [2] was downloaded from the RCSB protein data bank (http://www.pdb.org/pdb/home/home.do). A PDB file with EPHA3 kinase and juxtamembrane domain structure information (2QOC) [2] and the structural information of LKB1 tumor suppressor (2WTK) [3] was downloaded from the RCSB protein data bank (http://www.pdb.org/pdb/home/home.do). Mutation analysis, distance measurements and alignment analysis were performed using the PyMOL molecular visualisation system.

BrdU DNA replication analysis

For measurements of DNA replication, cells were transfected for 15h with pools of siRNAs and synchronised by treatment with 100 nM Nocodazole for 8h, followed by wash-out and release for 9 or 12h. During the last 30 minutes of release from Nocodazole, cells were pulsed with 50 μM 5-bromodeoxyuridine (BrdU, Sigma). Cells were trypsinised, washed twice in 1% BSA/PBS, fixed with cold 70% ethanol for at least 16h at -20°C. BrdU incorporation was determined with an anti-BrdU-FITC conjugate (Becton Dickinson) according to the manufacturer's protocol, followed by flow cytometric analysis on a FACScan (Becton Dickinson) using CellQuest software to quantitate the S phase fraction.

Immunostaining and fluorescence microscopy

hTERT-RPE1 Flp-In cells expressing stable LAP-tagged EPHA3 proteins with or without ephrin-A5 treatment were fixed on coverslips and immunostained for GFP (EPHA3-LAP)

and early endosomes (EEA1, BD Biosciences). Fluorescence microscopy imaging was performed with the Nikon 90i microscope using 60X objective. Image handling was done with Adobe Photoshop CS5 software.

Supplementary References

1. Torres JZ, Miller JJ, Jackson PK. High-throughput generation of tagged stable cell lines for proteomic analysis. Proteomics 2009; 9:2888-91.

2. Davis TL, Walker JR, Loppnau P, Butler-Cole C, Allali-Hassani A, Dhe-Paganon S. Autoregulation by the juxtamembrane region of the human ephrin receptor tyrosine kinase A3 (EphA3). Structure 2008; 16:873-84.

3. Zeqiraj E, Filippi BM, Deak M, Alessi DR, van Aalten DM. Structure of the LKB1-STRAD-MO25 complex reveals an allosteric mechanism of kinase activation. Science 2009; 326:1707-11.

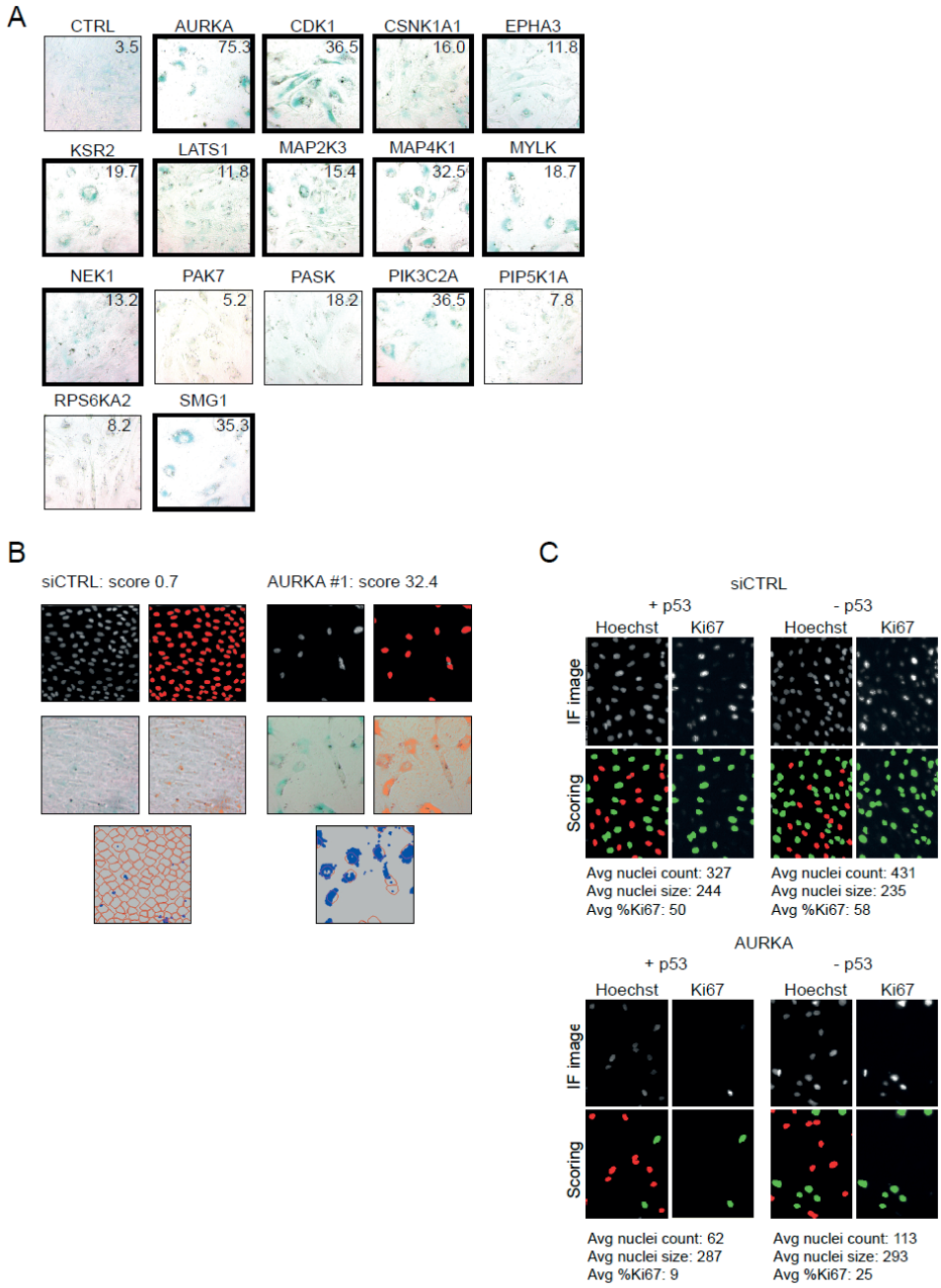

Fig. S1. Confirmation of senescence by quantitative SA-β-Gal staining.

(A) hTERT-RPE1 p53 shRNA cells were reverse transfected with pooled siGENOME siRNAs in the absence of doxycycline (p53+). Five days after siRNA transfection cells were fixed and stained for SA-β-Gal, and representative images are shown.

(B) Representative examples of senescence image processing and scoring for siCtrl and AURKA oligonucleotide #1 siRNAs. Five days after siRNA transfection cells were fixed and stained for SA-βGal, and DNA was counterstained with Hoechst. Images were binarised (right panels), and nuclear object regions were dilated by 15 pixels and overlaid with RGB images (bottom panels). The percentage of SA-β-Gal positive pixels per cell region was calculated, and cells were binned according to the average staining intensity per image (intensity/cell/image in bins of 0, 0-10%, 11-20% etc.). The senescence score was calculated as $\sum$ [(normalised #cells * maximum bin intensity)].

(C) Representative example of the HCS siRNA screen quantitative image analysis and scoring for siCtrl and AURKA pooled oligonucleotides.

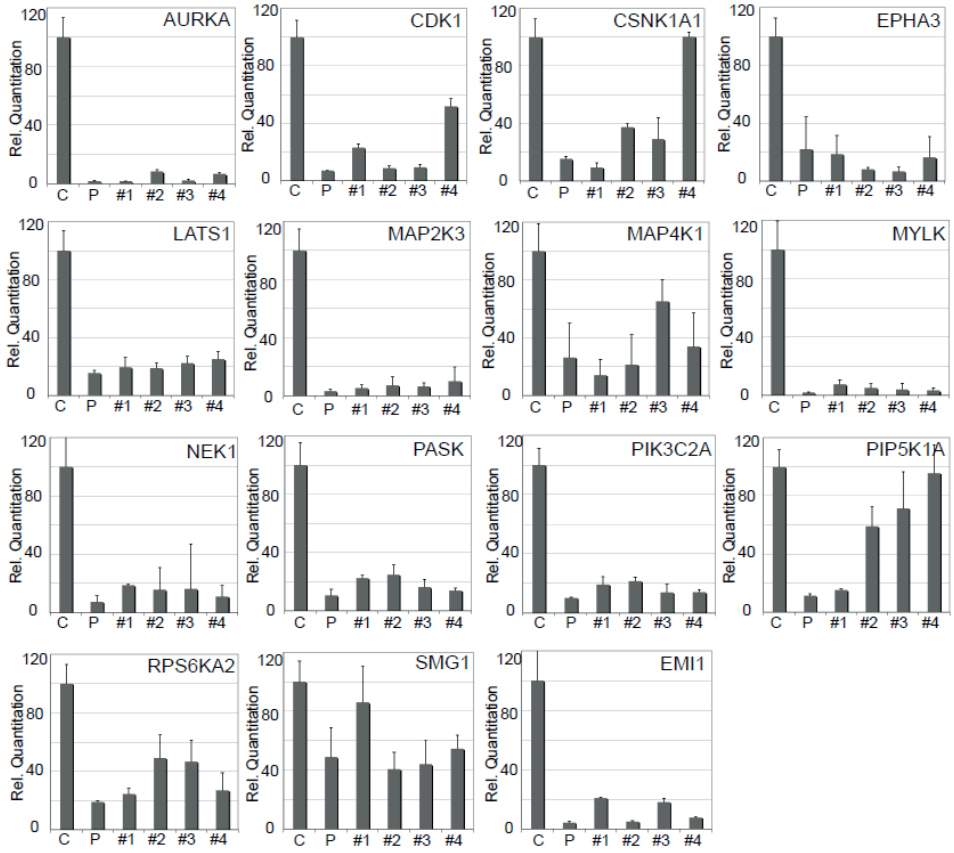

Fig. S2. Correlation of senescence with gene knockdown efficiency

Quantitative RNA expression analysis to measure gene knockdown efficiencies. hTERT-RPE1 p53 shRNA cells were reverse transfected with siRNAs in the absence of doxycycline (p53+). Total RNA was prepared three days later, and relative RNA expression was quantitated using TaqMan analyses. PAK7 RNA was not expressed in hTERT-RPE1 cells, correlating with its negative senescence score (Table S1), thus confirming it as a false negative; knockdown of RPS6KA2 was efficient but failed to induce senescence (Table S1). Three of four PIP5K1A siRNA oligonucleotides strongly induced senescence without efficient knockdown, implying an off-target effect. The expression levels of KSR2 were too low to be detected by the TaqMan probe, and its low expression level was confirmed in expression microarray analysis of hTERT-RPE1 cells.

However, since the pool and three of four KSR2 oligonucleotides scored positive, we assigned KSR2 siRNA as a genuine hit. Overall, no strict correlation between senescence scores and knockdown efficiency was detected; all senescence-inducing oligonucleotides showed 80-98% knockdown efficiency.

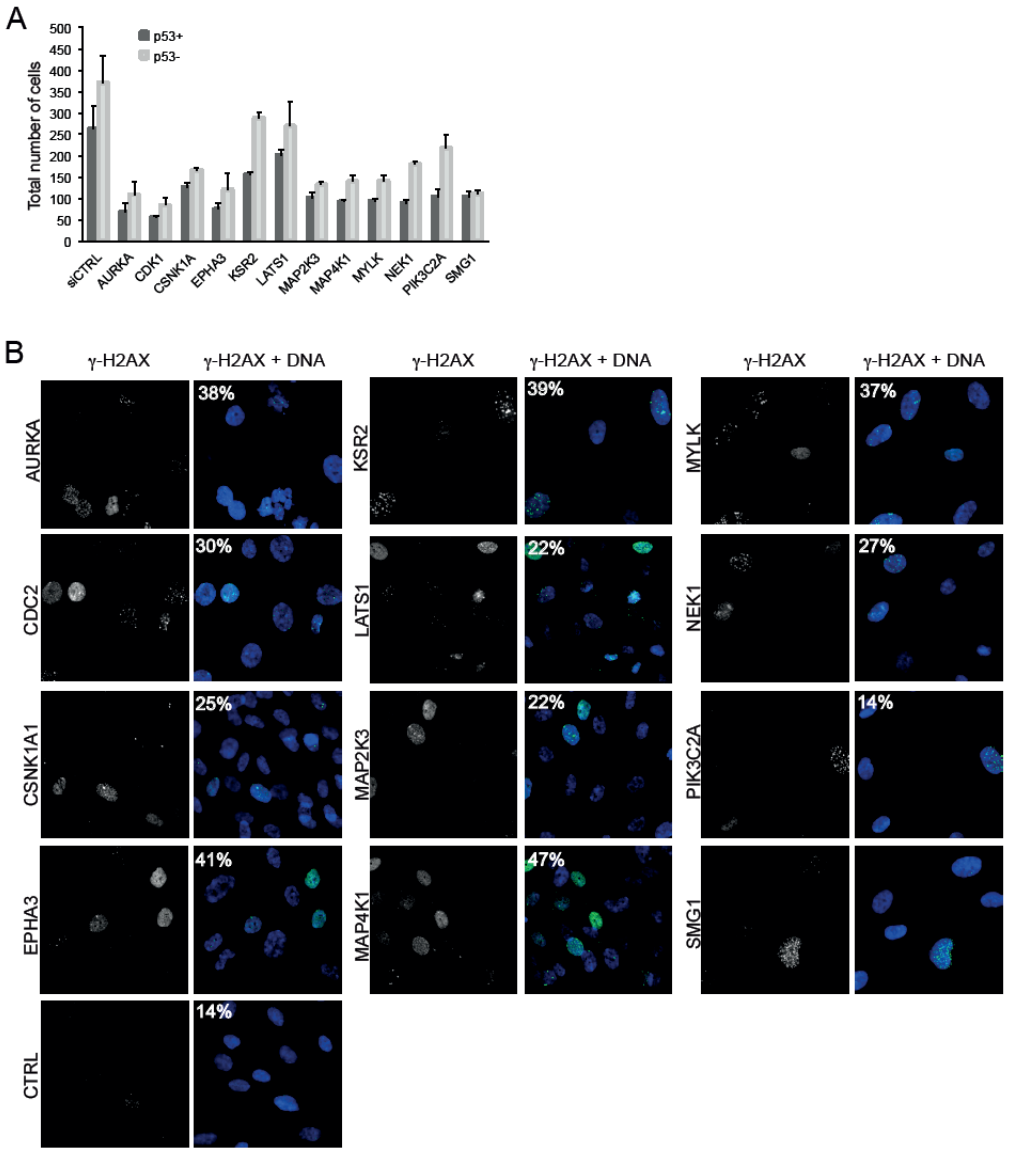

Fig. S3. Characterisation of senescence signatures.

(A) hTERT-RPE1 p53 shRNA cells (treated or not with doxycycline) were reverse transfected with indicated SMARTpool kinome siRNAs, and stained with Hoechst following 72h of culture. Total numbers of cells were calculated via MetaXpress image normalisation and analysis. HCS data shown are averaged percentages and standard deviations of cells from four 384 wells each.

(B) hTERT-RPE1 p53 shRNA cells (not treated with Doxycycline) were reverse transfected with indicated pooled siRNAs and immunostained for γ-H2AX and stained with Hoechst to mark the DNA following 96h of culture. A total of 300-500 cells were analysed, and percentages of cells containing discrete nuclear foci or staining are shown.

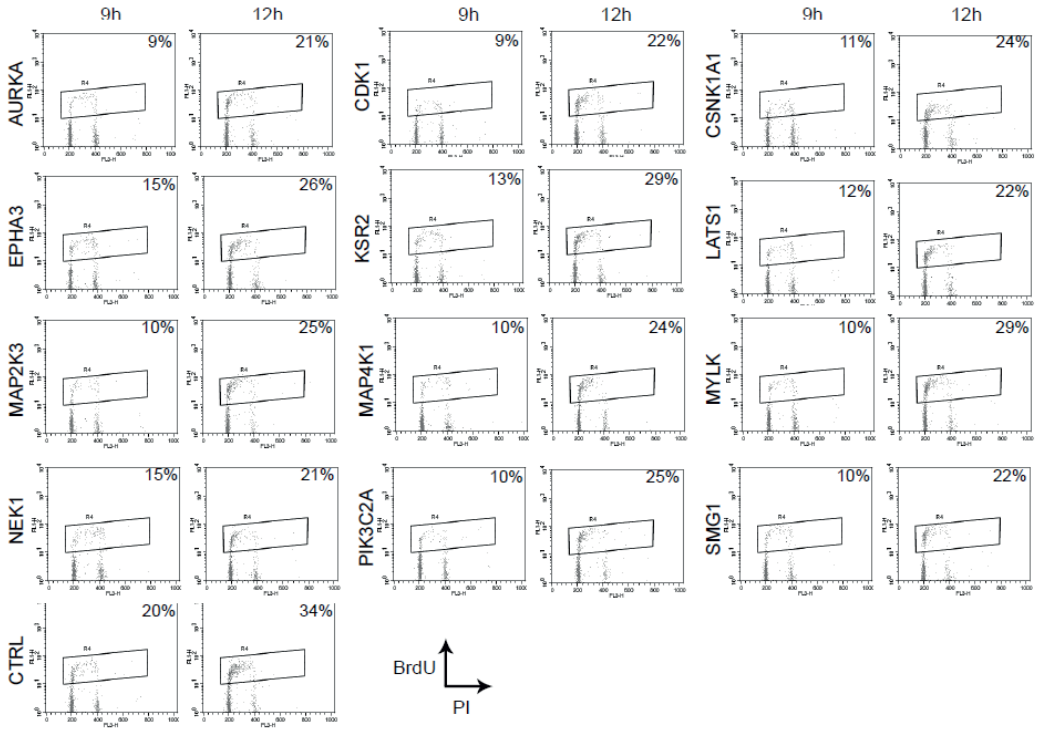

Fig. S4. DNA replication analysis after Nocodazole release.

hTERT-RPE1 p53 shRNA cells (not treated with Doxycycline) were transfected with control or senescence hit siRNAs for 15h, arrested in mitosis by Nocodazole treatment, and released by Nocodazole wash-out. Cells were harvested and fixed at the indicated timepoints, processed for BrdU and PI staining, and analysed by flow cytometry. Percentages of BrdU-positive cells are indicated.

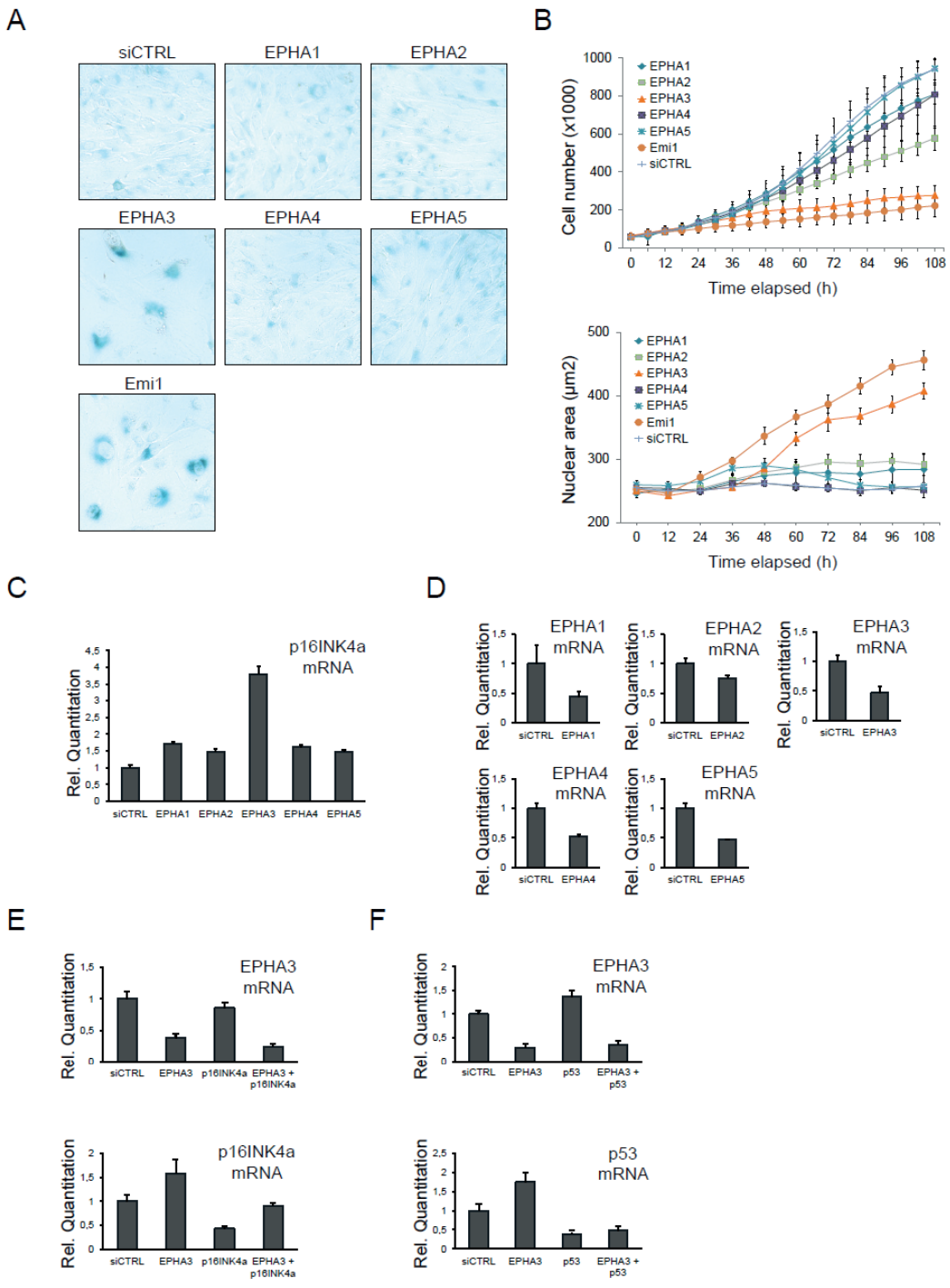

Fig. S5. EPHA receptor knockdown-associated cellular senescence.

(A) SA-β-Gal staining of EPHA receptor siRNA-treated hTERT-RPE1 cells assessed at five

days after siRNA transfection.

(B) Live cell imaging analysis of EPHA receptor siRNA treated hTERT-RPE1 cells. The cells were imaged during 6h intervals for five days after siRNA transfection.

(C) Quantitative $p16^{INK4a}$ RNA expression analysis of EPHA receptor siRNA treated hTERT-RPE1 cells. Total RNA was prepared from duplicate plate three days after siRNA transfection

(D) Knockdown verification of EPHA receptor depletion. Relative RNA expression three days after siRNA transfection was quantitated using quantitative real-time RT-PCR for indicated EPHA receptor mRNAs.

(E) Quantitative $p16^{INK4a}$, p53 and EPHA3 RNA expression analysis of siRNA treated hTERT-RPE1 cells. Total RNA was prepared from duplicate plate three days after siRNA transfection.

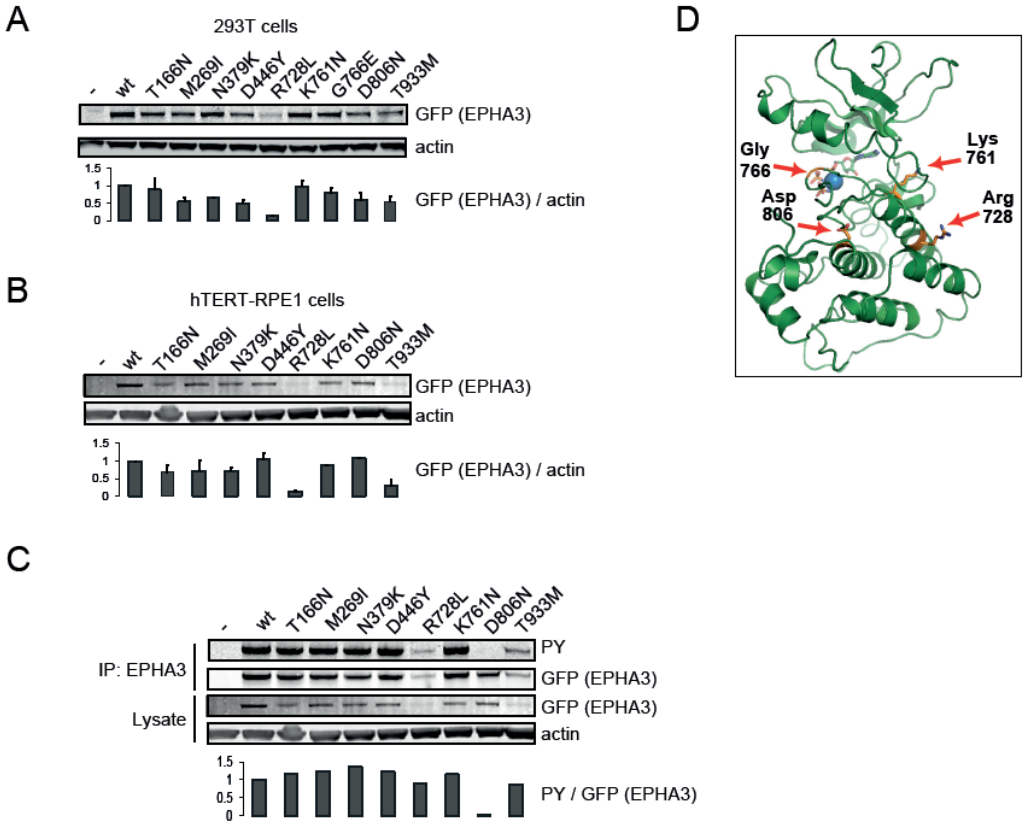

Fig. S6. Characterisation of EPHA3-LAP variant cell lines.

Verification of EPHA-LAP variant expression in 293T (A) and hTERT-RPE1 Flp-In cells (B). The samples were immunoblotted with the indicated antibodies.

(F) *In vitro* kinase assay of selected EPHA3 receptor cancer mutation variants. GFP immunoprecipitates from kinase assays or input lysate samples from hTERT-RPE1 stable EPHA3-LAP cell lines were immunoblotted with the indicated antibodies. GFP antibody was used for detection of EPHA3-LAP variants. Relative kinase activities were determined by normalisation of the PY (phosphotyrosine) against the EPHA3 signal where the normalised values are presented relative to WT.

(G) EPHA3 kinase and juxtamembrane domain (JMKIN) structure highlighting kinase domain residues in the kinase domain pertinent to this study (red arrows).

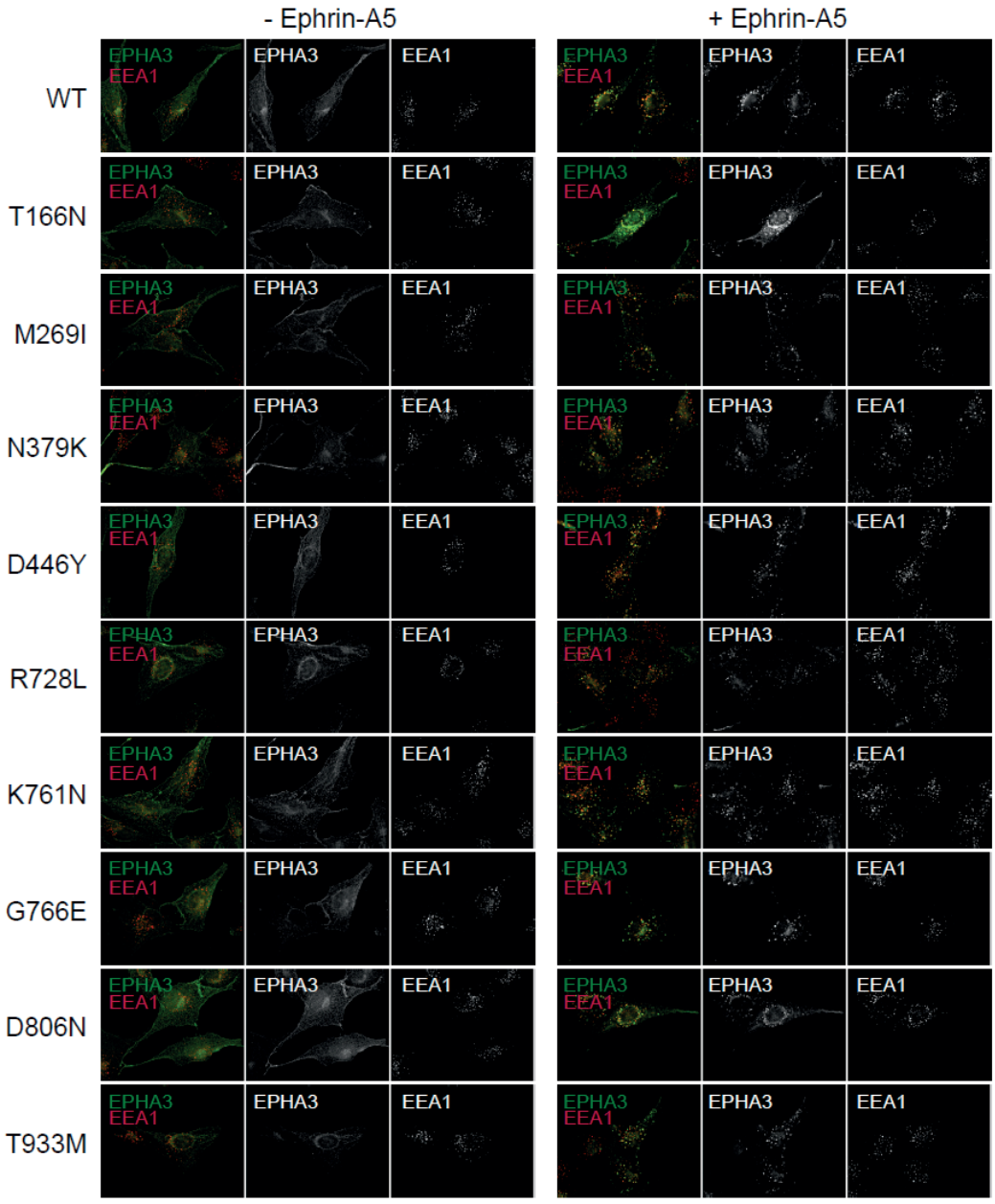

Fig. S7. EPHA3-LAP localises to early endosomes

EPHA3-LAP cancer variants localise to early endosomes after ephrin-A5 activation. hTERT-RPE1 stable EPHA3-LAP cell lines were stained with EEA1 and GFP (EPHA3) antibodies and imaged using fluorescence microscopy.

Supplementary Table S1. Kinome library information

Hit	Dharmacon Name	Oligo ID (Dharmacon siGENOME pools)	RefSeq#
	AAK1	M-005300-00	NM_014911
	AATK	M-005301-01	XM_375495
	ABI1	M-007290-00	NM_005470
	ABL1	M-003100-01	NM_007313
	ABL2	M-003101-01	NM_005158
	ACK1	M-003102-02	NM_005781
	ACVR1	M-004924-01	NM_001105
	ACVR1B	M-004925-01	NM_004302
	ACVR1C	M-004929-01	NM_145259
	ACVR2	M-004926-01	NM_001616
	ACVR2B	M-004927-00	NM_001106
	ACVRL1	M-005302-02	NM_000020
	ADAM9	M-004504-02	NM_003816
	ADCK1	M-005303-02	NM_020421
	ADCK2	M-005304-01	NM_052853
	ADCK4	M-005305-01	NM_024876
	ADCK5	M-018919-00	NM_174922
	ADK	M-004733-02	NM_001123
	ADRA1A	M-005419-00	NM_000680
	ADRA1B	M-005420-01	NM_000679
	ADRA2C	M-005424-01	NM_000683
	ADRB2	M-005426-01	NM_000024
	ADRBK1	M-004325-01	NM_001619
	ADRBK2	M-004326-00	NM_005160
	AGTR2	M-005429-01	NM_000686
	AK1	M-006811-01	NM_000476
	AK2	M-006812-00	NM_001625
	AK3	M-006700-01	NM_013410
	AK3L1	M-006701-00	NM_016282
	AK5	M-004897-02	NM_012093
	AK7	M-007257-00	NM_152327
	AKAP1	M-011426-01	NM_003488
	AKAP11	M-009277-01	NM_016248
	AKAP13	M-008868-01	NM_006738
	AKAP3	M-009765-01	NM_006422
	AKAP4	M-008442-00	NM_003886
	AKAP5	M-011954-00	NM_004857
	AKAP6	M-008497-01	NM_004274
	AKAP7	M-013371-00	NM_004842
	AKAP8	M-009656-01	NM_005858
	AKT1	M-003000-01	NM_005163
	AKT2	M-003001-01	NM_001626
	AKT3	M-003002-01	NM_005465

ALK	M-003103-02	NM_004304
ALS2CR2	M-005306-01	NM_018571
ALS2CR7	M-004685-01	NM_139158
AMHR2	M-005307-01	NM_020547
ANGPT4	M-007803-00	NM_015985
ANKK1	M-004930-01	NM_178510
ANKRD3	M-005308-02	NM_020639
APEG1	M-007687-01	NM_005876
APPL	M-005138-00	NM_012096
ARAF1	M-003563-02	NM_001654
ARK5	M-004931-00	NM_014840
ASK	M-004165-01	NM_006716
ASP	M-013023-00	NM_031916
ATM	M-003201-02	NM_138293
ATR	M-003202-04	NM_001184
AURKB	M-003326-02	NM_004217
AURKC	M-019573-01	NM_003160
AVPR1A	M-003631-01	NM_000706
AVPR1B	M-005431-00	NM_000707
AXL	M-003104-02	NM_001699
AY358257	M-032294-00	AY358257
AZU1	M-008914-00	NM_001700
BCKDK	M-004932-00	NM_005881
BCR	M-003875-04	NM_004327
BDKRB2	M-005436-00	NM_000623
BLK	M-003105-03	NM_001715
BLNK	M-020353-01	NM_013314
BMP2K	M-005071-00	NM_017593
BMPR1A	M-004933-03	NM_004329
BMPR1B	M-004934-01	NM_001203
BMPR2	M-005309-02	NM_001204
BMX	M-003106-02	NM_001721
BRAF	M-003460-01	NM_004333
BRD2	M-004935-01	NM_005104
BRDT	M-004938-01	NM_001726
BTK	M-003107-01	NM_000061
BUB1	M-004102-00	NM_004336
BUB1B	M-004101-00	NM_001211
C11ORF23	M-014646-00	NM_018312
C14ORF20	M-005310-00	NM_174944
C15ORF16	M-008841-00	NM_130901
C6ORF199	M-007254-01	NM_145025
C7ORF16	M-018324-01	NM_006658
C9ORF12	M-006703-02	NM_022755
C9ORF96	M-005347-00	XM_291304
C9ORF98	M-006803-00	NM_152572
CALM3	M-019939-01	NM_005184

	CAMK1	M-004940-00	NM_003656
	CAMK1D	M-004946-00	NM_020397
	CAMK1G	M-004941-01	NM_020439
	CAMK2A	M-004942-00	NM_015981
	CAMK2B	M-004943-03	NM_001220
	CAMK2D	M-004042-02	NM_001221
	CAMK2G	M-004536-01	NM_001222
	CAMK4	M-004944-01	NM_001744
	CAMKK1	M-004912-00	NM_172207
	CAMKK2	M-004842-01	NM_006549
	CARD10	M-004395-00	NM_014550
	CARD14	M-004397-00	NM_024110
	CARKL	M-006815-00	NM_013276
	CASK	M-005311-01	NM_003688
	CCL2	M-007831-00	NM_002982
	CCL4	M-007843-01	NM_002984
	CCRK	M-004686-01	NM_012119
	CD3E	M-003775-01	NM_000733
	CD4	M-005234-01	NM_000616
	CD7	M-013630-01	NM_006137
	CDADC1	M-007732-00	NM_030911
*	CDC2	M-003224-03	NM_001786
	CDC2L1	M-004687-01	NM_001787
	CDC2L2	M-004026-01	NM_024011
	CDC2L5	M-004688-00	NM_003718
	CDC42BPA	M-003814-02	NM_003607
	CDC42BPB	M-004075-01	NM_006035
	CDC7	M-003234-02	NM_003503
	CDK10	M-003235-04	NM_003674
	CDK11	M-004689-00	NM_015076
	CDK2	M-003236-04	NM_001798
	CDK3	M-003237-01	NM_001258
	CDK4	M-003238-02	NM_000075
	CDK5	M-003239-01	NM_004935
	CDK5R1	M-008988-00	NM_003885
	CDK5R2	M-008885-00	NM_003936
	CDK5RAP1	M-013297-01	NM_016082
	CDK5RAP3	M-012957-00	NM_025197
	CDK6	M-003240-02	NM_001259
	CDK7	M-003241-01	NM_001799
	CDK8	M-003242-02	NM_001260
	CDK9	M-003243-02	NM_001261
	CDKL1	M-004323-01	NM_004196
	CDKL2	M-004797-00	NM_003948
	CDKL3	M-004798-00	NM_016508
	CDKL4	M-022660-00	XM_293029
	CDKL5	M-004799-02	NM_003159

	CDKN1A	M-003471-00	NM_000389
	CDKN1B	M-003472-00	NM_004064
	CDKN1C	M-003244-03	NM_000076
	CDKN2B	M-003245-02	NM_004936
	CDKN2C	M-003246-01	NM_001262
	CDKN2D	M-003247-02	NM_001800
	CDKN3	M-003879-00	NM_005192
	CERK	M-004061-00	NM_022766
	CGI-77	M-008553-00	NM_016023
	CHEK1	M-003255-02	NM_001274
	CHEK2	M-003256-05	NM_007194
	CHKA	M-006704-00	NM_001277
	CHKB	M-006705-00	NM_005198
	CHRM1	M-005462-01	NM_000738
	CHUK	M-003473-01	NM_001278
	CILP	M-008295-00	NM_003613
	CINP	M-013591-01	NM_032630
	CIT	M-004613-00	NM_007174
	CKB	M-006706-01	NM_001823
	CKM	M-006707-00	NM_001824
	CKMT1	M-006708-00	NM_020990
	CKMT2	M-006709-00	NM_001825
	CKS1B	M-004586-01	NM_001826
	CKS2	M-007678-00	NM_001827
	CLK1	M-004800-00	NM_004071
	CLK2	M-004801-01	NM_001291
	CLK3	M-004802-01	NM_001292
	CLK4	M-004803-00	NM_020666
	CNKSR1	M-012217-00	NM_006314
	COASY	M-006751-00	NM_025233
	COL4A3BP	M-012101-00	NM_005713
	COPB2	M-019847-01	NM_004766
	CRK7	M-004031-02	NM_016507
	CRKL	M-012023-01	NM_005207
	CSF1R	M-003109-02	NM_005211
	CSK	M-003110-02	NM_004383
*	CSNK1A1	M-003957-03	NM_001892
	CSNK1A1L	M-004681-01	NM_145203
	CSNK1D	M-003478-00	NM_001893
	CSNK1E	M-003479-01	NM_001894
	CSNK1G1	M-004666-01	NM_022048
	CSNK1G2	M-004678-00	NM_001319
	CSNK1G3	M-004679-01	NM_004384
	CSNK2A1	M-003475-00	NM_001895
	CSNK2A2	M-004752-00	NM_001896
	CSNK2B	M-007679-00	NM_001320
	CTDSPL	M-020003-00	NM_005808

CXCL10	M-007871-00	NM_001565
DAPK1	M-004417-02	NM_004938
DAPK2	M-004418-02	NM_014326
DAPK3	M-004947-00	NM_001348
DCAMKL1	M-004884-01	NM_004734
DCK	M-006710-00	NM_000788
DCPS	M-021338-00	NM_014026
DDR1	M-003111-03	NM_001954
DDR2	M-003112-03	NM_006182
DGKA	M-006711-02	NM_001345
DGKB	M-006712-01	NM_004080
DGKD	M-006713-03	NM_003648
DGKE	M-011493-00	NM_003647
DGKG	M-006715-00	NM_001346
DGKI	M-006717-01	NM_004717
DGKQ	M-005079-02	NM_001347
DGKZ	M-006718-00	NM_003646
DGUOK	M-006719-02	NM_001929
DKFZP434C131	M-004949-00	XM_044630
DKFZP566K0524	M-013909-00	NM_015605
DKFZP586B1621	M-006808-00	NM_015533
DKFZP761A052	M-013823-00	NM_017602
DKFZP761G058	M-018772-00	NM_152542
DKFZP761P0423	M-025870-00	XM_291277
DKFZp434C1418	M-005313-01	NM_173655
DLG1	M-009415-00	NM_004087
DLG2	M-011252-01	NM_001364
DLG3	M-009462-01	NM_021120
DLG4	M-007882-01	NM_001365
DMPK	M-004637-00	NM_004409
DNAJC3	M-012251-00	NM_006260
DNAJC6	M-009885-00	NM_014787
DOK1	M-011254-00	NM_001381
DTYMK	M-006720-00	NM_012145
DUB3	M-027332-00	NM_201402
DUSP1	M-003484-02	NM_004417
DUSP10	M-003965-01	NM_007207
DUSP2	M-003565-01	NM_004418
DUSP22	M-004517-00	NM_020185
DUSP4	M-003963-02	NM_001394
DUSP5	M-003566-01	NM_004419
DUSP6	M-003964-01	NM_001946
DUSP7	M-003567-00	NM_001947
DUSP8	M-003568-00	NM_004420
DYRK1A	M-004805-00	NM_001396
DYRK1B	M-004806-01	NM_004714
DYRK2	M-004730-02	NM_003583

	DYRK3	M-004731-00	NM_003582
	DYRK4	M-004732-01	NM_003845
	EDN2	M-017723-01	NM_001956
	EEF2K	M-004950-00	NM_013302
	EGFR	M-003114-01	NM_005228
	EIF2AK3	M-004883-01	NM_004836
	EIF2AK4	M-005314-00	XM_031612
	EKI1	M-006721-01	NM_018638
	EPB41L5	M-010729-00	NM_020909
	EPHA1	M-003115-02	NM_005232
	EPHA10	M-005325-00	NM_173641
	EPHA2	M-003116-01	NM_004431
*	EPHA3	M-003117-02	NM_005233
	EPHA4	M-003118-01	NM_004438
	EPHA5	M-005315-02	NM_004439
	EPHA7	M-003119-01	NM_004440
	EPHA8	M-003120-02	NM_020526
	EPHB1	M-003121-01	NM_004441
	EPHB2	M-003122-01	NM_004442
	EPHB3	M-003123-02	NM_004443
	EPHB4	M-003124-01	NM_004444
	EPHB6		
	ERBB2	M-003126-01	NM_004448
	ERBB3	M-003127-02	NM_001982
	ERBB4	M-003128-02	NM_005235
	ERK8	M-004807-01	NM_139021
	ERN1	M-004951-01	NM_001433
	EVI1	M-006530-01	NM_005241
	EXOSC10	M-010904-00	NM_002685
	FAD104	M-017856-00	NM_022763
	FASTK	M-005317-02	NM_006712
	FER	M-003129-01	NM_005246
	FES	M-003130-01	NM_002005
	FGFR1	M-003131-02	NM_000604
	FGFR2	M-003132-01	NM_000141
	FGFR3	M-003133-01	NM_000142
	FGFR4	M-003134-01	NM_002011
	FGR	M-003135-02	NM_005248
	FKBP1B	M-009944-00	NM_004116
	FLJ10074	M-005318-00	NM_017988
	FLJ10761	M-005078-00	NM_018208
	FLJ10842	M-007256-00	NM_018238
	FLJ11767	M-016476-00	NM_024593
	FLJ12476	M-007726-00	NM_022784
	FLJ13052	M-006318-00	NM_023018
	FLJ16518	M-004847-00	XM_372199
	FLJ20574	M-005319-01	NM_017886

FLJ22405	M-016118-00	NM_022485
FLJ23074	M-004843-00	NM_025052
FLJ23356	M-005321-00	NM_032237
FLJ25006	M-004624-00	NM_144610
FLJ25449	M-015501-00	NM_144714
FLJ25756	M-022248-00	XM_370866
FLJ25831	M-032033-00	NM_207320
FLJ32332	M-016028-00	NM_144641
FLJ32658	M-015777-00	NM_144688
FLJ32685	M-004052-02	NM_152534
FLJ34389	M-005326-00	NM_152649
FLJ35107	M-007727-00	XM_496631
FLJ40125	M-009006-00	NM_178494
FLT1	M-003136-02	NM_002019
FLT3	M-003137-01	NM_004119
FLT4	M-003138-01	NM_002020
FN3K	M-006724-00	NM_022158
FN3KRP	M-006817-00	NM_024619
FNDC3	M-032215-00	NM_014923
FRAP1	M-003008-01	NM_004958
FRDA	M-006691-00	NM_000144
FRK	M-003139-01	NM_002031
FRMPD2	M-008854-00	NM_152428
FUK	M-007255-00	NM_145059
FYB	M-020174-01	NM_001465
FYN	M-003140-03	NM_002037
GAK	M-005005-01	NM_005255
GALK1	M-007728-01	NM_000154
GALK2	M-006725-00	NM_002044
GAP43	M-011663-00	NM_002045
GCK	M-010819-01	NM_000162
GFRA2	M-007914-00	NM_001495
GK	M-006727-00	NM_000167
GK2	M-015091-01	NM_033214
GMFB	M-019100-00	NM_004124
GMFG	M-019878-01	NM_004877
GNE	M-006729-00	NM_005476
GOLGA4	M-012396-00	NM_002078
GPR139	M-022522-00	XM_064062
GRK1	M-004662-00	NM_002929
GRK4	M-004625-00	NM_005307
GRK5	M-004626-00	NM_005308
GRK6	M-004627-01	NM_002082
GRK7	M-004628-00	NM_139209
GRSP1	M-023262-00	XM_114303
GSG2	M-005327-00	NM_031965
GSK3A	M-003009-01	NM_019884

GSK3B	M-003010-03	NM_002093
GTF2H1	M-010924-00	NM_005316
GUCY2C	M-005328-00	NM_004963
GUCY2D	M-005329-01	NM_000180
GUCY2F	M-004515-01	NM_001522
GUK1	M-006734-01	NM_000858
HAK	M-005330-02	NM_052947
HCK	M-003141-01	NM_002110
HIPK1	M-004809-02	NM_152696
HIPK2	M-003266-03	NM_022740
HIPK3	M-004810-00	NM_005734
HIPK4	M-004808-02	NM_144685
HK1	M-006820-01	NM_000188
HK2	M-006735-01	NM_000189
HK3	M-006736-00	NM_002115
HRI	M-005007-00	NM_014413
HSHIN1	M-009927-00	NM_017493
HSMDPKIN	M-007691-01	XM_290516
HSPB8	M-005006-00	NM_014365
HSPC121	M-010664-00	NM_016395
HUNK	M-004214-01	NM_014586
ICK	M-004811-01	NM_014920
IGF1R	M-003012-04	NM_000875
IHPK1	M-006737-01	NM_153273
IHPK2	M-006738-00	NM_016291
IHPK3	M-006739-00	NM_054111
IKBKAP	M-009371-00	NM_003640
IKBKB	M-003503-00	XM_032491
IKBKE	M-003723-02	NM_014002
IL2	M-007967-00	NM_000586
ILK	M-004499-00	NM_004517
ILKAP	M-010260-00	NM_030768
ILVBL	M-009658-00	NM_006844
IMPK	M-006740-01	NM_152230
INSR	M-003014-01	NM_000208
INSRR	M-005332-00	NM_014215
IRAK1	M-004760-02	NM_001569
IRAK2	M-004761-00	NM_001570
IRAK3	M-004762-00	NM_007199
IRS1	M-003015-01	NM_005544
ITGB1BP1	M-011927-00	NM_004763
ITK	M-003144-01	NM_005546
ITPK1	M-006741-00	NM_014216
ITPKA	M-006742-01	NM_002220
ITPKB	M-006743-02	NM_002221
ITPKC	M-006744-01	NM_025194
JAK1	M-003145-01	NM_002227

	JAK2	M-003146-02	NM_004972
	JAK3	M-003147-01	NM_000215
	JIK	M-004844-01	NM_016281
	KDR	M-003148-01	NM_002253
	KHK	M-006745-02	NM_000221
	KIAA0089	M-008514-00	NM_015141
	KIAA0685	M-021331-00	NM_014678
	KIAA0931	M-022586-00	XM_041191
	KIAA0999	M-004779-02	NM_025164
	KIAA1361	M-004846-01	XM_290796
	KIAA1399	M-023172-01	XM_046685
	KIAA1639	M-005336-00	XM_290923
	KIAA1765	M-005337-00	XM_047355
	KIAA1804	M-004063-00	NM_032435
	KIAA1811	M-004619-01	NM_032430
	KIAA2002	M-005339-00	XM_370878
	KIF13B	M-004963-00	NM_015254
	KIS	M-003981-01	NM_144624
	KIT	M-003150-01	NM_000222
*	KSR2	M-005322-01	NM_173598
	LAK	M-005009-01	NM_025144
*	LATS1	M-004632-00	NM_004690
	LATS2	M-003865-00	NM_014572
	LCK	M-003151-01	NM_005356
	LCP2	M-012120-00	NM_005565
	LIM	M-006930-00	NM_006457
	LIMK1	M-007730-01	NM_002314
	LIMK2	M-003311-02	NM_005569
	LMTK2	M-003149-01	NM_014916
	LMTK3	M-005338-01	XM_055866
	LOC115704	M-015901-01	NM_145245
	LOC149420	M-005011-01	NM_152835
	LOC254897	M-022066-00	XM_170950
	LOC340156	M-027171-00	XM_373109
	LOC340371	M-005340-01	NM_178564
	LOC388228	M-027174-00	XM_370948
	LOC390975	M-027175-00	XM_372749
	LOC391622	M-028355-00	NM_212553
	LOC401494	M-029537-00	XM_376819
	LOC91461	M-005341-01	XM_038576
	LOC91807	M-005342-02	NM_182493
	LRRK1	M-005320-01	NM_024652
	LRRK2	M-006323-00	XM_058513
	LTK	M-003152-01	NM_002344
	LYK5	M-005343-01	NM_153335
	LYN	M-003153-03	NM_002350
	MAGI-3	M-009453-01	NM_020965

	MAK	M-004813-01	NM_005906
	MALT1	M-005936-01	NM_006785
	MAP2K1	M-003571-01	NM_002755
	MAP2K1IP1	M-003572-02	NM_021970
	MAP2K2	M-003573-03	NM_030662
*	MAP2K3	M-003509-01	NM_002756
	MAP2K4	M-003574-02	NM_003010
	MAP2K5	M-003966-03	NM_002757
	MAP2K6	M-003967-00	NM_002758
	MAP2K7	M-004016-01	NM_145185
	MAP3K1	M-003575-01	XM_042066
	MAP3K10	M-003576-01	NM_002446
	MAP3K11	M-003577-02	NM_002419
	MAP3K12	M-003312-02	NM_006301
	MAP3K13	M-003579-01	NM_004721
	MAP3K14	M-003580-02	NM_003954
	MAP3K2	M-003582-01	NM_006609
	MAP3K3	M-003301-02	NM_002401
	MAP3K4	M-003789-02	NM_005922
	MAP3K5	M-003584-02	NM_005923
	MAP3K6	M-003969-00	NM_004672
	MAP3K7	M-003790-04	NM_003188
	MAP3K8	M-003511-00	NM_005204
	MAP3K9	M-003585-01	XM_027237
*	MAP4K1	M-003586-01	NM_007181
	MAP4K2	M-003587-01	NM_004579
	MAP4K3	M-003588-01	NM_003618
	MAP4K4	M-003971-02	NM_004834
	MAP4K5	M-003589-01	NM_006575
	MAPK1	M-003555-02	NM_002745
	MAPK10	M-004324-00	NM_002753
	MAPK11	M-003972-00	NM_002751
	MAPK12	M-003590-00	NM_002969
	MAPK13	M-003591-02	NM_002754
	MAPK14	M-003512-03	NM_001315
	MAPK3	M-003592-02	NM_002746
	MAPK4	M-003593-00	NM_002747
	MAPK6	M-003594-01	NM_002748
	MAPK7	M-003513-02	NM_002749
	MAPK8	M-003514-01	NM_002750
	MAPK8IP1	M-003595-00	NM_005456
	MAPK8IP2	M-012462-00	NM_012324
	MAPK8IP3	M-003596-01	NM_015133
	MAPK9	M-003505-02	NM_002752
	MAPKAPK2	M-003516-01	NM_004759
	MAPKAPK3	M-005014-00	NM_004635
	MAPKAPK5	M-005015-00	NM_003668

	MARK1	M-004259-02	NM_018650
	MARK2	M-004260-01	NM_004954
	MARK3	M-003517-03	NM_002376
	MARK4	M-005345-02	NM_031417
	MAST2	M-004633-00	NM_015112
	MAST3	M-004046-00	XM_038150
	MASTL	M-004020-03	NM_032844
	MATK	M-003154-03	NM_002378
	MBIP	M-021396-00	NM_016586
	MDM2		
	MELK	M-004029-01	NM_014791
	MERTK	M-003155-01	NM_006343
	MET	M-003156-02	NM_000245
	MGC16169	M-005346-00	NM_033115
	MGC20741	M-005945-01	NM_018561
	MGC26597	M-004783-00	NM_152700
	MGC42105	M-005016-01	NM_153361
	MGC45428	M-005017-01	NM_152619
	MGC4796	M-005348-00	NM_032017
	MGC5601	M-007684-01	NM_025247
	MGC5987	M-019407-00	NM_138476
	MGC75495	M-021702-01	XM_292160
	MGC8407	M-005349-01	NM_024046
	MIDORI	M-005350-01	NM_020778
	MINK	M-004861-02	NM_015716
	MKNK1	M-004879-01	NM_003684
	MKNK2	M-004908-01	NM_017572
	MOS	M-003859-02	NM_005372
	MPP1	M-010252-00	NM_002436
	MPP2	M-009729-00	NM_005374
	MPP3	M-010612-01	NM_001932
	MPZL1	M-015738-01	NM_003953
	MRC2	M-020064-00	NM_006039
	MST1R	M-003157-02	NM_002447
	MST4	M-003753-01	NM_016542
	MUSK	M-003158-01	NM_005592
	MVD	M-006748-00	NM_002461
	MVK	M-006749-00	NM_000431
*	MYLK	M-005351-04	NM_005965
	MYLK2	M-005352-02	NM_033118
	MYO3A	M-004862-00	NM_017433
	MYO3B	M-004863-00	NM_138995
	NAGK	M-006750-00	NM_017567
	NBEA	M-015419-00	NM_015678
*	NEK1	M-004864-00	XM_291107
	NEK11	M-004865-01	NM_024800
	NEK2	M-004090-03	NM_002497

NEK3	M-004867-01	NM_002498
NEK4	M-003519-01	NM_003157
NEK6	M-004166-01	NM_014397
NEK7	M-003795-02	NM_133494
NEK8	M-004866-00	NM_178170
NEK9	M-004869-01	NM_033116
NLK	M-004763-01	NM_016231
NME1	M-006821-01	NM_000269
NME2	M-005102-01	NM_002512
NME3	M-006753-00	NM_002513
NME4	M-006494-00	NM_005009
NME5	M-006754-00	NM_003551
NME6	M-006755-01	NM_005793
NME7	M-006756-02	NM_013330
NPR1	M-005354-00	NM_000906
NPR2	M-005355-01	NM_000907
NRBP	M-005356-01	NM_013392
NRG3	M-026286-00	XM_166086
NRK	M-024786-01	NM_198465
NTRK1	M-003159-01	NM_002529
NTRK2	M-003160-01	NM_006180
NTRK3	M-003161-01	NM_002530
NYD-SP25	M-007733-00	NM_033516
OPRD1	M-005683-00	NM_000911
OR4N4	M-032289-00	NM_001005241
OSR1	M-004870-01	NM_005109
OTUB2	M-010983-00	NM_023112
OTUD1	M-026487-00	XM_166659
P15RS	M-007734-01	NM_018170
P21		
P53		
PACE-1	M-005357-00	NM_020423
PACSIN1	M-007735-00	NM_020804
PAG	M-012956-01	NM_018440
PAK1	M-003521-03	NM_002576
PAK2	M-003597-02	NM_002577
PAK3	M-003614-00	NM_002578
PAK4	M-003615-02	NM_005884
PAK6	M-004338-02	NM_020168
PAK7	M-003973-02	NM_020341
PANK1	M-004057-02	NM_138316
PANK3	M-006758-00	NM_024594
PANK4	M-006759-00	NM_018216
PAPSS1	M-007736-01	NM_005443
PAPSS2	M-006760-01	NM_004670
PASK	M-005018-01	NM_015148
PCK1	M-006796-00	NM_002591

	PCK2	M-006797-01	NM_004563
	PCTK1	M-004313-00	NM_006201
	PCTK2	M-004835-01	NM_002595
	PCTK3	M-004836-02	NM_002596
	PDGFRA	M-003162-03	NM_006206
	PDGFRB	M-003163-02	NM_002609
	PDK1	M-005019-00	NM_002610
	PDK2	M-005020-00	NM_002611
	PDK3	M-005021-01	NM_005391
	PDK4	M-019425-00	NM_002612
	PDPK1	M-003017-01	NM_002613
	PDXK	M-005070-02	NM_003681
	PFKFB1	M-006761-00	NM_002625
	PFKFB2	M-006762-01	NM_006212
	PFKFB3	M-006763-00	NM_004566
	PFKFB4	M-006764-00	NM_004567
	PFKL	M-006822-00	NM_002626
	PFKM	M-006765-01	NM_000289
	PFKP	M-010253-01	NM_002627
	PFTK1	M-004837-01	NM_012395
	PGK1	M-006767-01	NM_000291
	PGK2	M-006768-01	NM_138733
	PHKA1	M-019682-00	NM_002637
	PHKA2	M-007669-00	NM_000292
	PHKG1	M-005023-01	NM_006213
	PHKG2	M-004881-00	NM_000294
	PI4K2B	M-006769-01	NM_018323
	PI4KII	M-006770-01	NM_018425
*	PIK3C2A	M-006771-00	NM_002645
	PIK3C2B	M-006772-01	NM_002646
	PIK3C2G	M-006773-00	NM_004570
	PIK3CA	M-003018-01	NM_006218
	PIK3CB	M-003019-02	NM_006219
	PIK3CG	M-005274-02	NM_002649
	PIK3R1	M-003020-02	NM_181504
	PIK3R2	M-003021-01	NM_005027
	PIK3R3	M-019546-00	NM_003629
	PIK3R4	M-005025-01	NM_014602
	PIK4CA	M-006776-03	NM_002650
	PIK4CB	M-006777-02	NM_002651
	PIM1	M-003923-00	NM_002648
	PIM2	M-005359-00	NM_006875
	PIM3	M-032287-00	NM_001001852
	PINK1	M-004030-01	NM_032409
	PIP5K1A	M-004780-02	NM_003557
	PIP5K2A	M-006778-00	NM_005028
	PIP5K2B	M-006779-02	NM_003559

PIP5K2C	M-004535-00	NM_024779
PIP5KL1	M-008770-00	NM_173492
PITPNM3	M-014699-00	NM_031220
PKIA	M-012321-00	NM_006823
PKIB	M-008224-01	NM_032471
PKLR	M-006780-00	NM_000298
PKM2	M-006781-01	NM_002654
PKMYT1	M-005026-02	NM_004203
PKN3	M-004647-00	NM_013355
PLK1	M-003290-01	NM_005030
PLK2	M-003325-03	NM_006622
PLK3	M-003257-02	NM_004073
PLK4	M-005036-01	NM_014264
PMVK	M-006782-00	NM_006556
PNCK	M-027176-00	NM_198452
PNKP	M-006783-02	NM_007254
PPP1R1B	M-012745-00	NM_032192
PPP2CA	M-003598-00	NM_002715
PPP2CB	M-003599-02	NM_004156
PPP4C	M-008486-01	NM_002720
PRKAA1	M-005027-01	NM_006251
PRKAA2	M-005361-01	NM_006252
PRKACA	M-004649-00	NM_002730
PRKACB	M-004650-00	NM_002731
PRKACG	M-004651-02	NM_002732
PRKAG1	M-009056-00	NM_002733
PRKAG3	M-009859-01	NM_017431
PRKAR1A	M-007670-01	NM_002734
PRKAR2A	M-007671-00	NM_004157
PRKAR2B	M-007673-00	NM_002736
PRKCA	M-003523-02	NM_002737
PRKCABP	M-020124-00	NM_012407
PRKCB1	M-003758-04	NM_002738
PRKCD	M-003524-01	NM_006254
PRKCE	M-004653-00	NM_005400
PRKCG	M-004654-01	NM_002739
PRKCH	M-004655-01	NM_006255
PRKCI	M-004656-01	NM_002740
PRKCL1	M-004175-02	NM_002741
PRKCL2	M-004612-02	NM_006256
PRKCM	M-005028-00	NM_002742
PRKCN	M-005029-01	NM_005813
PRKCQ	M-003525-01	NM_006257
PRKCSH	M-010618-00	NM_002743
PRKCZ	M-003526-02	NM_002744
PRKD2	M-004197-01	NM_016457
PRKDC	M-005030-01	NM_006904

PRKG1	M-004658-02	NM_006258
PRKG2	M-004659-00	NM_006259
PRKR	M-003527-00	NM_002759
PRKRA	M-006426-00	NM_003690
PRKWNK1	M-005362-00	NM_018979
PRKWNK2	M-005363-01	NM_006648
PRKWNK3	M-005364-02	NM_020922
PRKWNK4	M-005031-01	NM_032387
PRKX	M-004660-01	NM_005044
PRKY	M-004661-02	NM_002760
PRPF4B	M-004074-03	NM_003913
PRPS1	M-006784-00	NM_002764
PRPS1L1	M-006804-00	NM_175886
PRPS2	M-004877-01	NM_002765
PRPSAP1	M-006794-01	NM_002766
PRPSAP2	M-006795-01	NM_002767
PSKH1	M-005365-00	NM_006742
PSKH2	M-005366-00	NM_033126
PTK2	M-003164-02	NM_005607
PTK2B	M-003165-03	NM_004103
PTK6	M-003166-01	NM_005975
PTK7	M-003167-01	NM_002821
PTK9	M-003168-03	NM_002822
PTK9L	M-003169-01	NM_007284
PTPN5	M-003600-01	NM_032781
PTPRG	M-008069-00	NM_002841
PTPRJ	M-008476-01	NM_002843
PTPRQ	M-027185-01	AF169351
PTPRR	M-004017-01	NM_002849
PTPRT	M-008072-01	NM_007050
PXK	M-005367-00	NM_017771
PYCS	M-006785-00	NM_002860
RAC1	M-003560-02	NM_018890
RAF1	M-003601-00	NM_002880
RAGE	M-004838-01	NM_014226
RAPGEF3	M-007676-00	NM_006105
RAPGEF4	M-009511-00	NM_007023
RASGRF2	M-024516-01	NM_006909
RBKS	M-006786-00	NM_022128
RET	M-003170-01	NM_000323
RFK	M-007260-00	NM_018339
RFP	M-006552-00	NM_006510
RIOK1	M-005368-01	NM_031480
RIOK3	M-005040-01	NM_003831
RIPK1	M-004445-01	NM_003804
RIPK2	M-003602-00	NM_003821
RIPK3	M-003534-00	NM_006871

	RNASEL	M-005032-01	NM_021133
	ROCK1	M-003536-01	NM_005406
	ROCK2	M-004610-01	NM_004850
	ROR1	M-003171-01	NM_005012
	ROR2	M-003172-01	NM_004560
	ROS1	M-003173-01	NM_002944
	RP2	M-012350-01	NM_006915
	RPS6KA1	M-003025-03	NM_002953
	RPS6KA2	M-004663-01	NM_021135
	RPS6KA3	M-003026-01	NM_004586
	RPS6KA4	M-004664-00	NM_003942
	RPS6KA5	M-004665-01	NM_004755
	RPS6KA6	M-004670-00	NM_014496
	RPS6KB1	M-003616-02	NM_003161
	RPS6KB2	M-004671-00	NM_003952
	RPS6KC1	M-005371-01	NM_012424
	RPS6KL1	M-005372-00	NM_031464
	RYK	M-003174-02	NM_002958
	SAST	M-004672-01	NM_014975
	SBF1	M-021405-00	NM_002972
	SCAP1	M-011505-01	NM_003726
	SCYL1	M-005373-00	NM_020680
	SEPHS1	M-007737-00	NM_012247
	SEPHS2	M-007738-00	NM_012248
	SGK	M-003027-04	NM_005627
	SGK2	M-004673-01	NM_016276
	SGKL	M-004162-00	NM_013257
	SHC1	M-018841-00	NM_003029
	SIK2	M-004778-02	NM_015191
	SLK	M-003850-02	NM_014720
	SMAD7	M-020068-00	NM_005904
	SMAP-1	M-017653-00	NM_018671
*	SMG1	M-005033-00	NM_014006
	SNARK	M-005374-01	NM_030952
	SNF1LK	M-003959-04	NM_173354
	SNRK	M-004322-00	NM_017719
	SOCS1	M-011511-01	NM_003745
	SOCS5	M-017374-00	NM_014011
	SPA17	M-007677-01	NM_017425
	SPEC2	M-020826-00	NM_020240
	SPHK1	M-004172-02	NM_021972
	SPHK2	M-004831-00	NM_020126
	SQSTM1	M-010230-00	NM_003900
	SRC	M-003175-03	NM_005417
	SRMS	M-005376-00	NM_080823
	SRPK1	M-003982-02	NM_003137
	SRPK2	M-004839-01	NM_182691

	SSTK	M-005034-00	NM_032037
	STK10	M-004168-01	NM_005990
	STK11	M-005035-01	NM_000455
	STK16	M-004054-00	NM_003691
	STK17A	M-005377-00	NM_004760
	STK17B	M-004051-01	NM_004226
	STK19	M-005378-00	NM_004197
	STK22B	M-005379-01	NM_053006
	STK22C	M-004050-01	NM_052841
	STK22D	M-005038-02	NM_032028
	STK23	M-004840-02	NM_014370
	STK24	M-004872-02	NM_003576
	STK25	M-004873-00	NM_006374
	STK29	M-005381-02	NM_003957
	STK3	M-004874-01	NM_006281
	STK31	M-005382-00	NM_031414
	STK32A	M-004634-00	NM_145001
	STK32B	M-004618-00	NM_018401
	STK32C	M-004615-00	NM_173575
	STK33	M-005383-02	NM_030906
	STK35	M-005384-00	NM_080836
	STK36	M-005039-00	NM_015690
	STK38	M-004674-00	NM_007271
	STK38L	M-003313-02	NM_015000
	STK39	M-004875-01	NM_013233
	STK4	M-004157-01	NM_006282
*	STK6	M-003545-09	NM_003600
	STYK1	M-003113-01	NM_018423
	SYK	M-003176-03	NM_003177
	TAF1	M-005041-01	NM_004606
	TAF1L	M-005385-02	NM_153809
	TAO1	M-004171-02	NM_004783
	TBK1	M-003788-02	NM_013254
	TEC	M-003177-02	NM_003215
	TEK	M-003178-02	NM_000459
	TENS1	M-009997-00	NM_022748
	TESK1	M-005043-00	NM_006285
	TESK2	M-005044-00	NM_007170
	TEX14	M-005386-01	NM_031272
	TGFBR1	M-003929-01	NM_004612
	TGFBR2	M-003930-01	NM_003242
	THNSL1	M-007253-00	NM_024838
	TIE	M-003179-01	NM_005424
	TJP2	M-009932-01	NM_004817
	TK1	M-006787-00	NM_003258
	TK2	M-006788-02	NM_004614
	TLK1	M-004174-00	NM_012290

TLK2	M-005389-02	NM_006852
TLR1	M-008086-00	NM_003263
TLR3	M-007745-00	NM_003265
TLR4	M-008088-00	NM_003266
TLR6	M-005156-01	NM_006068
TNFRSF10A	M-008090-01	NM_003844
TNIK	M-004542-02	XM_039796
TNK1	M-003180-02	NM_003985
TNNI3K	M-005013-00	NM_015978
TOPK	M-005390-00	NM_018492
TP53RK	M-003108-01	NM_033550
TPK1	M-006789-00	NM_022445
TRAD	M-005045-00	NM_007064
TRIB1	M-003633-00	NM_025195
TRIB2	M-005391-01	NM_021643
TRIB3	M-003754-01	NM_021158
TRIM	M-020821-00	NM_016388
TRIO	M-005047-00	NM_007118
TRPM6	M-005048-01	NM_017662
TRPM7	M-005393-02	NM_017672
TSKS	M-013077-01	NM_021733
TTBK1	M-004680-01	XM_166453
TTBK2	M-004682-00	NM_173500
TTK	M-004105-00	NM_003318
TTN	M-005395-00	NM_003319
TXK	M-003181-01	NM_003328
TXNDC3	M-006791-00	NM_016616
TYK2	M-003182-01	NM_003331
TYRO3	M-003183-01	NM_006293
UCK1	M-004062-01	NM_031432
UGP2	M-007739-01	NM_006759
ULK1	M-005049-00	NM_003565
ULK2	M-005396-01	NM_014683
UMP-CMPK	M-004059-00	NM_016308
UMPK	M-005077-00	NM_012474
URKL1	M-006792-00	NM_017859
USP24	M-006073-01	XM_165973
USP32	M-006080-01	NM_032582
USP34	M-006082-00	XM_291018
USP39	M-006087-00	NM_006590
USP40	M-006088-00	NM_018218
USP41	M-031434-00	XM_036729
USP43	M-023019-00	XM_371015
USP45	M-010054-00	XM_371838
USP47	M-006093-00	NM_017944
USP48	M-006079-00	NM_032236
USP49	M-006094-00	NM_004275

USP50	M-031837-00	NM_203494
USP51	M-032247-00	NM_201286
USP53	M-027186-00	XM_052597
USP54	M-016853-00	NM_152586
VCIP135	M-019137-00	NM_025054
VRK1	M-004683-01	NM_003384
VRK2	M-004684-01	NM_006296
VRK3	M-005397-00	NM_016440
WEE1	M-005050-00	NM_003390
WIF1	M-012386-00	NM_007191
XYLB	M-006793-00	NM_005108
YES1	M-003184-02	NM_005433
YWHAH	M-010626-00	NM_003405
YWHAQ	M-012329-00	NM_006826
ZA20D1	M-008670-00	NM_020205
ZAK	M-005068-00	NM_133646
ZAP70	M-005398-01	NM_001079
ZRANB1	M-009270-00	NM_017580
CNTR siControl		
CNTR siTox		

Table S2. Normalised cellular senescence scores.

Gene	Pool	#1	#2	#3	#4	Sum[b]
1. AURKA	23.4	32.4	0.0	1.9	17.7	75.3
2. CDK1	12.5	9.5	7.3	2.4	4.8	36.5
3. CSNK1A1	1.5	4.4	1.8	8.4	2.2[a]	16.0
4. EPHA3	2.4	1.9	1.0	3.7	2.8	11.8
5. KSR2	7.4	5	3.1	1.1	3.1	19.7
6. LATS1	1.7	2.9	0.9	6.2	0.1	11.8
7. MAP2K3	2.1	1.5	1.3	3.7	6.8	15.4
8. MAP4K1	10.1	2.8	9.3	4.6[a]	10.3	32.5
9. MYLK	3.8	1.7	5.6	5.6	2.0	18.7
10. NEK1	1.7	5.4	0.6	4.1	1.5	13.2
11. PAK7[c]	1.5	0.9	0.0	0.7	2.1	5.2
12. PASK	0.5	3.8	6.0	3.6	4.3	18.2
13. PIK3C2A	1.9	6.2	6.6	2.3	19.5	36.5
14. PIP5K1A	0.2	7.6	2.4[a]	2.9[a]	11.6[a]	7.8
15. RPS6KA2	0.1	2.7	3.0	0.3	2.1	8.2
16. SMG1	11.3	3.8[a]	1.3	9.2	13.6	35.3
Pos. FBXO5	**5.9**	**2.0**	**2.7**	**1.0**	**5.9**	**17.5**
Neg. siCTRL	**0.7**	**0.7**	**0.7**	**0.7**	**0.7**	**3.5**

Cellular senescence scores per siRNA or siRNA pool were calculated as the sum of the staining intensities (in increasing bins of 10%) normalised against the total cell number per bin: ∑ [(normalised #cells * maximum bin intensity)]. Values lower than 1.4 (2-fold negative control value) and siRNAs conferring less than 50% knockdown efficiency were scored as negative (grey font). Genuine hits were assigned if both the pool AND two single siRNAs gave a positive score (black font). [a]siRNAs resulting in less than 50% knockdown of specific gene expression measured by RNA expression analysis (Fig S1B). [b]Sum of senescence scores excluding siRNAs conferring less than 50% knockdown. [c]No expression of Pak7 RNA is detected in hTERT-RPE1 cells.

Table S3. Normalised cellular senescence scores in p53 knockdown cells (doxycycline treatment).

Gene	Pool	#1	#2	#3	#4	Sum[b]
1. AURKA	14.2	2.5	0.1	0.4	5.5	22.6
2. CDK1	31.2	13.3	4.8	2.6	4.1	56.1
3. CSNK1A1	2.2	0.1	0.9	0.1	0.1[a]	3.3
4. EPHA3	5.7	3.3	1.6	7.9	2.0	20.5
5. KSR2	5.4	2.6	0.9	0.6	0.1	9.5
6. LATS1	1.3	1.0	2.2	4.8	0.7	9.9
7. MAP2K3	0.9	6.7	1.8	0.7	1.4	11.4
8. MAP4K1	8.6	1.3	8.7	5.9[a]	9.6	28.2
9. MYLK	1.1	2.4	3.8	11.9	0.2	19.3
10. NEK1	5.0	8.9	1.1	0.4	0.5	15.9
11. PIK3C2A	1.2	9.5	2.7	5.1	10.9	29.4
12. SMG1	1.6	6.1[a]	3.1	4.9	9.3	19.0
Pos. FBXO5	**8.9**	**0.0**	**2.9**	**1.3**	**1.3**	**14.4**
Neg. siCTRL	**0.3**	**0.3**	**0.3**	**0.3**	**0.3**	**1.3**

Cellular senescence scores per siRNA or siRNA pool were calculated as the sum of the staining intensities (in increasing bins of 10%) normalised against the total cell number per bin: ∑ [(normalised #cells * maximum bin intensity)]. Values lower than 0.6 (2-fold negative control value) and siRNAs conferring less than 50% knockdown efficiency were scored as negative (grey font). [a]siRNAs resulting in less than 50% knockdown of specific gene expression measured by RNA expression analysis (Fig S1B). [b]Sum of senescence scores excluding siRNAs conferring less than 50% knockdown.

II

© 2015. Published by The Company of Biologists Ltd | Disease Models & Mechanisms (2015) 8, 393-401 doi:10.1242/dmm.019257

RESEARCH ARTICLE

The putative tumor suppressor gene *EphA3* fails to demonstrate a crucial role in murine lung tumorigenesis or morphogenesis

Jenni Lahtela[1], Barun Pradhan[1], Katja Närhi[1], Annabrita Hemmes[1], Merja Särkioja[1], Panu E. Kovanen[2], Arthur Brown[3] and Emmy W. Verschuren[1,*]

ABSTRACT

Treatment of non-small cell lung cancer (NSCLC) is based on histological analysis and molecular profiling of targetable driver oncogenes. Therapeutic responses are further defined by the landscape of passenger mutations, or loss of tumor suppressor genes. We report here a thorough study to address the physiological role of the putative lung cancer tumor suppressor EPH receptor A3 (*EPHA3*), a gene that is frequently mutated in human lung adenocarcinomas. Our data shows that homozygous or heterozygous loss of *EphA3* does not alter the progression of murine adenocarcinomas that result from *Kras* mutation or loss of *Trp53*, and we detected negligible postnatal expression of *EphA3* in adult wild-type lungs. Yet, *EphA3* was expressed in the distal mesenchyme of developing mouse lungs, neighboring the epithelial expression of its *Efna1* ligand; this is consistent with the known roles of EPH receptors in embryonic development. However, the partial loss of *EphA3* leads only to subtle changes in epithelial *Nkx2-1*, endothelial *Cd31* and mesenchymal *Fgf10* RNA expression levels, and no macroscopic phenotypic effects on lung epithelial branching, mesenchymal cell proliferation, or abundance and localization of CD31-positive endothelia. The lack of a discernible lung phenotype in *EphA3*-null mice might indicate lack of an overt role for EPHA3 in the murine lung, or imply functional redundancy between EPHA receptors. Our study shows how biological complexity can challenge *in vivo* functional validation of mutations identified in sequencing efforts, and provides an incentive for the design of knock-in or conditional models to assign the role of *EPHA3* mutation during lung tumorigenesis.

KEY WORDS: *EPHA3*, EPH receptor A3, GEMM, Adenocarcinoma, Lung morphogenesis

INTRODUCTION

Lung cancer is a leading cause of cancer-related deaths worldwide. More than 85% of all lung cancers are classified as non-small cell lung cancer (NSCLC), which is further sub-classified as adenocarcinoma (ADC; ~50%) and squamous cell carcinoma (SCC; ~40%) (Chen et al., 2014). In recent years, excellent progress in molecular profiling of NSCLC has identified stratified patient groups that benefit from targeted therapies (Oxnard et al., 2013). Specifically, erlotinib or gefitinib are prescribed to patients that carry mutations in epidermal growth factor receptor (*EGFR*), and crizotinib to carriers of anaplastic lymphoma kinase (*ALK*) gene rearrangements. However, despite an increase in progression-free survival, the overall survival benefit of such tyrosine kinase inhibitors remains marginal, and profound intra- and inter-tumor genetic heterogeneity confounds effective long-term responses (de Bruin et al., 2014).

Next-generation sequencing of lung cancer patient tumors has identified numerous putative new cancer drivers, including EPH (also defined as erythropoietin-producing hepatocellular) receptor A3 (*EPHA3*), which is mutated in 6–16% of lung ADC samples (Cancer Genome Atlas Research Network, 2014; Ding et al., 2008; Imielinski et al., 2012). The EPH receptors make up the largest family of receptor tyrosine kinases (RTKs) and, together with their ephrin ligands, they control a variety of biological processes. They are classified into two subclasses based on sequence homologies, namely EPHA and EPHB receptors and their ephrin-A and ephrin-B ligands. Interaction between the EPH receptors and their ligands at cell-cell contacts triggers signaling into both the receptor- and ligand-expressing cell. Such bidirectional signaling induces changes in the actin cytoskeleton, cell-substrate adhesion, intercellular junctions and cell shape, impinging on cell movement and tissue patterning (Pasquale, 2010). Context-dependent cellular responses are finely tuned by the abundance and type of receptor-ligand pairs expressed in neighboring cells, leading to specialized cell functions known to control synaptic plasticity, insulin secretion, epithelial homeostasis and inflammatory immune responses (Gucciardo et al., 2014; Pasquale, 2010).

The expression pattern of *EphA3* in mammalian tissues suggests that there is a role for EPHA3 in neuronal development and formation of mesoderm-derived tissues (Kilpatrick et al., 1996; Kudo et al., 2005; Yue et al., 1999). However, in contrast to predictions made based on its expression in the developing medial motor column, constitutive loss of murine *EphA3* does not lead to abnormal motor axon topography (Vaidya et al., 2003). Instead, 75% of the null mice die at birth owing to cardiac abnormalities caused by defective endothelial-to-mesenchymal transition, a specific form of mesenchymal conversion that generates progenitors of the atrioventricular valves (Stephen et al., 2007).

With respect to its putative role in tumorigenesis, previous studies have indicated that EPHA3 can signal both in a kinase-dependent and kinase-independent manner, inducing both tumor-promoting and tumor-suppressing effects (Boyd et al., 2014). For example, in glioblastoma multiforme, EPHA3 is highly expressed in undifferentiated mesenchymal cells where it has been shown to confer a kinase-independent oncogenic role through regulating mitogen-activated protein kinase (MAPK) signaling (Day et al., 2013). A tumor-suppressive role of EPHA3, in particular for lung cancer, is supported by the reduction in receptor activity conferred by the point mutations found in cancers, and ligand- and EPHA3-

[1]Institute for Molecular Medicine Finland (FIMM), University of Helsinki, Helsinki FI-00014, Finland. [2]Department of Pathology, HUSLAB and Haartman Institute, Helsinki University Central Hospital and University of Helsinki FI-00014, Finland. [3]Spinal Cord Injury Team, Robarts Research Institute, University of Western Ontario, London, ON N6A 5K8, Canada.

*Author for correspondence (emmy.verschuren@helsinki.fi)

Received 19 November 2014; Accepted 12 February 2015

TRANSLATIONAL IMPACT

Clinical issue

Lung cancer is the leading cause of cancer-related deaths worldwide. Molecular profiling to identify targetable driver mutations is increasingly being applied in the clinic, and can stratify patient groups. However, pronounced patient- and tumor-specific lung tumor heterogeneity confounds long-term or predictable clinical responses. Hence, validation of *de novo* driver mutations using appropriate *in vivo* model systems is important. The EPH receptor A3 (*EPHA3*) tyrosine kinase is among the most frequently mutated cancer genes in human lung adenocarcinomas. However, we still lack mouse genetic studies to unequivocally validate its previously assigned putative tumor suppressor function in human lung adenocarcinomas.

Results

Here, the authors test the applicability of *EphA3*-null mice to address the functional importance of EPHA3 in mutant Kras- or p53-loss-driven mouse lung adenocarcinomas. The study shows that constitutive loss of *EphA3* does not alter mutant Kras-driven lung adenocarcinoma progression, nor the histopathology or latency of p53-loss-driven adenocarcinomas. Moreover, the study identifies EPHA3 as a receptor that is expressed in embryonic lung mesenchyme and describes subtle lung morphogenesis gene expression changes in *EphA3* heterozygous embryonic lungs. No gross phenotypic changes in morphogenesis-related functions are detected in *EphA3* heterozygous or null embryonic lungs.

Implications and future directions

This study highlights the importance of creating appropriate model systems to study the *in vivo* functional relevance of putative cancer drivers, such as EPHA3. Our studies utilizing *Epha3*-null mice fail to validate a putative tumor suppressor function for *EPHA3* in human lung cancer. Furthermore, the overlapping expression pattern of EPH receptors detected in the developing mouse embryonic lung might imply functional redundancy. Therefore this study provides an incentive to the design of sophisticated, possibly tissue-specific, knock-in or conditional mouse models using genome-editing tools such as the prokaryotic type II CRISPR/Cas-system to elucidate the role of EPHA3 mutations during lung tumorigenesis *in vivo*.

dependent apoptosis of tumor and stroma cells upon receptor agonist treatment, suggesting that wild-type EPHA3 has anti-tumorigenic properties (Lahtela et al., 2013; Lisabeth et al., 2012; Vail et al., 2014; Zhuang et al., 2012). Furthermore, the finding that senescence elicited by acute EPHA3 loss is rescued by loss of $p16^{INK4A}$ (encoded by *Cdkn2a*) or p53 (encoded by *Trp53*) suggests that EPHA3 mutation might promote tumorigenesis only in the absence of senescence-inducing pathways (Lahtela et al., 2013). Given the opposing outcomes of aberrant EPH-ephrin signaling, careful dissection of the tissue and cell-context-specific EPH receptor functions requires studies that utilize valid *in vivo* model systems.

Genetically engineered mouse models (GEMMs) are the most widely applied and functionally validated *in vivo* models of human lung cancer, in particular to validate gene cooperation concomitant with conditional expression of the oncogenic *Kras* gene (Jackson et al., 2001; Jackson et al., 2005; Ji et al., 2007; Schramek et al., 2011; Snyder et al., 2013). Importantly, murine clinical studies have shown that oncogenic signaling in *Kras*-driven GEMMs is crucially defined by the cooperating tumor suppressor, with loss of liver kinase B1 (*Lkb1*) conferring different therapeutic responses compared with loss of *Trp53* (Chen et al., 2012). Despite convincing data suggesting a tumor suppressor role for EPHA3 during lung tumor progression, thus far no studies have addressed its *in vivo* functional role. We therefore decided to utilize the *EphA3*-null mice to test the effect of constitutive loss of *EphA3* on lung ADC progression driven by mutant *Kras* (LSL-$Kras^{G12D/+}$) (Jackson et al., 2001) and loss of *Trp53* ($p53^{fl/fl}$) (Marino et al., 2000), hereafter referred to as *Kras* and *p53*. Our data shows that the constitutive loss of *EphA3* does not alter the progression of murine ADC in either of these models. Moreover, despite clear evidence for *EphA3* expression in the developing lung, similar to key regulators of morphogenesis known to regulate lung tumorigenesis (Clark et al., 2001; Snyder et al., 2013; Yin et al., 2013), an analysis of selected EphA family receptors shows that *EphA3* has a non-unique or minimal function during lung morphogenesis. Our study thus provides an incentive for rational design of novel GEMMs to unequivocally assign the role of *EPHA3* during lung tumorigenesis *in vivo*.

RESULTS

Constitutive loss of *EphA3* does not accelerate mutant *Kras*- or *p53*-loss-driven lung tumorigenesis

To test the hypothesis that EPHA3 acts as a lung tumor suppressor, we used a previously described constitutive *EphA3*-null mouse model (Stephen et al., 2007; Vaidya et al., 2003). *EphA3*-null mice did not show any marks of reduced survival during a 1-year follow-up period, indicating that mere *EphA3* loss does not drive tumorigenesis. We therefore assessed whether *EphA3* loss could accelerate tumorigenesis induced by conditional alleles known to initiate lung ADC, following a classic multi-allele paradigm. These 'first hit' conditional models comprised mutant *Kras* (Jackson et al., 2001) and loss of *p53* (Marino et al., 2000), which are also common drivers of human disease found in at 17% and 35% of ADCs, respectively (COSMIC, 2014; http://cancer.sanger.ac.uk/cancergenome/projects/cosmic/). In lung ADC, *EPHA3* mutations show a statistically significant tendency towards co-occurrence with mutations in *TP53* ($P<0.01$) and occasional, but not statistically significant, co-occurrence with *KRAS* mutations (supplementary material Fig. S1A). We established cohorts of 8-16 mice for each genetic combination (homozygous *p53* or heterozygous *Kras* with wild-type *EphA3*, or homozygous or heterozygous null *EphA3*). Lung-specific deletion of conditional alleles was achieved through intranasal inhalation of adenoviral Cre recombinase (CMV-AdCre), affording transduction of bronchiolar and alveolar progenitor cells, to initiate carcinoma progression. The infection efficacy was confirmed with a dual fluorescence *mT/mG* Cre-reporter strain that monitors *in vivo* integration efficiency through activating a Cre-dependent switch from membrane-tagged Tomato to GFP (supplementary material Fig. S1B) (Muzumdar et al., 2007). Tumor burden analysis at 19 weeks after CMV-AdCre infection showed that constitutive loss of *EphA3* did not alter mutant *Kras*-driven lung ADC progression (Fig. 1A,B; supplementary material Fig. S1C). Similar to previous findings in murine *Kras* lung cancer studies (Jackson et al., 2001), all *EphA3* genotype cohorts displayed distinct types of progressive lesions, including epithelial hyperplasia, adenomas and ADCs. In addition, we detected previously described profound inflammatory responses as infiltrations of macrophages and neutrophils (supplementary material Fig. S1C) (Ji et al., 2006). Furthermore, analysis of histopathology and NKX2-1 and tumor protein 63 (p63) biomarker expression to respectively depict ADC and SCC tissue, showed that constitutive absence of *EphA3* did not alter the tumor histology (Fig. 1C). We further found that the loss of *EphA3* did not alter the latency of *p53*-loss-driven ADCs (Fig. 1D). Thus, the constitutive absence of EPHA3 expression does not accelerate mutant *Kras*- or *p53*-loss-driven lung tumorigenesis.

Mesenchymal expression of *EphA3* suggests that it has a functional role during lung development

As previous studies have indicated a role for *EphA3* in embryonic development, we undertook a detailed expression analysis of *EphA3*

Disease Models & Mechanisms (2015) doi:10.1242/dmm.019257

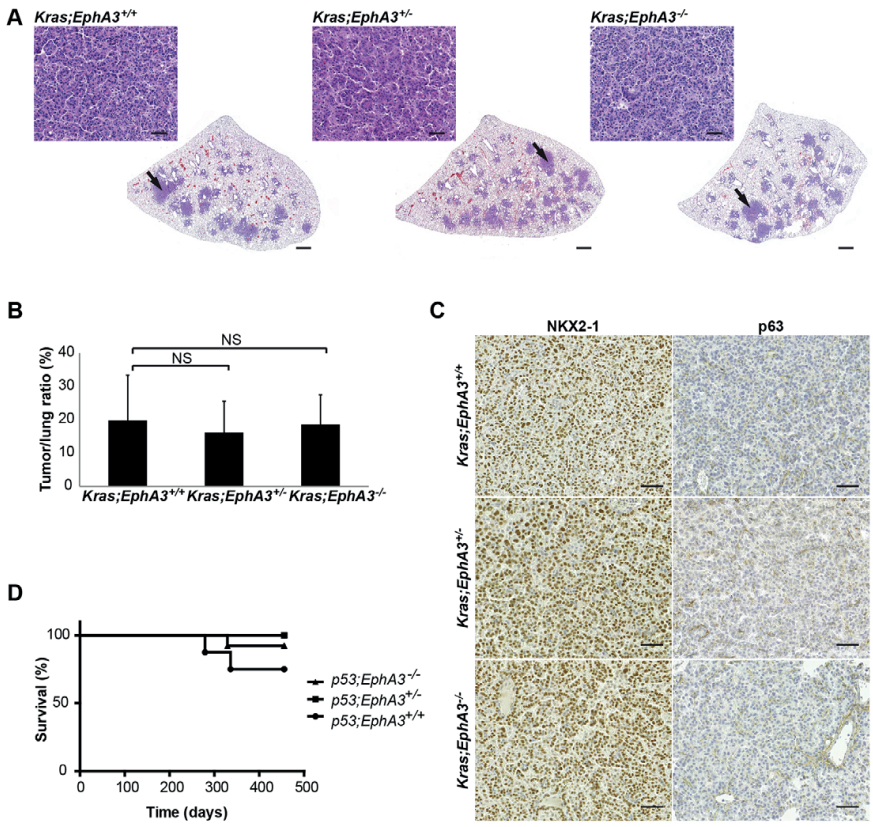

Fig. 1. Constitutive loss of *EphA3* does not alter mutant *Kras*-driven or *p53* loss-induced lung ADCs. (A) Representative sections (stained with H&E) depicting the tumor burden in *Kras;EphA3*$^{+/+}$, *Kras;EphA3*$^{+/-}$ and *Kras;EphA3*$^{-/-}$ lungs 19 weeks post CMV-AdCre infection (3.3×10^7 PFUs) show no difference between the genotypes. Black arrows indicate the site of magnified images. (B) Average tumor-to-lung area at 19 weeks after CMV-AdCre infection of the *Kras;EphA3*$^{+/+}$, *Kras;EphA3*$^{+/-}$ and *Kras;EphA3*$^{-/-}$ lungs. Two separate lung regions were used for tumor burden analysis. n=9 for *Kras;EphA3*$^{+/+}$, n=16 for *Kras;EphA3*$^{+/-}$ and n=8 for *Kras;EphA3*$^{-/-}$. Results are mean±s.d. (C) Immunohistochemical analysis of the ADC marker NKX2-1 and squamous cell carcinoma marker p63 in *Kras;EphA3*$^{+/+}$, *Kras;EphA3*$^{+/-}$ and *Kras;EphA3*$^{-/-}$ tumors, indicating positive nuclear staining for NKX2-1 and negative for p63. (D) Survival curves of n=7 for *p53;EphA3*$^{+/+}$, n=11 for *p53;EphA3*$^{+/-}$ and n=13 for *p53;EphA3*$^{-/-}$ mice treated with CMV-AdCre (3.3×10^8 pfu). Mice were monitored for 15 months, during which one out of seven *p53;EphA3*$^{+/+}$ and two out of 13 *p53;EphA3*$^{-/-}$ mice died due to CMV-AdCre-induced ADC formation. NS, P>0.05 (Student's t-test). Scale bars: 1 mm for whole lung lobes; 50 µm for magnified images.

in the developing mouse lung. Both RNA *in situ* hybridization (Fig. 2A) and immunohistochemical staining (Fig. 2B) demonstrated expression of *EphA3* in the distal mesenchyme of the embryonic lung. The specificity of the EPHA3 antibody was confirmed by absence of detectable immunohistochemical staining in *EphA3*-null embryos (Fig. 2A,B), as well as a decreased signal in hTERT-RPE1 cells treated with *EPHA3* small interfering RNA (siRNA) (supplementary material Fig. S1D). Expression of EPHA3 in the developing lung was detected during embryonic ages E11.5 to E15.5 (Fig. 2B,C), which falls into the pseudoglandular (E9.5-E16.5) stage of murine lung development. During this stage, the newly generated primary lung buds develop into a complex branched tree-like structure ending in thousands of epithelial terminal tubules, accompanied by continued mesenchymal growth around the growing epithelia (Morrisey and Hogan, 2010). Based on this mesenchymal expression in the developing mouse lungs we hypothesized that EPHA3 might function during the pseudoglandular stage of lung development.

Expression of multiple EPH receptors in the developing mouse lung suggests involvement in lung morphogenesis

We next asked how mRNA expression of *EphA3* during murine lung morphogenesis might correlate with or impact on mRNA expression of other EphA receptors in epithelial and mesenchymal cells at E11.5, E13.5 and E15.5 of lung development (Fig. 3A). At E11.5 we performed quantitative PCR (q-PCR) expression analysis on both proximal and distal epithelium and mesenchyme. At E13.5 and E15.5, the analysis was restricted to the distal regions, approximating the terminal epithelial buds and their surrounding mesenchyme. We found that among the studied EphA receptors, only expression of *EphA3* was restricted to the developing lung mesenchyme, and closely overlapped with expression of known mesenchymal *Fgf10* and endothelial *Cd31* (also known as *Pecam1*) genes (Fig. 3B; supplementary material Fig. S2A). *EphA7* expression was detected both in the mesenchyme and epithelia, and was the only other EphA receptor co-expressed with *EphA3* in the mesenchyme (Fig. 3B). Importantly, we did not detect any

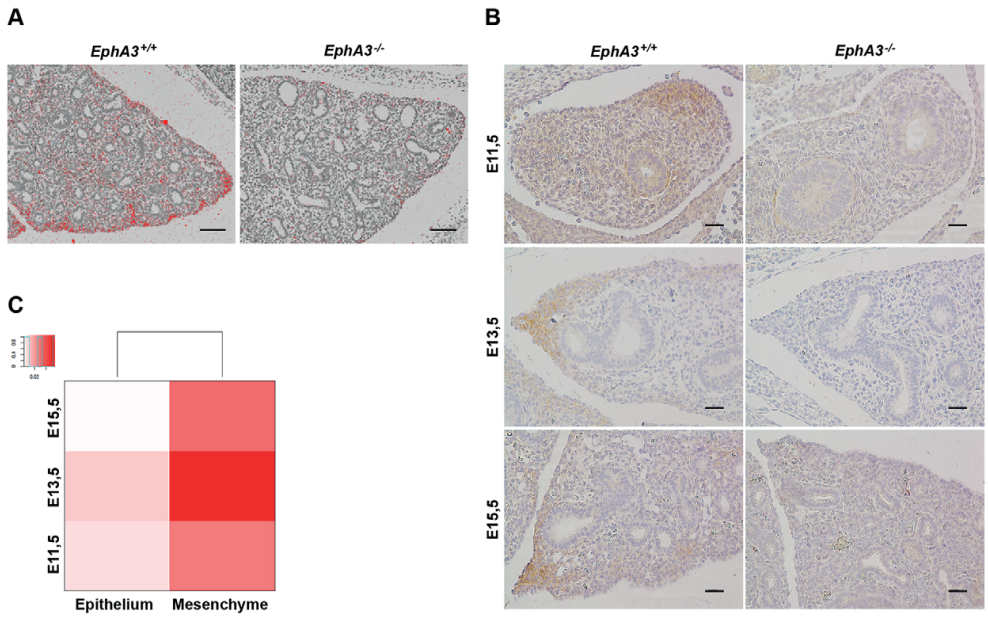

Fig. 2. Mesenchymal expression of *EphA3* during lung development. (A) *In situ* hybridization analysis of *EphA3* expression in embryonic mouse lungs at E14.5, showing its distal mesenchymal expression. (B) Immunohistochemical analysis of EPHA3 protein in embryonic mouse lungs at E11.5, E13.5 and E15.5 confirms the distal mesenchymal expression. (C) Quantitative PCR analysis of epithelial and mesenchymal mRNA expression of *EphA3* at E11.5, E13.5 and E15.5 indicating strongest expression at E13.5. The inset shows the distribution of the samples within the observed expression values. Scale bars: 100 µm.

compensatory changes in *EphA7* expression levels in the heterozygous or homozygous *EphA3*-null embryonic lungs (supplementary material Fig. S2B). *EphA2* and *EphA4* were found to be expressed mainly in epithelial cells, whereas expression of *EphA1* and *EphA5* was absent in both tissue compartments (Fig. 3B). These results correlate with *in situ* hybridization data described by the Allen Institute for Brain Science, with the exception of *EphA1*, for which moderate expression was detected in murine lung epithelia (Allen Institute for Brain Science, 2013). We further confirmed the epithelial expression of the known ligand of EPHA3, ephrin-A1 (encoded by *Efna1*), at E11.5, E13.3 and E15.5 (Fig. 3B; supplementary material Fig. S2C). Finally, postnatal murine lung expression analysis revealed very low *EphA3* and *EphA7* expression levels when compared to that of the embryonic mesenchyme (E13.5), whereas *EphA2* and *EphA4* expression were higher in the adult tissue (supplementary material Fig. S3A). Taken together, our data identifies *EphA3* as a mesenchymal EPH receptor and suggests that its ligand ephrin-A1 is expressed in the adjacent branching epithelia. Furthermore, the low expression of *EphA3* in adult tissue suggests that EPHA3 is absent or has a minimal role in postnatal lung homeostasis.

EphA3 heterozygosity is associated with altered expression of branching morphogenesis and vasculogenesis genes

Next, we investigated whether constitutive loss of *EphA3* affected the mRNA expression of known lung morphogenesis genes. A targeted q-PCR analysis of known regulators of lung morphogenesis identified a small but significant increase in the expression of *Nkx2-1* in heterozygous *EphA3* embryonic epithelium at E13.5 when compared with wild-type tissue (Fig. 3C). Furthermore, similar expression increases were detected in endothelial *Cd31* and mesenchymal *Fgf10* (Fig. 3C). In contrast, analysis at E15.5 failed to show statistically significant expression differences for these three genes (supplementary material Fig. S3B) suggesting that any role for *EphA3* during pseudoglandular lung development is transitory. Taken together, the partial loss of *EphA3* appears to induce subtle and transitory alterations in epithelial *Nkx2-1*, endothelial *Cd31* and mesenchymal *Fgf10* mRNA expression, suggesting that EPHA3 function might modulate lung morphogenesis.

Constitutive loss of *EphA3* does not overtly affect murine lung morphogenesis

We next asked whether the constitutive loss of *EphA3* was directly associated with altered lung branching morphogenesis. We first performed a quantitative analysis of lung branch end-points at E13.5 by E-cadherin whole-mount immunohistochemistry staining and optical projection tomography (OPT) to visualize branching epithelia. The number of terminal branches was found to be identical in *EphA3* heterozygous (average 113) and null embryonic lungs (average 110) when compared to age-matched littermate controls (average 108) (Fig. 4A,B). Additional qualitative analysis using E-cadherin-stained E11.5 and E15.5 whole-mount lungs further confirmed that EPHA3 does not overtly affect lung branching morphogenesis (supplementary material Fig. S3C). Next, we assessed whether loss of *EphA3* was associated with an alteration in distal mesenchymal cell proliferation. Analysis of *in vivo* BrdU incorporation showed that there was no statistically significant increase in the percentage of mesenchymal S phase cells in *EphA3* heterozygous (36%) or *EphA3*-null (26%) lungs at E13.5 when compared to littermate controls (26%) (Fig. 4C). Finally, we studied whether the pulmonary vasculature formation was altered by loss of *EphA3* by analyzing CD31 expression at E13.5. In both *EphA3*-null

Disease Models & Mechanisms (2015) doi:10.1242/dmm.019257

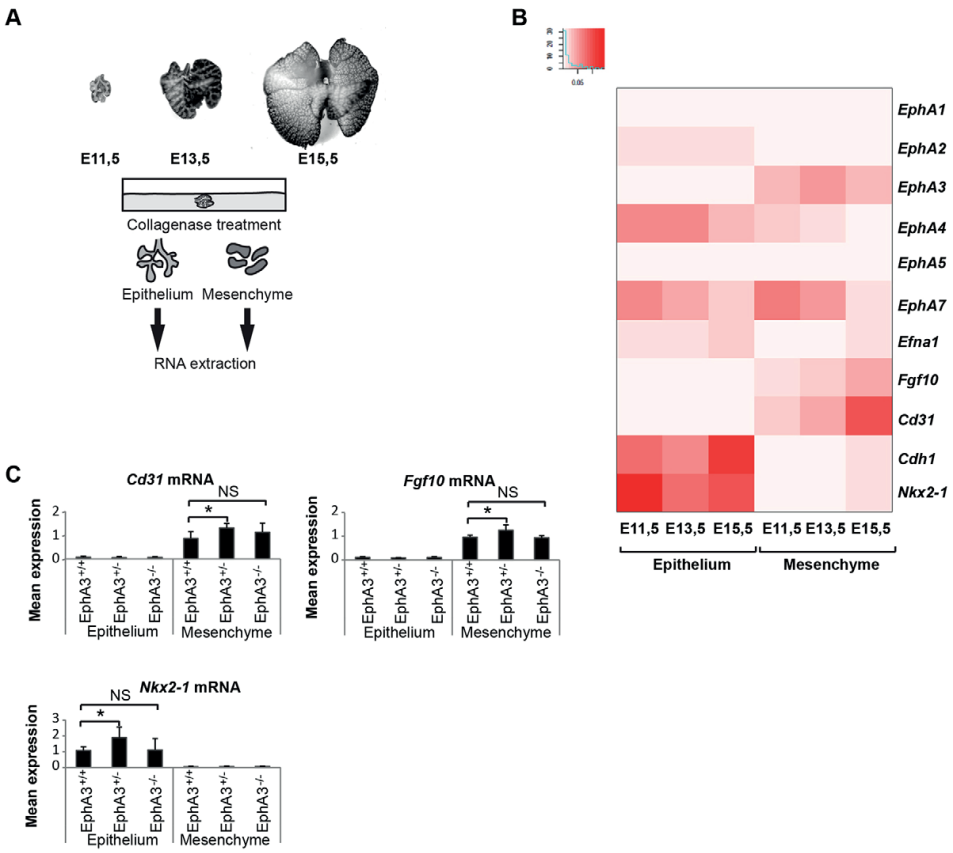

Fig. 3. Embryonic lung gene expression analysis of selected EphA family and morphogenesis genes. (A) Schematic workflow describing the mRNA expression analysis of E11.5, E13.5 and E15.5 embryonic lung epithelium and mesenchyme. (B) Average mRNA expression levels of selected EphA family receptors and *Efna1* ligand. Expression of epithelial *Nkx2-1* and *Cdh1*, mesenchymal *Fgf10* and endothelial *Cd31*, correlates with their known expression patterns. E11.5, n=2, E13.5 and E15.5, n=4. The inset shows the distribution of the samples within the observed expression values. (C) Comparative mRNA expression analysis of *EphA3*$^{+/+}$, *EphA3*$^{+/-}$ and *EphA3*$^{-/-}$ dissected embryos at E13.5 shows a minor but statistically significant difference between *EphA3*$^{+/+}$and *EphA3*$^{+/-}$ in epithelial *Nkx2-1* and mesenchymal *Fgf10* and *Cd31* expression. Results are mean±s.d. (n=4).*P<0.05 (Student's t-test).

and heterozygous lungs, the number of CD31-positive endothelial cells at E13.5 was identical to that of the controls (Fig. 4D). Taken together, the data presented here show that constitutive loss of *EphA3* does not overtly alter murine lung morphogenesis.

DISCUSSION

The functional validation of *de novo* mutations identified in lung cancer sequencing efforts is a prerequisite for the development of novel targeted therapies. *EPHA3* is among the most frequently mutated RTKs in human lung ADCs, and has been assigned a candidate tumor suppressor role based on its mutation spectrum and findings from *in vitro* and *in vivo* studies (Lahtela et al., 2013; Lisabeth et al., 2012; Vail et al., 2014; Zhuang et al., 2012). However, the actual role of EPHA3 during lung tumor progression has not been investigated nor validated using GEMMs. Our previous findings linked loss of EPHA3 to p53 activation (Lahtela et al., 2013), and *EPHA3* and *TP53* point mutations display statistically significant co-occurrence in lung ADC (supplementary material Fig. S1A). We hence asked whether the absence of *EphA3* enhanced the incidence of *p53*-loss-driven lung cancer progression. Additionally, we asked whether loss of *EphA3* accelerated lung ADC progression caused by the commonly mutated *Kras* oncogene. We here show that the constitutive absence of EPHA3 does not affect tumor progression and histopathology of both *p53*-loss- and mutant *Kras*-driven lung ADCs. Thus, *EphA3*-null mice fail to validate a putative tumor suppressor function for *EPHA3* in human lung cancer, perhaps owing to functional redundancy between murine EphA receptors expressed in adult lungs. Interestingly, sequencing of murine small cell lung cancer (SCLC) tumors initiated by loss of *p53* and retinoblastoma 1 (Rb1) revealed that there were recurrent somatically acquired *EphA5* and *EphA7* mutations (McFadden et al., 2014). This means that there is a strong case for further lung tumorigenesis studies to study the role of EphA receptor biology in GEMMs, and in particular the physiological role of *EphA5* and *EphA7*.

Re-activation of EPH-receptor–ephrin pathways, generally known to contribute to cell sorting and tissue patterning in embryonic development, has been causally linked with tumorigenesis

Disease Models & Mechanisms (2015) doi:10.1242/dmm.019257

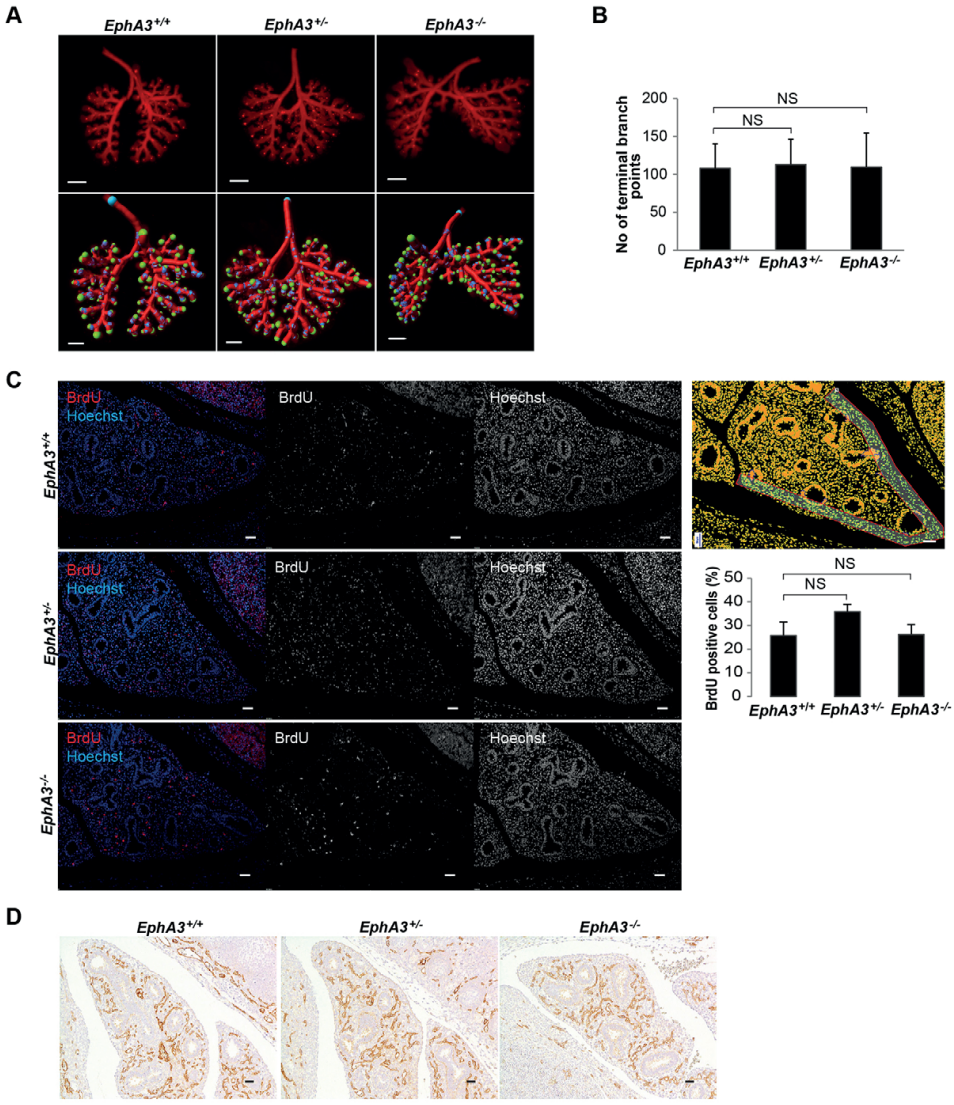

Fig. 4. Constitutive loss of *EphA3* does not alter morphogenesis of murine lungs. (A) Representative E-cadherin whole-mount images of *EphA3*$^{+/+}$, *EphA3*$^{+/-}$ and *EphA3*$^{-/-}$ embryonic lungs at E13.5 and corresponding images from branch end-point analyses, indicating end points in green. (B) Mean±s.d. of the branch end-point number from *EphA3*$^{+/+}$, *EphA3*$^{+/-}$ and *EphA3*$^{-/-}$ lungs at E13.5 shows no difference between *EphA3*$^{+/-}$ and *EphA3*$^{-/-}$ embryonic lungs when compared to *EphA3*$^{+/+}$ lungs; *n*=6 in all three genotypes. (C) Representative images from BrdU and nuclear Hoechst immunohistochemical staining in *EphA3*$^{+/+}$, *EphA3*$^{+/-}$ and *EphA3*$^{-/-}$ embryonic lungs at E13.5. Segmentation of representative images was performed to calculate distal-mesenchyme-specific BrdU proliferation analysis. Mean±s.d. values of the amount of BrdU-positive cells relative to the total number of Hoechst-stained nuclei shows no difference between *EphA3*$^{+/+}$, *EphA3*$^{+/-}$ and *EphA3*$^{-/-}$ embryonic lungs at E13.5. *n*=3 for *EphA3*$^{+/+}$ and *EphA3*$^{-/-}$; *n*=1 for *EphA3*$^{+/-}$. Analysis was done on two separate regions of the embryonic lungs. NS, *P*<0.05 (Student's *t*-test). (D) Representative images of CD31-positive endothelial cells of *EphA3*$^{+/+}$, *EphA3*$^{+/-}$ and *EphA3*$^{-/-}$ embryonic lungs at E13.5. Scale bars: 300 µm in E-cadherin whole-mount images; 200 µm in the branch end-point images; and 100 µm in BrdU images.

(Nievergall et al., 2012). Moreover, expression of key regulators of embryonic lung morphogenesis, *Fgf9* and *Fgf10* (Colvin et al., 2001; Min et al., 1998; White et al., 2006), has been shown to trigger ADC and adenoma progression, respectively (Clark et al., 2001; Yin et al., 2013). Thus far, of all EphA receptors and ligands, only a role of the ephrin-B2 ligand has been described during lung development. Specifically, ephrin-B2 has been shown to regulate alveolar epithelial and endothelial viability and vascular growth in hyperoxic rats (Vadivel et al., 2012), as well as pulmonary compliance in mice (Bennett et al., 2013). Our current data shows that *EphA3* is expressed specifically in the mesenchymal distal lung tips during the pseudoglandular stage of branching morphogenesis,

albeit at low levels. However, whereas for example the removal of *Fgf10* results in dramatic defects in lung organogenesis (Min et al., 1998), partial loss of *EphA3* appears to induce only subtle increases in epithelial *Nkx2-1*, endothelial *Cd31* and mesenchymal *Fgf10* mRNA expression levels. Furthermore, no macroscopic phenotypic effect on lung epithelial branching, mesenchymal cell proliferation, or abundance and localization of CD31-positive endothelia was measured. This lack of a discernible phenotype might indicate: (1) lack of an overt, or a different, role for EPHA3 in the murine lung; (2) functional redundancy between lung-expressed EphA receptors; or (3) a partial penetrance of the *EphA3*-null genotype.

Of the selected EphA receptors, we found that only *EphA7* was co-expressed with *EphA3* in the lung mesenchyme. Interestingly, a recent study has suggested that there is functional compensation of *EphA3* loss by *EphA7* co-expression during palate development, as compound homozygous mutation of *EphA3* and *EphA4* failed to cause defective midfacial development (Agrawal et al., 2014). Furthermore, a truncated form of EPHA7 has been reported to act as a tumor suppressor in follicular lymphoma (Oricchio et al., 2011), and it would thus be interesting to study its potential role in lung tumor suppression in conjunction with *EphA3* loss of function.

Taken together, we report that loss of *EphA3* does not lead to measurable effects on lung ADC progression, nor lung morphogenesis, in the applied constitutive null GEMM. Importantly, we cannot exclude the possibility that other EphA receptors co-expressed in the (developing) lung, most notably *EphA7*, can compensate for the decreased expression of *EphA3*. Our findings therefore provide an incentive to perform a rational design of tissue-specific knock-in or conditional mouse models to unequivocally assign the role of *EPHA3* mutation or loss of expression, possibly in the context of compound EPHA-ephrin network mutations, on lung tumorigenesis *in vivo*. In this respect, the ability to apply prokaryotic type II CRISPR/Cas genome editing tools to introduce somatic germline mutations in mice (Sanchez-Rivera et al., 2014; Yang et al., 2013) provides promise for future tumor modeling approaches.

MATERIALS AND METHODS

Mouse cohorts and tissue preparation

Animal studies were carried out in accordance with guidelines from the Finnish National Board of Animal Experimentation, and were approved by the Experimental Animal Committee of the University of Helsinki and the State Provincial Office of Southern Finland (License number ESAVI-2010-04855/Ym-23). *EphA3*-null mice lacking a genetic region encompassing the first exon of *EphA3* were previously described (Stephen et al., 2007; Vaidya et al., 2003). Mice carrying a conditional mutant allele of *Kras* (LSL-*Kras*$^{G12D/+}$) (Jackson et al., 2001) or a loss-of-function allele of *Trp53* (*p53*$^{fl/fl}$) (Marino et al., 2000) were purchased from The Jackson Laboratory. *EphA3*-null mice were bred with *Kras* and *p53* mice to generate the study cohorts, and were maintained on a mixed genetic background using littermates as controls. Multiple litters of the same age were used to provide sufficient numbers of each genotype. Lung tumorigenesis was initiated by infecting mice at 6-10 weeks of age with 3.3×10^7 (*Kras*) or with 3.3×10^8 (*p53*) plaque-forming units (PFUs) of recombinant adenovirus expressing the Cre recombinase (University of Turku, Finland), using intranasal instillation as described elsewhere (Jackson et al., 2001). Viruses were administered in a Biosafety Level 2+ room according to the guidelines of the Finnish Board for Gene Technology. Lungs from mice were fixed in 4% formaldehyde, and all lobes were embedded in paraffin.

Tumor burden analysis and survival curves

Lungs from *Kras;EphA3*$^{-/-}$, *Kras;EphA3*$^{+/-}$ and *Kras;EphA3*$^{+/+}$ mice at 19 weeks post infection were processed as described above and paraffin sections (4 µm) were cut from two distinct zones (middle and bottom) of each paraffin block, thus generating two sections each representing the whole lung surface area, which were stained with H&E. Whole slide scans of the H&E-stained lung sections were acquired with a Pannoramic 250 3DHISTECH (3DHISTECH Kft., Budapest, Hungary) digital slide scanner with a 20× objective. Whole slide images were assessed for tumor burden using the Tissue studio image analysis solution of the Definiens Developer XD 64 2.1 software (Definiens, Munich, Germany). The histopathology of the lesions and inflammatory infiltrations were diagnosed by an expert pathologist. Long-term follow up of infected *p53;EphA3*$^{-/-}$, *p53;EphA3*$^{+/-}$ and *p53;EphA3*$^{+/+}$ mice was performed until 15 months, and mice were killed when showing labored breathing. Sections (4 µm) were cut from two distinct zones (middle and bottom) of each paraffin block, stained with H&E and qualitatively analyzed for tumor appearance. Kaplan-Meier survival curves were generated using Prism (GraphPad Software, Inc., San Diego, CA).

Histology and immunohistochemistry

Immunohistochemistry was performed on paraffin-embedded sections (4 µm). Sections were dehydrated and antigenic epitopes were exposed by heating in 10-mM citrate buffer (pH 6.0) or by incubation in 0.05% trypsin at +37°C. Sections were incubated with the following antibodies: anti-NKX2-1 (Abcam, Cambridge, UK); anti-p63 (Abcam, Cambridge, UK); anti-EPHA3 (Invitrogen/Thermo Fisher Scientific Inc., Waltham, MA); anti-CD31 (Becton, Dickinson and Company, Franklin Lakes, NJ); anti-GFP (polyclonal rabbit serum 8 mg/ml, generated in house). Primary antibody staining was detected using Bright vision poly-horseradish peroxidase (HRP)-conjugated goat anti-rabbit IgG (ImmunoLogic, Duiven, The Netherlands), HRP-conjugated goat anti-rat IgG (Invitrogen/Thermo Fisher Scientific Inc., Waltham, MA) and 3,3′-diaminobenzidine (DAB) (Immunologic, Duiven, The Netherlands) or Alexa-Fluor-488-conjugated anti-rabbit IgG (Life Technologies/Thermo Fisher Scientific Inc., Waltham, MA). Sections were counterstained with Mayers hemalum solution (Millipore, Billerica, MA) or Hoechst 33342 dye (Invitrogen/Thermo Fisher Scientific Inc., Waltham, MA). Image acquisition was performed either using a Nikon 90i Eclipse microscope (Nikon Instruments Europe BV, The Netherlands) and DS-Fi2 5 MP camera, or a Pannoramic 250 3DHISTECH (3DHISTECH Kft., Budapest, Hungary) digital slide scanner with a 20× objective.

In situ hybridization

Radioactive *in situ* hybridization was performed on paraffin sections according to the standard protocols using probes labeled with ^{35}[S]-UTP. Dark-field images were inverted, linearly thresholded and combined with brightfield images in Adobe Photoshop CS6 (Adobe Systems Software, Dublin, Ireland). The mouse *EphA3* probe was an 817-bp fragment (nucleotides 658-1474) inserted into pGEM-3Zf- vector. The mouse *Efna1* probe was a 402-bp fragment (nucleotides 20-421) inserted into pGEM-3Zf- vector. The *Fgf10* probe was a 584-bp fragment (nucleotides 11-579) inserted into Bluescript KSII+ vector.

BrdU proliferation assay

A timed pregnant mouse was injected with 5-bromo-2′-deoxyuridine (BrdU) (Sigma, St Louis, MO) and killed 4 hours later to harvest embryos at embryonic age of 13.5. Embryos were fixed in 4% formaldehyde and embedded in paraffin. Sections (4 µm) were cut from two distinct zones of the embryonic lungs. BrdU-positive cells were detected using anti-BrdU antibody (Cell Signaling Technology, Danvers, MA) and counterstained with Hoechst 33342 using standard immunohistochemical methods. Image acquisition was performed with a Nikon 90i Eclipse microscope (Nikon Instruments Europe BV, The Netherlands) and DS-Fi2 5 MP camera. Image analysis was done using NIS-Elements AR 4.2 software (Nikon Instruments Europe BV, The Netherlands).

Preparation of embryonic lung tissue

Embryonic lung dissection and epithelial and mesenchymal cell separation was performed as previously described (del Moral and Warburton, 2010), with small modifications. Briefly, pregnant mice were killed to harvest embryos at E11.5, E13.5 and E15.5 by CO_2 administration. Collected embryos were dissected under a stereoscopic microscope in a glass Petri dish immersed in PBS. Isolated lungs were then transferred to 24-well plates

containing CO_2-independent medium (Gibco by Life Technologies/Thermo Fisher Scientific Inc., Waltham, MA). Epithelial and mesenchymal tissues were separated by treating with 10 mg/ml collagenase (collagenase from *Clostridium histolyticum*, Sigma) in CO_2-independent medium at 37°C for 20 minutes. Enzymatic degradation was stopped by adding CO_2-independent medium supplemented with 5 U/ml RNase-free DNase (RQ1 RNase free DNase, M6101, Promega, WI). Depending on the embryonic age, mesenchymal and epithelial cells from one to five embryos were used to reach high enough RNA yields.

Quantitative PCR analysis

Normal adult lung tissue was homogenized using a Precellys homogenization kit (Bertin Technologies, Montigny-le-Bretonneux, France). Total RNA was extracted using NucleoSpin RNA II kit (MACHEREY-NAGEL, Düren, Germany) and quantified using NanoDrop 1000 (Thermo Fisher Scientific Inc.). Complementary DNA (cDNA) was synthesized from the extracted RNA using a High-capacity cDNA reverse transcription kit (Applied Biosystems by Life Technologies/Thermo Fisher Scientific Inc.). The q-PCR amplification was performed using iQ™ SYBR® Green Supermix (Bio-Rad, Hercules, CA) or iQ™ Supermix (Bio-Rad) and CFX384 Touch™ Real-Time PCR Detection System C1000 Touch (Bio-Rad). The following TaqMan® probes were used to measure the *EPHA3* expression in hTERT-RPE1 cells: EPHA3 Hs00739096_m1 and RPL19 Hs02338565_gH (Applied Biosystems by Life Technologies/Thermo Fisher Scientific Inc.). q-PCR primers were designed to flank exon-exon boundaries and to give specific amplification. Following 3 minutes denaturation at 95°C, 40 cycles of 15 seconds at 95°C and 1 minute in 60°C were run. A melting curve ranging from 57°C to 95°C was included in every analysis to confirm the specific amplification. Primer details are listed in supplementary material Table S1. An exponential expression (ΔCq Expression) was obtained with formula ΔCq Expression=$2^{-\Delta Cq}$, where ΔCq=Cq (target) – Cq (reference). The average of the ΔCq expression values of the specific genotypes and time points were visualized with heatmaps generated using an R statistical programing language heatmap function from the Heatplus Bioconductor package. We used R version 2.15.3 freely available at http://www.r-project.org/.

Whole-mount immunohistochemistry and optical tomography scanning

Sample processing and whole-mount immunohistochemistry of dissected embryonic lungs at E11.5-E15.5 were performed as described previously (Alanentalo et al., 2007). Briefly, fixed lungs were dehydrated with methanol followed by rehydration and processing to immunohistochemical staining. Localization of anti-E-cadherin (Cell Signaling Technology) was detected either by fluorescently labeled secondary antibody conjugated to Alexa-Fluor-594-conjugated anti-rabbit IgG (Life Technologies/Thermo Fisher Scientific Inc.) or visualized by using the chromogenic DAB substrate (Immunologic, Duiven, The Netherlands) following the incubation with poly-HRP-conjugated anti-rabbit IgG antibody (Immunologic, Duiven, The Netherlands). Fluorescently labeled lungs were processed for OPT scanning as described previously (Alanentalo et al., 2007), using a Bioptonics OPT 3001M Scanner. Three-dimensional (3D) visualization and branch end-point analysis was performed with Imaris 3D and 4D data software, using the Filament analysis function (Bitplane AG, Switzerland). Chromogenically stained samples were imaged using a Leica MZFLIII stereomicroscope (Leica, Germany) and Colorview camera (Software imaging system, Olympus, Japan).

Cell culture and transfections

hTERT-RPE1 cells (Clontech, CA) were maintained in DMEM with F-12 (Sigma) containing 10% FBS, 2 mM L-glutamine, 0.348% sodium bicarbonate and penicillin-streptomycin (all Gibco by Life Technologies/Thermo Fisher Scientific Inc.), following the manufacturer's recommendations. For gene knockdown, hTERT-RPE1 cells were treated with 50 nM pooled siRNAs against *EPHA3* (GE Dharmacon, Denver, CO) or siCONTROL non-targeting siRNA #3 (SiCtrl; GE Dharmacon, Denver, CO) after transfection with Oligofectamine reagent (Invitrogen/Thermo Fisher Scientific Inc.) on 15-cm culture dishes. One fifth of the transfected cells was pelleted for RNA extraction and *EPHA3* mRNA quantification.

Acknowledgements

We thank Irma Thesleff (University of Helsinki, Finland) for providing *in situ* hybridization facilities, Hernán Espinoza (Stanford University School of Medicine and Howard Hughes Medical Institute, USA) for the *EphA3* probe sequence, and Merja Mäkinen and Raija Savolainen (University of Helsinki, Finland) for assistance with the *in situ* hybridization assays. We further thank Jussi Kenkkilä (Biomedicum Imaging Unit) and Sami Blom (University of Helsinki, Finland) for guidance and support in OPT and whole-tissue slide scanning, the Laboratory Animal Centre animal caretakers for expert support in mouse husbandry, and members of the Verschuren laboratory for valuable scientific discussions.

Competing interests

The authors declare no competing or financial interests.

Author contributions

All work was performed in the laboratory of E.W.V. The *EphA3*-null mice were generated in the laboratory of A.B. J.L., B.P., K.N. and E.W.V. conducted aspects of the experimental design. J.L., B.P., A.S. and M.S. performed experiments. J.L., B.P., P.K. and E.W.V. conducted data interpretation. J.L., B.P. and E.W.V. wrote the manuscript.

Funding

Research was supported by a European Union Framework Programme 7 (EU-FP7) Marie Curie Grant [grant number PIRG06-GA-2009–256485 to E.W.V.]; the Sigrid Juselius and Orion-Farmos Foundations (E.W.V.); and a University of Helsinki Graduate Program scholarship to J.L.

Supplementary material

Supplementary material available online at
http://dmm.biologists.org/lookup/suppl/doi:10.1242/dmm.019257/-/DC1

References

Agrawal, P., Wang, M., Kim, S., Lewis, A. E. and Bush, J. O. (2014). Embryonic expression of EphA receptor genes in mice supports their candidacy for involvement in cleft lip and palate. *Dev. Dyn.* **243**, 1470-1476.

Alanentalo, T., Asayesh, A., Morrison, H., Lorén, C. E., Holmberg, D., Sharpe, J. and Ahlgren, U. (2007). Tomographic molecular imaging and 3D quantification within adult mouse organs. *Nat. Methods* **4**, 31-33.

Allen Institute for Brain Science (2013). *Allen Developing Mouse Brain Atlas*.

Bennett, K. M., Afanador, M. D., Lal, C. V., Xu, H., Persad, E., Legan, S. K., Chenaux, G., Dellinger, M., Savani, R. C., Dravis, C. et al. (2013). Ephrin-B2 reverse signaling increases α5β1 integrin-mediated fibronectin deposition and reduces distal lung compliance. *Am. J. Respir. Cell Mol. Biol.* **49**, 680-687.

Boyd, A. W., Bartlett, P. F. and Lackmann, M. (2014). Therapeutic targeting of EPH receptors and their ligands. *Nat. Rev. Drug Discov.* **13**, 39-62.

Cancer Genome Atlas Research Network (2014). Comprehensive molecular profiling of lung adenocarcinoma. *Nature* **511**, 543-550.

Chen, Z., Cheng, K., Walton, Z., Wang, Y., Ebi, H., Shimamura, T., Liu, Y., Tupper, T., Ouyang, J., Li, J. et al. (2012). A murine lung cancer co-clinical trial identifies genetic modifiers of therapeutic response. *Nature* **483**, 613-617.

Chen, Z., Fillmore, C. M., Hammerman, P. S., Kim, C. F. and Wong, K. K. (2014). Non-small-cell lung cancers: a heterogeneous set of diseases. *Nat. Rev. Cancer* **14**, 535-546.

Clark, J. C., Tichelaar, J. W., Wert, S. E., Itoh, N., Perl, A. K., Stahlman, M. T. and Whitsett, J. A. (2001). FGF-10 disrupts lung morphogenesis and causes pulmonary adenomas in vivo. *Am. J. Physiol.* **280**, L705-L715.

Colvin, J. S., White, A. C., Pratt, S. J. and Ornitz, D. M. (2001). Lung hypoplasia and neonatal death in Fgf9-null mice identify this gene as an essential regulator of lung mesenchyme. *Development* **128**, 2095-2106.

Day, B. W., Stringer, B. W., Al-Ejeh, F., Ting, M. J., Wilson, J., Ensbey, K. S., Jamieson, P. R., Bruce, Z. C., Lim, Y. C., Offenhäuser, C. et al. (2013). EphA3 maintains tumorigenicity and is a therapeutic target in glioblastoma multiforme. *Cancer Cell* **23**, 238-248.

de Bruin, E. C., McGranahan, N., Mitter, R., Salm, M., Wedge, D. C., Yates, L., Jamal-Hanjani, M., Shafi, S., Murugaesu, N., Rowan, A. J. et al. (2014). Spatial and temporal diversity in genomic instability processes defines lung cancer evolution. *Science* **346**, 251-256.

del Moral, P. M. and Warburton, D. (2010). Explant culture of mouse embryonic whole lung, isolated epithelium, or mesenchyme under chemically defined conditions as a system to evaluate the molecular mechanism of branching morphogenesis and cellular differentiation. *Methods Mol. Biol.* **633**, 71-79.

Ding, L., Getz, G., Wheeler, D. A., Mardis, E. R., McLellan, M. D., Cibulskis, K., Sougnez, C., Greulich, H., Muzny, D. M., Morgan, M. B. et al. (2008). Somatic mutations affect key pathways in lung adenocarcinoma. *Nature* **455**, 1069-1075.

Gucciardo, E., Sugiyama, N. and Lehti, K. (2014). Eph- and ephrin-dependent mechanisms in tumor and stem cell dynamics. *Cell. Mol. Life Sci.* **71**, 3685-3710.

Imielinski, M., Berger, A. H., Hammerman, P. S., Hernandez, B., Pugh, T. J., Hodis, E., Cho, J., Suh, J., Capelletti, M., Sivachenko, A. et al. (2012). Mapping the hallmarks of lung adenocarcinoma with massively parallel sequencing. *Cell* **150**, 1107-1120.

Jackson, E. L., Willis, N., Mercer, K., Bronson, R. T., Crowley, D., Montoya, R., Jacks, T. and Tuveson, D. A. (2001). Analysis of lung tumor initiation and progression using conditional expression of oncogenic K-ras. *Genes Dev.* **15**, 3243-3248.

Jackson, E. L., Olive, K. P., Tuveson, D. A., Bronson, R., Crowley, D., Brown, M. and Jacks, T. (2005). The differential effects of mutant p53 alleles on advanced murine lung cancer. *Cancer Res.* **65**, 10280-10288.

Ji, H., Houghton, A. M., Mariani, T. J., Perera, S., Kim, C. B., Padera, R., Tonon, G., McNamara, K., Marconcini, L. A., Hezel, A. et al. (2006). K-ras activation generates an inflammatory response in lung tumors. *Oncogene* **25**, 2105-2112.

Ji, H., Ramsey, M. R., Hayes, D. N., Fan, C., McNamara, K., Kozlowski, P., Torrice, C., Wu, M. C., Shimamura, T., Perera, S. A. et al. (2007). LKB1 modulates lung cancer differentiation and metastasis. *Nature* **448**, 807-810.

Kilpatrick, T. J., Brown, A., Lai, C., Gassmann, M., Goulding, M. and Lemke, G. (1996). Expression of the Tyro4/Mek4/Cek4 gene specifically marks a subset of embryonic motor neurons and their muscle targets. *Mol. Cell. Neurosci.* **7**, 62-74.

Kudo, C., Ajioka, I., Hirata, Y. and Nakajima, K. (2005). Expression profiles of EphA3 at both the RNA and protein level in the developing mammalian forebrain. *J. Comp. Neurol.* **487**, 255-269.

Lahtela, J., Corson, L. B., Hemmes, A., Brauer, M. J., Koopal, S., Lee, J., Hunsaker, T. L., Jackson, P. K. and Verschuren, E. W. (2013). A high-content cellular senescence screen identifies candidate tumor suppressors, including EPHA3. *Cell Cycle* **12**, 625-634.

Lisabeth, E. M., Fernandez, C. and Pasquale, E. B. (2012). Cancer somatic mutations disrupt functions of the EphA3 receptor tyrosine kinase through multiple mechanisms. *Biochemistry* **51**, 1464-1475.

Marino, S., Vooijs, M., van Der Gulden, H., Jonkers, J. and Berns, A. (2000). Induction of medulloblastomas in p53-null mutant mice by somatic inactivation of Rb in the external granular layer cells of the cerebellum. *Genes Dev.* **14**, 994-1004.

McFadden, D. G., Papagiannakopoulos, T., Taylor-Weiner, A., Stewart, C., Carter, S. L., Cibulskis, K., Bhutkar, A., McKenna, A., Dooley, A., Vernon, A. et al. (2014). Genetic and clonal dissection of murine small cell lung carcinoma progression by genome sequencing. *Cell* **156**, 1298-1311.

Min, H., Danilenko, D. M., Scully, S. A., Bolon, B., Ring, B. D., Tarpley, J. E., DeRose, M. and Simonet, W. S. (1998). Fgf-10 is required for both limb and lung development and exhibits striking functional similarity to Drosophila branchless. *Genes Dev.* **12**, 3156-3161.

Morrisey, E. E. and Hogan, B. L. (2010). Preparing for the first breath: genetic and cellular mechanisms in lung development. *Dev. Cell* **18**, 8-23.

Muzumdar, M. D., Tasic, B., Miyamichi, K., Li, L. and Luo, L. (2007). A global double-fluorescent Cre reporter mouse. *Genesis* **45**, 593-605.

Nievergall, E., Lackmann, M. and Janes, P. W. (2012). Eph-dependent cell-cell adhesion and segregation in development and cancer. *Cell. Mol. Life Sci.* **69**, 1813-1842.

Oricchio, E., Nanjangud, G., Wolfe, A. L., Schatz, J. H., Mavrakis, K. J., Jiang, M., Liu, X., Bruno, J., Heguy, A., Olshen, A. B. et al. (2011). The Eph-receptor A7 is a soluble tumor suppressor for follicular lymphoma. *Cell* **147**, 554-564.

Oxnard, G. R., Binder, A. and Jänne, P. A. (2013). New targetable oncogenes in non-small-cell lung cancer. *J. Clin. Oncol.* **31**, 1097-1104.

Pasquale, E. B. (2010). Eph receptors and ephrins in cancer: bidirectional signalling and beyond. *Nat. Rev. Cancer* **10**, 165-180.

Sanchez-Rivera, F. J., Papagiannakopoulos, T., Romero, R., Tammela, T., Bauer, M. R., Bhutkar, A., Joshi, N. S., Subbaraj, L., Bronson, R. T., Xue, W. et al. (2014). Rapid modelling of cooperating genetic events in cancer through somatic genome editing. *Nature* **516**, 428-431.

Schramek, D., Kotsinas, A., Meixner, A., Wada, T., Elling, U., Pospisilik, J. A., Neely, G. G., Zwick, R. H., Sigl, V., Forni, G. et al. (2011). The stress kinase MKK7 couples oncogenic stress to p53 stability and tumor suppression. *Nat. Genet.* **43**, 212-219.

Snyder, E. L., Watanabe, H., Magendantz, M., Hoersch, S., Chen, T. A., Wang, D. G., Crowley, D., Whittaker, C. A., Meyerson, M., Kimura, S. et al. (2013). Nkx2-1 represses a latent gastric differentiation program in lung adenocarcinoma. *Mol. Cell* **50**, 185-199.

Stephen, L. J., Fawkes, A. L., Verhoeve, A., Lemke, G. and Brown, A. (2007). A critical role for the EphA3 receptor tyrosine kinase in heart development. *Dev. Biol.* **302**, 66-79.

Vadivel, A., van Haaften, T., Alphonse, R. S., Rey-Parra, G. J., Ionescu, L., Haromy, A., Eaton, F., Michelakis, E. and Thébaud, B. (2012). Critical role of the axonal guidance cue EphrinB2 in lung growth, angiogenesis, and repair. *Am. J. Respir. Crit. Care Med.* **185**, 564-574.

Vaidya, A., Pniak, A., Lemke, G. and Brown, A. (2003). EphA3 null mutants do not demonstrate motor axon guidance defects. *Mol. Cell. Biol.* **23**, 8092-8098.

Vail, M. E., Murone, C., Tan, A., Hii, L., Abebe, D., Janes, P. W., Lee, F. T., Baer, M., Palath, V., Bebbington, C. et al. (2014). Targeting EphA3 inhibits cancer growth by disrupting the tumor stromal microenvironment. *Cancer Res.* **74**, 4470-4481.

White, A. C., Xu, J., Yin, Y., Smith, C., Schmid, G. and Ornitz, D. M. (2006). FGF9 and SHH signaling coordinate lung growth and development through regulation of distinct mesenchymal domains. *Development* **133**, 1507-1517.

Yang, H., Wang, H., Shivalila, C. S., Cheng, A. W., Shi, L. and Jaenisch, R. (2013). One-step generation of mice carrying reporter and conditional alleles by CRISPR/Cas-mediated genome engineering. *Cell* **154**, 1370-1379.

Yin, Y., Betsuyaku, T., Garbow, J. R., Miao, J., Govindan, R. and Ornitz, D. M. (2013). Rapid induction of lung adenocarcinoma by fibroblast growth factor 9 signaling through FGF receptor 3. *Cancer Res.* **73**, 5730-5741.

Yue, Y., Su, J., Cerretti, D. P., Fox, G. M., Jing, S. and Zhou, R. (1999). Selective inhibition of spinal cord neurite outgrowth and cell survival by the Eph family ligand ephrin-A5. *J. Neurosci.* **19**, 10026-10035.

Zhuang, G., Song, W., Amato, K., Hwang, Y., Lee, K., Boothby, M., Ye, F., Guo, Y., Shyr, Y., Lin, L. et al. (2012). Effects of cancer-associated EPHA3 mutations on lung cancer. *J. Natl. Cancer Inst.* **104**, 1183-1198.

SUPPLEMENTARY MATERIAL

Supplementary Table 1. List of primers used in the quantitative PCR analysis of mouse epithelial and mesenchymal cells. Primer sequences for *EphA1* and *EphA4* were from the indicated references.

Gene	Primer sequence	Primer efficiency
EphA1 (Forward)	CAAGATTGCAAGACTGTGGC (Abdul-Aziz et al., 2009)	E=98.3% R^2=0.949 Slope= -3.363
EphA1 (Reverse)	CCTCCCACATTACAATCCCA (Abdul-Aziz et al., 2009)	
EphA2 (Forward)	GTCTATAAAGGGACGCTGAAGG	E=96.3% R^2=0.987 Slope= -3.414
EphA2 (Reverse)	CGCTCCATTCTCCATGTACTC	
EphA3 (Forward)	GAGACAGTATGCCGCAGTCA	E=99.0% R^2=1.000 Slope= -3.346
EphA3 (Reverse)	GCCTCTTGCTCTCAAAATGG	
EphA4 (Forward)	CCGAAGCAGCCTACACTACC (Andersson et al., 2011)	E= 98.7 R^2= 0.996 Slope= -3.354
EphA4 (Reverse)	GCCAGCAGTCCAGCATTAAC (Andersson et al., 2011)	
EphA5 (Forward)	AGTGACAGTGGGAGTCATCT	E=90.7% R^2=0.943 Slope= -3.566
EphA5 (Reverse)	GCAGTTTAATGTGCCCGTTATG	
EphA7 (Forward)	CAGCAGACGGGATTAGAGGA	E=100.4% R^2=0.988 Slope= -3.313
EphA7 (Reverse)	GATGACTCCATTGGGATGCT	
Efna1 (Forward)	CAGGAATCCCAGTGCTTGAA	E=94.2% R^2=0.998 Slope= -3.468
Efna1 (Reverse)	CAGCAGTGGTAGGAGCAATAC	
Efna5 (Forward)	GAGATGTTGACGCTGCTCTT	E=102.4% R^2=0.996 Slope= -3.266
Efna5 (Reverse)	TTCTGGGACAGAGTCCTCATAG	
Efnb2 (Forward)	CCAGACAAGAGCCATGAAGAT	E=74.6% R^2=0.975 Slope= -4.130
Efnb2 (Reverse)	TGCGATCCCTGCGAATAAG	
Fgf10 (Forward)	GCTGTTCTCCTTCACCAAGTA	E=95.1% R^2=0.969 Slope= -3.445
Fgf10 (Reverse)	ACTCCGATTTCCACTGATGTT	
Pecam1 (Forward)	GTGGTCATCGCCACCTTAATA	E=96.7% R^2=0.997 Slope= -3.404
Pecam1 (Reverse)	TTCTCGCTGTTGGAGTTCAG	
Nkx2.1(Forward)	CTACTGCAACGGCAACCTG	E=92.3% R^2=0.997 Slope= -3.522
Nkx2.1 (Reverse)	CCATGCCACTCATATTCATGC	
Cdh1 (Forward)	CAGGTCTCCTCATGGCTTTGC	E=89.6% R^2=0.994 Slope=-3.599
Cdh1 (Reverse)	CTTCCGAAAAGAAGGCTGTCC	
Rpl19 (Forward)	CGGGAATCCAAGAAGATTGA	E=93.4% R^2=0.997 Slope= -3.492
Rpl19 (Reverse)	TTCAGCTTGTGGATGTGCTC	

Supplementary figure legends

Supplementary Figure 1. (A) *EPHA3* mutations co-occur with mutations in common drivers of human lung adenocarcinoma. Grey bars represent patients with mutations in any of the three genes. Green mark indicates existence of point mutation in the assigned gene. Mutation information is based on the data from Cancer Genome Atlas Research Network (Cancer Genome Atlas Research Network, 2014) and was exported from cBioportal (Cerami et al., 2012;Gao et al., 2013). (B) Lungs from dual fluorescence mT/mG Cre-reporter mice at two weeks post CMV-AdCre infection ($3{,}3 \times 10^7$ pfu) show Cre activity-induced GFP expression in bronchiolar [Br] and alveolar [Av] progenitor cells. Image acquisition was performed at 20x magnification. (C) Representative image of H&E stained lung section from *Kras;EphA3* lungs and the corresponding pseudo-colored image describing the tissue segmentation performed with Definiens software. The quantitation of cancer area [C] including epithelial hyperplasia, adenomas, and adenocarcinomas in all samples was measured in relation to the area of combined normal [N] and stromal regions [S] including infiltration of immune cells. Scale bars: 100 µm. (D) Validation of a polyclonal rabbit anti-EPHA3 antibody via siRNA-mediated downregulation of *EPHA3* in human hTERT-RPE1 cells. Cells were treated with *EPHA3* siRNA or siRNA control for 72 hours and processed for immunohistochemistry. Image acquisition was performed at 20x magnification. *EPHA3* mRNA quantitation confirms the knockdown upon siRNA treatment. Results are mean±s.d.

Supplementary Figure 2. (A) In situ hybridization analysis of *Fgf10* expression in embryonic mouse lungs at E14.5 shows mesenchymal expression. Scale bars: 100 µm. (B) Constitutive loss of *EphA3* does not trigger altered expression of *EphA7* in embryonic lung mesenchyme. Comparative expression analysis of $EphA3^{+/+}$, $EphA3^{+/-}$ and $EphA3^{-/-}$ embryonic lungs at E11.5, E13.5 and E15.5 shows statistically significant differences between $EphA3^{+/+}$and $EphA3^{-/-}$ only in epithelial *EphA7* expression. Results are mean±s.d. E11.5: n=2-3; E13.5 n=1-4; E15.5 n=3-4, *P < 0,05 (Student's t-test). (C) In situ hybridization of *Efna1* expression in embryonic mouse lungs at E14.5 shows epithelial expression. Scale bars: 100 µm.

Supplementary Figure 3. (A) *EphA3* is expressed at low levels in adult mouse lungs when compared with selected EphA receptors. Heatmap presentation of the comparative expression

analysis shows average expression values in *EphA3* -wild type and -null adult mouse lung and embryonic mesenchyme at E13.5 without scaling. Histogram presentation of the comparative expression analysis shows scaled average expression values in *EphA3* -wild type and -null adult mouse lung and embryonic mesenchyme at E13.5. Results are mean±s.d. N=3 for all four groups. (B) Comparative expression analysis of $EphA3^{+/+}$, $EphA3^{+/-}$ and $EphA3^{-/-}$ embryonic lungs at E15.5 shows a statistically significant difference between $EphA3^{+/+}$ and $EphA3^{-/-}$ only in epithelial Nkx2-1 expression. Results are mean±s.d. N=3-4 *P < 0,05 (Student's t-test). (C) Constitutive loss of *EphA3* does not have gross effect on embryonic lung branching morphogenesis. Representative E-cadherin whole mount images of $EphA3^{+/+}$, $EphA3^{+/-}$ and $EphA3^{-/-}$ embryonic lungs at E11.5 and E15.5. Image acquisition was performed at 8x magnification for E11.5 lungs, and at 2x for E15.5 lungs.

Supplementary figure 1.

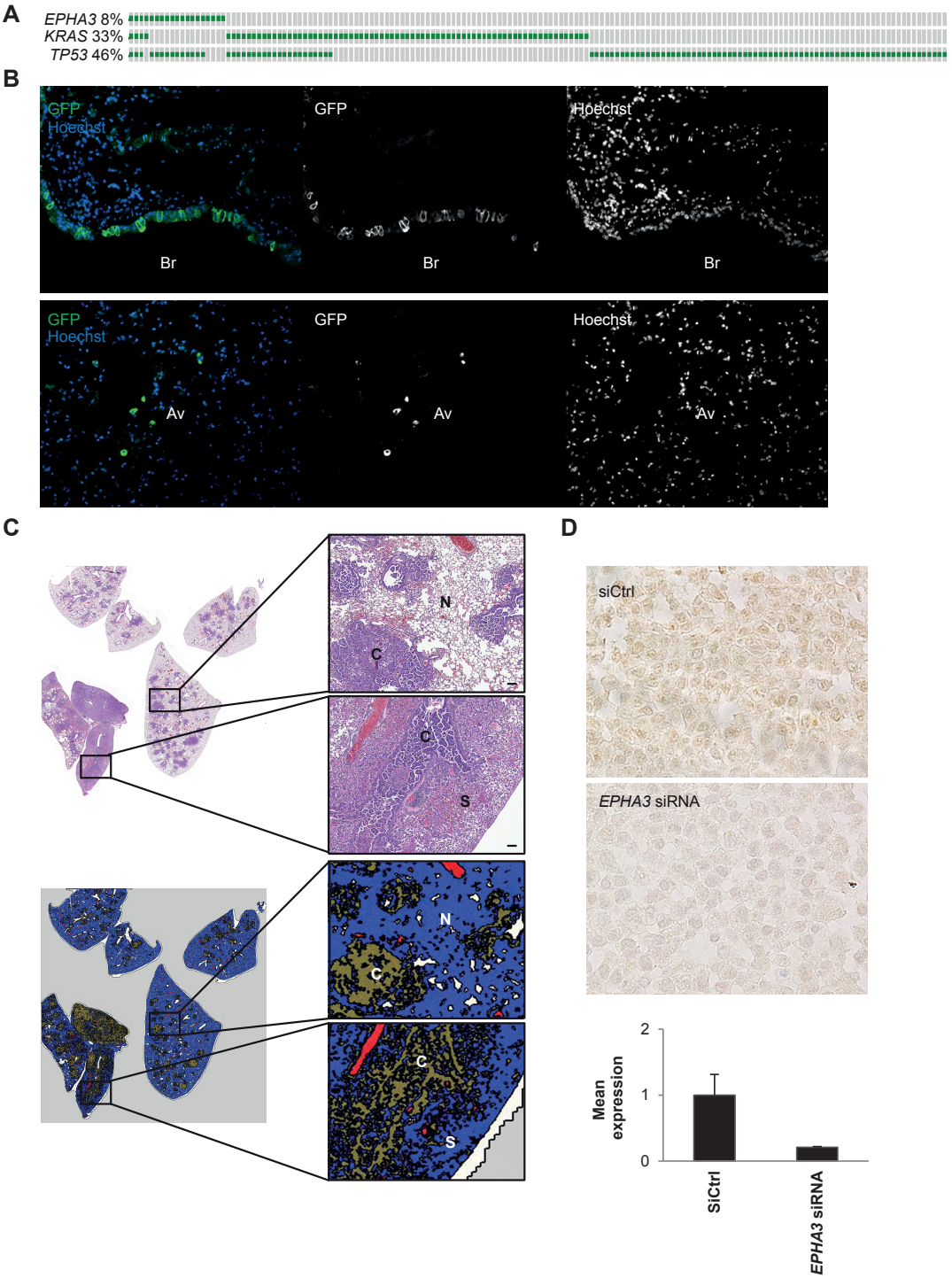

Supplementary figure 2.

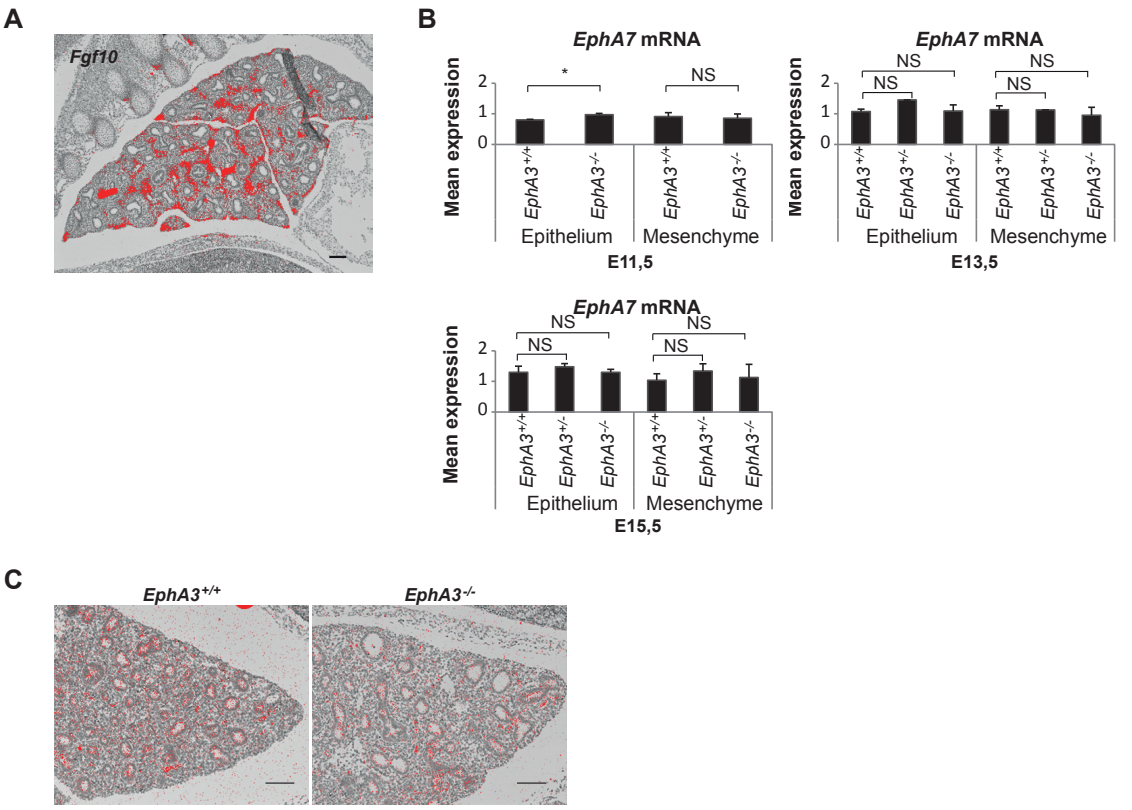

Supplementary figure 3.

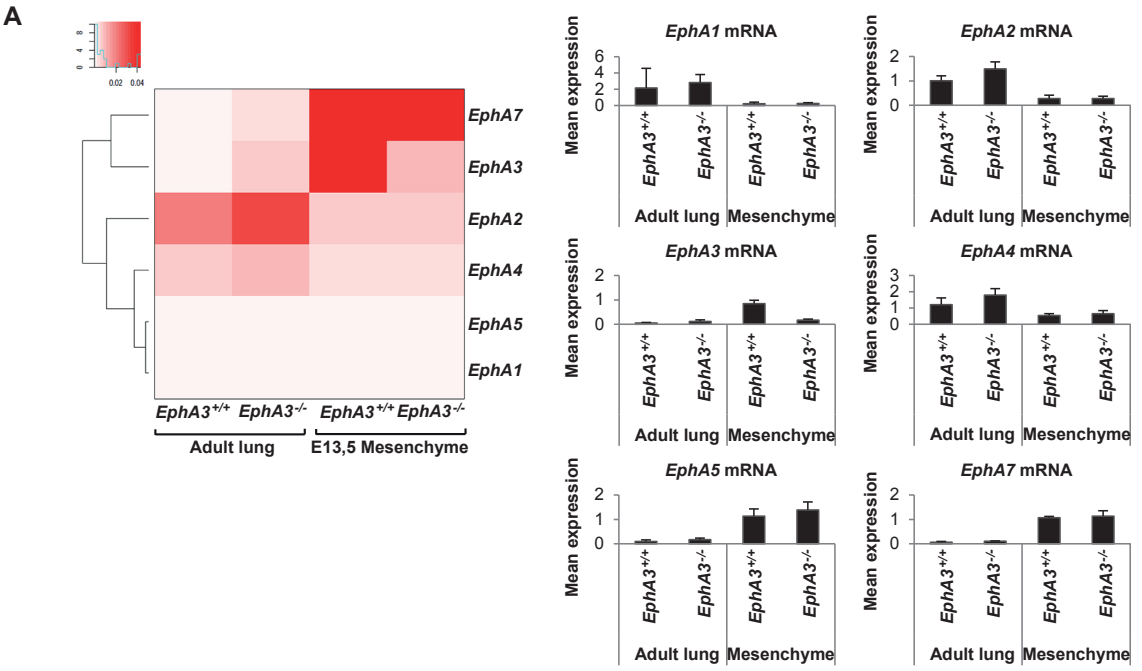

III

Cell-of-origin links histotype spectrum to immune microenvironment diversity in non-small cell lung cancer driven by mutant *Kras* and loss of *Lkb1*

Ashwini Nagaraj[1, 3], Jenni Lahtela[1, 3], Annabrita Hemmes[1], Kaisa Salmenkivi[2], Katja Närhi[1], and Emmy W. Verschuren[1]

[1]Institute for Molecular Medicine Finland (FIMM), University of Helsinki, Helsinki FI-00014, Finland.

[2]Department of Pathology, HUSLAB and Haartman Institute, Helsinki University Central Hospital and University of Helsinki FI-00014, Finland.

[3]Co-first author.

Correspondence: Emmy Verschuren, emmy.verschuren@helsinki.fi

Summary

Lung cancers exhibit pronounced histological and genomic heterogeneity, confounding precision medicine. We studied how the cell-of-origin contributes to phenotypic and immune microenvironment heterogeneity following conditional expression of *Kras*^{G12D} and loss of *Lkb1 (Kras;Lkb1)*. Using progenitor cell type-restricted adenoviral-Cre targeting cells expressing Surfactant Protein C (SPC) or Clara cell antigen 10 (CC10), we show that Ad5-CC10-Cre infected mice exhibit a shorter latency compared with Ad5-SPC-Cre cohorts. We further demonstrate that CC10^{+} cells are the predominant progenitors of adenosquamous carcinoma (ASC) tumors, and give rise to a wider spectrum of histotypes that uniquely include mucinous and acinar invasive adenocarcinomas. Transcriptome analysis indicates ASC histotype-specific downregulation of Class I MHC genes, and upregulation of pro-inflammatory and immunomodulatory genes. ASC-specific immunosuppression is evidenced by recruitment of Gr-1^{+}CD11b^{+} myeloid derived suppressor cells and decreased CD3^{+} T cell infiltration. We conclude that progenitor cell-specific etiology influences the *Kras;Lkb1*-driven tumor histopathology spectrum and histotype-specific immune microenvironment.

Highlights

- Cell-of-origin crucially defines tumor proliferation and histopathology spectrum
- CC10^{+} cells are the predominant progenitors of adenosquamous carcinoma in *Kras;Lkb1* mice
- CC10^{+} cells uniquely give rise to pure mucinous and acinar adenocarcinoma histotypes
- Adenosquamous tumors but not papillary adenocarcinomas have immunosuppressive microenvironments

Introduction

Lung cancers are relatively intractable with respect to detection and treatment, and pronounced histological and genomic heterogeneity compromises prognosis and treatment success (Chen et al., 2014). Factors contributing to tumor progression and therapy resistance may include genetic modifiers of signaling responses, or stromal and immune regulators residing in the tumor-specific microenvironment. In addition, disease etiology can be influenced by niche-specific stem or progenitor cell functions (Leeman et al., 2014). In the murine lung, multiple stem/progenitor cell types have been identified based on their capacities to self-renew and/or differentiate following lung injury, and include $Krt5^{+}/p63^{+}$ tracheal basal cells in the proximal airways, $CC10^{+}$ Clara cells and dual $CC10^{+}/SPC^{+}$ bronchioalveolar stem cells (BASCs) in the distal airways and SPC^{+} alveolar type 2 (AT2) cells in the air spaces (Asselin-Labat and Filby, 2012). However, the relative roles of progenitor cells in establishing potential histotype-specific tumor microenvironments remain poorly understood.

Clinically, non-small cell lung cancer (NSCLC) accounts for around 85% of total lung cancers, with adenocarcinoma (AC; 40%) and squamous cell carcinoma (SCC; 30%) representing the major sub-histotypes (Travis et al., 2013). Lesions containing both AC and SCC features are classified as adenosquamous carcinoma (ASC; 0.4-4%), a rare disease with poor prognosis (Nakagawa et al., 2003). NSCLC subtypes can be enriched for certain genetic alterations: activating mutations in *EGFR*, *KRAS* or loss of function mutations in serine/threonine kinase 11 (*STK11*, also known as *LKB1*) are common for AC and ASC, while loss of function mutations in *TP53, PTEN,* or *SOX2* amplification are common for SCC (Gridelli et al., 2015). *KRAS* mutation concurrent with loss of *LKB1* is detected in around 30% of NSCLC, and represents a more aggressive metastasis-prone NSCLC type recapitulated by the preclinical $Kras^{G12D/+};Lkb1^{fl/fl}$ (*Kras;Lkb1*) model (Calles et al.,

2015; Ji et al., 2007). This highlights the need for deeper understanding of this genetic subtype of lung cancers.

Various genetically engineered mouse models (GEMMs) of NSCLC, utilizing conditional genetic or viral induction, have been used to address the relative contributions of genetic drivers and cells-of-origin to the generation of histopathological diversity and proliferative phenotypes (Leeman et al., 2014). Specifically, expression of oncogenic *Kras* with or without additional loss of the *Trp53* (*p53*) tumor suppressor drives transformation of $CC10^+$ cells in the terminal bronchioles, bronchioalveolar duct junctions (BADJ) including dual $CC10^+/SPC^+$ BASCs (Kim et al., 2005; Xu et al., 2012), as well as of SPC^+ AT2 cells (Sutherland et al., 2014). Interestingly, $CC10^+$ and SPC^+ progenitors appear to distinctly contribute to AC tumorigenesis, evidenced by differential *Kras*- or *Kras;p53*-induced histopathology spectra (Lin et al., 2012; Sutherland et al., 2014). In addition, $Kras^{G12V}$ yields malignant AC mostly from SPC^+ progenitors, whereas $CC10^+$ cells develop more benign lesions requiring an adenoviral inflammatory response (Mainardi et al., 2014). Thus, $CC10^+$ Clara cells or BASCs appear to show partial resistance to malignant transformation by oncogenic *Kras*, possibly due to differential Notch activity (Xu et al., 2014b).

While progenitor-specific etiologies of lung ACs are well described, this is less clear for ASC and SCC histotypes. Airway basal cells have been proposed to act as SCC progenitors following loss of *Pten* with *Tgfbr2* or *Lkb1* (Malkoski et al., 2014; Xu et al., 2014a). Recent studies have further shown that AC derived from SPC^+ cells can transdifferentiate into SCCs via an intermediate ASC stage (Han et al., 2014; Li et al., 2015). Among NSCLC GEMMs, *Kras;Lkb1* mice infected with Ad5-CMV-Cre uniquely produce the full spectrum of histotypes, namely AC, SCC, ASC and large cell carcinomas (Ji et al., 2007). This prompted us to employ $CC10^+$ and SPC^+ progenitor cell-restricted adeno-Cre viruses previously used to identify cells-of-origin in lung GEMMs (Sutherland et al., 2011), to dissect progenitor cell roles in establishing NSCLC phenotypic and

microenvironmental heterogeneity in conditional *Kras;Lkb1* mice. Our results show that $CC10^+$ and SPC^+ progenitor cells differentially contribute to histotype diversity, and that $CC10^+$-derived tumors are more proliferative. Furthermore, we establish $CC10^+$ cells as the predominant progenitors of the ASC histotype, and establish that ASCs exhibit a unique histotype-specific immunosuppressive microenvironment conducive for tumorigenesis.

Results

Cell-of-origin defines survival of mice following oncogenic *Kras* expression and loss of *Lkb1*

To investigate the relative contribution of lung progenitors in determining disease progression and histopathology in the *Kras;Lkb1* GEMM, mice were intranasally infected with $1x10^7$ plaque forming units (pfu) or $2.5x10^9$ pfu of Ad5-CC10-Cre virus or Ad5-SPC-Cre virus, respectively. Titers were set based on their ability to achieve comparable infection rates using *mT/mG* Cre-reporter mice (Muzumdar et al., 2007), as distal airway-located SPC^+ AT2 cells are not targeted as readily. Lungs of fluorescent Cre-reporter *Kras;Lkb1;Rosa26*$^{mT/mG}$ mice were examined at 2-4 wk post infection, and accurate alveolar and bronchiolar mGFP labeling following Ad5-SPC-Cre or Ad5-CC10-Cre infection was detected, respectively (Fig. S1A). Similar to previous data (Sutherland et al., 2014), BADJ areas were readily targeted by Ad5-CC10-Cre, which was not observed with Ad5-SPC-Cre; no alveolar cells were targeted by Ad5-CC10-Cre. We next followed cohorts for late-stage tumor formation and euthanized mice when moribund. Tumors from Ad5-CC10-Cre and Ad5-SPC-Cre infection showed loss of LKB1 expression, confirming dual gene recombination (Fig. S1B). Kaplan-Meier survival analysis showed that mice infected with Ad5-CC10-Cre had a shorter latency compared with Ad5-SPC-Cre (median survival 79 *vs* 120 days; Fig. 1A), suggesting that tumors initiated from $CC10^+$ progenitor cells developed faster and/or more aggressive lung disease.

Cell-of-origin defines the *Kras;Lkb1*-driven histopathology spectrum

Next, histopathological analyses of lesions formed in the full set of lung lobes from moribund *Kras;Lkb1* mice were performed. We hereto adhered to the IASLC/ATS/ERS NSCLC classification system (Travis et al., 2011), guided by an expert lung pathologist (Fig. 1B). Two major histotypes were detected, namely (1) ASCs which contain an inner AC core expressing the NKX2-1 AC

biomarker surrounded by an outer squamous region co-expressing the p63 squamous biomarker and NKX2-1, and (2) ACs with invasive characteristics conferring loss of the alveolar structure. ASCs were predominantly detected in the Ad5-CC10-Cre cohort (5/5 mice, 20 tumors total) when compared to the Ad5-SPC-Cre cohort (1/5 mice, 3 tumors total) (Fig. 1C & S1C). All ASCs expressed the cytokeratin 5 (KRT5) squamous cell marker, but no staining for the nuclear SOX2 SCC marker was detected (Fig. S1D).

Both Ad5-CC10-Cre and Ad5-SPC-Cre induced invasive ACs, comprised of well or moderately differentiated lesions, and invasive ACs were accompanied with pre-invasive adenocarcinoma in situ (AIS). Deeper analysis of moderately differentiated invasive ACs based on growth pattern revealed a spectrum of three AC subtypes, namely pure mucinous AC, papillary AC, and acinar AC. Tumors with a lepidic growth pattern at the lesion border, but otherwise invasive, were considered invasive AC (Fig. S1E). Of these five lesion types, pure mucinous and acinar ACs were uniquely detected following Ad5-CC10-Cre infection (Fig. 1B & 1C). The number of cells positive for the AC biomarker NKX2-1, a differentiation marker frequently lost during invasive progression, was highest in invasive ACs with or without papillary growth, whereas mucinous and acinar ACs uniquely induced by Ad5-CC10-Cre showed less NKX2-1 positive cells (Fig. 1B). The majority of invasive AC subtypes were negative for p63 (Fig. 1B), although few Ad5-CC10-Cre-induced papillary and mucinous ACs showed sporadic p63 staining (Fig. S1F). The latter resembles clinical ACs, where 30% of lesions show some p63 expression, yet are classified as AC based on morphological features (Au et al., 2004).

Inspection of *Kras;Lkb1* lesions during early-stage tumorigenesis showed that both viruses induced detectable lesions at six wk post infection (Fig. S1G). At this stage, Ad5-CC10-Cre induced NKX2-1 positive luminal papillary hyperplasias of epithelial cells in the terminal bronchioles, with sparse

staining for p63. Ad5-SPC-Cre-induced lesions at 6 wk were NKX2-1 positive pre-invasive AIS located in the alveoli. At nine wk post infection, Ad5-CC10-Cre lesions consisted of AIS, invasive AC, papillary AC, mucinous AC and ASC similar to the histopathology types detected in moribund mice. At this time point we observed SCC in one of four mice (Fig. S1G), while no SCC was seen at later stages. Lesions at nine wk following Ad5-SPC-Cre infections were invasive or papillary ACs and lacked squamous features altogether. Taken together, expression of oncogenic *Kras* with *Lkb1* loss elicited a progenitor cell-specific difference in histopathology spectrum formation; $CC10^{+}$-driven lesions showed a wider spectrum of AC histotypes to include pure mucinous and acinar AC, and were predominantly of the adenosquamous histotype, while SPC^{+}-driven tumors were primarily ACs.

$CC10^{+}$-derived lesions are more proliferative and often less differentiated

To investigate histotype-specific proliferation rates, percentages of Ki67 positive nuclei across all lesions were quantified at the end stage. This showed that Ad5-CC10-Cre-induced lesions exhibited increased proliferation rates compared with Ad5-SPC-Cre infections, and that the squamous regions of ASCs were more proliferative than the AC regions (Fig. 1D & S2A). We further analysed expression of the high mobility group AT-hook 2 (HMGA2) transcription factor commonly expressed in more poorly differentiated and invasive tumors (Snyder et al., 2013; Sutherland et al., 2014; Winslow et al., 2011). Homogeneous expression of HMGA2 in ASCs was seen, whereas all other histopathologies had negative to low expression (Fig. S2B). Furthermore, macroscopically all ASCs were much bigger in size, ranging from 20-30 mm^2 compared to smaller than 3 mm^2 lesions for all other histotypes (Fig. 1E). The shorter survival of Ad5-CC10-Cre infected mice thus correlated with an increased propensity for progression of highly proliferative and larger ASC tumors.

Since the molecular basis and etiology of AC subtypes is thus far unknown, we decided to more deeply study the mucinous ACs, a subtype of human lung cancer here uniquely detected upon Ad5-CC10-Cre infection. First, mucin production was confirmed with periodic acid Schiff's (PAS) staining (Fig. S2C). Consistent with the finding that haploinsufficiency of NKX2-1 cooperates with *Kras*^{G12D} in mucinous AC progression (Maeda et al., 2012; Snyder et al., 2013), we further observed reduced expression of NKX2-1 in PAS positive mucinous tumors compared to well-differentiated papillary ACs (Fig. 1F, 1G, S2D & S2E). PAS positivity was also detected in the AC regions of ASCs, bronchiolar luminal papillary hyperplasias, and in some of the invasive ACs (Fig. S2C & S2F). This suggests that progression to mucinous AC may involve bronchiolar luminal papillary hyperplasias or invasive AC as an intermediate state. Taken together, CC10^{+} progenitor cells have the unique ability to give rise to advanced AC with mucinous differentiation.

***Kras;Lkb1* tumors show histotype-specific gene expression signatures**

To gain insights in histotype-specific molecular heterogeneities, we compared RNA expression profiles of Ad5-CC10-Cre-derived ASCs and Ad5-SPC-Cre-derived papillary ACs, representing the predominant progenitor-specific *Kras;Lkb1* histotypes at the end stage of the disease progression (Fig. S3A). Tumor histopathology was confirmed by expression of p63 protein specifically in ASCs (Fig. S3B). Unsupervised hierarchical clustering using adjusted p value <0,01 LogFC>1 as a cut-off revealed 340 differentially expressed genes showing distinct clustering of ASC and papillary AC tumors (Fig. 2A). We next asked how these gene signatures related to previously published histotype-specific gene signatures. Since no human ASC gene signatures are available, we instead utilized SCC vs AC comparative gene expression data. These were comprised of a recently described comparison of SCC elicited by conditional *Lkb1* and *Pten* loss to *Kras*$^{G12D/+}$-derived AC tumors (Xu et al., 2014a), and a human SCC vs AC comparative gene expression study (Kuner et al., 2009). Using a cut-off value of p<0,01 LogFC>1, we identified 29 and 11 commonly

upregulated or downregulated genes, respectively (Fig 2B & Table S1). SCC-enriched genes encompassed known human SCC biomarkers transformation related protein 63 (*Trp63*) and multiple basal cytokeratins (Krt) (Fig. 2C). Interestingly, the recently described AC biomarker napsin A (*Napsa*), a pepsin family aspartic proteinase (Turner et al., 2012), was found enriched in our murine ACs.

We further compared our dataset to untransformed murine airway basal cell expression profiles, to determine if basal or epithelial signatures contribute to ASC (Rock et al., 2009). This identified 108 genes commonly enriched in Ad5-CC10-Cre-derived ASC and airway basal cells (Fig S3C & Table S1). In addition to known stratified squamous epithelial marker genes *Trp63*, basonuclin (*Bnc1*), stratifin (*Sfn*) and cytokeratins, we found common enrichment of pro-inflammatory cytokine interleukin 1β (*Il1b*) and its type II interleukin 1 receptor (*Il1r2*). As expected, the AC biomarker SPC was commonly downregulated in airway basal cells and ASC. Finally, our dataset was compared with published ASC gene expression signatures from the *Kras;Lkb1* GEMMs (Ji et al., 2007), showing 23 commonly enriched genes (Fig. S3C & Table S1), including SCC signature genes such as *Trp63* and cytokeratins. Collectively, our results show that even though $CC10^{+}$ lung progenitor cell-derived ASCs display features of AC at the histological level, they exhibit SCC histotype-specific gene signatures.

Histotype-specific expression of immune-related genes

Interestingly, analysis of *Kras;Lkb1* histotype-specific gene signatures by Ingenuity Pathway Analysis (IPA) revealed several immune-related canonical pathways, implying differences in immune-related functions (Fig. 3A). We thus asked if this apparent histotype-specific difference in immune-related signatures might exist independently of the genetic drivers. Indeed, by comparing RNA expression profiles of *Kras;p53* Ad5-CC10-Cre- and Ad5-SPC-Cre-derived ACs to

Kras;Lkb1 expression data, we found that selected cytokine, chemokine and antigen presentation pathway genes showed histopathology-dependent expression differences (Fig. 3B). Pro-inflammatory cytokine *Il1b* and the arginase 1 enzyme gene (*Arg1*), a key mediator of T cell immunosuppression (Munder et al., 2006), were specifically enriched in ASCs. ASCs further showed downregulation of class II (*H2-DMa, H2-Ab1, H2-DMb1*) major histocompatibility complex (MHC) genes, and class II MHC associated gene *Cd74* as well as the lymphocyte and monocyte chemoattractant chemokines *Ccl17, Ccl*6, and the chemokine *Cxcl15*. Notable exceptions were class I (*H2-M2, H2-D1*) MHC genes, which expression was lower in *Kras;Lkb1* Ad5-CC10-Cre-derived ASCs when compared to *Kras;Lkb1* Ad5-SPC-Cre-derived papillary ACs but showed variable expression in *Kras;p53* ACs. *Cxcl5*, a downstream chemokine target of *Il1b*, showed elevated levels in both *Kras;Lkb1* ASCs and *Kras;p53* ACs, suggesting a potential association with tumor grade rather than histopathology. Quantitative real-time PCR (qPCR) analysis on a select set of inflammatory genes confirmed increased *Il1b* and *Arg1* expression in *Kras;Lkb1* ASC histotype tumors and variable expression of class I (*H2-M2, H2-D1*) MHC genes in ACs (Fig. 3C). Finally, to assess whether the cell-of-origin has an effect on histotype-specific expression of immune-related genes, we included in the validation panel also a rare Ad5-CC10-Cre-derived papillary AC and two rare Ad5-SPC-Cre-derived *Kras;Lkb1* ASCs. Validation by qPCR also in this set confirmed the ASC histotype-specific expression of *Il1b* and *Arg1,* as well as decreased MHC gene expression (Fig. S3D). In summary, our data indicates that immune-related genes are expressed in a histotype-specific manner, independent of the driver genotype, cell-of-origin, or potential adenovirus-associated inflammatory response.

ASC histotype-specific recruitment of Gr-1^{+}CD11b^{+} myeloid derived suppressor cells (MDSCs)

Tumor tissue-expressed interleukin 1β (encoded by *Il1b*) has been shown to activate and mobilize MDSCs, a heterogeneous population of activated immature myeloid cells that mediate immunosuppression among others by expression of arginase 1, an enzyme responsible for depletion of extracellular L-arginine required for T cell proliferation (Coffelt et al., 2015; Monu and Frey, 2012; Raber et al., 2012; Tu et al., 2008). Since we identified ASC-specific expression of both *Il1b* and *Arg1*, we next studied *Kras;Lkb1* tumor histotype-specific immune cell infiltration by immunostaining. This confirmed the enrichment of Gr-1^{+} and CD11b^{+} cells, concomitant with a reduced number of CD3^{+} T cells specifically in ASCs compared to papillary ACs (Fig. 4A, 4B & S3E). Flow cytometric analysis identified MDSC cell populations by virtue of double Gr-1 and CD11b staining, and further verified the enrichment of Gr-1^{+}CD11b^{+} MDSCs in multiple ASC tumors (Fig. 4C & 4D). Interestingly, although spleen-derived Ly-6C^{hi}CD11b^{+} monocytic and Ly-6G^{hi}CD11b^{+} granulocytic cells have been shown to promote tumorigenesis of *Kras;p53* ACs (Cortez-Retamozo et al., 2012), our *Kras;p53* tumor analysis showed low yet highly variable amounts of Gr-1^{+}CD11b^{+} cells (Fig. S3F & G). This suggests that MDSC infiltration in the *Kras;p53* model could be dependent on tumor differentiation status. Taken together, we provide evidence that Ad5-CC10-Cre-derived *Kras;Lkb1* ASC tumors exhibit an immunosuppressive microenvironment and, importantly, this appears to be a histotype-specific phenomenon.

Discussion

Until now the relative roles of progenitor cells in establishing potential histotype-specific tumor microenvironments remain poorly understood. We show here that $CC10^+$ and SPC^+ progenitor cells differentially contribute to histotype diversity, with $CC10^+$ cells being the predominant progenitor of the ASC histotype. Furthermore, we show that $CC10^+$-derived tumors are more proliferative and that ASCs create an immune suppressive microenvironment conducive for tumorigenesis (Fig. 4E). Interestingly, similar to our observations, human ASCs often contain PAS positive AC regions (Kanazawa et al., 2000) indicating recapitulation of human ASC features in our *Kras;Lkb1* model.

Clinically, AC is the most common lung cancer subtype, further sub-classified as pre-invasive, minimally invasive, and invasive AC (Travis et al., 2011). We here find that *Kras;Lkb1* progenitors have a capacity to generate three subtypes of invasive AC, namely papillary, acinar and mucinous AC, thus closely resembling the mixed histotype spectrum typical of human disease. Importantly, mucinous and acinar ACs are exclusively initiated from the $CC10^+$ progenitors, implying unique niche/stem cell-dependent contributions to histotype diversity. Phenotypic diversity could hence be causally linked to targeting of functionally distinct, albeit CC10 expressing, progenitors lining the lung epithelium. One such progenitors could be airway goblet cells co-expressing mucin and CC10, located near the terminal bronchioles (Boers et al., 1999), as we observe many PAS positive cells in early bronchiolar luminal papillary hyperplasias. Mucinous AC may thus arise from a secretory cell conferring dual goblet and Clara cell features. In line with our observations in *Kras;Lkb1* ASCs, a recent study detected mucin-encoding *Muc5b* also in CC10-Cre induced *Pten;Smad4* ASCs (Liu et al., 2015). Importantly, this is the first study addressing progenitor-specific histotype diversity in the *Kras;Lkb1* GEMM, revealing a previously underappreciated capacity to model human ACs, where *LKB1* mutation is enriched across the spectrum of AC (13%) and adenosquamous NSCLC

(22%) (Koivunen et al., 2008). Our data hence warrants deeper dissection of progenitor cell subtypes contributing to histotype diversity, possibly by using bimodal promoters.

We show novel evidence for a clear propensity of bronchiolar $CC10^+$ progenitors to form adenosquamous lesions, with all Ad5-CC10-Cre treated animals developing ASC, while SPC^+ progenitors gave rise to ASCs at a low incidence of one in five mice. These rare ASCs may transdifferentiate from papillary ACs, as reported earlier (Li et al., 2015). Alternatively, this may reflect Ad5-SPC-Cre infection of rare SPC+ cells around the BADJ area. Interestingly we observed rare SCC among the invasive AC and ASC at nine wk following Ad5-CC10-Cre infection, whereas at later stages no pure SCC lesions were detected. This stands in stark contrast to previous studies describing transdifferentiation of AC lesions to SCC via an intermediate ASC stage in the identical *Kras;Lkb1* GEMM (Han et al., 2014). The same group recently showed Ad5-SPC-Cre-induced SCC and ASC at respective incidences of 40% and 60% (Li et al., 2015). One factor contributing to these differences could be the appreciated influence of mouse genetic background on tumor incidence and histotype spectrum formation. Future lineage-tracing studies could confirm whether ASCs transdifferentiate from a specific precursor histotype lesion, and further if SPC^+ BADJ cells and/or BASCs act as a cell-of-origin for ASC.

Comparative gene expression analysis displayed that *Kras;Lkb1* ASCs show characters of murine and human SCCs. Furthermore, the analysis of *Kras;Lkb1* and *Kras;p53* tumor histotype specific expression profiles revealed differential immune-related gene signatures, which in *Kras;Lkb1* ASCs were associated with recruitment of MDSCs and concomitant low T cell numbers, while ACs expressed chemoattractants and showed higher yet variable T cell infiltration. Furthermore, ASCs may escape tumor antigen presentation and hence T cell-mediated toxicity due to decreased Class Ia/b MHC gene expression. We thus provide evidence that lung histotype-specific pathogenesis and

disease progression are closely intertwined with immune modulation. Some ASC-specific immune modulatory features may be shared with SCC tumors, which showed a partial immune signature overlap (Table S1). Indeed, MDSC recruitment has been reported in SCCs of the *Lkb1;Pten* GEMM (Xu et al., 2014a). Furthermore, data from a recent human lung cancer immune cell profiling suggests higher infiltration of neutrophils, possibly representing a subpopulation of MDSCs, in ASCs and SCCs when compared to papillary ACs (Banat et al., 2015). This conceivably indicates that the identified murine histotype-specific immunosuppressive microenvironment translates to human disease. However, while *Lkb1;Pten* SCC tumors express the PD-L1 checkpoint molecule, we found no increased expression of PD-L1 in *Kras;Lkb1* ASCs or papillary ACs compared with normal lung epithelium (data not shown). Tumor-specific mechanisms of immune regulation may thus vary depending on tumor model or histotype. Outstanding questions are how such functional heterogeneity is tied with expression of the *Il1b* cytokine, already expressed at baseline in untransformed tracheal cells (Rock et al., 2009), and how such heterogeneity may relate to human disease. Interestingly, polymorphisms in *IL1B* have been associated with increased lung cancer risk, in particular SCC (Landvik et al., 2009). Furthermore, loss of function mutations in the HLA class I MHC gene have been reported for human lung SCC (Cancer Genome Atlas Research, 2012), indicating that immunosuppression may be a feature of human squamous lesions.

In conclusion, our study provides important insights in the etiology of lung cancer histotype diversity, implying that the niche and cell-of-origin biology crucially define histopathology-specific tumorigenesis and formation of an immune microenvironment. Our data further imply that progenitor cell-specific tumor phenotypes are dominant over their driver genotype as *Kras;Lkb1* SPC^{+} progenitors drive AC features similar to *Kras;p53*. Such phenotypic dominance possibly relates to clinical evidence for clonal heterogeneity in the genetic makeup of tumor cells in histopathologically indistinct lesions (Heim et al., 2014). Future approaches will need to address

which molecular aspects of $CC10^{+}$ and SPC^{+} progenitors cooperate with *Kras;Lkb1* drivers to define histopathology diversity. It will further be interesting to find how this GEMM can be used for development of immune modulatory targets to achieve better control of ASC, an aggressive subtype of NSCLC (Nakagawa et al., 2003). Specifically, strategies to target pro-tumorigenic MDSC functions are under investigation, and re-priming of the anti-tumor T cell response by epigenetic modifiers inducing Class I MHC expression could be considered. Finally, our data suggest that the profiling of patient tumor histotype-specific functions and immune microenvironments should be taken into consideration together with stratified driver mutations.

Experimental Procedures

Mouse strain information

Animal studies followed guidelines from the Finnish National Board of Animal Experimentation, and were approved by the Experimental Animal Committee of the University of Helsinki and the State Provincial Office of Southern Finland (Licence number ESAVI-2010-04855/Ym-23). Mice harboring a conditional allele of mutant *Kras* (*LSL-Kras*$^{G12D/+}$; (Jackson et al., 2001) or loss of function *Trp53* allele (*p53*$^{fl/fl}$; (Marino et al., 2000) were purchased from The Jackson Laboratory. Conditional loss of function *Stk11/Lkb1* mice (*Lkb1*$^{fl/fl}$; (Bardeesy et al., 2002) were received from Ron DePinho (MD Anderson, Houston, USA). Further details are explained in the Supplemental Information.

Survival analysis, tissue preparation and histopathology analysis

Mice were sacrificed when showing symptoms of labored breathing and loss of weight. Kaplan-Meier survival curves were created with GraphPad Prism (GraphPad Software, Inc. San Diego, USA). Histopathology analysis was performed for whole slide scans of H&E-stained paraffin sections. Details are explained in the Supplemental Information.

Immunohistochemistry

Immunistochemistry was performed on 4% formaldehyde fixed lungs and paraffin embedded lungs using standard protocols. Quantitation of whole slide scans acquired from PAS or immunohistological stained sections was performed using the Tissue Studio™ image analysis solution of the Definiens Developer XD 64 2.1 software (Definiens, Munich, Germany). Details are explained in the Supplemental Information.

Microarray gene expression profiling and quantitative PCR analysis

Total RNA from snap-frozen tumors was extracted using the NucleoSpin RNA II kit (MACHEREY-NAGEL, Duren, Germany). Expression profiling was done with Illumina Mouse WT-6 version 2 expression arrays (Illumina, San Diego, CA, USA). Microarray data is made available by GEO, accession no. GSE69552 (http://www.ncbi.nlm.nih.gov/geo/query/acc.cgi?token=yjafiucynxyftmj&acc=GSE69552).

Quantitative PCR was performed for total mRNA extracted from snap-frozen tissue using iQ™ SYBR® Green Supermix (Bio-Rad, Hercules, USA). Further details are explained in the Supplemental Information.

Comparative gene expression analysis

Differentially expressed genes were compared to publicly available gene expression data sets made available via the NCBI-GEO (http://www.ncbi.nlm.nih.gov/geo/) database. Details are explained in the Supplemental Information.

Flow cytometry analysis

Tumors were dissected from moribund mice and single-cell suspensions were incubated with rat anti-mouse antibodies. Detailed processing of the samples and antibody information can be found in the Supplemental Information.

Author Contributions

EWV, AN and KN conducted the experimental design; AN, JL, KN and AS performed the experiments; AN, KN, JL and KS conducted data interpretation. AN, JL and EWV wrote the manuscript.

Acknowledgements

We are grateful to Kate Sutherland and Anton Berns for progenitor cell-directed adenoviruses, and Ronald DePinho for *Lkb1*$^{fl/fl}$ mice. We thank the FIMM WebMicroscope team and Sami Blom for scanning histological slides, the Laboratory Animal Centre for husbandry support, FuGU for expression profiling support, John-Patrick Mpindi for bioinformatics advice, Carolina Pereira and Virva Uotinen for technical support, and Panu Kovanen and Ori Brenner for histopathological guidance. Kate Sutherland is thanked for critical reading of the manuscript. Research was supported by the Innovative Medicines Initiative Joint Undertaking under grant agreement n˚115188 (IMI-PREDECT), resources of which are composed of financial contribution from the European Union's Seventh Framework Programme (FP7/2007-2013) and EFPIA companies in kind contribution (EWV); the Sigrid Juselius and Orion-Farmos Foundations (EWV); Finnish Cultural Foundation (JL) and University of Helsinki Doctoral Programme in Biomedicine scholarships (AN and JL).

References

Asselin-Labat, M.L., and Filby, C.E. (2012). Adult lung stem cells and their contribution to lung tumourigenesis. Open Biol *2*, 120094.

Au, N.H., Gown, A.M., Cheang, M., Huntsman, D., Yorida, E., Elliott, W.M., Flint, J., English, J., Gilks, C.B., and Grimes, H.L. (2004). P63 expression in lung carcinoma: a tissue microarray study of 408 cases. Appl Immunohistochem Mol Morphol *12*, 240-247.

Banat, G.A., Tretyn, A., Pullamsetti, S.S., Wilhelm, J., Weigert, A., Olesch, C., Ebel, K., Stiewe, T., Grimminger, F., Seeger, W., *et al.* (2015). Immune and Inflammatory Cell Composition of Human Lung Cancer Stroma. PLoS One *10*, e0139073.

Bardeesy, N., Sinha, M., Hezel, A.F., Signoretti, S., Hathaway, N.A., Sharpless, N.E., Loda, M., Carrasco, D.R., and DePinho, R.A. (2002). Loss of the Lkb1 tumour suppressor provokes intestinal polyposis but resistance to transformation. Nature *419*, 162-167.

Boers, J.E., Ambergen, A.W., and Thunnissen, F.B. (1999). Number and proliferation of clara cells in normal human airway epithelium. Am J Respir Crit Care Med *159*, 1585-1591.
Calles, A., Sholl, L.M., Rodig, S.J., Pelton, A.K., Hornick, J.L., Butaney, M., Lydon, C., Dahlberg, S.E., Oxnard, G.R., Jackman, D.M., *et al.* (2015). Immunohistochemical Loss of LKB1 Is a Biomarker for More Aggressive Biology in KRAS-Mutant Lung Adenocarcinoma. Clin Cancer Res.
Cancer Genome Atlas Research, N. (2012). Comprehensive genomic characterization of squamous cell lung cancers. Nature *489*, 519-525.
Chen, Z., Fillmore, C.M., Hammerman, P.S., Kim, C.F., and Wong, K.K. (2014). Non-small-cell lung cancers: a heterogeneous set of diseases. Nat Rev Cancer *14*, 535-546.
Coffelt, S.B., Kersten, K., Doornebal, C.W., Weiden, J., Vrijland, K., Hau, C.S., Verstegen, N.J., Ciampricotti, M., Hawinkels, L.J., Jonkers, J., *et al.* (2015). IL-17-producing gammadelta T cells and neutrophils conspire to promote breast cancer metastasis. Nature *522*, 345-348.
Cortez-Retamozo, V., Etzrodt, M., Newton, A., Rauch, P.J., Chudnovskiy, A., Berger, C., Ryan, R.J., Iwamoto, Y., Marinelli, B., Gorbatov, R., *et al.* (2012). Origins of tumor-associated macrophages and neutrophils. Proc Natl Acad Sci U S A *109*, 2491-2496.
Gridelli, C., Rossi, A., Carbone, D.P., Guarize, J., Karachaliou, N., Mok, T., Petrella, F., Spaggiari, L., and Rosell, R. (2015). Non-small-cell lung cancer. Nature Reviews Disease Primers *1*, 16.
Han, X., Li, F., Fang, Z., Gao, Y., Li, F., Fang, R., Yao, S., Sun, Y., Li, L., Zhang, W., *et al.* (2014). Transdifferentiation of lung adenocarcinoma in mice with Lkb1 deficiency to squamous cell carcinoma. Nat Commun *5*, 3261.
Heim, D., Budczies, J., Stenzinger, A., Treue, D., Hufnagl, P., Denkert, C., Dietel, M., and Klauschen, F. (2014). Cancer beyond organ and tissue specificity: next-generation-sequencing gene mutation data reveal complex genetic similarities across major cancers. Int J Cancer *135*, 2362-2369.
Jackson, E.L., Willis, N., Mercer, K., Bronson, R.T., Crowley, D., Montoya, R., Jacks, T., and Tuveson, D.A. (2001). Analysis of lung tumor initiation and progression using conditional expression of oncogenic K-ras. Genes Dev *15*, 3243-3248.
Ji, H., Ramsey, M.R., Hayes, D.N., Fan, C., McNamara, K., Kozlowski, P., Torrice, C., Wu, M.C., Shimamura, T., Perera, S.A., *et al.* (2007). LKB1 modulates lung cancer differentiation and metastasis. Nature *448*, 807-810.
Kanazawa, H., Ebina, M., Ino-Oka, N., Shimizukawa, M., Takahashi, T., Fujimura, S., Imai, T., and Nukiwa, T. (2000). Transition from squamous cell carcinoma to adenocarcinoma in adenosquamous carcinoma of the lung. Am J Pathol *156*, 1289-1298.
Kim, C.F., Jackson, E.L., Woolfenden, A.E., Lawrence, S., Babar, I., Vogel, S., Crowley, D., Bronson, R.T., and Jacks, T. (2005). Identification of bronchioalveolar stem cells in normal lung and lung cancer. Cell *121*, 823-835.
Koivunen, J.P., Kim, J., Lee, J., Rogers, A.M., Park, J.O., Zhao, X., Naoki, K., Okamoto, I., Nakagawa, K., Yeap, B.Y., *et al.* (2008). Mutations in the LKB1 tumour suppressor are frequently detected in tumours from Caucasian but not Asian lung cancer patients. Br J Cancer *99*, 245-252.
Kuner, R., Muley, T., Meister, M., Ruschhaupt, M., Buness, A., Xu, E.C., Schnabel, P., Warth, A., Poustka, A., Sultmann, H., *et al.* (2009). Global gene expression analysis reveals specific patterns of cell junctions in non-small cell lung cancer subtypes. Lung Cancer *63*, 32-38.
Landvik, N.E., Hart, K., Skaug, V., Stangeland, L.B., Haugen, A., and Zienolddiny, S. (2009). A specific interleukin-1B haplotype correlates with high levels of IL1B mRNA in the lung and increased risk of non-small cell lung cancer. Carcinogenesis *30*, 1186-1192.
Leeman, K.T., Fillmore, C.M., and Kim, C.F. (2014). Lung stem and progenitor cells in tissue homeostasis and disease. Curr Top Dev Biol *107*, 207-233.

Li, F., Han, X., Li, F., Wang, R., Wang, H., Gao, Y., Wang, X., Fang, Z., Zhang, W., Yao, S., *et al.* (2015). LKB1 Inactivation Elicits a Redox Imbalance to Modulate Non-small Cell Lung Cancer Plasticity and Therapeutic Response. Cancer Cell *27*, 698-711.
Lin, C., Song, H., Huang, C., Yao, E., Gacayan, R., Xu, S.M., and Chuang, P.T. (2012). Alveolar type II cells possess the capability of initiating lung tumor development. PLoS One *7*, e53817.
Liu, J., Cho, S.N., Akkanti, B., Jin, N., Mao, J., Long, W., Chen, T., Zhang, Y., Tang, X., Wistub, II, *et al.* (2015). ErbB2 Pathway Activation upon Smad4 Loss Promotes Lung Tumor Growth and Metastasis. Cell Rep.
Maeda, Y., Tsuchiya, T., Hao, H., Tompkins, D.H., Xu, Y., Mucenski, M.L., Du, L., Keiser, A.R., Fukazawa, T., Naomoto, Y., *et al.* (2012). Kras(G12D) and Nkx2-1 haploinsufficiency induce mucinous adenocarcinoma of the lung. J Clin Invest *122*, 4388-4400.
Mainardi, S., Mijimolle, N., Francoz, S., Vicente-Duenas, C., Sanchez-Garcia, I., and Barbacid, M. (2014). Identification of cancer initiating cells in K-Ras driven lung adenocarcinoma. Proc Natl Acad Sci U S A *111*, 255-260.
Malkoski, S.P., Cleaver, T.G., Thompson, J.J., Sutton, W.P., Haeger, S.M., Rodriguez, K.J., Lu, S.L., Merrick, D., and Wang, X.J. (2014). Role of PTEN in basal cell derived lung carcinogenesis. Mol Carcinog *53*, 841-846.
Marino, S., Vooijs, M., van Der Gulden, H., Jonkers, J., and Berns, A. (2000). Induction of medulloblastomas in p53-null mutant mice by somatic inactivation of Rb in the external granular layer cells of the cerebellum. Genes Dev *14*, 994-1004.
Monu, N.R., and Frey, A.B. (2012). Myeloid-derived suppressor cells and anti-tumor T cells: a complex relationship. Immunol Invest *41*, 595-613.
Munder, M., Schneider, H., Luckner, C., Giese, T., Langhans, C.D., Fuentes, J.M., Kropf, P., Mueller, I., Kolb, A., Modolell, M., *et al.* (2006). Suppression of T-cell functions by human granulocyte arginase. Blood *108*, 1627-1634.
Muzumdar, M.D., Tasic, B., Miyamichi, K., Li, L., and Luo, L. (2007). A global double-fluorescent Cre reporter mouse. Genesis *45*, 593-605.
Nakagawa, K., Yasumitu, T., Fukuhara, K., Shiono, H., and Kikui, M. (2003). Poor prognosis after lung resection for patients with adenosquamous carcinoma of the lung. Ann Thorac Surg *75*, 1740-1744.
Raber, P., Ochoa, A.C., and Rodriguez, P.C. (2012). Metabolism of L-arginine by myeloid-derived suppressor cells in cancer: mechanisms of T cell suppression and therapeutic perspectives. Immunol Invest *41*, 614-634.
Rock, J.R., Onaitis, M.W., Rawlins, E.L., Lu, Y., Clark, C.P., Xue, Y., Randell, S.H., and Hogan, B.L. (2009). Basal cells as stem cells of the mouse trachea and human airway epithelium. Proc Natl Acad Sci U S A *106*, 12771-12775.
Snyder, E.L., Watanabe, H., Magendantz, M., Hoersch, S., Chen, T.A., Wang, D.G., Crowley, D., Whittaker, C.A., Meyerson, M., Kimura, S., *et al.* (2013). Nkx2-1 represses a latent gastric differentiation program in lung adenocarcinoma. Mol Cell *50*, 185-199.
Sutherland, K.D., Proost, N., Brouns, I., Adriaensen, D., Song, J.Y., and Berns, A. (2011). Cell of origin of small cell lung cancer: inactivation of Trp53 and Rb1 in distinct cell types of adult mouse lung. Cancer Cell *19*, 754-764.
Sutherland, K.D., Song, J.Y., Kwon, M.C., Proost, N., Zevenhoven, J., and Berns, A. (2014). Multiple cells-of-origin of mutant K-Ras-induced mouse lung adenocarcinoma. Proc Natl Acad Sci U S A *111*, 4952-4957.
Travis, W.D., Brambilla, E., Noguchi, M., Nicholson, A.G., Geisinger, K., Yatabe, Y., Powell, C.A., Beer, D., Riely, G., Garg, K., *et al.* (2011). International Association for the Study of Lung Cancer/American Thoracic Society/European Respiratory Society: international multidisciplinary classification of lung adenocarcinoma: executive summary. Proc Am Thorac Soc *8*, 381-385.

Travis, W.D., Brambilla, E., and Riely, G.J. (2013). New pathologic classification of lung cancer: relevance for clinical practice and clinical trials. J Clin Oncol *31*, 992-1001.
Tu, S., Bhagat, G., Cui, G., Takaishi, S., Kurt-Jones, E.A., Rickman, B., Betz, K.S., Penz-Oesterreicher, M., Bjorkdahl, O., Fox, J.G., *et al.* (2008). Overexpression of interleukin-1beta induces gastric inflammation and cancer and mobilizes myeloid-derived suppressor cells in mice. Cancer Cell *14*, 408-419.
Turner, B.M., Cagle, P.T., Sainz, I.M., Fukuoka, J., Shen, S.S., and Jagirdar, J. (2012). Napsin A, a new marker for lung adenocarcinoma, is complementary and more sensitive and specific than thyroid transcription factor 1 in the differential diagnosis of primary pulmonary carcinoma: evaluation of 1674 cases by tissue microarray. Arch Pathol Lab Med *136*, 163-171.
Winslow, M.M., Dayton, T.L., Verhaak, R.G., Kim-Kiselak, C., Snyder, E.L., Feldser, D.M., Hubbard, D.D., DuPage, M.J., Whittaker, C.A., Hoersch, S., *et al.* (2011). Suppression of lung adenocarcinoma progression by Nkx2-1. Nature *473*, 101-104.
Xu, C., Fillmore, C.M., Koyama, S., Wu, H., Zhao, Y., Chen, Z., Herter-Sprie, G.S., Akbay, E.A., Tchaicha, J.H., Altabef, A., *et al.* (2014a). Loss of Lkb1 and Pten leads to lung squamous cell carcinoma with elevated PD-L1 expression. Cancer Cell *25*, 590-604.
Xu, X., Huang, L., Futtner, C., Schwab, B., Rampersad, R.R., Lu, Y., Sporn, T.A., Hogan, B.L., and Onaitis, M.W. (2014b). The cell of origin and subtype of K-Ras-induced lung tumors are modified by Notch and Sox2. Genes Dev *28*, 1929-1939.
Xu, X., Rock, J.R., Lu, Y., Futtner, C., Schwab, B., Guinney, J., Hogan, B.L., and Onaitis, M.W. (2012). Evidence for type II cells as cells of origin of K-Ras-induced distal lung adenocarcinoma. Proc Natl Acad Sci U S A *109*, 4910-4915.

Figure Legends

Figure 1. Cell-of-origin defines the histopathology spectrum and associated survival differences of *Kras;Lkb1*-driven lung tumors. (A) Kaplan-Meier survival curves of *Kras;Lkb1* mice, showing median survival of 79 days for Ad5-CC10-Cre ($1x10^7$ pfu, black symbols) vs 120 days for Ad5-SPC-Cre infections ($2.5x10^9$ pfu, white symbols). Significance value p=0,0125 with a Gehan-Breslow-Wilcoxon Test. (B) Histopathology analysis for tumors harvested from moribund Ad5-CC10-Cre and Ad5-SPC-Cre mice. Arrows indicate areas depicted in higher magnification IHC analyses with indicated antibodies. (C) Quantification of histopathology-specific lesions from n=5 animals per virus, showing ASC as the predominant histopathology for Ad5-CC10-Cre, and invasive AC for Ad5-SPC-Cre treated mice. (D) Histopathology-specific quantification of Ki67 positive nuclei in lesions from animals analyzed in (C). (E) Lesion size quantification of animals analyzed in (C) showing that ASC tumors are the largest lesions. (F) Quantification of PAS positive

tumor areas for lung lesions infected with Ad5-CC10-Cre virus (n=4). (G) Quantification of NKX2-1 positive nuclei on samples analyzed in (F). Error bars represent mean ± StDev. Student's t test p value is *p< 0.5, ***p< 0.001. Scale bars: 2000 μM for lung lobes, 50 μM for magnified images.

Figure 2. Comparative gene expression analysis indicates squamous expression profile in Ad5-CC10-Cre derived ASC tumors. (A) Unsupervised hierarchical clustering of Ad5-CC10-Cre-derived ASC and Ad5-SPC-Cre-derived papillary AC tumors with p<0,01 LogFC>1 as a cut-off, showing distinct histopathology-specific gene expression signatures. (B) Venn diagram illustrating comparative expression analyses of Ad5-CC10-Cre-derived *Kras;Lkb1* ASC vs Ad5-SPC-Cre-derived *Kras;Lkb1* papillary AC, *Lkb1;Pten* SCC vs *Kras* AC (Xu et al. 2014, GSE54353) and human SCC vs AC tumors (Kuner et al., GSE10245). Upregulated and downregulated genes are in red and green fonts, respectively. (C) Common up- and downregulated genes of datasets shown in figure (B) represented as a heatmap of gene expression values from *Kras;Lkb1* ASC vs papillary AC datasets. Insets in (A) and (C) show the distribution of samples within scaled expression values.

Figure 3. Distinct immune-related gene expression signatures suggest ASC vs papillary AC histopathology-dependent tumor immune microenvironments. (A) IPA canonical pathway analysis shows enrichment of several immune-related genes in *Kras;Lkb1* Ad5-CC10-Cre-derived ASCs compared with Ad5-SPC-Cre-derived papillary ACs. A –log(p-value) greater than 2 is used as a cut-off. (B) Heatmap representing immune-related genes differentially expressed in *Kras;Lkb1* (KL) Ad5-CC10-Cre-derived ASC and Ad5-SPC-Cre-derived papillary AC, and *Kras;p53* (KP) Ad5-CC10-Cre-derived and Ad5-SPC-Cre-derived AC tumors with p<0,01 LogFC>1 as a cut-off. The inset shows the distribution of samples within scaled expression values. (C) qPCR validation of *Il-1β, Arg1, H2-M2* and *H2-D1* gene expression in ASC (n=13 tumors) and papillary AC (PAC, n=8 tumors) from *Kras;Lkb1*, and Ad5-CC10-Cre-derived (n=4 tumors) and Ad5-SPC-Cre-derived

(n=7 tumors) PACs from *Kras;p53* genotypes. Gene expression was normalized against the housekeeping *Rpl19* mRNA. Error bars represent mean ± StDev. Student's t test p value is **p<0.01, ***p<0.001.

Figure 4. The presence of MDSCs in ASC tumors reveals histopathology-specific tumor immune microenvironments. (A) Representative immunohistochemical stainings for Gr-1, CD11b, and CD3 in Ad5-CC10-Cre-derived ASC and Ad5-SPC-Cre-derived papillary AC (PAC) from *Kras;Lkb1* mice. (B) Quantification of immunostainings for Gr-1, CD11b and CD3 (n=5 mice). (C) Representative flow cytometry plots showing Gr-1 and CD11b expression in Ad5-CC10-Cre-derived ASC and Ad5-SPC-Cre-derived papillary AC from *Kras;Lkb1* mice. Plots are gated for live cells. Percentages of Gr-1$^+$CD11b$^+$ cells are presented in the upper right quadrant of the plot. (D) Quantification of Gr-1$^+$CD11b$^+$ MDSCs in Ad5-CC10-Cre-derived ASC (n=4) and Ad5-SPC-Cre-derived papillary AC (PAC, n=4) from *Kras;Lkb1* mice assessed by flow cytometry. (E) Schematic representation summarizing lung progenitor cell-specific lesion etiology following expression of oncogenic *Kras* concomitant with loss of *Lkb1* in CC10$^+$ or SPC$^+$ cells. Both CC10$^+$ and SPC$^+$ progenitors can give rise to invasive AC, AIS, papillary AC and ASC, with ASC most prevalent for CC10$^+$ cells. CC10$^+$ cells uniquely give rise to pure mucinous and acinar AC. ASCs exhibit an immunosuppressive microenvironment, showing MDSCs recruitment and decreased T cells. Error bars represent mean ± StDev. Student's t test values are *p<0.5, ***p<0.001. Scale bar 50 μM.

Figure 1

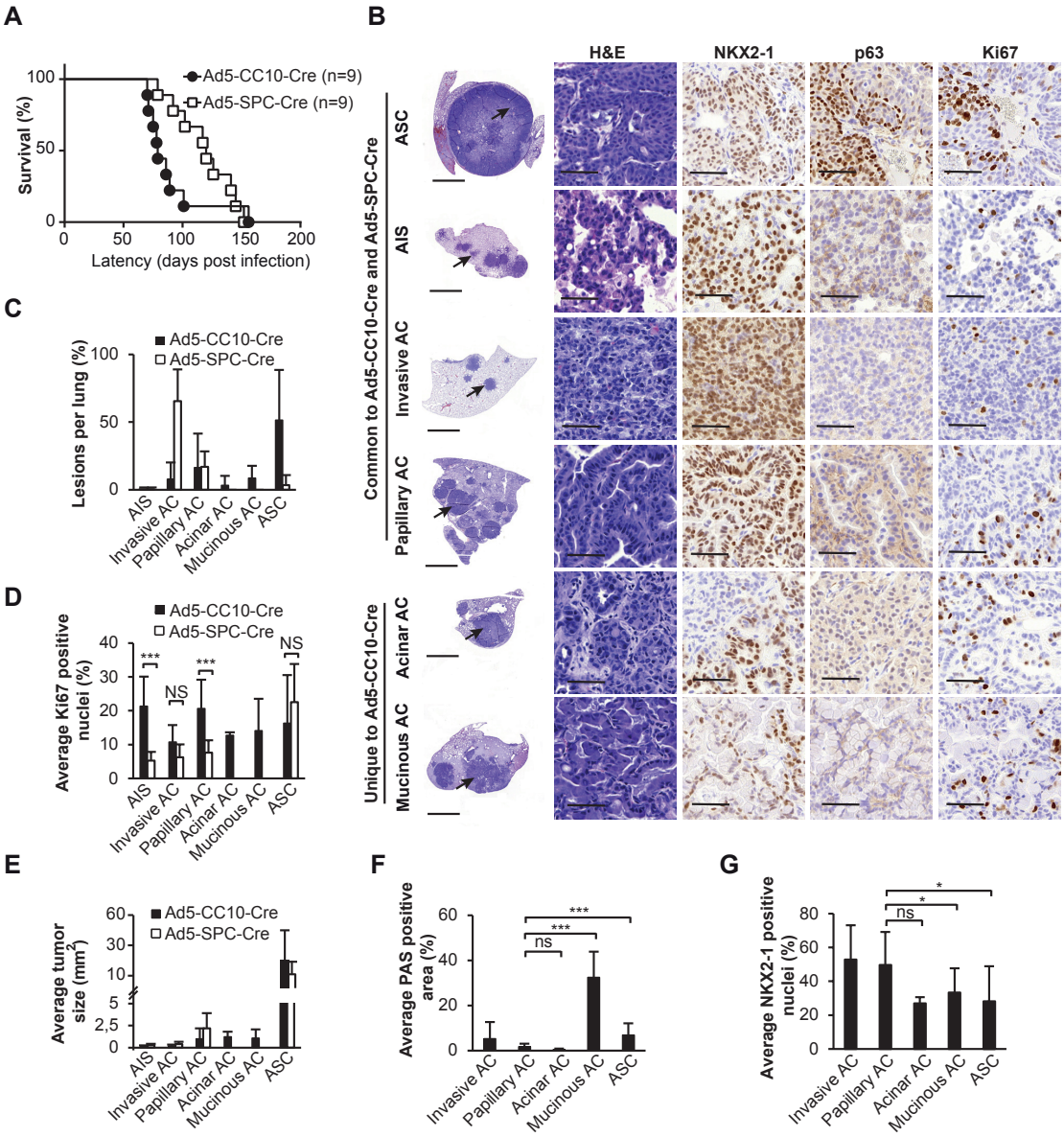
A
Survival (%)
Latency (days post infection)
Ad5-CC10-Cre (n=9)
Ad5-SPC-Cre (n=9)
B
H&E
NKX2-1
p63
Ki67
Common to Ad5-CC10-Cre and Ad5-SPC-Cre
Unique to Ad5-CC10-Cre
ASC
AIS
Invasive AC
Papillary AC
Acinar AC
Mucinous AC
C
Lesions per lung (%)
Ad5-CC10-Cre
Ad5-SPC-Cre
D
Average Ki67 positive nuclei (%)
NS
E
Average tumor size (mm²)
F
Average PAS positive area (%)
ns
G
Average NKX2-1 positive nuclei (%)

Figure 2

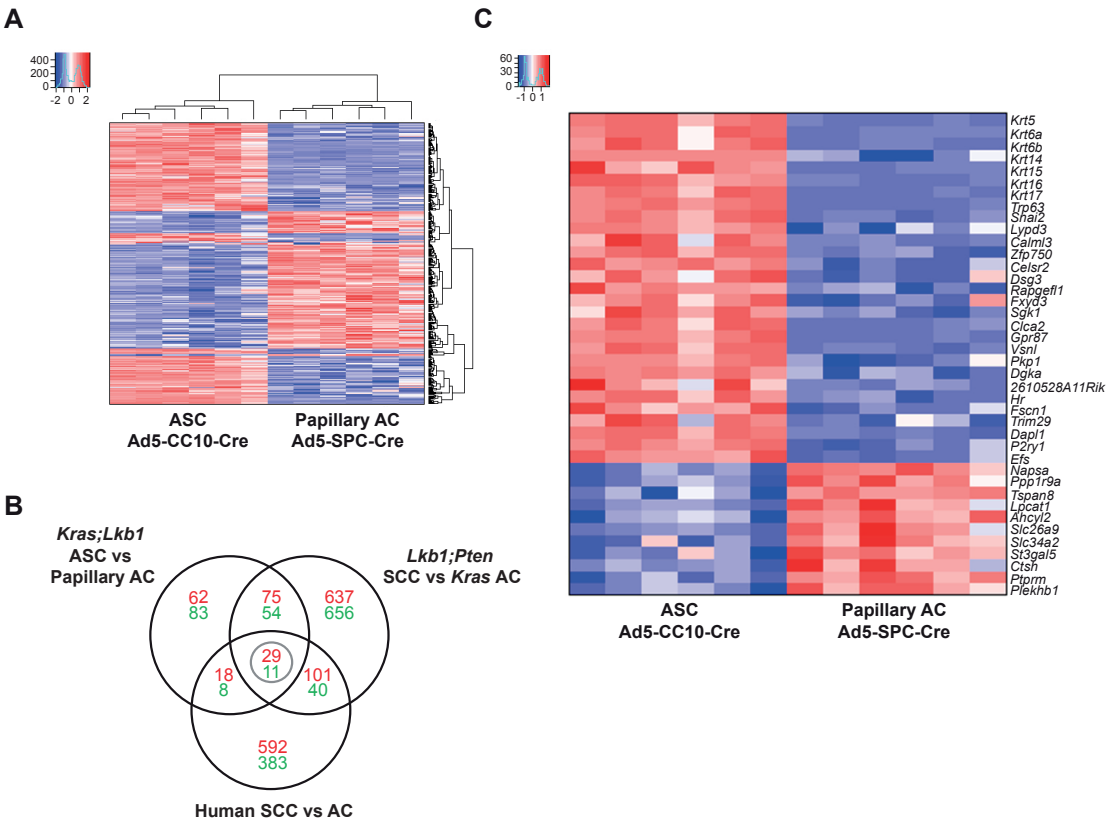
A
400
200
0
-2 0 2
ASC
Ad5-CC10-Cre
Papillary AC
Ad5-SPC-Cre
B
Kras;Lkb1
ASC vs
Papillary AC
Lkb1;Pten
SCC vs Kras AC
62
83
75
54
637
656
29
11
18
8
101
40
592
383
Human SCC vs AC
C
60
30
0
-1 0 1
Krt5
Krt6a
Krt6b
Krt14
Krt15
Krt16
Krt17
Trp63
Shai2
Lypd3
Calml3
Zfp750
Celsr2
Dsg3
Rapgefl1
Fxyd3
Sgk1
Clca2
Gpr87
Vsnl
Pkp1
Dgka
2610528A11Rik
Hr
Fscn1
Trim29
Dapl1
P2ry1
Efs
Napsa
Ppp1r9a
Tspan8
Lpcat1
Ahcyl2
Slc26a9
Slc34a2
St3gal5
Ctsh
Ptprm
Plekhb1
ASC
Ad5-CC10-Cre
Papillary AC
Ad5-SPC-Cre

Figure 3

A

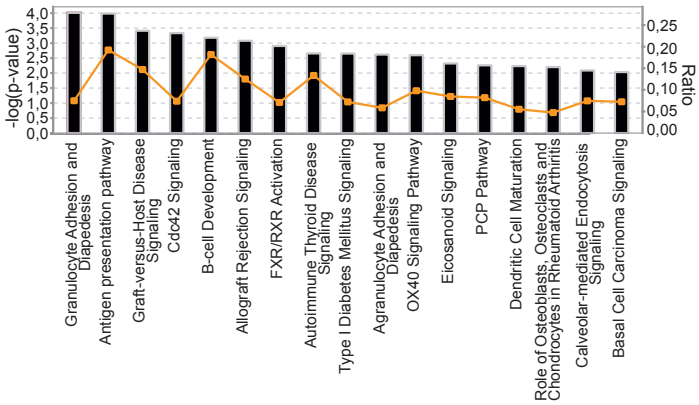
-log(p-value)
Ratio
Granulocyte Adhesion and Diapedesis
Antigen presentation pathway
Graft-versus-Host Disease Signaling
Cdc42 Signaling
B-cell Development
Allograft Rejection Signaling
FXR/RXR Activation
Autoimmune Thyroid Disease Signaling
Type I Diabetes Mellitus Signaling
Agranulocyte Adhesion and Diapedesis
OX40 Signaling Pathway
Eicosanoid Signaling
PCP Pathway
Dendritic Cell Maturation
Role of Osteoblasts, Osteoclasts and Chondrocytes in Rheumatoid Arthritis
Calveolar-mediated Endocytosis Signaling
Basal Cell Carcinoma Signaling

B

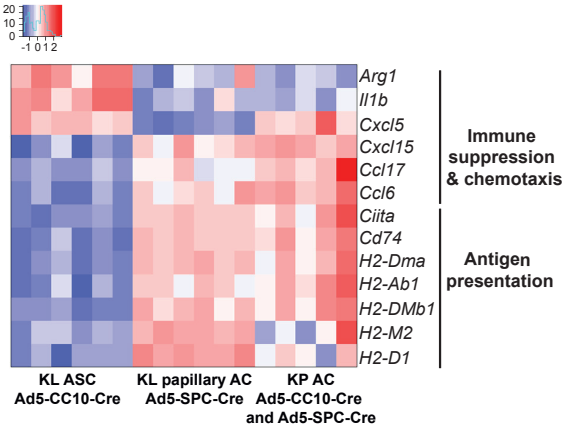
Arg1
Il1b
Cxcl5
Cxcl15
Ccl17
Ccl6
Ciita
Cd74
H2-Dma
H2-Ab1
H2-DMb1
H2-M2
H2-D1
Immune suppression & chemotaxis
Antigen presentation
KL ASC Ad5-CC10-Cre
KL papillary AC Ad5-SPC-Cre
KP AC Ad5-CC10-Cre and Ad5-SPC-Cre

C

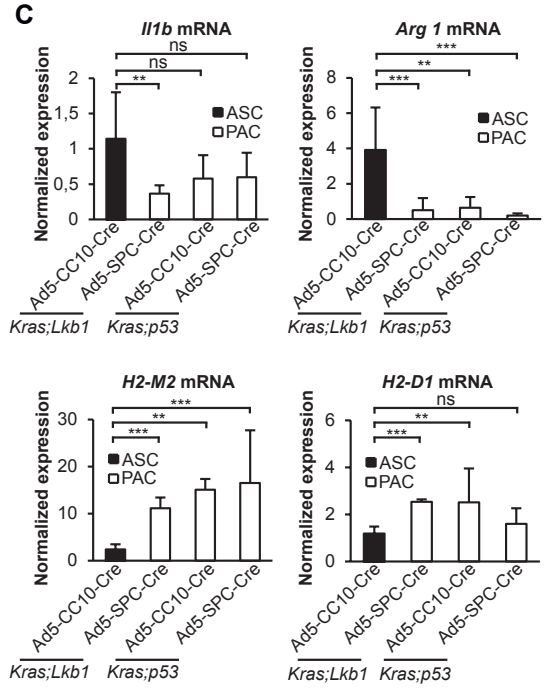
Il1b mRNA
Arg 1 mRNA
H2-M2 mRNA
H2-D1 mRNA
Normalized expression
ASC
PAC
ns
**
***
Ad5-CC10-Cre
Ad5-SPC-Cre
Kras;Lkb1
Kras;p53

Figure 4

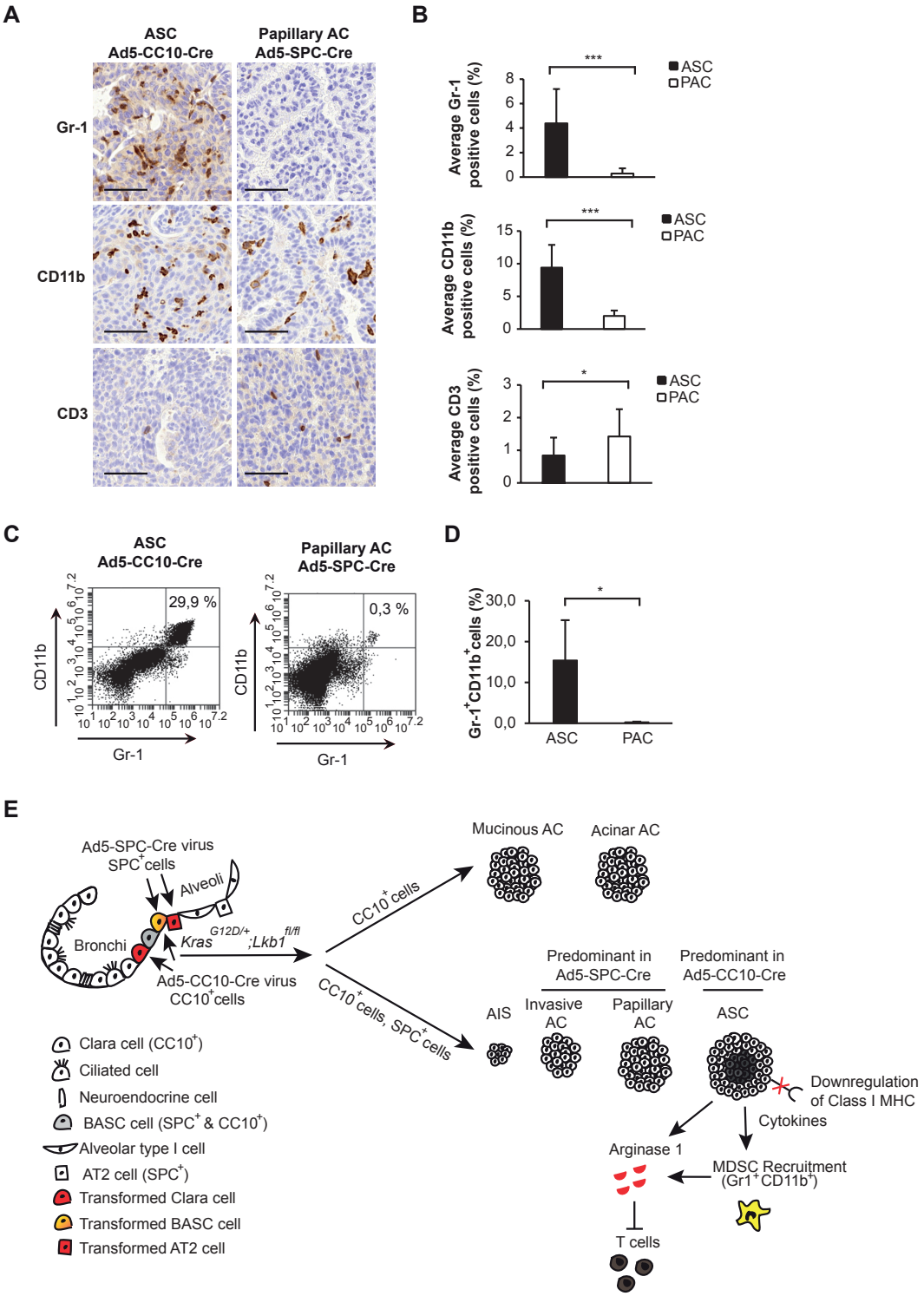
A
ASC
Ad5-CC10-Cre
Papillary AC
Ad5-SPC-Cre
Gr-1
CD11b
CD3
B
Average Gr-1 positive cells (%)
Average CD11b positive cells (%)
Average CD3 positive cells (%)
***
*
ASC
PAC
C
ASC
Ad5-CC10-Cre
Papillary AC
Ad5-SPC-Cre
29,9 %
0,3 %
CD11b
Gr-1
D
Gr-1+CD11b+cells (%)
ASC
PAC
E
Ad5-SPC-Cre virus
SPC+cells
Alveoli
Bronchi
Kras G12D/+ ;Lkb1 fl/fl
Ad5-CC10-Cre virus
CC10+cells
CC10+cells
CC10+cells, SPC+cells
Mucinous AC
Acinar AC
Predominant in Ad5-SPC-Cre
Predominant in Ad5-CC10-Cre
AIS
Invasive AC
Papillary AC
ASC
Downregulation of Class I MHC
Cytokines
Arginase 1
MDSC Recruitment (Gr1+CD11b+)
T cells
Clara cell (CC10+)
Ciliated cell
Neuroendocrine cell
BASC cell (SPC+ & CC10+)
Alveolar type I cell
AT2 cell (SPC+)
Transformed Clara cell
Transformed BASC cell
Transformed AT2 cell

Figure S1, related to Figure 1

Cell-of-origin defines histopathology spectrum in *Kras;Lkb1* mice. (A) Representative images of anti-GFP stained Ad5-CC10-Cre and Ad5-SPC-Cre infected *Kras;Lkb1;Rosa26*$^{mT/mG}$ mice at two and four weeks post infection, respectively. The majority of GFP positive cells in Ad5-CC10-Cre infected lungs were located in bronchiolar regions (arrows), occasionally at bronchioalveolar duct junctions (arrowhead). GFP positive cells in Ad5-SPC-Cre virus infected lungs were mainly seen in the alveolar region (arrows). Scale bars: 100 μm. (B) Representative images of anti-LKB1 stained Ad5-CC10-Cre- and Ad5-SPC-Cre-infected *Kras;Lkb1* and *Kras;p53* lungs. All *Kras;Lkb1* tumors were negative for LKB1. Arrows indicate areas depicted in higher magnification. Scale bars: 2000 μM for lung lobes, 50 μM for magnified images. (C) Tumor lesion quantification. Representative image of H&E-stained lung sections from Ad5-CC10-Cre infected *Kras;Lkb1* mice, and corresponding pseudo-colored image depicting tumor segmentation performed with Definiens software. PAC: Papillary AC, MAC: Mucinous AC, IAC: in situ AC. (D) Representative IHC images of KRT5 and SOX2 for Ad5-CC10-Cre-induced ASC tumors. All ASCs showed expression of KRT5, but lacked SOX2 expression. Scale bars: 50 μm. (E) Representative images from H&E-stained lung sections from Ad5-CC10-Cre infected *Kras;Lkb1* mice showing invasive AC histopathology class. Scale bars: 100 μm. (F) Representative images of anti-p63 stained Ad5-CC10-Cre ASC mucinous and papillary ACs, showing rare p63 positive nuclei. Scale bars: 50 μm. (G) Time point analysis of *Kras;Lkb1* mice infected with Ad5-CC10-Cre and Ad5-SPC-Cre viruses. Representative images of H&E, anti-NKX2-1 and anti-p63 stained lungs show papillary hyperplasias of bronchiolar epithelial cells in Ad5-CC10-Cre-infected lungs and adenocarcinoma in situ (AIS) lesions in Ad5-SPC-Cre infected lungs at six wk post infection (n=2). At nine wk post infection pure squamous cell carcinoma (SCC) was detected in one out of four mice in Ad5-CC10-Cre-infected lungs, and invasive AC or invasive papillary AC in Ad5-SPC-Cre infected lungs (n=4). Arrows indicate areas depicted in higher magnification. Scale bars: 2000 μM for lung lobes, 50 μM for magnified images.

Figure S2, related to Figure 1

Cell-of-origin defines histopathology spectrum in *Kras;Lkb1* mice. (A) Ki67 IHC quantification. Representative image of anti-Ki67 stained lung sections from Ad5-CC10-Cre-infected *Kras;Lkb1* mice, and the corresponding pseudo-colored images describing Ki67 positive (yellow) and negative (blue) nuclear detection performed with Definiens. Scale bars: 50 µm. (B) Representative images of anti-HMGA2 stained Ad5-CC10-Cre- and Ad5-SPC-Cre-induced *Kras;Lkb1* tumors. All ASCs showed homogenous staining for HMGA2, whereas all other histopathologies showed negative staining or pockets of positive regions. Arrows indicate areas depicted in higher magnification. Scale bars: 1000 µM for lung lobes, 50 µM for magnified images. (C) Representative images of PAS and NKX2-1 immunostaining of Ad5-CC10-Cre-derived lesions. Scale bars: 100 µm. (D) PAS staining quantification. Representative image of lung sections from Ad5-CC10-Cre infected *Kras;Lkb1* mice, and corresponding pseudo-colored images showing PAS positive (yellow) and negative (purple) area detection performed with Definiens. Scale bars: 50 µm. (E) NKX2-1 immunohistochemistry quantification. Representative image of anti-NKX2-1 stained lung sections from Ad5-CC10-Cre-infected *Kras;Lkb1* mice, and corresponding pseudo-colored image describing NKX2-1 low (yellow), NKX2-1 medium (orange), NKX2-1 high (dark brown) and negative (blue) nuclear detection performed with Definiens. Scale bars: 50 µm. (F) Representative images of PAS and anti-NKX2-1 immunostaining of Ad5-CC10-Cre-derived bronchiolar hyperplasia. Scale bars: 100 µm.

Figure S3, related to Figure 2

***Kras*$^{G12D/+}$*;Lkb1*$^{fl/fl}$ tumors exhibit histotype-specific gene expression signatures** (A) Workflow describing comparative gene expression analysis of ASC and papillary AC tumors from *Kras;Lkb1* mice. (B) Western blot analysis of tumors selected for microarray profiling using anti-p63 and anti-ß-actin antibodies. (C) Comparison of *Kras;Lkb1* Ad5-CC10-Cre ASC vs Ad5-SPC-Cre papillary AC differentially expressed genes with normal airway basal cells vs epithelial differentially expressed genes (GSE15724) and *Kras;Lkb1* Ad5-CMV-Cre ASC vs AC tumors (GSE6135). (D) qPCR

validation of immune-related genes in Ad5-SPC-Cre-induced ASC tumors (n=2) and Ad5-CC10-Cre-induced papillary AC (n=1). Gene expression was normalized against the housekeeping *Rpl19* mRNA. Error bars represent mean ± StDev. (E) Gr-1 immunohistochemistry quantification. Representative image of anti-Gr-1 stained lung sections from Ad5-CC10-Cre-infected *Kras;Lkb1* mice, and the corresponding pseudo-colored image describing Gr-1 low (yellow), Gr-1 medium (orange), Gr-1 high (dark brown) and negative (blue) nuclear detection performed with Definiens. Tightened filtering was performed to exclude any false positive staining detection (grey nuclei). Identical quantification settings were used for CD11b and CD3 stainings. Scale bars: 50 µm. (F) Representative images of anti-Gr-1, anti-CD11b and anti-CD3 stained Ad5-CC10-Cre and Ad5-SPC-Cre-induced *Kras;p53* tumors. Scale bars: 50 µm. (G) Quantification of immunostainings for Gr-1, CD11b and CD3 in *Kras;p53* mice infected with Ad5-CC10-Cre (n=2) and Ad5-SPC-Cre (n=2). Error bars represent mean ± StDev.

Table S1, related to Figure 2 and Figure S3.

List of commonly up- and downregulated genes from the comparative gene expression analysis represented as log fold changes and p-values from the *Kras;Lkb1* Ad5-CC10-Cre ASC vs Ad5-SPC-Cre papillary AC comparison.

Supplemental Experimental Procedures

Mouse breeding and recombinant adenovirus administration

Kras mice were crossed with *Lkb1*$^{fl/fl}$ or *p53*$^{fl/fl}$ mice to generate *Kras;Lkb1* or *Kras;p53* mice on a C57Bl/6J background. *Kras;Lkb1* mice were crossed with *Rosa26*$^{mT/mG}$ Cre-reporter mice (Muzumdar et al., 2007), resulting in mixed background cohorts (C57Bl/6J;29X1/SvJ;ICR). Eight to ten wk old mice were intranasally or intratracheally administered with 1-20x10^7 pfu of Ad5-CC10-Cre or 2.5-7.5x10^9 pfu of Ad5-SPC-Cre viruses (Viral Vector Core Facility, University of Iowa, USA) under isofluorane anaesthesia.

Tissue preparation and histopathology analysis

Histopathology analysis was performed for H&E-stained paraffin sections. Whole slide scans of stained tissue sections were acquired with a Pannoramic 250 3DHISTECH digital slide scanner. Scans were assessed for lesion numbers and sizes using the Tissue studio image analysis solution of Definiens Developer XD 64 2.1 software (Definiens, Munich, Germany). Histopathology diagnoses were made by an expert pathologist.

Antibodies

The following antibodies were used for immunohistochemistry and immunoblotting.

Antibody	Company	Catalogue no.	Antigen retrieval
LKB1	Cell Signaling Technology	D60C5F10	10mM sodium citrate pH 6.0
p63	Abcam	ab53039	10mM sodium citrate pH 6.0
NKX2-1	Abcam	ab133638	10mM sodium citrate pH 6.0
Ki67	Thermo Fisher scientific	RM-9106-S0	10mM sodium citrate pH 6.0
GFP (polyclonal rabbit serum 8 mg/ml)	Generated in house (1)		10mM sodium citrate pH 6.0
Keratin 5	Abcam	ab52635	10mM sodium citrate pH 6.0
Gr-1	E-Bioscience	14-5931	Trypsin
CD11b	BioSB	BSB6441	10mM sodium citrate pH 6.0
CD3	Abcam	ab5690	10mM sodium citrate pH 6.0
SOX2	Santa Cruz Biotechnology	sc-17320	10mM sodium citrate pH 6.0
β-actin	Sigma	A1978	

Immunohistochemistry and quantitation

For immunistochemistry, lungs were fixed overnight at room temperature in 4% formaldehyde, embedded in paraffin, sectioned (5 µm) from two distinct regions representing the surface and middle regions of the lungs. Sections were dehydrated and antigenic epitopes were exposed using an optimized antigen retrieval method (see more details in the table for used antibodies). Tissue sections were blocked with 1% BSA and 10% Normal Goat Serum in 1x PBS. Primary antibody staining was overnight at 4°C (SOX2) or 1h at ambient temperature or (all others). Primary antibodies were detected using secondary antibody BrightVision poly-HRP anti-rabbit (IL ImmunoLogic, AD Duiven, the Netherlands), or Peroxidase-Goat Anti-Rat IgG (H+L) (Invitrogen Corporation, Camarillo, CA) for 30 min at

ambient temperature. Detection was done with DAB (Bright DAB, IL ImmunoLogic, Duiven, The Netherlands). Whole slide scans of immunohistologically stained lung sections were acquired with a Pannoramic 250 3DHISTECH (3DHISTECH Kft., Budapest, Hungary) digital slide scanner using a 20x objective. Scans were assessed for quantitation of PAS or immunohistological stainings using the Tissue Studio^{TM} image analysis solution of the Definiens Developer XD 64 2.1 software (Definiens, Munich, Germany). Inflammatory infiltrations were diagnosed by an expert pathologist.

Microarray gene expression data analysis

Data analysis consisted of data pre-processing, quality analysis and detection of statistically differentially expressed genes between different samples. All methods used were implemented in the beadarray, limma, and BioMart packages of the Bioconductor Project. The result sheets from GenomeStudio were loaded to R, normalized, log2-transformed and background corrected. Additional gene information was extracted from Ensembl using BioMart. Matching was done via Ensembl gene names.

Comparative gene expression analysis

Differentially expressed genes were compared to publicly available gene expression data sets made available via the NCBI-GEO (http://www.ncbi.nlm.nih.gov/geo/) database. Differentially expressed genes using a $p<0,01$ and LogFC>1 cut-off value from the following studies were included in the analysis: GSE54352 (2), GSE15724 (3), GSE10245 (4) and GSE6135 (5). Venn diagrams were generated using Venny 2.0.2 (http://bioinfogp.cnb.csic.es/tools/venny/). Heatmaps were generated using the R statistical programming language heatmap function from the Heatplus Bioconductor package. R version

2.15.3 (http://www.r-project.org/) was used to visualize genes commonly upregulated across data sets.

Microarray gene expression profiling and quantitative PCR analysis

For gene expression analyses, two tumors per tumor-bearing mouse were excised from the lung lobes. Each tumor was divided into three parts; one each for RNA and protein isolation, and one as a histology reference. Total RNA from snap-frozen tumors was extracted using the NucleoSpin RNA II kit (MACHEREY-NAGEL, Duren, Germany). Expression profiling was done with Illumina Mouse WT-6 version 2 expression arrays (Illumina, San Diego, CA, USA). For the quantitative PCR analysis the total RNA isolated from snap-frozen tumors was quantified using the NanoDrop 1000 (Thermo Fisher Scientific Inc., Waltham, USA). A high-capacity cDNA reverse transcription kit (Life technologies, Waltham, USA) was used to synthesize complementary DNA (cDNA). Triplicate reactions using iQ™ SYBR® Green Supermix (Bio-Rad, Hercules, USA) were run and analyzed on a CFX384 Touch™ Real-Time PCR Detection System (Bio-Rad, Hercules, USA), using relative quantitation against the housekeeping *Rpl19* mRNA. The following primers flanking exon-exon boundaries were designed and verified for specific amplification: *Il-1β*, fwd 5'TGCCACCTTTTGACAGTGATGAGA3' rev 5'CCTGGAAGGTCCACGGGAA3'; *Arginase1*, fwd 5'TCGTGTACATTGGCTTGCGA3' rev 5'GCCAATCCCCAGCTTGTCTA3'; *H2-D1*, fwd 5'CTGAAGAACGGGAACGCGAC3' rev 5'TGTAAGAGTCAGTGGACGGAGG3'; *H2-M2*, fwd 5'GTGCCTTGGATGGAACAGAT3'; rev 5'CCAGTCATCCTTTGGATGGT3'; Rpl19 fwd 5'CGGGAATCCAAGAAGATTGA3' rev 5'TTCAGCTTGTGGATGTGCTC3'. Cycles started with three minutes denaturation at 95 °C, followed by 40 cycles of 15s at 95°C, and

1m at 60°C. A melting curve ranging from 57°C to 95°C was included in every analysis to confirm specific amplification. For *Arginase 1*, an annealing temperature of 58°C was used.

Immunoblotting analysis

Protein lysates from snap-frozen tissues were prepared using a Precellys® tissue homogenizer (Bertin technologies, France). Cell lysates were prepared in RIPA buffer and protein concentrations were measured using a BCA kit. Protein samples (20 µg) were analyzed by immunoblotting.

Flow cytometry analysis

Tumors were dissected from the lungs of moribund mice and single cell suspensions were prepared by incubating the tumor tissue in HBSS containing 2mg/ml Collagenase 1A (Sigma Aldrich, USA) and 0,3 mg/ml Dispase (Life Technologies, Thermo Fisher Scientific, USA) for 30 minutes at 37°C, after which the tissue was disrupted using the gentle MACS Dissociator (Miltenyi Biotec, Germany) in DMEM medium containing 20mM Hepes and 5U/ml DNAse (Promega, USA). Single cell suspensions were stained using APC conjugated Rat anti-Gr-1 (Biolegend, USA) and FITC conjugated Rat anti-CD11b (Biolegend, USA) antibodies. The antibodies were incubated in HBSS/2%BSA for 30 minutes at 4°C at 1:25 dilution. Dead cells were stained with 1µg/ml Propidium Iodide (Sigma Aldrich, USA). Analysis of the cells was performed using a BD Accuri flow cytometer, and data were analyzed with the BD Accuri C6 software (Becton, Dickinson and Company, USA).

Statistical analysis

For the statistical analysis of we used Student's t test (two-tailed and equal variance). A p-value < 0.05 was considered significant. Error bars indicate SD.

References

1. Lahtela J, Corson LB, Hemmes A, Brauer MJ, Koopal S, Lee J, et al. A high-content cellular senescence screen identifies candidate tumor suppressors, including EPHA3. Cell cycle. 2013;12:625-34.

2. Xu C, Fillmore CM, Koyama S, Wu H, Zhao Y, Chen Z, et al. Loss of Lkb1 and Pten leads to lung squamous cell carcinoma with elevated PD-L1 expression. Cancer cell. 2014;25:590-604.

3. Rock JR, Onaitis MW, Rawlins EL, Lu Y, Clark CP, Xue Y, et al. Basal cells as stem cells of the mouse trachea and human airway epithelium. Proceedings of the National Academy of Sciences of the United States of America. 2009;106:12771-5.

4. Kuner R, Muley T, Meister M, Ruschhaupt M, Buness A, Xu EC, et al. Global gene expression analysis reveals specific patterns of cell junctions in non-small cell lung cancer subtypes. Lung cancer. 2009;63:32-8.

5. Ji H, Ramsey MR, Hayes DN, Fan C, McNamara K, Kozlowski P, et al. LKB1 modulates lung cancer differentiation and metastasis. Nature. 2007;448:807-10.

Figure S1

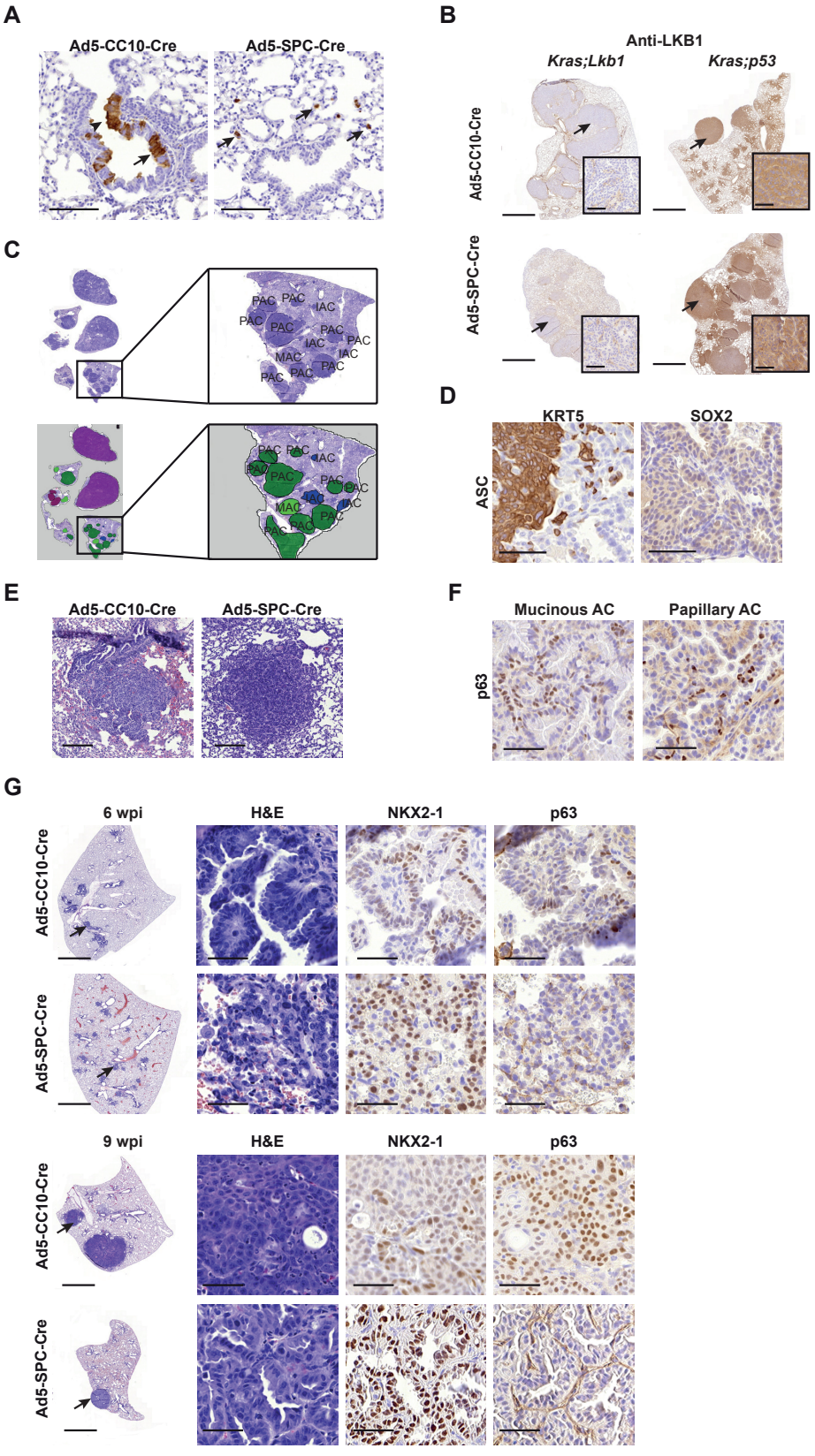
A
Ad5-CC10-Cre
Ad5-SPC-Cre
B
Anti-LKB1
Kras;Lkb1
Kras;p53
Ad5-CC10-Cre
Ad5-SPC-Cre
C
PAC
IAC
MAC
D
KRT5
SOX2
ASC
E
Ad5-CC10-Cre
Ad5-SPC-Cre
F
Mucinous AC
Papillary AC
p63
G
6 wpi
H&E
NKX2-1
p63
Ad5-CC10-Cre
Ad5-SPC-Cre
9 wpi
H&E
NKX2-1
p63
Ad5-CC10-Cre
Ad5-SPC-Cre

Figure S2

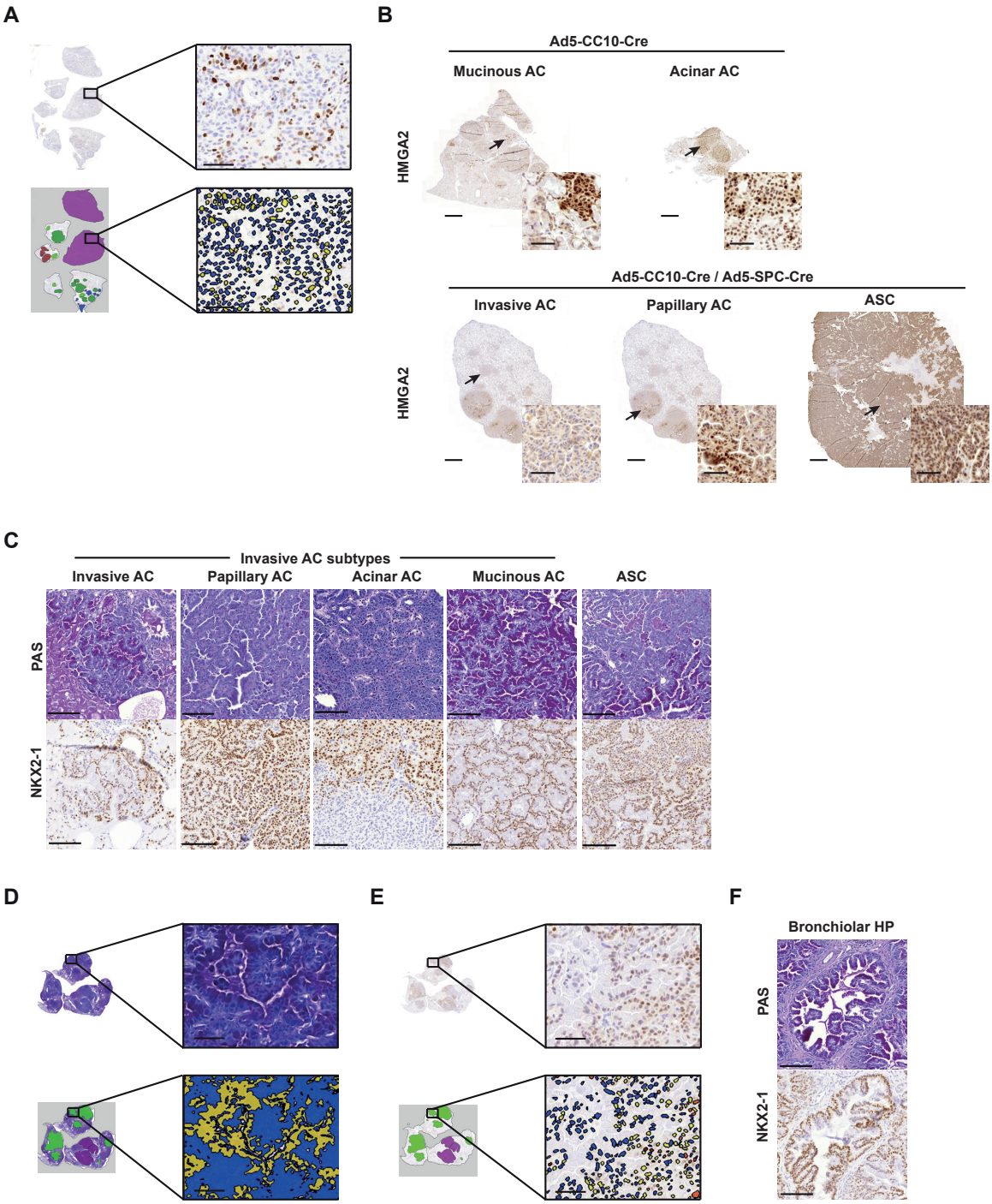
A
B
Ad5-CC10-Cre
Mucinous AC
Acinar AC
HMGA2
Ad5-CC10-Cre / Ad5-SPC-Cre
Invasive AC
Papillary AC
ASC
HMGA2
C
Invasive AC subtypes
Invasive AC
Papillary AC
Acinar AC
Mucinous AC
ASC
PAS
NKX2-1
D
E
F
Bronchiolar HP
PAS
NKX2-1

Figure S3

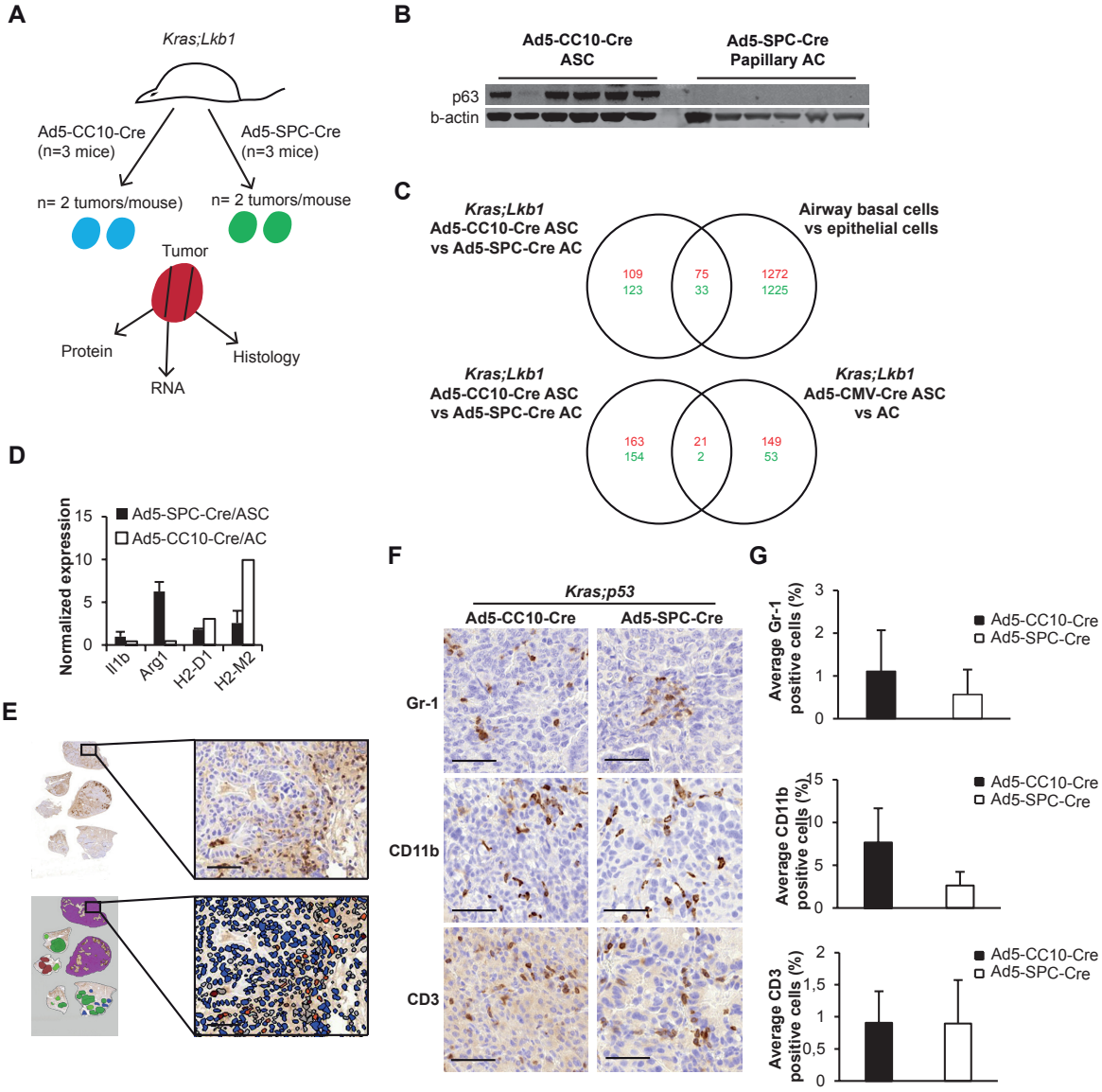
A
Kras;Lkb1
Ad5-CC10-Cre
(n=3 mice)
Ad5-SPC-Cre
(n=3 mice)
n= 2 tumors/mouse)
n= 2 tumors/mouse
Tumor
Protein
RNA
Histology
B
Ad5-CC10-Cre
ASC
Ad5-SPC-Cre
Papillary AC
p63
b-actin
C
Kras;Lkb1
Ad5-CC10-Cre ASC
vs Ad5-SPC-Cre AC
109
123
75
33
1272
1225
Airway basal cells
vs epithelial cells
Kras;Lkb1
Ad5-CC10-Cre ASC
vs Ad5-SPC-Cre AC
163
154
21
2
149
53
Kras;Lkb1
Ad5-CMV-Cre ASC
vs AC
D
Normalized expression
Ad5-SPC-Cre/ASC
Ad5-CC10-Cre/AC
Il1b
Arg1
H2-D1
H2-M2
E
F
Kras;p53
Ad5-CC10-Cre
Ad5-SPC-Cre
Gr-1
CD11b
CD3
G
Average Gr-1 positive cells (%)
Average CD11b positive cells (%)
Average CD3 positive cells (%)
Ad5-CC10-Cre
Ad5-SPC-Cre

Supplementary Table 1, related to Figure 2 and Supplementary Figure 3.

List of commonly up- and downregulated genes from the comparative gene expression analysis represented as log fold changes and p-values from the *Kras;Lkb1* Ad5-CC10-Cre ASC vs Ad5-SPC-Cre papillary AC comparison.

Ad5-CC10-Cre derived Kras;Lkb1 ASC vs Ad5-SPC-Cre derived Kras;Lkb1 papillary AC; Lkb1;Pten SCC vs Kras AC (Xu et al. 2014, GSE54353); human SCC vs AC tumors (Kuner et al., GSE10245)

Gene	LogFC	P.Value	Adj.P.Val
Krt6b	4,064895218	2,86E-09	1,90E-06
Krt6a	2,88010548	1,11E-07	2,03E-05
Zfp750	2,586819988	1,85E-08	5,70E-06
Calml3	2,508817568	8,84E-06	0,000434838
Krt15	1,98725044	2,75E-07	3,75E-05
Sgk1	1,235556478	2,48E-06	0,000180144
Fxyd3	1,21776195	0,000465713	0,007121127
Rapgefl1	1,023115374	9,46E-07	8,78E-05
Dsg3	1,013274283	0,000186607	0,003677196
Celsr2	1,009851937	2,39E-07	3,46E-05
Krt17	6,480742841	1,23E-09	1,21E-06
Krt5	4,741898945	2,46E-10	4,61E-07
Krt14	4,729042034	1,42E-05	0,000591751
Gpr87	3,750789294	2,96E-11	8,72E-08
Clca5	3,421039565	9,55E-08	1,82E-05
Lypd3	3,091228646	3,22E-05	0,001033619
Krt16	3,038105964	4,04E-09	2,29E-06
Pkp1	2,997180129	1,01E-05	0,000477906
Vsnl1	2,656167403	1,11E-08	4,77E-06
Trp63	2,572210067	6,06E-12	3,12E-08
Snai2	2,543222344	2,73E-09	1,88E-06
Efs	2,312028751	6,14E-08	1,33E-05
P2ry1	1,814915127	3,79E-08	8,99E-06
Dapl1	1,690803978	7,50E-10	9,10E-07
Trim29	1,655666154	0,00010719	0,002449449
Fscn1	1,556296265	4,20E-06	0,000259199
Hr	1,506296829	1,47E-07	2,49E-05
2610528A11Rik	1,087798271	0,000137464	0,002927555
Dgka	1,026082285	1,31E-07	2,25E-05
Plekhb1	-1,033836655	2,36E-05	0,000833556
Ptprm	-1,084496704	1,67E-06	0,000132517
Ctsh	-1,135088307	0,000222835	0,004173821
St3gal5	-1,16689992	0,000713279	0,009770334
Slc34a2	-1,229963288	0,000128328	0,002793128
Slc26a9	-1,24239973	5,47E-05	0,001512401
Ahcyl2	-1,361390926	3,54E-05	0,00110697

Lpcat1	-1,441100162	8,87E-05	0,002133149
Tspan8	-1,460808859	1,76E-05	0,000690221
Ppp1r9a	-2,397095416	1,30E-05	0,000562926
Napsa	-2,834033514	4,24E-07	5,15E-05

Ad5-CC10-Cre derived Kras;Lkb1 ASC vs Ad5-SPC-Cre derived Kras;Lkb1 papillary AC;Pten SCC vs Kras AC (Xu et al. 2014, GSE54353)

Gene	LogFC	P.Value	Adj.P.Val
Ppbp	4,301742649	1,99E-07	2,99E-05
Klk8	3,28244013	1,95E-08	5,91E-06
Ifitm1	3,163843669	8,39E-08	1,68E-05
Gp2	3,095473571	1,02E-05	0,000480819
Clic6	3,029312411	8,07E-08	1,65E-05
Ltf	3,0232633	4,34E-05	0,001261855
Gabrp	2,953742698	3,29E-09	2,06E-06
Tbx1	2,941031317	5,66E-07	6,17E-05
Otx1	2,834533016	1,34E-08	5,22E-06
Scgb3a1	2,761557199	2,39E-06	0,000175119
Aqp4	2,659834182	5,01E-05	0,001412095
Slitrk6	2,268185779	3,70E-08	8,95E-06
Tiam1	2,256112596	2,35E-09	1,88E-06
Ifitm6	2,225760594	5,12E-07	5,83E-05
Casp1	2,111535318	1,28E-07	2,24E-05
Cyp27a1	2,068398574	1,16E-08	4,77E-06
Wfdc3	2,046900637	0,000388975	0,006263711
Ifitm2	1,968165166	1,12E-05	0,000514802
Tmc5	1,936153678	6,52E-08	1,38E-05
Sox21	1,879990049	9,41992E-10	1,01988E-06
Mycl	1,836297296	1,30E-05	0,000562926
Cldn23	1,725283844	7,28E-06	0,0003763
Klk10	1,673587873	3,66E-06	0,000235662
2300002M23Rik	1,651265077	1,67E-07	2,72E-05
Sprr2g	1,597072081	7,65E-07	7,41E-05
Tmprss13	1,547035273	9,90E-10	1,02E-06
Cxcl5	1,517714154	1,23E-08	4,88E-06
Ecm1	1,449986118	0,000571094	0,008319006
Adamtsl4	1,434630129	5,09E-06	0,000297819
Irf7	1,377473649	1,05E-05	0,000489333
Clec2d	1,351667467	1,77E-05	0,000690221
Gsta3	1,304378526	0,000440771	0,006820704
Tspan33	1,205872993	9,13E-05	0,002183905
Fam46b	1,203360757	3,23E-06	0,000217193
Arhgef3	1,182057533	5,92E-07	6,32E-05
Lrrc26	1,177261765	0,000184909	0,003661204
Frrs1	1,149864462	7,39E-06	0,000379877
Slc39a6	1,141665357	2,42E-05	0,000838141

Wnt7b	1,100742247	0,000282215	0,004967559
Tfap2c	1,100684979	6,38E-06	0,000346721
Pof1b	1,057734366	1,25E-07	2,22E-05
Hsd17b2	1,043678599	0,000270183	0,004797763
Cyp2b10	1,031397057	0,000614385	0,008784004
Slc7a8	1,029435891	3,78E-05	0,001157115
Gsto1	1,028154614	1,44E-05	0,000595884
Mall	1,020838641	2,57E-06	0,000184608
Msantd3	1,015503827	3,83E-06	0,000243003
Krt6b	4,064895218	2,86E-09	1,90E-06
Krt6a	2,88010548	1,11E-07	2,03E-05
Zfp750	2,586819988	1,85E-08	5,70E-06
Calml3	2,508817568	8,84E-06	0,000434838
Krt15	1,98725044	2,75E-07	3,75E-05
Sgk1	1,235556478	2,48E-06	0,000180144
Fxyd3	1,21776195	0,000465713	0,007121127
Rapgefl1	1,023115374	9,46E-07	8,78E-05
Dsg3	1,013274283	0,000186607	0,003677196
Celsr2	1,009851937	2,39E-07	3,46E-05
Krt17	6,480742841	1,23E-09	1,21E-06
Krt5	4,741898945	2,46E-10	4,61E-07
Krt14	4,729042034	1,42E-05	0,000591751
Gpr87	3,750789294	2,96E-11	8,72E-08
Clca5	3,421039565	9,55E-08	1,82E-05
Lypd3	3,091228646	3,22E-05	0,001033619
Krt16	3,038105964	4,04E-09	2,29E-06
Pkp1	2,997180129	1,01E-05	0,000477906
Vsnl1	2,656167403	1,11E-08	4,77E-06
Trp63	2,572210067	6,06E-12	3,12E-08
Snai2	2,543222344	2,73E-09	1,88E-06
Efs	2,312028751	6,14E-08	1,33E-05
P2ry1	1,814915127	3,79E-08	8,99E-06
Dapl1	1,690803978	7,50E-10	9,10E-07
Trim29	1,655666154	0,00010719	0,002449449
Fscn1	1,556296265	4,20E-06	0,000259199
Hr	1,506296829	1,47E-07	2,49E-05
2610528A11Rik	1,087798271	0,000137464	0,002927555
Dgka	1,026082285	1,31E-07	2,25E-05
Col17a1	5,025445094	8,31E-13	1,71E-08
Tmprss11g	3,612988155	1,40E-06	0,00011442
Aqp3	3,049499899	4,37E-06	0,000267141
Upk3bl	2,3645967	1,06E-05	0,000491014
Cwh43	2,255775512	3,39E-07	4,46E-05
Tpbg	2,213087982	5,11E-07	5,83E-05
Wnt10a	2,202487002	9,04E-07	8,53E-05
Lrig3	2,133480927	1,86E-09	1,59E-06

Htra1	1,9742672	5,41E-06	0,000309994
Rgs12	1,768790397	2,69E-07	3,74E-05
Evpl	1,664523823	3,18E-05	0,001024405
Apcdd1	1,564060909	3,64E-07	4,66E-05
Fbln1	1,41345374	1,76E-07	2,82E-05
Barx2	1,405121172	2,69E-07	3,74E-05
Ngfr	1,372386307	1,22E-08	4,88E-06
Cdh3	1,36896438	9,15E-09	4,15E-06
Ccdc3	1,348661482	2,38E-05	0,000836316
Kif21a	1,316708116	2,42E-05	0,000838141
Fam57a	1,305612112	3,27E-06	0,000218401
Plch2	1,298860294	6,83E-09	3,43E-06
Wnt4	1,240429909	3,14E-10	4,97E-07
Itgb4	1,225887923	1,26776E-05	0,000555194
Niacr1	1,223207012	8,65E-08	1,69E-05
Psapl1	1,191536251	0,000506668	0,007611832
Pkp3	1,104825926	3,56E-05	0,001109329
Arhgap32	1,084767013	8,35E-08	1,68E-05
Man2a1	1,02980095	0,0002011	0,003881589
Ces2g	1,012728291	1,73E-07	2,78E-05
Pcbd1	-1,01266118	2,90E-05	0,000954445
Ptgs1	-1,035525417	6,50E-05	0,001718979
Cideb	-1,085190992	0,000261821	0,004676485
Kdm3a	-1,098249847	3,89E-05	0,001171753
Elovl1	-1,101061635	0,000404124	0,006413027
Adk	-1,105024856	1,53E-06	0,00012255
Mylk	-1,118321309	3,81E-05	0,001161981
Pros1	-1,13322592	0,000646362	0,009106255
Spr	-1,147862815	3,58E-06	0,000233416
Ciita	-1,153590497	1,21E-10	2,58E-07
4921507P07Rik	-1,154570617	1,34E-05	0,000573774
Egr2	-1,159479858	0,000361639	0,005940529
Susd2	-1,186784613	0,000538464	0,007968748
Eva1a	-1,219646097	1,10E-06	9,55E-05
Acot7	-1,230953503	7,43E-05	0,001880742
Unc13d	-1,232479494	3,67E-06	0,000235662
Crlf1	-1,275587664	0,000465018	0,007115781
Adssl1	-1,275843818	6,16E-07	6,41E-05
Car4	-1,320714106	0,000303357	0,005236842
Scarf2	-1,388910549	1,01E-06	9,17E-05
H2-Ab1	-1,470348395	1,43E-05	0,000593517
Lrrc8c	-1,477330207	9,26E-09	4,15E-06
Ager	-1,579816873	3,06E-06	0,000209391
H2-DMa	-1,60921388	8,73E-09	4,15E-06
Lamp3	-1,6403467	7,30E-06	0,0003763
Chrnb1	-1,642160635	2,13E-07	3,18E-05

Bmp4	-1,673468291	3,84E-07	4,82E-05
Npw	-1,688474342	0,000342705	0,005738839
Renbp	-1,72252724	3,85E-08	9,02E-06
Cdh16	-1,748131739	6,95E-07	6,92E-05
Dpep2	-2,007282021	6,82E-07	6,86E-05
Cd74	-2,023164975	1,89E-07	2,91E-05
Fbp2	-2,054643897	8,94E-05	0,002146234
Chi3l1	-2,056055903	7,83E-05	0,001957923
Gata6	-2,104007907	9,80E-09	4,30E-06
Lgi3	-2,12757937	7,46E-07	7,34E-05
Hhex	-2,28415459	2,17E-07	3,21E-05
Adam19	-2,318299424	2,37E-11	8,15E-08
Cldn18	-2,428907714	1,08E-06	9,40E-05
Itih4	-2,61812704	1,86E-07	2,91E-05
Vsig2	-2,8978702	2,07E-08	6,09E-06
Nrn1	-2,995940883	2,31E-05	0,000825158
Aif1l	-3,164038231	1,66E-08	5,43E-06
Ctse	-3,421681314	1,43E-05	0,000593517
Plekhb1	-1,033836655	2,36E-05	0,000833556
Ptprm	-1,084496704	1,67E-06	0,000132517
Ctsh	-1,135088307	0,000222835	0,004173821
St3gal5	-1,16689992	0,000713279	0,009770334
Slc34a2	-1,229963288	0,000128328	0,002793128
Slc26a9	-1,24239973	5,47E-05	0,001512401
Ahcyl2	-1,361390926	3,54E-05	0,00110697
Lpcat1	-1,441100162	8,87E-05	0,002133149
Tspan8	-1,460808859	1,76E-05	0,000690221
Ppp1r9a	-2,397095416	1,30E-05	0,000562926
Napsa	-2,834033514	4,24E-07	5,15E-05
Sftpc	-1,013479428	3,18E-06	0,000214909
Lcp1	-1,023140496	1,54E-07	2,56E-05
Atp2a3	-1,349662184	1,26E-06	0,000106311
Plekhd1	-1,536838606	0,000382373	0,006196131
Pip5k1b	-1,770073039	1,27E-06	0,000107061
Sftpb	-1,959551374	6,01E-06	0,00033471
Cxcl15	-2,061399013	2,32E-05	0,000825158
Sftpa1	-2,11503717	0,00015855	0,003255014
Fbp1	-2,60215319	4,13E-06	0,000255393
Pla2g1b	-2,642586558	4,02E-05	0,00119669

Ad5-CC10-Cre derived Kras;Lkb1 ASC vs Ad5-SPC-Cre derived Kras;Lkb1 papillary AC; human SCC vs AC tumors (Kuner et al., GSE10245)

Gene	LogFC	P.Value	Adj.P.Val
Car12	3,636862829	2,63E-09	1,88E-06
Pdpn	1,744004733	0,000156923	0,003235567
Igf2bp2	1,587802928	0,000222947	0,004173821

Gm684	1,429416585	6,12E-07	6,41E-05
Hspb1	1,420229376	4,98E-07	5,83E-05
Has3	1,261680584	6,23E-05	0,001667649
Ltb4r1	1,243028669	9,54E-07	8,82E-05
Fgfbp1	1,020884122	4,05E-05	0,001200011
Krt6b	4,064895218	2,86E-09	1,90E-06
Krt6a	2,88010548	1,11E-07	2,03E-05
Zfp750	2,586819988	1,85E-08	5,70E-06
Calml3	2,508817568	8,84E-06	0,000434838
Krt15	1,98725044	2,75E-07	3,75E-05
Sgk1	1,235556478	2,48E-06	0,000180144
Fxyd3	1,21776195	0,000465713	0,007121127
Rapgefl1	1,023115374	9,46E-07	8,78E-05
Dsg3	1,013274283	0,000186607	0,003677196
Celsr2	1,009851937	2,39E-07	3,46E-05
Krt17	6,480742841	1,23E-09	1,21E-06
Krt5	4,741898945	2,46E-10	4,61E-07
Krt14	4,729042034	1,42E-05	0,000591751
Gpr87	3,750789294	2,96E-11	8,72E-08
Clca5	3,421039565	9,55E-08	1,82E-05
Lypd3	3,091228646	3,22E-05	0,001033619
Krt16	3,038105964	4,04E-09	2,29E-06
Pkp1	2,997180129	1,01E-05	0,000477906
Vsnl1	2,656167403	1,11E-08	4,77E-06
Trp63	2,572210067	6,06E-12	3,12E-08
Snai2	2,543222344	2,73E-09	1,88E-06
Efs	2,312028751	6,14E-08	1,33E-05
P2ry1	1,814915127	3,79E-08	8,99E-06
Dapl1	1,690803978	7,50E-10	9,10E-07
Trim29	1,655666154	0,00010719	0,002449449
Fscn1	1,556296265	4,20E-06	0,000259199
Hr	1,506296829	1,47E-07	2,49E-05
2610528A11Rik	1,087798271	0,000137464	0,002927555
Dgka	1,026082285	1,31E-07	2,25E-05
Sostdc1	2,930147281	0,000660051	0,009223703
Pard6g	2,765215384	6,52E-10	8,91E-07
Bnc1	2,377164297	2,71E-09	1,88E-06
Sfn	2,251581488	3,08E-09	1,98E-06
S100a8	1,889118575	0,000116966	0,002614854
Pthlh	1,459110393	0,000165801	0,0033703
Clip4	1,409097502	0,000130502	0,002819601
Col7a1	1,329498769	3,78E-07	4,81E-05
Amotl1	1,179282851	1,05E-06	9,31E-05
Trim59	1,046473677	7,29E-05	0,001863426
Gdf15	-1,065481026	0,000247593	0,004489287
Gprc5a	-1,066873106	2,18E-05	0,000792638

Errfi1	-1,232325325	7,52E-06	0,000385737
Cpm	-1,251867026	0,000693469	0,009593146
Hkdc1	-2,155174339	2,36E-06	0,000174026
Plekhb1	-1,033836655	2,36E-05	0,000833556
Ptprm	-1,084496704	1,67E-06	0,000132517
Ctsh	-1,135088307	0,000222835	0,004173821
St3gal5	-1,16689992	0,000713279	0,009770334
Slc34a2	-1,229963288	0,000128328	0,002793128
Slc26a9	-1,24239973	5,47E-05	0,001512401
Ahcyl2	-1,361390926	3,54E-05	0,00110697
Lpcat1	-1,441100162	8,87E-05	0,002133149
Tspan8	-1,460808859	1,76E-05	0,000690221
Ppp1r9a	-2,397095416	1,30E-05	0,000562926
Napsa	-2,834033514	4,24E-07	5,15E-05
Cmtm8	-1,032511879	0,000238502	0,004369773
Cd55	-1,446457341	0,000102306	0,002385451
Acox2	-1,64064951	9,63E-07	8,86E-05

Ad5-CC10-Cre derived Kras;Lkb1 ASC vs Ad5-SPC-Cre derived Kras;Lkb1 papillary AC; mouse lung basal cells vs epithelial cells (Rock et al. 2009, GSE15724)

Gene	LogFC	P.Value	Adj.P.Val
Sncg	1,839855318	5,87E-06	0,000327761
Scin	1,674641271	2,95E-05	0,000964679
Nxn	1,57921197	9,10E-06	0,000444586
Il1r2	1,433847403	0,000233918	0,004328114
Il1b	1,410776466	2,63E-05	0,000884856
Cib2	1,286434757	1,32E-06	0,000110423
Cav1	1,279630393	9,97E-05	0,002334545
Notch1	1,26558021	7,18E-07	7,11E-05
Fads1	1,206201817	0,000263389	0,004696351
Sytl1	1,19770372	1,90E-05	0,00073062
B3gnt8	1,166292081	4,15E-07	5,09E-05
Pcdhb22	1,164517777	0,000134662	0,002894312
Dlk2	1,152847829	2,42E-06	0,000176611
Fam101b	1,106656825	3,33E-07	4,43E-05
Tacstd2	1,092475614	3,58E-05	0,001112435
Enho	1,055377066	0,000521062	0,007792835
Ptk7	1,04865216	1,71E-06	0,00013465
Def6	1,007300675	5,06E-07	5,83E-05
Sostdc1	2,930147281	0,000660051	0,009223703
Pard6g	2,765215384	6,52E-10	8,91E-07
Bnc1	2,377164297	2,71E-09	1,88E-06
Sfn	2,251581488	3,08E-09	1,98E-06
S100a8	1,889118575	0,000116966	0,002614854
Pthlh	1,459110393	0,000165801	0,0033703
Clip4	1,409097502	0,000130502	0,002819601

Col7a1	1,329498769	3,78E-07	4,81E-05
Amotl1	1,179282851	1,05E-06	9,31E-05
Trim59	1,046473677	7,29E-05	0,001863426
Krt17	6,480742841	1,23E-09	1,21E-06
Krt5	4,741898945	2,46E-10	4,61E-07
Krt14	4,729042034	1,42E-05	0,000591751
Gpr87	3,750789294	2,96E-11	8,72E-08
Clca5	3,421039565	9,55E-08	1,82E-05
Lypd3	3,091228646	3,22E-05	0,001033619
Krt16	3,038105964	4,04E-09	2,29E-06
Pkp1	2,997180129	1,01E-05	0,000477906
Vsnl1	2,656167403	1,11E-08	4,77E-06
Trp63	2,572210067	6,06E-12	3,12E-08
Snai2	2,543222344	2,73E-09	1,88E-06
Efs	2,312028751	6,14E-08	1,33E-05
P2ry1	1,814915127	3,79E-08	8,99E-06
Dapl1	1,690803978	7,50E-10	9,10E-07
Trim29	1,655666154	0,00010719	0,002449449
Fscn1	1,556296265	4,20E-06	0,000259199
Hr	1,506296829	1,47E-07	2,49E-05
2610528A11Rik	1,087798271	0,000137464	0,002927555
Dgka	1,026082285	1,31E-07	2,25E-05
Col17a1	5,025445094	8,31E-13	1,71E-08
Tmprss11g	3,612988155	1,40E-06	0,00011442
Aqp3	3,049499899	4,37E-06	0,000267141
Upk3bl	2,3645967	1,06E-05	0,000491014
Cwh43	2,255775512	3,39E-07	4,46E-05
Tpbg	2,213087982	5,11E-07	5,83E-05
Wnt10a	2,202487002	9,04E-07	8,53E-05
Lrig3	2,133480927	1,86E-09	1,59E-06
Htra1	1,9742672	5,41E-06	0,000309994
Rgs12	1,768790397	2,69E-07	3,74E-05
Evpl	1,664523823	3,18E-05	0,001024405
Apcdd1	1,564060909	3,64E-07	4,66E-05
Fbln1	1,41345374	1,76E-07	2,82E-05
Barx2	1,405121172	2,69E-07	3,74E-05
Ngfr	1,372386307	1,22E-08	4,88E-06
Cdh3	1,36896438	9,15E-09	4,15E-06
Ccdc3	1,348661482	2,38E-05	0,000836316
Kif21a	1,316708116	2,42E-05	0,000838141
Fam57a	1,305612112	3,27E-06	0,000218401
Plch2	1,298860294	6,83E-09	3,43E-06
Wnt4	1,240429909	3,14E-10	4,97E-07
Itgb4	1,225887923	1,26776E-05	0,000555194
Niacr1	1,223207012	8,65E-08	1,69E-05
Psapl1	1,191536251	0,000506668	0,007611832

Pkp3	1,104825926	3,56E-05	0,001109329
Arhgap32	1,084767013	8,35E-08	1,68E-05
Man2a1	1,02980095	0,0002011	0,003881589
Ces2g	1,012728291	1,73E-07	2,78E-05
Slc17a9	-1,034249167	1,07E-05	0,000494843
Atp6v0e2	-1,054769326	5,79E-05	0,00156945
Trim30a	-1,095484355	0,0003617	0,005940529
Lgals3bp	-1,109622465	8,25E-05	0,002035775
Gstk1	-1,166952407	1,92E-05	0,00073299
Sdcbp2	-1,18348163	0,000548512	0,008081441
Fam174b	-1,189204298	6,26E-05	0,001672841
Plaur	-1,233099763	3,57E-05	0,001109329
Tmem8	-1,270742422	4,05E-06	0,000253829
Degs2	-1,310245338	0,000549681	0,008092879
Cacna1h	-1,392371714	1,48E-05	0,000607006
Hdc	-1,488481365	0,000108002	0,002457095
Foxa3	-1,821006491	5,37E-06	0,000308658
Fcna	-1,99503127	0,000524527	0,00782879
Tmem54	-2,004014539	6,25E-06	0,000342662
Cmtm8	-1,032511879	0,000238502	0,004369773
Cd55	-1,446457341	0,000102306	0,002385451
Acox2	-1,64064951	9,63E-07	8,86E-05
Plekhb1	-1,033836655	2,36E-05	0,000833556
St3gal5	-1,16689992	0,000713279	0,009770334
Slc34a2	-1,229963288	0,000128328	0,002793128
Ahcyl2	-1,361390926	3,54E-05	0,00110697
Ppp1r9a	-2,397095416	1,30E-05	0,000562926
Sftpc	-1,013479428	3,18E-06	0,000214909
Lcp1	-1,023140496	1,54E-07	2,56E-05
Atp2a3	-1,349662184	1,26E-06	0,000106311
Plekhd1	-1,536838606	0,000382373	0,006196131
Pip5k1b	-1,770073039	1,27E-06	0,000107061
Sftpb	-1,959551374	6,01E-06	0,00033471
Cxcl15	-2,061399013	2,32E-05	0,000825158
Sftpa1	-2,11503717	0,00015855	0,003255014
Fbp1	-2,60215319	4,13E-06	0,000255393
Pla2g1b	-2,642586558	4,02E-05	0,00119669

Ad5-CC10-Cre derived Kras;Lkb1 ASC vs Ad5-SPC-Cre derived Kras;Lkb1 papillary AC; Ad5-CMV-Cre derived Kras;Lkb1 ASC vs AC (Ji et al. 2015, GSE6135)

Gene	LogFC	P.Value	Adj.P.Val
Wfdc1	2,432883241	1,34E-07	2,28E-05
Hspa2	1,247619569	2,68E-07	3,74E-05
Hsph1	1,243515918	5,41E-07	6,02E-05
Car12	3,636862829	2,63E-09	1,88E-06
Bnc1	2,377164297	2,71E-09	1,88E-06

Sfn	2,251581488	3,08E-09	1,98E-06
Has3	1,261680584	6,23E-05	0,001667649
Krt5	4,741898945	2,46E-10	4,61E-07
Gpr87	3,750789294	2,96E-11	8,72E-08
Lypd3	3,091228646	3,22E-05	0,001033619
Krt6a	2,88010548	1,11E-07	2,03E-05
Trp63	2,572210067	6,06E-12	3,12E-08
Krt15	1,98725044	2,75E-07	3,75E-05
Col17a1	5,025445094	8,31E-13	1,71E-08
Aqp3	3,049499899	4,37E-06	0,000267141
Aqp4	2,659834182	5,01E-05	0,001412095
Tiam1	2,256112596	2,35E-09	1,88E-06
Cyp27a1	2,068398574	1,16E-08	4,77E-06
Psapl1	1,191536251	0,000506668	0,007611832
Pkp3	1,104825926	3,56E-05	0,001109329
Ces2g	1,012728291	1,73E-07	2,78E-05
Ccl6	-1,238072525	1,56E-05	0,000629781
Hkdc1	-2,155174339	2,36E-06	0,000174026